



HAL
open science

Optimisation de la transmission de phonie et vidéophonie sur les réseaux à larges bandes PMR

Alina Alexandra Florea

► **To cite this version:**

Alina Alexandra Florea. Optimisation de la transmission de phonie et vidéophonie sur les réseaux à larges bandes PMR. Economies et finances. Institut National des Télécommunications, 2013. Français. NNT : 2013TELE0006 . tel-00873686

HAL Id: tel-00873686

<https://theses.hal.science/tel-00873686>

Submitted on 16 Oct 2013

HAL is a multi-disciplinary open access archive for the deposit and dissemination of scientific research documents, whether they are published or not. The documents may come from teaching and research institutions in France or abroad, or from public or private research centers.

L'archive ouverte pluridisciplinaire **HAL**, est destinée au dépôt et à la diffusion de documents scientifiques de niveau recherche, publiés ou non, émanant des établissements d'enseignement et de recherche français ou étrangers, des laboratoires publics ou privés.



THESE DE DOCTORAT CONJOINT

TELECOM SUDPARIS et L'UNIVERSITE PIERRE ET MARIE CURIE

Spécialité: Télécommunications

Ecole doctorale: Informatique, Télécommunications et Electronique de Paris



Optimisation de la transmission de la phonie et vidéophonie sur les réseaux à larges bandes PMR

Thèse n° : 2013TELE0006

Thèse de doctorat présentée par
Mlle Alina Alexandra FLOREA

Pour obtenir le grade de: Docteur

Soutenue le 25 février 2013

Devant le jury composé de:

M. Djamel ZEGHLACHE	<i>Directeur de thèse</i>	Professeur, Telecom SudParis
Mme. Hang NGUYEN	<i>Encadrant Académique</i>	Directeur d'Etudes, Telecom SudParis
M. Laurent MARTINOD	<i>Encadrant Industriel</i>	Ingénieur, Cassidian
M. Philippe MEGE	<i>Encadrant Industriel</i>	Expert Senior, Cassidian
M. Fumiyuki ADACHI	<i>Rapporteur</i>	Professeur Emérite, Université de Tohoku
M. Xavier LAGRANGE	<i>Rapporteur</i>	Professeur, Telecom Bretagne
M. Pierre SENS	<i>Examineur</i>	Professeur, Université Pierre et Marie Curie



JOINT DOCTORATE

TELECOM SUDPARIS and UNIVERSITY PIERRE AND MARIE CURIE

Field: Telecommunications

Doctoral school: Computer Science, Telecommunications and Electronics, Paris



Optimization of Speech and Video Transmission over Broadband PMR

Dissertation N°: 2013TELE0006

*A PhD dissertation presented by
Miss Alina Alexandra FLOREA*

Submitted for the degree of: Doctor of Philosophy

Presented the 25th February 2013

Accepted on the recommendation of:

Mr. Djamel ZEGHLACHE	<i>Academic Supervisor</i>	Professor, Telecom SudParis
Mrs. Hang NGUYEN	<i>Academic Supervisor</i>	Professor, Telecom SudParis
Mr. Laurent MARTINOD	<i>Industrial Supervisor</i>	Engineer, Cassidian
Mr. Philippe MEGE	<i>Industrial Supervisor</i>	Senior Expert, Cassidian
Mr. Fumiyuki ADACHI	<i>Reporter</i>	Distinguished Professor, Tohoku University
Mr. Xavier LAGRANGE	<i>Reporter</i>	Professor, Telecom Bretagne
Mr. Pierre SENS	<i>Examiner</i>	Professor, Pierre and Marie Curie University



Cette thèse a été réalisée de 2009 à 2012 dans le cadre d'un contrat CIFRE chez CASSIDIAN.

This thesis has been performed from 2009 to 2012 in the frame of a CIFRE contract within CASSIDIAN.



Ce travail a été partiellement financé par l'Agence Nationale Recherche Technologie (ANRT), à travers le dispositif des Conventions Industrielles de Formation par la Recherche (CIFRE).

This work has been partly supported by the Industrial Convention of Education through Reasearch (CIFRE) program, from the National Agency for Research and Technology (ANRT).



Cette thèse de doctorat a été supervisé académiquement et conjointement par l'Ecole Doctorale d'Informatique, Télécommunications et Electronique (Université Pierre et Marie Curie), et le laboratoire de recherche SAMOVAR (Telecom SudParis). Des copies de cette thèse sont disponibles aux bibliothèques de l'UPMC et de Telecom SudParis.

This PhD has been academically supervised by both the Informatics, Telecommunications and Electronics Department (Pierre and Marie Curie University), and the research laboratory SAMOVAR (Telecom SudParis). Catalog records for this publication are available from the UPMC and Telecom SudParis libraries.

Remerciements

Je remercie les professeurs Hang Nguyen et Djamel Zeghlache de m'avoir donné l'occasion de poursuivre mes études avec cette thèse de doctorat. Egalement, je les remercie pour leurs précieux conseils sur l'approche de recherche académique et l'accueil au sein de l'équipe du laboratoire SAMOVAR.

J'adresse mes remerciements aux nombreux ingénieurs et experts de chez EADS Cassidian, qui m'ont souvent aidée et fourni des indications techniques importantes. Merci à Laurent pour son encadrement, pour son suivi technique, et pour les nombreux conseils sur la transmission radio, l'architecture LTE, les problèmes Matlab. Merci à Christophe qui m'a souvent corrigée sur les notions de codage canal. Merci à Philippe aussi, qui a suivi de près les travaux de cette thèse et m'a fait bénéficier de son expertise technique. Merci à Laurent pour les remarques sur l'analyse de la qualité audio. Merci à Antte pour les discussions constructives sur l'architecture LTE. Merci à Olivier aussi pour ses encouragements. Je remercie toute l'équipe pour son accueil et pour la bonne humeur. Egalement, merci aux experts et ingénieurs EADS Cassidian, Christophe, Laurent, Arthur, Eric, Gerard qui m'ont fourni des informations indispensables dans mon étude concernant les caractéristiques de la voix et de la vidéo, ainsi que sur les standards 3GPP et leurs évolutions.

Je tiens également à adresser des remerciements au professeur Didier Le Ruyet, du CNAM de Paris. Merci pour vos conseils et pour vos cours fournis sur les turbo codes et leurs caractéristiques théoriques.

Merci à mes amis pour leurs pensées d'encouragement et conseils utiles. J'aimerais particulièrement remercier Iulia, qui, par sa compréhension et vision roumaine et autrichienne à la fois sur la thèse de doctorat, m'a souvent rappelé l'importance du doctorat à l'international. Egalement, je tiens à saluer les lauréats de la Fondation Georges Besse, Andreea et Ghiles, pour leurs conseils et pour leurs archives LaTeX qui se sont avérés très utiles pour la rédaction de la thèse .

Et, bien sûr, un grand merci à ma famille, pour le soutien psychologique très important. Merci à mes parents et grands-parents qui ont fait de nombreux efforts pour que je puisse venir faire mes études en France. Merci de m'avoir souvent rappelé la chance et l'opportunité que les études à l'étranger représentent. Merci également à mon frère pour ses encouragements et son optimisme. Et merci à mon cher Davy pour sa patience, sa compréhension, sa joie de vivre et ses nombreux conseils, qui m'ont souvent aidé à surpasser les moments les plus difficiles durant ces trois années de thèse.

Je vous remercie tous pour votre soutien, vos encouragements et vos nombreux conseils!

Résumé Court

Le monde de la sécurité publique se prépare à l'évolution des réseaux de radiocommunications vers les larges bandes. Les technologies radio mobiles privées ou professionnelles (PMR) actuelles ne peuvent pas concourir avec les tendances de la nouvelle génération. Pendant que le standard 3GPP, Long Term Evolution (LTE), a été adopté de façon générale comme la prochaine évolution des réseaux radio mobiles publics, des questions surgissent aussi sur sa possible utilisation avec les communications critiques.

Dans cet exposé, nous présentons une étude préliminaire et une évaluation des performances du candidat LTE dans un contexte de sécurité publique. Nous mettons en évidence non seulement quelques-uns des points clés qui doivent être adressés, mais nous proposons aussi une évolution du codage canal de l'interface air. Cette nouvelle proposition est basée sur une technologie existante du standard et raffine la protection de données de la couche physique LTE d'une perspective PMR.

Nous commençons par introduire le contexte de la sécurité publique dans le chapitre 1, ainsi que la définition des communications critiques de mission. Les caractéristiques les plus importantes de la PMR sont mises en évidence, avec des références aux cas typiques d'utilisation.

Le chapitre 2 propose une évaluation objective des perspectives larges bandes de la PMR. Nous fournissons une courte introduction aux technologies PMR et leurs caractéristiques les plus importantes en terme d'architecture de transmission. La sphère des technologies larges bandes est par la suite discutée, en rappelant WIMAX comme une possible technologie niche. Pourtant, LTE a été choisi comme le candidat préféré. Nous avons concentré notre analyse sur l'architecture protocolaire de la version 9 de LTE et sur sa couche physique. Des contraintes typiques PMR sont incluses, comme la canalisation de 1.4 MHz, déployée dans les bandes UHF autour de 400 MHz. Des communications de voix et vidéo bas débit sont prises comme référence, et l'encapsulation IP est considérée. Les paramètres d'allocation de l'interface air sont aussi introduits pour une évaluation des en-têtes supplémentaires et des ressources radio disponibles. Nous réalisons une évaluation réaliste de la capacité voix et vidéo de LTE, pour les deux voies montante et descendante. L'efficacité spectrale LTE est calculée, pour une évaluation objective de ses performances comparables aux technologies PMR existantes. Nous identifions ainsi quelques aspects clés de LTE, qui devraient être adressés dans un environnement de missions critiques.

Un de ces points clés est le codage canal proposé à l'interface air. LTE propose une protection uniforme à travers les puissants codages turbo. Mais un aspect particulier dans l'optimisation des performances du système est de considérer l'analyse multi-couches. Les applications voix et vidéo à bas débit ont des propriétés spécifiques de protection non-uniforme qui, exploitées au niveau de la couche physique, augmenteraient certainement l'efficacité du système. Ainsi, nous nous concentrons dans le chapitre 3 sur la conception d'un codage turbo à protection non-uniforme. Associer des propriétés de protection non-uniforme avec les très efficaces codages turbo peut se montrer très performant. Les codages turbo ont été amplement discutés dans la littérature scientifique et ont été adoptés par de nombreux standards mobiles. Nous proposons leur évolution à travers l'intégration des concepts UEP dans leurs structures parallèles et séries, avec le codage turbo parallèle progressif et hiérarchique (PPHTC) et le codage turbo série progressif et hiérarchique (SPHTC). Les idées sur lesquelles reposent les structures parallèles et séries ont été brevetées. Dans ce chapitre, nous décrivons en détail leurs architectures pour le cas particulier d'un encodage/décodage à deux dimensions, ainsi que pour leur encodage/décodage généralisé à n dimensions. Nous mettons également en évidence une propriété particulière dans le décodage itératif turbo à travers un développement mathématique. Les comportements itératifs

et propriétés des codes sont analysés théoriquement, ainsi qu'à l'aide des simulations numériques. Leurs performances sont évaluées sur deux plateformes différentes, basées sur des éléments aléatoires et repris du standard 3GPP LTE. Les résultats sont donnés pour les environnements statiques et dynamiques. Leur comportement non-uniforme est particulièrement intéressant comparé aux codages turbo et convolutionnels pris comme références.

Le travail du chapitre 4 se concentre sur l'analyse du comportement du codage parallèle dans certains cas d'utilisation spécifiques à la transmission de voix dans le domaine de la PMR. L'idée présentée dans ce chapitre a également été brevetée. Ainsi, le PPHTC est inséré dans l'architecture LTE, à travers la proposition d'une nouvelle approche du schéma de modulation et de codage. Cette nouvelle perspective propose l'utilisation d'une protection non-uniforme intégrée à ce schéma, qui corrèlerait les performances du PPHTC et de la modulation avec la qualité de la voix perçue par l'utilisateur final. Les performances de ce schéma à protection non-uniforme pour la transmission de la voix sont comparées avec deux références LTE. Les résultats sont présentés en terme de taux d'erreur de la couche physique, ainsi que la qualité de voix correspondante mesurée. L'utilité du code et ses avantages sont mis en évidence et fournissent des perspectives de développement intéressantes.

Enfin, nous concluons et proposons les perspectives d'évolution dans le chapitre 5. Même si LTE est technologiquement très avancé comparé aux solutions PMR existantes, son adoption pour la sécurité publique va être conditionnée par son efficacité dans des scénarios critiques. Quelques modifications consistantes seront néanmoins nécessaires pour l'amélioration de LTE et son utilisation optimale pour les communications des missions critiques.

Résumé Long

Le monde de la sécurité publique a pendant longtemps utilisé des réseaux dédiés, conçus pour ses besoins propres. Ces réseaux, appelés réseaux radio mobiles privés ou professionnelles PMR, sont basés sur des technologies développées il y a plus de dix ans. Même si leurs performances sont remarquables en terme d'efficacité d'utilisation du spectre radio, les technologies PMR, aujourd'hui en utilisation, ne peuvent plus concourir avec les nouvelles tendances: un plus grand débit, un plus grand nombre d'applications possibles, de l'envoi de données voix ou vidéo temps réel. Ces nouvelles demandes des clients PMR surviennent suite aux évolutions rapides des réseaux mobiles grand public, ce qu'on appelle les réseaux à larges bandes.

En Europe, c'est le standard Long Term Evolution ou 3GPP LTE qui s'est imposé comme la prochaine génération de technologies radio mobiles. Les grands opérateurs publics commencent déjà à l'adopter et à planifier son déploiement. Mais LTE est configuré pour l'utilisation avec les contraintes du grand public. Ces contraintes sont beaucoup moins restrictives que pour la sécurité publique.

Typiquement, les réseaux PMR sont conçus avec un niveau de fiabilité de 99,99%, car ils doivent fonctionner dans toute situation critique, que ce soit un désastre naturel ou bien un événement public. Les communications de voix et de données ne sont pas uniquement cryptées, mais également assurées. Tout utilisateur doit se voir garantir l'accès au réseau, donc le taux d'établissement de communications abouti doit être de 99,99% sur toute la largeur de la cellule radio, même en bordure de cellule. Ceci implique une haute protection des données, fournie par des codages canal puissants. Les communications de groupe sont particulièrement spécifiques aux réseaux PMR. Non seulement le réseau doit gérer les membres d'un seul groupe, mais doit également décider de la priorité des utilisateurs autant dans un seul groupe, que parmi tous les groupes.

Une des caractéristiques importantes des réseaux PMR est leur efficacité d'utilisation du spectre fréquentiel. Suite à leurs applications dédiées d'encodage de la parole, de transmission de données, ainsi qu'aux techniques très rigoureuses de gestion du spectre, ces réseaux présentent une grande efficacité spectrale. Ainsi, toute ressource disponible est utilisée de façon optimale pour maximiser le nombre de communications que le réseau peut gérer simultanément. Ceci est aussi dû à la nature de leurs applications dédiées, qui sont conçues pour transmettre les messages de façon compréhensible, visant une bonne qualité, mais avec un fort taux de compression. Un exemple serait les applications dédiées de parole, qui encodent uniquement les caractéristiques très importantes de la voix humaine, pour que, après transmission, on puisse reconstruire le message avec le minimum d'information. Ainsi, la transmission de phonie sur le réseaux est faite avec le minimum de débit voix, visant les 2400 bits/s, ce qui économise des ressources radio importantes. En utilisant ces encodeurs de parole bas débit, le monde de la PMR gagne en terme de capacité de phonie et d'efficacité spectrale.

Le bas débit semble être le choix stratégique pour une future efficacité spectrale importante des réseaux de nouvelle génération aussi, comme LTE. On préconise l'utilisation en parallèle des réseaux PMR existants et des réseaux LTE. Les réseaux PMR existants seraient ainsi utilisés pour la transmission des communications de phonie, pendant que LTE transporterait le trafic plus grand débit, comme la vidéo. Pourtant, le trafic de la vidéo restera dans les normes de communications PMR, soit environ 350 kbits/s, ce qui est largement inférieur au taux de haut débit que les grands opérateurs annoncent pour LTE. Ce réseau de nouvelle technologie ne va pas forcément apporter le haut débit à la PMR, mais de plus grandes capacités acquises à travers des technologies plus performantes. A terme, LTE doit remplacer les anciennes technologies PMR, et ainsi assurer une couverture permanente pour la phonie, la vidéo et d'autres types de données. Comme LTE n'est pas conçu pour les contraintes rigoureuses de la PMR, des questions surgissent sur sa possible utilisation avec les communications

critiques, et particulièrement pour les communications de phonie. Ces dernières, avec leur nature très bas débit, semblent poser un problème particulier d'efficacité.

Une première étude, abordée dans le chapitre 2, met en évidence les caractéristiques de la PMR, ainsi que quelques uns des points clés qui doivent être adressés dans LTE pour agrandir son efficacité. Les réseaux PMR demandent une grande efficacité pour les communications de voix, et, dans le futur, pour les communications vidéo ou vidéophonie. Mais ces communications doivent également être fortement protégées, pour couvrir uniformément toute la surface d'une cellule radio. Ces dernières sont particulièrement étendues pour les réseaux PMR et peuvent atteindre de quelques kilomètres en milieu urbain jusqu'à plusieurs dizaines de kilomètres en milieu rural. Ceci est dû aux fréquences utilisées, allouées dans les bandes fréquentielles de 400 MHz en Europe et 700 MHz aux Etats-Unis. Ces très hautes fréquences ou UHF ont de plus grandes couvertures et sont moins atténuées par les pertes que les fréquences plus hautes (900 à 2000 MHz) utilisées dans le grand public. Donc, avec un coût limité, les réseaux PMR peuvent aller jusqu'à couvrir un territoire national. Mais le spectre alloué reste limité et donc il doit être utilisé avec un maximum d'efficacité.

Nous soulignons par la suite des contraintes de transmission de la voix et de la vidéo, qui font partie intégrante de la philosophie de développement de la PMR. Les notions d'efficacité et de qualité sont perçues de manière différente. Ainsi, la bonne qualité de parole est définie comme un message compréhensible, intelligible, dont le bruit de fond est fortement atténué. Egalement, pour une forte compression de la parole, les codeurs source éliminent des caractéristiques typiques de la voix humaine, comme par exemple son contenu émotionnel. Ceci requiert des techniques particulières d'encodage source de la voix, et des applications dédiées existent. A un tel taux de compression audio, les caractéristiques source sont prises en compte par la couche radio pour une protection optimale de l'information. Ainsi, la protection non-uniforme est introduite, ce qui fournit une très haute protection aux informations essentielles de reconstruction du signal, et moins de robustesse aux bits de poids faibles.

Les communications vidéos sont sensées ramener plus d'outils de travail pour les professionnels. Des techniques modernes seraient nécessaires pour la transmission et l'analyse des images et vidéos prises en temps réel. Ceci pourrait s'appliquer par exemple à la télé-médecine, où des images des patients pourraient aider les médecins à identifier le problème sans forcément se déplacer sur place. Ou bien dans le cas des désastres naturels, où la présence humaine serait impossible, des robots pourraient fournir des images en temps réel des événements sur place.

L'architecture de transmission des technologies PMR et leurs caractéristiques les plus importantes sont présentées par la suite. Ainsi, nous passons en revue une première famille de standards: APCO25, TETRA, TETRAPOL. Ces derniers font partie de la génération à bande étroite, puisqu'ils utilisent des canalisations comprises entre 10 et 25 kHz. On pourrait également les identifier comme la deuxième génération ou 2G, à cause des technologies qu'ils incorporent. Cette génération permet la transmission de la parole bas débit et de données de types message court sur une architecture simple, de type circuit. Le mode circuit se traduit par la simple transmission des trames de voix à la couche physique radio, sans même passer par d'autres protocoles intermédiaires. Ainsi, ces trames subissent une forte protection canal, une modulation robuste et une émission sur des ressources radio allouées sur toute la durée de la communication. Pour une efficacité agrandie, la protection canal est de type non-uniforme et adaptée aux caractéristiques de l'encodeur source.

Un standard PMR de nouvelle génération est présenté également, TEDS. Il s'agit de l'évolution de TETRA à des technologies à bande élargie, qui peuvent être considérées de troisième génération ou 3G. Avec TEDS, la transmission de la vidéo est introduite dans les réseaux PMR. L'architecture de TEDS présente déjà des éléments de nouvelle génération, comme les turbo codes, des schémas de codages et modulations adaptatifs, modulations multi-porteuses similaires à l'OFDM, antennes sectorielles et bien sûr de plus grandes bandes passantes, allant jusqu'à 150 kHz.

Dans la sphère des technologies à larges bandes, WIMAX a été également proposé en tant que candidat à l'évolution de la PMR. Cependant, il semblerait que ce standard resterait plutôt une possible technologie niche. En comparant LTE à WIMAX, plusieurs caractéristiques clés de ces réseaux de nouvelle génération se distinguent, parmi lesquelles les couches protocolaires plus complexes, dont l'IP, ou "Internet Protocol", devient

indispensable, les turbo codes, modulations multi-porteuses OFDM, les systèmes d'antennes adaptatives. Ces éléments nous permettent de mieux comprendre les perspectives d'évolution des réseaux PMR également, puisqu'ils désignent les briques des réseaux radio mobiles de nouvelle génération.

Nous analysons ensuite les perspectives de convergence de LTE vers le monde de la PMR. LTE a été conçu pour le grand public et représente une évolution des technologies radio mobiles grand public. La couche physique présente donc de nombreux principes de ses prédécesseurs. On retrouve les couches protocolaires incluant le transport IP, la compression des en-têtes supplémentaires au niveau 3 de la couche physique, le transfert des paquets de données des canaux logiques sur les canaux physiques à l'aide des blocs de transport standardisés. Le standard LTE définit un grand nombre de ces blocs, qui, en fonction du niveau de protection des paquets, seront transmis sur un nombre de ressources radio adéquates sur le canal de données correspondant. LTE propose également des mécanismes complexes d'adaptation de lien, en fonction desquels le niveau de protection des données est choisi (turbo codage suivi par un poinçonnage performant). Les paquets protégés et modulés sont transmis sur la trame radio en utilisant des technologies performantes, comme l'OFDM et le SC-FDMA, qui éparpillent les symboles sur les multi-porteuses radio en fréquence. Ces trames radio sur les liens montant et descendant présentent une structure complexe, avec des canaux spécifiques à chaque type d'information traitée par le réseau: les données utilisateur, les données de contrôle, les données de synchronisation, les données d'adaptation de lien. Chaque trame radio est divisée en sous-trames de 1 ms, qui constituent l'intervalle de temps d'émission. Ces mécanismes représentent une évolution de l'héritage des réseaux de troisième génération existants.

Mais la grande nouveauté de cette nouvelle génération à large bande ou "broadband" consiste à vouloir faire converger tous les services sur un seul réseau, dont la voix. Mais sur les réseaux existants, les communications de voix utilisent surtout les réseaux GSM qui sont configurés pour une grande efficacité de transmission. Et les réseaux de troisième génération transmettent les données de plus grand débit sur paquets IP, comme la vidéo, les jeux, les applications. Et uniquement en heure de pointe les paquets de voix peuvent être relayés de façon transparente comme des paquets de données sur IP. LTE propose justement la réunification de tous ces services sur un seul réseau, avec des configurations standard. Les questions qui ont surgi donc sont relatives à l'efficacité de la transmission sur IP de la parole, et particulièrement des applications à bas débit, caractéristiques à la PMR.

Dans ce chapitre, nous modélisons la chaîne de transmission théorique pour les paquets de voix et de vidéo dans le seul but d'estimer l'efficacité de LTE. Nous prenons en compte des contraintes PMR: communications de parole et de vidéo bas-débit, allocations des ressources radio dans la bande spectrale de 1.4 MHz. Même si l'étude reste théorique, l'approche reste réaliste, avec la prise en compte des paramètres de transmission multicouches. Ainsi, les en-têtes des couches protocolaires sont pris en compte pour une modélisation objective de leur impact sur l'allocation radio et donc la capacité maximale LTE en nombre de communications. Le choix des paramètres d'allocations radio est fait en suivant de près les indications du standard LTE, autant pour la couche physique, que pour la trame radio et son affectation aux données utiles de l'utilisateur. Nous réalisons une évaluation réaliste de la capacité voix et vidéo de LTE, pour les deux voies montante et descendante.

La transmission de la voix sur LTE est un sujet de grande actualité, en vue de l'utilisation de LTE pour le grand public. Des études sur la faisabilité ont été réalisées, mais surtout pour la transmission de la voix sur IP pour les codeurs sources grand public, comme par exemple AMR, dont le débit peut aller de 6 à 12 fois le débit ciblé par la PMR. Les organismes de standardisation ont également proposé plusieurs approches pour la migration en douceur des communications de voix du mode circuit au mode IP. Ainsi, deux solutions reposent sur l'utilisation des réseaux circuit existants pour les communications de voix. Dans un premier cas, il s'agit de l'utilisation de GSM en attendant le déploiement de LTE. Par contre, dans un deuxième cas, on envisagerait l'utilisation simultanée de LTE, de telle façon à faire passer le grand débit sur LTE et la voix sur GSM pour une bonne efficacité du système. Une troisième solution propose l'utilisation de LTE pour l'ensemble des communications, quelle que soit leur nature. Cette dernière suppose l'utilisation des paquets IP pour la transmission de toute donnée de manière transparente pour le réseau. Il s'agit ici d'une vraie solution pure IP, appelée MMTel. Cette plateforme de service bénéficie de normes d'interopérabilité déjà existantes, qui s'appliquent tout aussi bien aux terminaux mobiles et fixes. Pour ce qui est de service de téléphonie sur internet, comme par exemple Skype, ces derniers ne présentent pas d'interface d'utilisation commune aux opérateurs, qui soit standardisée, et ne supportent pas les appels aux numéros d'urgences.

Pour l'évaluation de l'efficacité LTE pour la transmission de voix type PMR, nous avons considéré un codeur source de voix de très bas débit, soit 2400 bits/s. Les paquets de parole sont encapsulés pour une transmission temps réel, en utilisant les différents protocoles de transmission, comme RTP, UDP, IP et la compression des en-têtes au niveau 3 de la couche physique LTE, à l'aide du protocole ROHC. Les différents en-têtes des couches LTE sont également considérés: PDCP, RLC, MAC, ainsi que les mécanismes de détection d'erreur type CRC. Le standard LTE envisage une multitude de schémas de protection des données pour l'émission radio. Ainsi, tout paquet de données arrivant des couches supérieures se voit attribuer un bloc de transmission ou TBS. Le standard propose la corrélation du TBS au niveau de protection des données et aux ressources radio alloués à travers un algorithme. Mais cet algorithme s'est avéré très peu efficace pour le bas débit de la voix sur la PMR. Nous avons donc modifié cet algorithme, en normalisant ses paramètres pour une utilisation optimale. Nous trouvons ainsi les TBS et les ressources radio correspondantes à la transmission des paquets de voix bas débit sur LTE. En utilisant des valeurs réalistes des en-têtes protocolaires, nous évaluons la capacité maximale de LTE pour les communications de voix type PMR. Egalement, nous évaluons le devenir de cette capacité dans le cas idéal des en-têtes protocolaires quasi-inexistants. Ces derniers chiffres nous permettent d'évaluer le comportement de LTE, au cas où une transmission quasi-circuit de la voix serait envisagée.

La transmission de la vidéo sur LTE est un sujet qui a également généré beaucoup d'études, mais surtout pour la vidéo grand et très grand débit. Pour la PMR, les débits vidéo envisagés seraient plus modestes, donc nous modélisons un système de transmission similaire à la transmission de la voix, mais en utilisant judicieusement les indications du standard. Nous envisageons ainsi des communications vidéo pour trois débits différents, dans trois optiques différentes. Un premier flux vidéo de base est émis à très bas débit, et est destiné à l'ensemble des utilisateurs de la cellule. Ayant une protection très robuste, ce flux représente le message essentiel que tous les utilisateurs doivent recevoir impérativement. Les deux autres flux bénéficient d'un débit plus élevé et leur but est d'améliorer la qualité de la vidéo reçue. Donc, leur protection est moins élevée et ils s'adressent à un nombre d'utilisateurs restreint.

Les résultats donnent une estimation réaliste de la capacité LTE pour la transmission de la voix et de la vidéo bas-débit sur ce nouveau réseau. Les chiffres montrent une utilisation possible pour les paquets de vidéo, mais ils mettent en évidence un manque d'optimisation en ce qui concerne les paquets de voix.

Ainsi, en utilisant des valeurs réelles pour les en-têtes protocolaires, ainsi que pour la trame air, LTE montre une capacité maximale de 60 communications de voix dans la bande de 1.4 MHz, sur la voie descendante. En n'utilisant quasiment pas d'en-têtes protocolaires, ou bien en les remplaçant avec des protocoles plus efficaces pour la transmission radio, la capacité maximale de LTE atteindrait 120 communications, soit le double. Sur la voie montante, dans la même bande de 1.4 MHz, la capacité passerait de 40 à 160 communications établies simultanément, pour le cas des en-têtes réalistes et idéaux respectivement. Dans les bandes supérieures, la situation est similaire, le nombre de communications fait plus que doubler en réduisant le poids des en-têtes protocolaires. Le problème est posé par l'ensemble des protocoles de transport réseau, qui ne sont simplement pas dimensionnés pour une transmission sur la couche radio, et surtout pour des paquets de voix. L'en-tête IP reste largement surdimensionné par rapport aux bas débits de la voix type PMR. LTE fournit pourtant un mécanisme de compression des en-têtes réseau performant, le ROHC. Mais même avec une compression très haute des en-têtes protocolaires, le pourcentage de perte dans le cas des paquets de parole reste trop élevé, au delà de 50%.

Pour une évaluation objective des performances comparables aux technologies PMR existantes, nous avons donc calculé l'efficacité spectrale LTE pour ces communications de voix. En prenant des hypothèses bien définies, nous comparons LTE, une technologie à transmission de paquets, aux technologies de type circuit, PMR et GSM. Ces dernières sont hautement efficaces pour la transmission de la voix et utilisent des technologies inférieures à LTE. Pourtant, les résultats sont surprenants. L'efficacité spectrale de transmission de la voix sur LTE est à peine supérieure, même comparable, à l'efficacité de ces réseaux circuit. Il est évident que les réseaux PMR et GSM utilisent des encodeurs source de voix, ainsi que des allocations qui ont été conçus pour la voix. Quand à LTE, nous modélisons le système en considérant un codec voix très bas débit, un débit cible pour la PMR. LTE n'est donc pas optimisé pour cet encodeur de voix. Mais cette étude nous permet de souligner les failles de cette nouvelle génération, qui semble avoir oublié de prévoir la transmission de bas débits.

La transmission de la vidéo sur LTE semble fournir des chiffres plus satisfaisants. Même si notre modélisation reste simple, elle nous permet d'acquérir une vision sur les capacités de ce nouveau système. Les communications de vidéo à trois débits différents prouvent la nécessité d'optimiser la transmission bas débit, car nous mettons en évidence le pourcentage de données de bourrage envoyées par paquet vidéo et le débit maximal atteignable par le système. Ainsi, dans la bande de 1.4 MHz en voie descendante, le flux vidéo de débit faible permettrait d'envisager 3 utilisateurs toutes les milisecondes. Mais pour un débit constant, approximativement 20% du paquet transmis est constitué par des données de bourrage. Donc le flux vidéo devrait être modifié ou bufferisé pour une meilleure efficacité du système. En voie montante, le même flux transmis à débit constant serait possible pour 2 utilisateurs toutes les milisecondes. Pour ce débit, et pour un taux de protection forte, le système ne propose que très peu de choix, ce qui peut générer des pertes en données de bourrage jusqu'à 40 % d'un paquet. Donc, pour une meilleure efficacité, pour un même débit, on devrait envisager des taux de protection moins performants, ou l'inverse, envisager des débits plus élevés pour que le taux de protection soit respecté. Ce taux est essentiel puisque tous les utilisateurs doivent impérativement recevoir ce flux vidéo. Or, le seul choix efficace permis par LTE actuellement est de transmettre un flux à un débit supérieur pour ce taux de forte protection. Ceci n'est pas forcément un empêchement pour l'utilisation de LTE dans le monde de la PMR, mais souligne surtout l'inefficacité de LTE pour les bas débits. Pour un réseau LTE dédié à la PMR, les paramètres devraient être conçus pour pouvoir basculer d'une optique grand débit à une optique grande capacité utilisateurs. Dans le cas d'un désastre naturel par exemple, le système devrait être capable de satisfaire les requêtes de communications voix et/ou vidéo d'un plus grand nombre d'utilisateurs, en leur offrant un débit plus bas. Ainsi, tous les utilisateurs ont un accès garanti au réseau, pour recevoir des messages d'urgences, de contrôle et de gestion des événements. Mais, comme nous l'avons souligné ici, LTE ne possède pas cette flexibilité pour l'instant.

Ce chapitre nous permet ainsi d'identifier quelques aspects clés de LTE, qui devraient être adressés dans un environnement de missions critiques pour une efficacité agrandie, et surtout dans le cas de la voix sur IP. A la couche physique, les tailles des paquets de transport ne sont pas adaptées non plus à une protection robuste de ce bas débit de la voix, et donc les allocations radio correspondantes sont supérieures aux taux nécessaires. Les protections canal proposées sont uniquement à protection uniforme, et donc non adaptables aux caractéristiques des encodages sources parole et vidéo, sauf s'ils sont utilisés indépendamment. Ceci veut dire que plusieurs schémas de codage et modulations doivent être prévues pour la transmission d'un seul flux vidéo ou voix. Autant ce scénario est envisageable pour la vidéo et est utilisé même dans les réseaux de troisième génération, il risque d'être hautement inefficace s'il est appliqué aux bas débits des communications de parole. En conclusion, même si LTE reste acceptable pour la transmission de la vidéo bas débit, son efficacité est encore fortement réduite pour la parole, et particulièrement pour la parole bas débit utilisée dans les réseaux PMR.

Parmi les points identifiés comme sensibles et non efficaces pour les réseaux PMR, nous avons choisi de concentrer nos efforts sur la protection canal. Le codage canal proposé à la couche physique LTE est un codage très performant, de type turbo. Il s'agit des codes turbo parallèles, suivi par un poinçonnage pour la modification des taux de transmission canal. Mais ces codes ne proposent pas une protection adaptative aux contraintes des codecs sources, qui permettrait d'envisager une meilleure allocation radio. Les applications voix et vidéo à bas débit ont des propriétés spécifiques de protection non-uniforme, qui, exploitées au niveau de la couche physique, augmenteraient certainement l'efficacité du système.

La philosophie de protection non uniforme (ou "unequal error protection - UEP" en anglais) est très simple, mais pourtant très efficace. Chaque paquet de données vidéo ou de parole présente des caractéristiques de sensibilités différentes aux erreurs du canal de transmission. Chaque bit présente un niveau d'importance différent dans la reconstruction du signal analogique en réception. Donc, le niveau d'erreur sur chacun des bits va être perçu différemment par l'utilisateur final. Si un des bits essentiel à la reconstruction du message est gravement endommagé, il sera impossible d'identifier le message. Le principe de l'UEP consiste à dire que les bits les plus importants pour la reconstruction du signal en réception seront mieux protégés que les bits les moins importants. Ainsi, même si le canal présente un taux très élevé d'erreur, le décodeur en réception pourra corriger au moins les bits les plus importants, puisque leur protection était supérieure, et pouvoir reconstruire un message compréhensible. Ce principe de protection UEP est déjà largement utilisé et bien ancré dans les moeurs de l'architecture GSM et PMR. Ces réseaux sont des réseaux hautement efficaces pour la transmission

de la parole. Donc, si nous voulons augmenter l'efficacité des communications de voix sur LTE, la piste d'une protection UEP hautement performante pourrait donner des résultats intéressants.

Ainsi, nous nous concentrons dans le chapitre 3 sur la conception d'un codage turbo à protection non-uniforme, qui permettrait l'encodage d'un seul flux à des niveaux de sensibilités différentes. Les concepts de protection non-uniforme ou UEP sont connus depuis 1967, quand les codes linéaires UEP ont été investigués. Plus tard, ces concepts ont été adoptés par des standards radio mobiles, comme le GSM, pour la transmission de la parole. Ainsi, dans le GSM, la transmission de la voix se fait en utilisant trois classes de bits différentes, qui bénéficient de niveaux de protection canal appropriés. Dans cette philosophie UEP, une classe est d'autant plus protégée qu'elle est sensible aux erreurs canal.

Associer des propriétés de protection non-uniforme avec les très efficaces codages turbo peut se montrer très performant. Une telle évolution éviterait l'utilisation des schémas de protection indépendamment les uns des autres pour transmettre les sous-flux vidéo ou voix par niveaux de sensibilité.

Les turbo codes ont été largement investigués dans la littérature scientifique. Proposés sous leur forme parallèle (PCCC) ou série (SCCC), les turbo codes offrent un large panel de structures et dérivations. Le principe même des turbo codes est basé sur la concaténation de plusieurs codes séparés par un entrelaceur. Ceci permet un décodage performant, aux entrées et sorties souples, qui estime les valeurs décodées à l'aide du calcul du maximum à posteriori ou MAP. L'entrelaceur joue un rôle essentiel pour les performances des turbo codes. Il casse les blocs d'erreur introduits par le canal de transmission, et permet aussi le décodage de plusieurs versions des mêmes informations transmises. Même si les structures PCCC et SCCC sont construites sur les mêmes principes, il a été prouvé que les performances du SCCC peuvent dépasser celle du PCCC à des niveaux très bas de taux d'erreur.

Les codages turbo aux propriétés UEP ont été amplement discutés dans la littérature scientifique également. La grande majorité des techniques UEP existantes sont basées sur des schémas de poinçonnages accompagnés parfois d'entrelaceurs adaptés. Ainsi, ces schémas proposent l'entrelacement des classes de bits sans mélanger les bits des différentes classes, et l'utilisation d'un poinçonnage non uniforme en sortie, appliqué aux classes moins importantes uniquement. Ces schémas ne modifient pas la structure même des codages turbo, mais viennent simplement compléter la protection offerte.

Une autre famille de turbo codes UEP traite des architectures hybrides. Ces dernières sont le résultat de différentes concaténations de codes pour modifier le taux de transmission à travers des techniques de codage supplémentaires. Les codes irréguliers proposent la répétition des bits les plus importants avant l'encodage turbo. Ainsi, les bits les plus protégés se voient offrir une redondance supplémentaire propre.

D'autres dérivations turbo introduisent les structures multiples. Habituellement constitués de deux codes concaténés, les turbo codes sont étendus à plus de codes concaténés. Ces concaténations multiples offrent non seulement un plus grand choix de taux de transmissions, mais également une flexibilité agrandie en architectures de décodage. Les codes woven et multifold présentent des architectures multiples très intéressantes, dont l'adaptation UEP peut s'avérer très flexible et performante. Ainsi, les codes woven proposent un code hybride de SCCC et PCCC, soit une concaténation série de deux blocs de codes parallèles. Chacun de ces deux blocs parallèles est constitué d'une multitude de codes concaténés en parallèle. Si chacun des codes constituants de ces blocs possède un taux de transmission différent, alors la trame encodée bénéficiera d'une protection non uniforme. Les codes multifold sont basés sur le PCCC seul. La trame de données est partagée en trois classes, qui sont concaténées deux par deux, et chaque nouveau bloc ainsi obtenu est encodé par un code convolusionnel récursif. Le décodage des codes multifold est très performant, car il est constitué de trois branches indépendantes, qui s'échangent des informations sur les bits qu'ils ont en commun. Ce concept est exploité avec de bons résultats pour la transmission UEP des images.

Un autre concept intéressant est introduit par les turbo codes en trois dimensions ou 3D. Ces codes sont basés sur un PCCC, qui possède déjà deux dimensions de codage, suivi par un code de taux égal à un. Ce dernier représente la troisième dimension de codage, et permet d'encoder une fraction des bits en sortie du PCCC. En fonction du pourcentage de bits encodé en 3D, le poids des mots codes en sortie est modifié, ce qui peut engendrer une modification des performances du décodage.

Dans ce chapitre, nous proposons l'évolution des turbo codes à travers l'intégration des concepts UEP dans leurs structures parallèles et séries, avec le codage turbo parallèle progressif et hiérarchique (PPHTC) et le codage turbo série progressif et hiérarchique (SPHTC). Les idées sur lesquelles reposent les structures parallèles et séries ont été brevetées. Nous décrivons en détail leur architecture pour le cas particulier d'un encodage/décodage à deux dimensions, ainsi que pour un encodage/décodage généralisé à n dimensions. Leur structure est basée sur la concaténation de deux ou n codes récursifs convolutionnels, que nous identifions par le terme de niveau d'encodage. En restant fidèles aux modèles de turbo codage, dans ces structures, deux codes successifs sont séparés par un entrelaceur.

La nouveauté de ces structures repose sur le principe d'encodage progressif des données dont la protection doit être non uniforme. Ainsi, un flux de données à n niveaux de sensibilités canal différentes sera encodé aux n niveaux de codage. La première classe de bits sera encodée en premier, la deuxième classe de bits sera introduite dans le processus de codage au niveau suivant, et les prochaines classes seront encodées hiérarchiquement aux niveaux inférieurs. Grâce à leurs conceptions, les codes PPHTC et SPHTC offrent une protection progressive, qui fournit à la première classe le niveau de redondance le plus élevé, et à la dernière classe le niveau de redondance le plus bas.

Il est impératif que l'introduction de nouvelles données dans le processus d'encodage se fasse avant l'entrelaceur. Le rôle de ce dernier n'est pas uniquement de fournir une nouvelle version de la trame à encoder au deuxième code constituant du turbo code, mais également de mieux répartir les bits de la classe moins protégée parmi ceux des classes supérieures. Cette répartition permet aux classes inférieures de pleinement profiter de la redondance supplémentaire acquise par les classes supérieures, et va être particulièrement visible dans le processus de décodage.

Pour le décodage non-uniforme progressif et hiérarchique, nous proposons une adaptation du bien connu décodage itératif turbo. Ce dernier est basé sur la concaténation de plusieurs blocs de décodage, chacun utilisant le principe de calcul de maximum a posteriori. Le maximum a posteriori ou MAP, qui tient compte des probabilités des bits en entrée, calcule la probabilité de maximiser la valeur d'un bit par rapport à la trame reçue. Un autre algorithme, le maximum de vraisemblance ou ML, maximise la probabilité de réception de la trame correcte par rapport à la valeur d'un bit. Ce qui différencie ces deux approches repose sur la présence des probabilités a priori.

Dans les structures de décodage du PPHTC et SPHTC, nous mettons en évidence la dualité de ces deux algorithmes pour le cas particulier à deux dimensions. Nous développons l'algorithme du maximum a posteriori et nous soulignons les propriétés qui sont exploitées dans le processus de décodage UEP. La première classe de bits, qui a été encodée par un processus fortement ressemblant aux codes turbo, par deux codes concaténés, est décodée avec un gain turbo important. Mais ce qui est particulièrement intéressant avec ces nouvelles structures est que la deuxième classe de bits, qui a été uniquement encodée par un seul code convolutionnel, puisse acquérir des gains considérables à travers le décodage itératif UEP. Ce flux de protection moindre exploite la redondance cachée des flux à une protection supérieure. Dans le décodage itératif, même si cette deuxième classe de bits ne possède pas d'information a priori propre, elle peut gagner de un à plusieurs dB entre sa première et sa dernière itération. Il s'agit ici de l'exploitation de la propriété du décodage itératif MAP d'influence réciproque, qui, utilisé dans un contexte UEP, donne des résultats surprenants. Le décodage itératif est détaillé pour mettre en évidence cette propriété exploitée et expliquer l'influence de la redondance cachée, que les classes inférieures gagnent en étant éparpillée parmi les classes de redondance supérieure. Ainsi, l'algorithme du BCJR et l'application mathématique aux expressions logarithmiques sont également analysés.

Nous analysons par la suite plusieurs des propriétés des codes brevetés. Ainsi, nous présentons leur représentation graphique et visuellement compréhensible à l'aide des graphes factoriels ou de type Forney. En nous basant sur ces représentations géométriques, nous mettons en évidence la propriété de taux de transmission virtuel. Ce taux est acquis grâce à la structure propre de ces codes, qui n'encodent pas un seul bloc de données mais imbriquent effectivement les données les unes dans les autres. Ainsi, chaque sous-paquet se verra envoyé sur le canal radio accompagné non seulement de sa redondance propre, mais également de la redondance des autres sous-paquets cachés dans la trame. Le taux propre de chaque sous-paquet est virtuellement modifié pour la

transmission sur le canal radio. La redondance qui n'est pas propre à un paquet agit en tant que données de bourage, d'où le taux de transmission virtuel.

Mais ces données ne sont pas tout à fait de données de bourage, leur influence étant visible dans le processus de décodage. Donc, nous sommes penchés sur l'analyse des similitudes aux codes pilotes. Ces codes pilotes représentent une famille de codes qui utilisent des séquences connues pour améliorer le taux de confiance des probabilités dans le décodeur. Leur but est uniquement de rendre le décodage plus rapide et plus performant. Ce qui devient très intéressant dans les structures PPHTC et SPHTC, c'est que chacune des classes supérieures encodées se comporte comme un pilote pour les classes moins importantes. Il s'avère que les classes qui bénéficient pleinement des à priori turbo propres, sont corrigées plus rapidement, et accélèrent, en l'améliorant, le décodage des classes encodées à un niveau moins élevé. Cet aspect est particulièrement visible sur la deuxième classe dans le cas particulier de deux dimensions d'encodage.

Enfin, cette interdépendance des données encodées est soulignée par l'analyse mathématique des poids des deux codes, PPHTC et SPHTC. Cette analyse met en évidence la modification des poids propres des entrées et sorties des codes, qui peut engendrer une modification des performances. Effectivement, modifier les poids de mots codes influence particulièrement le décodeur. Les équations mathématiques pour l'encodage à deux niveaux mettent en évidence les deux comportements des deux classes de bits. La première classe, qui a été encodée par deux codes concaténés se comporte naturellement comme étant turbo encodée et turbo décodée. Ces résultats sont pourtant influencés par la présence des poids des mots codes de la deuxième classe, ce qui la différenciera d'un codage turbo classique. Par contre, la deuxième classe a été encodée par un code convolutionnel uniquement et il n'y aurait pas de raison qu'elle gagne à travers les itérations du décodage. Mais ce que nous permet de voir ces équations de poids c'est qu'elle n'a pas vraiment un comportement turbo, mais que les poids des mots codes ont amélioré le comportement du code convolutionnel. Les poids des mots codes de la première classe ont agi comme une redondance cachée qui a modifié les performances du décodage de la deuxième classe.

Les performances et les comportements des codes PPHTC et SPHTC sont mis en évidence et testés à l'aide de deux plateformes de tests différentes, ainsi que dans deux environnements de propagations différents. Une des plateformes est basée sur des éléments de nature aléatoire, tandis que la deuxième plateforme utilise des éléments du standard LTE. Les résultats des simulations par ordinateur sont donnés pour le canal statique AWGN, ainsi que dans un environnement dynamique de Rayleigh. Pour chaque code, deux scénarios différents sont utilisés, définis en fonction des tailles des classes en entrée.

Les codes sont évalués sur les deux plateformes pour mettre en évidence leur comportement itératif dans un premier temps. Ainsi, pour chacune des structures, nous soulignons l'importance des tailles des classes sur le comportement itératif et donc sur les gains de codage. Le comportement turbo est d'autant plus puissant que la taille de la classe une est importante. Également, les gains de la classe deux sont d'autant plus importants que sa taille propre est inférieure à la première classe. Ces courbes présentent bien l'influence des poids des mots codes en entrée et en sortie des codes. Les mots codes qui présentent le poids le plus important dictent les performances du décodeur. Si la classe une est beaucoup plus importante, l'influence des poids de la deuxième classe est minimale, et donc les performances approchent fortement celles d'un codage turbo classique. La deuxième classe, même si elle a été encodée par un seul code convolutionnel, gagne en performance de façon considérable. Ceci peut s'expliquer par le poids des mots codes en entrée de ce code convolutionnel, qui ne reçoit pas uniquement la classe deux, mais également la classe une. Donc, tout le poids de la classe une peut être également exploité dans le décodage de la classe deux. Dans le scénario contraire, où la classe deux est largement supérieure à la classe une, il devient évident d'observer le comportement contraire. Le gain de la classe deux devient inférieur au scénario précédent et approche considérablement celui d'un code convolutionnel. La classe une garde un gain turbo, mais qui devient moins important que le scénario précédent. Le ratio des poids des mots codes en entrée des codes a changé et donc le ratio des performances mêmes a changé.

Les propriétés des codes pilotes sont évaluées sur les deux plateformes également. Ainsi, nos attentes par rapport aux comportements des deux classes se vérifient parfaitement. Dans les deux scénarios, si la classe deux est utilisée en tant que pilote, et devient donc parfaitement connue par le décodeur, le résultat se traduit par une nette amélioration des performances de la classe une. Dans le cas contraire, où la première classe devient pilote,

la classe deux atteint en maximum deux itérations son état de décodage normal. C'est à dire, les performances de la classe deux ne sont pas améliorées, mais la convergence est seulement plus rapide. Ceci est normal si nous considérons la discussion sur les poids des mots codes et que cette deuxième classe ne fait que bénéficier du comportement amélioré de son code convolutionnel.

Pour une évaluation objective des résultats des codes PPHTC et SPHTC, nous les comparons par la suite à plusieurs codes de référence. Ces codes ont été choisis d'un côté par leur affiliation à la famille des turbo codes, ce qui nous permet de comparer les performances des deux classes à leur variantes turbo pures. D'un autre côté, nous avons choisi de mettre en référence deux codes convolutionnels aussi, pour leur comparaison directe aux performances UEP de la classe deux. Quelques mots sur la complexité de ces structures nous permettent de mettre en évidence leurs similitudes et différences en nombres d'opérations et de calcul.

Les comparaisons des performances des PPHTC et SPHTC montrent de très bons résultats. Les codes de références auxquels les comparaisons sont faites sont configurés aux mêmes taux de transmissions que les cas UEP. Chaque classe subit ainsi soit un codage UEP, soit un codage de référence. Notre approche est très pragmatique et permet d'évaluer les gains absolus du point de vue de l'ingénierie du système. Ce principe est basé sur la comparaison des performances des codes ayant la même trame en entrée et le même taux de transmission, ce qui équivaut à la même occupation spectrale.

Les deux classes encodées ensemble avec ces nouvelles structures UEP ont de très bonnes performances et leur comportement pourrait contenter les attentes des réseaux PMR. La première classe approche fortement les performances des turbo codes, pendant que la classe deux présente des gains importants par rapport aux codes convolutionnels et même par rapport aux codes turbo de taux de transmission équivalent. Les performances de la classe la plus protégée sont légèrement moins puissantes que si cette classe avait subi uniquement un codage turbo. Mais ceci n'est pas interprété comme un défaut dans le monde de la PMR, où la zone d'intérêt se situe au niveau des mauvais rapports signaux à bruits. Pour la reconstruction des signaux audio, la PMR privilégie les taux d'erreur d'environ 10^{-2} , et donc constater une réduction des performances à des taux d'erreur très bas, de l'ordre de 10^{-5} ne devient pas dérangeant. Au contraire, il s'avère que cette légère perte sur la première classe se traduit par des gains importants pour la deuxième classe, et ce dans la région d'intérêt, soit à 10^{-2} . Le même comportement se vérifie dans les deux environnements, en statique et en dynamique. Les courbes d'évaluation présentées en statique sont beaucoup plus marquées par les gains et montrent les gains théoriques maximaux qu'on peut atteindre. Les courbes en dynamique sont lissées par le manque de diversité de ce canal de transmission. Mais ces courbes montrent également des gains pour les deux classes. Le chapitre 3 nous permet ainsi de présenter et d'analyser de plusieurs perspectives les codes brevetés, PPHTC et SPHTC.

Compte tenu du grand nombre de résultats obtenus, nous avons inclus dans le chapitre 3 uniquement les résultats présentés en taux d'erreur bit et pour les scénarios à deux classes UEP seulement. Les résultats correspondants mesurés en taux d'erreur trame sont donnés dans les annexes. Egalement, nous avons inclus dans les annexes des résultats supplémentaires qui permettent de mettre en évidence le comportement des codes pour d'autres cas d'utilisation. Nous avons particulièrement souligné leur comportement pour trois classes UEP. Les hypothèses dégagées par l'analyse à deux dimensions sont parfaitement vérifiées pour le cas à trois dimensions. Les deux premières classes les plus protégées montrent des comportements turbo puissants, les performances de la deuxième classe se rapprochent fortement de celles de la première classe. La troisième classe, qui devient la classe la moins protégée, présente donc un gain considérable à travers les itérations de décodage.

Les annexes incluent quelques résultats significatifs pour les performances avec poinçonnage. Puisque dans le monde de la PMR, on utilise souvent des poinçonnages très puissants, nous montrons dans les annexes le comportement du PPHTC fortement poinçonné et évalué sur une plateforme LTE. Ce qui reste impressionnant avec ce code c'est qu'il arrive à donner du gain à la classe envoyée à taux 1 sur le canal. Ceci équivaut à dire que cette classe ne possède quasiment pas de redondance qui puisse être exploitée pour sa correction. Mais grâce à la structure UEP, c'est bien la redondance cachée qui est pleinement exploitée pour la correction d'erreurs.

Dans les annexes et toujours relatif aux codes PPHTC et SPHTC, nous fournissons une étude sur les limites théoriques des performances de décodage. Il s'agit d'une estimation théorique des performances du maximum de vraisemblance qui peuvent être calculées à l'aide des caractéristiques de poids des mots codes. Nous fournissons cette annexe en information complémentaire à l'étude des poids des codes. Mais compte tenu de la

complexité considérable de ce calcul théorique, nous montrons une évaluation faite sur des mots codes très courts. Les limites théoriques permettent de mettre en évidence les différences entre les performances de la classe une et celle de la classe deux, pour le cas particulier à deux dimensions. La classe une fait partie à travers ces limites des codes turbo. Quand à la classe deux, elle gagne légèrement en crédibilité turbo, mais se comporte comme un turbo qui a atteint son palier de taux d'erreur maximal plus tôt. Ou bien, ceci peut être interprété également comme un code convolutionnel supérieur, dont le comportement est amélioré à cause des mots codes de poids important en entrée.

Les codes proposés, sous la forme du PPHTC et du SPHTC, prouvent donc être des codes très performants, qui encodent les données à sensibilités différentes de façon progressive et hiérarchique. Leur puissance, ainsi que leur faiblesse, repose dans la redondance cachée qui est exploitée par le décodage itératif à travers les informations a priori. Ces codages peuvent s'avérer des outils intéressants pour la protection non uniforme des applications comme la parole et la vidéo.

Le travail du chapitre 4 se concentre sur l'analyse du comportement du codage parallèle dans certains cas d'utilisation spécifiques à la transmission de voix sur la PMR. Etant donnée l'importance des communications de voix sur les réseaux PMR, il est essentiel d'optimiser la transmission de la voix sur IP sur LTE. L'utilisation donc d'un codage performant à protection non uniforme permettrait d'envisager une meilleure utilisation du spectre radio pour une réception de bonne qualité par l'utilisateur. Dans ce chapitre, nous nous concentrons sur deux axes. Le premier axe permet de comprendre les mécanismes qui ont été envisagés pour la transmission de la voix sur IP dans le réseau LTE. Et le deuxième axe se concentre sur l'évaluation du PPHTC pour la transmission de la voix sur LTE. Notre but est de prouver que le PPHTC peut prétendre être un bon choix pour un codage canal de LTE, si LTE venait à être adopté pour l'évolution de la PMR. L'idée présentée dans ce chapitre a également été brevetée.

Nous commençons donc par l'analyse et la discussion sur l'architecture de transmission de la voix par paquet sur LTE. Cette architecture représente une évolution considérable du point de vue des communications de voix, puisque, jusqu'ici, on n'avait pas encore envisagé l'utilisation à grande échelle de la voix sur IP par les opérateurs mobiles. La nouveauté introduite par LTE est la communication IP de bout en bout. Mais les appels de voix ont des contraintes très strictes de temps réel, donc de délai de transmission des paquets, de perte de paquets et d'établissement de la communication. Ces paramètres sont fixés sur LTE à des limites bien définies, et sont associés à des tunnels configurés qui portent le nom de "bearer" ou porteurs. Ces bearers portent les paquets de voix à travers les couches protocolaires et radio, et assurent l'acheminement de ces paquets en respectant tous les paramètres de configuration de la qualité de service.

Mais ce qui ne semble pas particulièrement adapté sur LTE est l'association de ces paquets de voix aux différentes qualités de service. LTE définit donc le transfert d'un paquet IP sur un seul bearer avec des niveaux de protections bien définis. La technologie ne prévoit pas encore de moyens de transmission à protection non uniforme. Ce problème persiste depuis plusieurs générations de réseaux mobiles, où le concept UEP n'a pas été proprement optimisé. Il a été plutôt simulé avec les paramètres existants, technique appelé émulation d'UEP. Par exemple, dans le cas des deux classes UEP, la protection UEP est émulée en séparant le paquet de données dans deux sous-paquets, et ces deux sous-paquets sont transmis l'un indépendamment de l'autre. Mais contrairement à la transmission vidéo, où ce genre de solution peut être envisagée sans pertes considérables d'efficacité, cette solution n'est pas utilisable pour la transmission bas débit de la parole dans la PMR. L'étude théorique du chapitre 2 nous a montré que la transmission d'un paquet de voix sur le réseau LTE n'est pas efficace. De nouvelles solutions de transmissions de la voix à protection non-uniforme doivent être envisagées.

Nous proposons l'optimisation de la transmission de voix sur LTE en utilisant le concept de turbo codes à protection non-uniforme intégrée, le PPHTC. Ce code a été conçu pour s'adapter au réseau LTE et les tests nous ont montré que son utilisation avec des éléments constituants propres à LTE restait performante. La littérature scientifique prouve aussi que l'utilisation des codes turbo à protection non uniforme a déjà été envisagée par d'autres auteurs et pour d'autres réseaux. Pourtant, toutes les techniques UEP utilisent des schémas de poinçonnage ou d'émulation d'UEP. Le PPHTC proposerait une technique plus simple et plus efficace pour une protection UEP. Nous modélisons ainsi le système de transmission LTE, en remplaçant le code turbo propre à LTE par sa version PPHTC. Tout paquet en provenance des couches supérieures peut être encodé non

uniformément à l'aide du PPHTC. Inclure ce nouveau type de codage nécessiterait le minimum d'adaptation aux couches supérieures, où seulement la définition d'un mode de transmission à protection UEP intégré serait nécessaire.

Les performances du PPHTC pour les communications de voix sont évaluées sur une plateforme LTE, qui simule la couche physique de façon simplifiée. Les paquets de voix des couches supérieures sont multiplexés par groupes de trois, et leurs bits respectifs sont regroupés dans deux classes de sensibilités différentes. Les niveaux d'importance de ces bits sont prédéfinis par le constructeur. Pour une évaluation réaliste du système, les en-têtes supplémentaires introduites par les couches protocolaires sont pris en compte. Le paquet obtenu doit être transporté par un bloc de transport ou TBS, comme défini par le standard. L'allocation de ressources est faite en considérant les études du chapitre 2.

Les résultats du PPHTC sont comparés avec deux autres schémas de transmission de la voix sur LTE, constitués par l'émulation d'UEP et la transmission uniforme. Les deux références utilisent le standard LTE avec son code turbo propre, ainsi que son poinçonnage. Le même paquet de données en provenance des couches supérieures peut être transmis en utilisant un des trois schémas de transmission, appelés schémas de codage et modulation ou MCS. Le premier MCS à protection non uniforme intégrée (MCS UEP) est représenté par le regroupement du PPHTC avec le type de modulation. Le deuxième MCS propose l'émulation UEP, soit l'utilisation de deux MCS de taux de protection différents. Le paquet reçu est divisé en deux sous-paquets de sensibilités différentes. Chacun de ces deux sous-paquets est transmis sur le canal radio avec un MCS approprié, qui propose une protection uniforme pour le sous-paquet respectif. Et le troisième MCS regroupe le code LTE, PCCC, et le type de modulation, et représente le MCS à protection uniforme pour l'ensemble du paquet.

Pour une évaluation objective des performances, les résultats du PPHTC en MCS UEP sont comparés aux résultats des deux autres MCS à entrées-sorties équivalents. Chaque MCS ou groupe de MCS reçoit le même paquet en entrée, et va occuper la même quantité de ressources radio. Ainsi, tout gain peut être directement quantifié en niveau de qualité audio, pour des taux d'utilisation du spectre parfaitement équivalents.

Les performances du PPHTC par rapport aux références sont évaluées à l'aide des taux d'erreur trames, le taux d'erreur bit résiduel et la qualité de la parole en réception. Ainsi, le taux d'erreur trame nous donne des informations sur le nombre de trames correctes reçues. Ce dernier est un indicatif important surtout pour la première classe de bits. Ces bits sont essentiels pour la reconstruction correcte du signal et donc toute erreur sur l'ensemble de ces paquets peut être ressentie dans la qualité finale de la parole. C'est pour cela que la première classe de bits est également protégée par un code détecteur d'erreur ou CRC. Le rôle du CRC est de détecter les trames fausses par rapport à la première classe de bits et de les rejeter. Le décodeur source de parole va remplacer ces trames détectées fausses par des répétitions et des trames de silence pour empêcher la reconstruction d'un son fortement bruité et désagréable. Le taux d'erreur bit résiduel mesure le nombre de bits erronés qui sont laissés passer au décodeur source de parole. Ce taux résiduel mesure surtout l'influence des bits de la deuxième classe sur la qualité de la parole. Et enfin, ces deux mesures de la couche physique sont corrélées à la qualité de parole, mesurée par des outils spécifiques.

La qualité de parole obtenue est moyennée sur un nombre de 60 fichiers de voix d'hommes et femmes, qui sont transmis pour chacun des cas MCS étudié. Sur les 60 fichiers, quatre langues européennes sont présentes: anglais, français, allemand et espagnol. Un nombre exhaustif de trames a été utilisé en simulation numérique pour pouvoir évaluer la qualité audio sur 600 secondes de signal audio. La qualité audio est évaluée à deux niveaux. Le premier niveau mesure l'influence des erreurs du canal de transmission radio uniquement sur le signal de parole. Le deuxième niveau est normalisé, soit il donne la qualité de voix absolue perçue par rapport aux fichiers d'origine. Cette dernière méthode tient compte des erreurs du canal de transmission radio, ainsi que des quantifications faites par le décodeur de voix bas-débit.

Tous les résultats sont donnés dans un environnement statique et dynamique. Ainsi, nous pouvons estimer les performances théoriques atteignables, ainsi que les performances réelles mesurées dans un environnement de propagation fortement perturbé. Les courbes en taux d'erreur nous offrent une estimation quantitative des résultats bruts du codage canal et montrent un compromis entre le niveau de protection de la première classe et celui de la deuxième classe. Mais la mesure de la qualité de la parole donne une mesure qualitative de l'impact

de ces performances sur l'utilisateur final. Le PPHTC présente de très bons résultats et s'impose comme une nouvelle approche intéressante et performante.

Enfin, nous concluons et proposons les perspectives d'évolution dans le chapitre 5. Les codes proposés, PPHTC et SPHTC, représentent deux approches différentes et performantes pour la transmission plus efficace des données applicatives. La protection non-uniforme des données permet la corrélation des paramètres radio aux contraintes des encodeurs sources. Ainsi, les ressources radio sont exploitées pour un rendu optimal de la qualité au niveau de l'utilisateur final.

Les perspectives d'évolutions des deux codes sont riches. Etant donné leur flexibilité et leur adaptabilité, le PPHTC et le SPHTC peuvent bénéficier d'optimisations portant sur différentes techniques de codage, entrelacement et poinçonnage. Chacune de ces techniques peut considérablement changer les performances des codes et peut engendrer des études conséquentes. Des approches d'optimisation UEP peuvent être envisagées également à travers les éléments constitutifs, et pour différents types d'applications.

Mais à travers leurs structures, ces codes peuvent être utilisés également dans d'autres contextes. Au niveau de la couche physique, les estimations du décodeur pourraient être améliorées à l'aide des informations source. Des solutions d'optimisations propres à la couche radio peuvent être envisagées aussi. En exploitant les différentes branches des encodeurs, le système pourrait proposer de nouvelles techniques de transmission répétitive ou HARQ. L'égalisation de canal peut bénéficier d'améliorations, par les corrélations des informations du décodeur avec celles de l'égaliseur canal.

Du point de vue de la technologie LTE et son évolution, de nombreuses pistes d'optimisations restent possibles pour le PPHTC et la transmission UEP. Les paramètres de codage canal peuvent être pris en compte par le scheduler, pour une meilleure adaptation aux transmissions voix et vidéo. Egalement, des optimisations pour les couches protocolaires sont à envisager sur LTE, étant donné leur inefficacité pour la transmission de la voix. Quand aux allocations radio, les propositions du standard LTE restent non optimales pour la PMR.

Même si LTE est technologiquement très avancé comparé aux solutions PMR existantes, son adoption pour la sécurité publique va être conditionnée par son efficacité dans des scénarios critiques. Quelques modifications consistantes seront néanmoins nécessaires pour l'amélioration de LTE et sa transformation pour une utilisation optimale dans les communications de missions critiques.

Acknowledgments

I thank my teachers, Professors Hang Nguyen and Djamel Zeglache, for having given me the opportunity of pursuing my education with this PhD. Also, I thank them for their valuable advices regarding the academic research approach, and for the welcome in the research team of SAMOVAR laboratory.

I also address my thanks to the many EADS Cassidian engineers and experts, who have often helped me and provided important technical insights. I thank Laurent for his supervising, for his technical overview, for his many advices regarding radio transmission, LTE architecture, Matlab problems. Thank you to Christophe who has often corrected the channel coding aspects. Thank you to Philippe also, who has closely followed the progress of this thesis. Thank you to Laurent for his remarks on audio quality analysis. I also thank Antte for the constructive discussions on the LTE architecture. Thank you to Olivier for his encouragements. I thank the entire team for their warm welcome and their good humor. Also, thank you to the EADS Cassidian engineers and experts, Christophe, Laurent, Arthur, Eric, Gerard, who have provided essential informations regarding voice and video characteristics, as well as 3GPP standards and their respective evolutions.

I would also like to thank Professor Didier Le Ruyet, from the CNAM Paris. Thank you for your advices et courses regarding turbo codes and their theoretical characteristics.

I thank my friends for their encouraging thoughts, and useful advices. I would particularly like to thank my friend Iulia, who, with her comprehension and Romanian and Austrian visions of the doctorate, has reminded me many times of the importance of the PhD at the international level. Also, I would like to salute some of the winners of the Georges Besse Foundation scholarship, Andreea and Ghiles, for their useful advices and LaTeX archives, which have proved very helpful for the dissertation's writing.

And, of course, a considerable thank you to my family, for the very important psychological support. I would like to thank my parents and grand-parents for their considerable efforts to have me pursue my studies in France. Thank you for reminding me what a benefit and an incredible opportunity represents an over broad education. I also thank my brother for his encouragements and optimism. And thank you to my dear Davy for his patience, his comprehension, his joy of life and many advices, which have often helped me to overcome the most difficult moments during these past three years of doctorate.

Thank you all for your help, your encouragements and many advices!

Abstract

The public safety world is preparing for the broadband evolution. Existent Private Mobile Radio (PMR) technologies can not compete with the new generation trend. While the Long Term Evolution (LTE) standard has been generally adopted as the next public radio evolution, questions regarding its possible use with critical communications as well have arisen.

In this dissertation, we present a preliminary study and evaluation of the LTE candidate performances in a public safety context. Not only we point out several key points that must be addressed, but we also propose an evolution of the air interface channel codec. This new proposition is based on existent standard technology and refines the LTE physical layer data protection from a PMR perspective.

We begin by introducing the context of public safety in chapter 1, as well as the definition of mission critical communications. Most important characteristics of PMR are highlighted, with references to typical use cases.

Chapter 2 proposes an objective evaluation of the PMR broadband perspectives. We provide a short introduction to PMR technologies and their main characteristics in terms of transmission architecture. The broadband sphere of technologies is then discussed, reminding WIMAX as a possible niche technology. However, LTE has been chosen as the preferred candidate. We have focused our analysis on the LTE Release 9 stack architecture and its physical layer. Typical PMR constraints are included, as the 1.4 MHz frequency bandwidth, deployed in the 450 MHz transmission frequency spectrum. Low rate voice and video communications are supposed, and IP encapsulation is considered. The air interface allocation parameters are also introduced for an evaluation of the air overhead and available radio resources. We perform a realistic evaluation of the LTE voice and video capacity, in both downlink and uplink. The LTE voice spectral efficiency is calculated, for an objective evaluation of its performances compared with existent PMR technologies. We thus identify several key aspects of LTE that should be addressed in a mission critical environment.

One of these key aspects is the air interface proposed channel protection, i.e. the channel codec. LTE proposes an uniform protection through the powerful turbo codes. But one particular aspect in optimizing system performance is considering the multi-layer analysis. Low rate voice and video applications have specific unequal error protection properties, that exploited at the physical layer, would certainly enhance the system efficiency. Thus, we concentrate in chapter 3 on the design of an unequal error protection (UEP) turbo code. Associating unequal error protection properties with highly efficient turbo codes can prove very performing. Turbo codes have been widely discussed in scientific literature and adopted in many mobile standards. We propose their evolution through the embedding of UEP concepts into their parallel and serial structures, with the parallel progressive hierarchical turbo codes (PPHTC) and the serial progressive hierarchical turbo codes (SPHTC). The ideas behind the parallel and serial turbo structures have been patented. In this chapter, we describe in detail their architectures for the particular case of two dimensions encoding/decoding, as well as for their generalized n -dimensions encoding/decoding. We also highlight a particular property in the iterative turbo decoding through mathematical development. The codes iterative behaviors and properties are analyzed theoretically, as well as through computer simulations. Their performances are evaluated on two different platforms, based on random and LTE elements. Also, the results are given for static and dynamic environments. Their UEP behavior is particularly interesting compared with benchmark turbo and convolutional codes.

Chapter 4 work is concentrating on analyzing the parallel code's behavior in certain use cases specific to PMR voice transmission. The idea presented in this chapter has been also patented. Thus, the PPHTC is inserted in the LTE architecture, through the proposal of a new perspective modulation and coding scheme (MCS).

This new approach proposes the use of an embedded UEP MCS, that would correlate PPHTC and modulation performances to the end-user perceived voice quality. The voice transmission UEP MCS's performances are compared with two LTE benchmarks. Results are presented in terms of physical layer error rates, as well as corresponding measured voice quality. The code utility and advantages are highlighted and provide interesting development perspectives.

Finally, we conclude and propose evolution perspectives in chapter 5. Even though LTE is technologically very advanced compared to existent PMR solutions, its adoption for the public safety will be conditioned by its effectiveness in critical scenarios. Some consistent modifications will, nevertheless, be necessary for the improvement of LTE and its transformation for optimal use in mission critical communications.

Table of Contents

Remerciements	vii
Résumé Court	ix
Résumé Long	xi
Acknowledgments	xxiii
Abstract	xxv
Table of Contents	xxvii
List of Acronyms	xxxi
List of Figures	xxxv
List of Tables	xxxix
1 Introduction	1
1.1 Towards the Professional Broadband Era	1
1.2 Mission Critical Communications over LTE	2
2 PMR Broadband Perspectives	5
2.1 Introduction	5
2.2 PMR Key Issues	6
2.2.1 Voice Communications Constraints	7
2.2.2 Data and Video Transmissions Issues	7
2.3 2G Narrowband Digital PMR	8
2.3.1 APCO25	9
2.3.2 TETRAPOL	10
2.3.3 TETRA	10
2.4 3G Wideband Evolution: TEDS	11
2.5 Broadband Perspectives	12
2.6 LTE and PMR Convergence Analysis	13
2.6.1 LTE Technical Overview	13
2.6.2 Voice over LTE: a PMR use case	16
2.6.3 Video over LTE: PMR Use Cases	18
2.7 Theoretical Analysis and Results	20
2.7.1 LTE Voice Capacity Evaluation	20
2.7.2 LTE Video Capacity Evaluation	22

2.7.3	LTE Voice Spectral Efficiency	24
2.8	Conclusion	28
3	Progressive Hierarchical Turbo Codes	33
3.1	Turbo Codes & UEP Enhancements	33
3.2	PPHTC & SPHTC: Enabling UEP Turbo Adaptation	38
3.2.1	2-D Architecture Design	38
3.2.1.1	UEP Encoder Description	38
3.2.1.2	UEP Decoder Description	41
3.2.1.3	UEP MAP Decoding Analysis	42
3.2.1.4	BCJR Algorithm UEP Characteristics	45
3.2.1.5	Log Likelihood UEP Adaptation	48
3.2.2	n -D Extended UEP Architecture	49
3.2.2.1	UEP Turbo Multiple Encoding	50
3.2.2.2	UEP Multiple Decoding Description	51
3.2.2.3	n -D Progressive UEP MAP	55
3.2.2.4	BCJR Algorithm n -D Extension	56
3.2.2.5	Log Likelihood Extended Interpretation	56
3.3	Code Properties Analysis	57
3.3.1	Factor Graph	57
3.3.2	Pilot Insertion Codes	60
3.3.3	Virtual Code Rate	61
3.3.4	Weight Characteristics	61
3.4	Performance Analysis: Methods and Results	66
3.4.1	Evaluation Platforms & Benchmarks Description	66
3.4.2	Simulation Parameters and Complexity Issues	69
3.4.3	Code Performance Results	72
3.4.3.1	UEP Turbo Behavior	72
3.4.3.2	Pilot insertion codes	80
3.4.3.3	AWGN Channel Performance Comparison	84
3.4.3.4	Rayleigh Channel Results	89
3.5	Conclusion	94
4	PMR Evolution: Design of Radio Efficient Voice over LTE	99
4.1	Introduction	99
4.2	Voice Services over Packet Switched Network	100
4.2.1	Packet Bearer Architecture	100
4.2.2	Design of Embedded UEP MCS	102
4.3	LTE Evaluation Platform	104
4.4	Results and Comments	106
4.5	Conclusion	111
5	Conclusions and Perspectives	115
A	List of Publications	119
B	Puncturing Adaptation	121
B.1	Puncturing Mechanisms	121
B.2	Illustrative Results	121

C The Tangential Sphere Bound	125
D Complementary Results	131
D.1 2-D Results	131
D.1.1 UEP Turbo behavior: AWGN FER Performances	131
D.1.2 UEP Turbo behavior: HT200 FER Performances	133
D.1.3 HT200 Pilot Code Performances	136
D.1.4 AWGN FER Performance Comparison	138
D.1.5 HT200 FER Performance Comparison	140
D.2 3-D Performances	142

List of Acronyms

1G	First Generation Technology
2G	Second Generation Technology
3G	Third Generation Technology
3GPP	Third Generation Partnership Project
4G	Fourth Generation Technology
$\Pi/4$ DQPSK	$\Pi/4$ Offset Differential Quaternary Phase Shift Keying
ACELP	Algebraic Code Excited Linear Prediction
AMBE	Advanced MultiBand Excitation
AMR	Adaptive Multi-Rate
APCO25	Association of Public Safety Communications Officials' Project 25
APCO25 φ 1	Association of Public Safety Communications Officials' Project 25 Phase 1
APCO25 φ 2	Association of Public Safety Communications Officials' Project 25 Phase 2
APP	A Posteriori Probability
ARP	Allocation Retention Priority
ARQ	Automatic Repeat Request
AWGN	Additive White Gaussian Noise
BCJR	Bahl-Cocke-Jelinek-Raviv algorithm
BER	Bit Error Rates
BW	Bandwidth
C4FM	Continuous Four Level Frequency Modulation
CC	Convolutional Codes
CDMA	Code Division Multiple Access
CP	Cyclic Prefix
CQI	Channel Quality Information
CRC	Cyclic Redundancy Checked
CS	Circuit Switched
DiffServ	Differentiated Service
DL	Downlink
DMR	Digital Mobile Radio
DMRS	Demodulation Reference Signal
EADS	European Aeronautic Defence and Space
EDGE	Enhanced Data for GSM Evolution
EEP	Equal Error Protection
EF	Expedited Forwarding
EGPRS	Enhanced GPRS
EPC	Evolved Packet Core
EPS	Evolved Packet System
ETSI	European Telecommunications Standards Institute
FCC	Chairman of the Federal Communications Commission
FEC	Forward Error Correction Coding
FER	Frame Error Rates
FDD	Frequency Division Duplexing

FDMA	Frequency Division Multiple Access
GBR	Guaranteed Bit Rate
GERAN	GSM Evolution Radio Access Network
GF	Galois Field
GMSK	Gaussian Minimum Shift Keying
GPRS	General Packet Radio Service
GSM	Global System for Mobile Communications
HARQ	Hybrid ARQ
H-CPM	Harmonized Continuous Phase Modulation
H-DQPSK	Harmonized Differential Quadrature Phase Shift Keyed Modulation
H-FDD	Half-duplex Frequency Division Duplex
HT	Hilly Terrain
ID	Identity
IEEE	Institute of Electrical and Electronics Engineers
IMBE	Improved MultiBand Excitation
IMT	International Mobile Telecommunications
IMS	IP Multimedia Sub-system
IntServ	Integrated Services
ITU	International Telecommunications Union
IP	Internet Protocol
LDPC	Low-Density Parity-Check
LLR	Log Likelihood Ratios
LTE	Long Term Evolution
MAC	Medium Access Layer
MAP	Maximum A Posteriori
MCS	Modulation and Coding Scheme
MIMO	Multiple-Input Multiple-Output
ML	Maximum Likelihood
MMTel	IMS Telephony
NTIA	National Telecommunications and Information Administration
OFDM	Orthogonal Frequency Division Multiplexing
P25	Project 25
PAMR	Public Access Mobile Radio
PAPR	Peak Average Power Ratio
PCCC	Parallel Concatenated Convolutional Codes
PDCCH	Physical Downlink Control Channel
PDCP	Packet Data Convergence Protocol
PDSCH	Physical Downlink Shared Channel
PDN-ID	Packet Data Network Identification
PDU	Packet Data Unit
PESQ	Perceptual Evaluation of Speech Quality
PMI	Precoding Matrix Indicator
PMR	Private/Professional Mobile Radio
PPHTC	Parallel Progressive Hierarchical Turbo Codes
PRBs	Physical Resource Blocks
PSWAC	Public Safety Wireless Advisory Committee
PUCCH	Physical Uplink Control Channel
PUSCH	Physical Uplink Shared Channel
QAM	Quadrature Amplitude Modulation
QCI	QoS Class Identifier
QoS	Quality of Service
QPP	Quadratic Permutation Polynomial

QPSK	Quadrature Phase Shift Keying
RACH	Random Access channel
RE	Resource Element
RI	Rank Indicator
RLC	Radio Link Control
RM	Rate Matching
ROHC	Robust Header Compression
RPCELP	Regular Pulse Code-Excited Linear Prediction
RSC	Recursive Systematic Convolutional Code
RTP	Real-time Transport Protocol
SAFECOM	Program document released by the USA Department of Homeland Security in 2006
SCCC	Serial Concatenated Convolutional Codes
SC-FDMA	Single Carrier FDMA
SDF	Service Data Flows
SDU	Service Data Unit
SMS	Short Messaging System
SNDCP	Sub-Network Dependent Convergence Protocol
SPHTC	Serial Progressive Hierarchical Turbo Codes
SRVCC	IMS telephony with handover to CS domain
SVC	Scalable Video Coder
TBS	Transport Block Sizes
TCP	Transport Control Protocol
TDMA	Time Division Multiple Access
TEDS	TETRA Enhanced Data System
TETRA	Terrestrial Trunked Radio
TETRAPOL	Proprietary solution of the EADS company
TIA	Telecommunications Industry Association
TTI	Time Transmission Interval
UDP	User Datagram Protocol
UE	User Element
UEP	Unequal Error Protection
UHF	Ultra High frequencies
UL	Uplink
UM	Unacknowledged Mode
USA	United States of America
VHF	Very High Frequencies
VoLGA	Voice over LTE Generic Access
WIMAX	Worldwide Interoperability for Microwave Access

List of Figures

1.1	PMR networks' market position.	2
2.1	Circuit-switched like voice transmission mechanisms over PMR.	9
2.2	LTE transmission system model for voice and video packets.	14
2.3	LTE DL radio frame configuration (1 ms spanning 1 PRB).	16
2.4	LTE UL radio frame configuration (1 ms spanning the allocated bandwidth).	16
3.1	Transmission system for PPHTC $n = 2$	39
3.2	Transmission system for SPHTC $n = 2$	40
3.3	General form for the PPHTC encoder.	50
3.4	General form for the SPHTC encoder.	51
3.5	General form for the PPHTC decoder.	52
3.6	General form for the SPHTC decoder.	54
3.7	PPHTC factor graph representation.	58
3.8	SPHTC factor graph representation.	59
3.9	The state diagram for the 8 state RSC.	63
3.10	Input output weight representations for PPHTC.	65
3.11	Input output weight representations for SPHTC.	66
3.12	Simulation platform.	67
3.13	AWGN $PPHTC^{(1)}$ turbo iterative behavior, LTE platform.	73
3.14	AWGN $PPHTC^{(1)}$ turbo iterative behavior, random platform.	73
3.15	HT200 $PPHTC^{(1)}$ turbo iterative behavior, LTE platform.	74
3.16	HT200 $PPHTC^{(1)}$ turbo iterative behavior, random platform.	74
3.17	AWGN $PPHTC^{(2)}$ turbo iterative behavior, LTE platform.	75
3.18	AWGN $PPHTC^{(2)}$ turbo iterative behavior, random platform.	75
3.19	HT200 $PPHTC^{(2)}$ turbo iterative behavior, LTE platform.	76
3.20	HT200 $PPHTC^{(2)}$ turbo iterative behavior, random platform.	76
3.21	AWGN $SPHTC^{(1)}$ turbo iterative behavior, LTE platform.	77
3.22	AWGN $SPHTC^{(1)}$ turbo iterative behavior, random platform.	77
3.23	HT200 $SPHTC^{(1)}$ turbo iterative behavior, LTE platform.	78
3.24	HT200 $SPHTC^{(1)}$ turbo iterative behavior, random platform.	78
3.25	AWGN $SPHTC^{(2)}$ turbo iterative behavior, LTE platform.	79
3.26	AWGN $SPHTC^{(2)}$ turbo iterative behavior, random platform.	79
3.27	HT200 $SPHTC^{(2)}$ turbo iterative behavior, LTE platform.	80
3.28	HT200 $SPHTC^{(2)}$ turbo iterative behavior, random platform.	80
3.29	AWGN $PPHTC^{(1)}$ pilot insertion behavior, LTE platform.	81
3.30	AWGN $PPHTC^{(1)}$ pilot insertion behavior, random platform.	81
3.31	AWGN $PPHTC^{(2)}$ pilot insertion behavior, LTE platform.	82

3.32	AWGN $PPHTC^{(2)}$ pilot insertion behavior, random platform.	82
3.33	AWGN $SPHTC^{(1)}$ pilot insertion behavior, LTE platform.	83
3.34	AWGN $SPHTC^{(1)}$ pilot insertion behavior, random platform.	83
3.35	AWGN $SPHTC^{(2)}$ pilot insertion behavior, LTE platform.	84
3.36	AWGN $SPHTC^{(2)}$ pilot insertion behavior, random platform.	84
3.37	AWGN $PPHTC^{(1)}$ turbo performances comparison, LTE platform.	85
3.38	AWGN $PPHTC^{(1)}$ turbo performances comparison, random platform.	85
3.39	AWGN $PPHTC^{(2)}$ turbo performances comparison, LTE platform.	86
3.40	AWGN $PPHTC^{(2)}$ turbo performances comparison, random platform.	86
3.41	AWGN $SPHTC^{(1)}$ turbo performances comparison, LTE platform.	88
3.42	AWGN $SPHTC^{(1)}$ turbo performances comparison, random platform.	88
3.43	AWGN $SPHTC^{(2)}$ turbo performances comparison, LTE platform.	89
3.44	AWGN $SPHTC^{(2)}$ turbo performances comparison, random platform.	89
3.45	HT200 $PPHTC^{(1)}$ turbo performances comparison, LTE platform.	90
3.46	HT200 $PPHTC^{(1)}$ turbo performances comparison, random platform.	90
3.47	HT200 $PPHTC^{(2)}$ turbo performances comparison, LTE platform	91
3.48	HT200 $PPHTC^{(2)}$ turbo performances comparison, random platform.	91
3.49	HT200 $SPHTC^{(1)}$ turbo performances comparison, LTE platform.	92
3.50	HT200 $SPHTC^{(1)}$ turbo performances comparison, random platform.	92
3.51	HT200 $SPHTC^{(2)}$ turbo performances comparison, LTE platform.	93
3.52	HT200 $SPHTC^{(2)}$ turbo performances comparison, random platform.	93
4.1	EPC bearer architecture.	102
4.2	UEP embedded MCS.	104
4.3	Emulated UEP simulated MCS.	105
4.4	EEP simulated MCS.	105
4.5	Average frame error rate (FER) for the AWGN transmission (for both physical layer classes - PLC).	108
4.6	Average residual bit error rate (RBER) for the AWGN channel transmission (for the physical layer class 2 only - PLC2).	108
4.7	Average frame error rate (FER) for the HT200 transmission (for both physical layer classes - PLC).	109
4.8	Average residual bit error rate (RBER) for the HT200 channel transmission (for the physical layer class 2 only - PLC2).	109
4.9	Average PESQ for the AWGN transmission, estimated considering radio distortions only, and both radio and speech reconstruction distortions.	110
4.10	Average PESQ for the HT200 transmission, estimated considering radio distortions only, and both radio and speech reconstruction distortions.	110
B.1	$PPHTC$ turbo iterative behavior without puncturing, $r_{A_1} = 1/3$ and $r_{A_2} = 1/2$ - average BER, LTE platform	122
B.2	Punctured $PPHTC$ turbo iterative behavior, $r_{A_1} = 1/2$ and $r_{A_2} = 1$ - average BER, LTE platform	122
B.3	$PPHTC$ turbo iterative behavior, $r_{A_1} = 2/3$ and $r_{A_2} = 1$ - average BER, LTE platform	122
C.1	Comparison of the bit error probability theoretical upper bound for theoretical ML decoding with $PPHTC$ simulations results for iterative decoding, random platform.	127
C.2	Comparison of the bit error probability theoretical upper bound for ML decoding with $SPHTC$ simulations results for iterative decoding, random platform.	127

D.1	AWGN $PPHTC^{(1)}$ turbo iterative behavior - average FER, LTE platform	131
D.2	AWGN $PPHTC^{(1)}$ turbo iterative behavior - average FER, random platform	131
D.3	AWGN $PPHTC^{(2)}$ turbo iterative behavior - average FER, LTE platform	132
D.4	AWGN $PPHTC^{(2)}$ turbo iterative behavior - average FER, random platform	132
D.5	AWGN $SPHTC^{(1)}$ turbo iterative behavior - average FER, LTE platform	132
D.6	AWGN $SPHTC^{(1)}$ turbo iterative behavior - average FER, random platform	132
D.7	AWGN $SPHTC^{(2)}$ turbo iterative behavior - average FER, LTE platform	133
D.8	AWGN $SPHTC^{(2)}$ turbo iterative behavior - average FER, LTE platform	133
D.9	HT200 $PPHTC^{(1)}$ turbo iterative behavior - average FER, LTE platform.	133
D.10	HT200 $PPHTC^{(1)}$ turbo iterative behavior - average FER, random platform.	134
D.11	HT200 $PPHTC^{(2)}$ turbo iterative behavior - average FER, LTE platform.	134
D.12	HT200 $PPHTC^{(2)}$ turbo iterative behavior - average FER, random platform.	134
D.13	HT200 $SPHTC^{(1)}$ turbo iterative behavior - average FER, LTE platform.	134
D.14	HT200 $SPHTC^{(1)}$ turbo iterative behavior - average FER, random platform.	135
D.15	HT200 $SPHTC^{(2)}$ turbo iterative behavior - average FER, LTE platform.	135
D.16	HT200 $SPHTC^{(2)}$ turbo iterative behavior - average FER, random platform.	135
D.17	HT200 $PPHTC^{(1)}$ pilot insertion behavior, LTE platform.	136
D.18	HT200 $PPHTC^{(1)}$ pilot insertion behavior, random platform.	136
D.19	HT200 $PPHTC^{(2)}$ pilot insertion behavior, LTE platform.	136
D.20	HT200 $PPHTC^{(2)}$ pilot insertion behavior, random platform.	137
D.21	HT200 $SPHTC^{(1)}$ pilot insertion behavior, LTE platform.	137
D.22	HT200 $SPHTC^{(1)}$ pilot insertion behavior, random platform.	137
D.23	HT200 $SPHTC^{(2)}$ pilot insertion behavior, LTE platform.	137
D.24	HT200 $SPHTC^{(2)}$ pilot insertion behavior, random platform.	138
D.25	AWGN $PPHTC^{(1)}$ turbo performances comparison - average FER, LTE platform.	138
D.26	AWGN $PPHTC^{(1)}$ turbo performances comparison - average FER, random platform.	138
D.27	AWGN $PPHTC^{(2)}$ turbo performances comparison - average FER, LTE platform.	139
D.28	AWGN $PPHTC^{(2)}$ turbo performances comparison - average FER, random platform.	139
D.29	AWGN $SPHTC^{(1)}$ turbo performances comparison - average FER, LTE platform.	139
D.30	AWGN $SPHTC^{(1)}$ turbo performances comparison - average FER, random platform.	139
D.31	AWGN $SPHTC^{(2)}$ turbo performances comparison - average FER, LTE platform.	140
D.32	AWGN $SPHTC^{(2)}$ turbo performances comparison - average FER, random platform.	140
D.33	$PPHTC^{(1)}$ turbo performances comparison - average FER, LTE platform, HT200.	140
D.34	$PPHTC^{(1)}$ turbo performances comparison - average FER, random platform, HT200.	141
D.35	$PPHTC^{(2)}$ turbo performances comparison - average FER, LTE platform, HT200.	141
D.36	$PPHTC^{(2)}$ turbo performances comparison - average FER, random platform, HT200.	141
D.37	$SPHTC^{(1)}$ turbo performances comparison - average FER, LTE platform, HT200.	141
D.38	$SPHTC^{(1)}$ turbo performances comparison - average FER, random platform, HT200.	142
D.39	$SPHTC^{(2)}$ turbo performances comparison - average FER, LTE platform, HT200.	142
D.40	$SPHTC^{(2)}$ turbo performances comparison - average FER, random platform, HT200.	142
D.41	AWGN $PPHTC^{(n=3)}$ convergence behavior $A_1 > A_2 > A_3$ - average BER, random platform.	143
D.42	AWGN $PPHTC^{(n=3)}$ convergence behavior $A_1 < A_2 < A_3$ - average BER, random platform.	143
D.43	HT200 $PPHTC^{(n=3)}$ convergence behavior $A_1 > A_2 > A_3$ - average BER, random platform.	143
D.44	HT200 $PPHTC^{(n=3)}$ convergence behavior $A_1 < A_2 < A_3$ - average BER, random platform.	143
D.45	AWGN $SPHTC^{(n=3)}$ convergence behavior $A_1 > A_2 > A_3$ - average BER, random platform.	144
D.46	AWGN $SPHTC^{(n=3)}$ convergence behavior $A_1 < A_2 < A_3$ - average BER, random platform.	144
D.47	HT200 $SPHTC^{(n=3)}$ convergence behavior $A_1 > A_2 > A_3$ - average BER, random platform.	144

D.48 HT200 $SPHTC^{(n=3)}$ convergence behavior $A_1 < A_2 < A_3$ - average BER, random platform. 144

List of Tables

2.1	LTE PMR voice capacity in DL and UL.	21
2.2	LTE PMR video capacity in DL and UL.	23
2.3	LTE spectral efficiency comparison with PMR and GSM.	26
3.1	UEP scenarios code parameters & respective complexities.	71
4.1	QCI values for voice transmission.	101
4.2	LTE simulation platform parameters.	107

Chapter 1

Introduction

1.1 Towards the Professional Broadband Era

”In times of emergencies, the public looks to government, particularly their Public Safety officials, to act swiftly and correctly, and do the things which must be done to save lives, help the injured, and restore order. Most disasters occur without warning, but people still expect a rapid and flawless response on the part of government. There is no room for error. Whether a vehicle accident, crime, plane crash, special event, or any other Public Safety activity, one of the major components of responding to and mitigating a disaster is wireless communications. These wireless communications systems are critical to Public Safety agencies’ ability to protect lives and property, and the welfare of Public Safety officials.”

This statement comes from the highly regarded Public Safety Wireless Advisory Committee (PSWAC) Final Report, presented to the Chairman of the Federal Communications Commission (FCC) and the Administrator of the National Telecommunications and Information Administration (NTIA) in September 1996. It highlights very well the essential role that wireless communications can play in times of emergencies, or what one might call public safety.

The private or professional mobile radio, or shortly called PMR, address the public safety requirements and not only. These standardized technologies describe radio communications systems that can be used in both public safety sectors, and for business and industry professionals (petrochemicals, transport and utilities). The market position of PMR technologies is presented in Fig. 1.1.

But PMR technologies being deployed nowadays are still based on standards of over ten years old. On the contrary, in the public field, radio products have evolved rapidly in recent years with the introduction of broadband technologies. An important gap has been created between the PMR proposed solutions and those of public operators. Thus, the public safety industry has reached a crossroads where the future of their own products is uncertain and must be considered.

In consequence, industry contributors as well as standardization organisms have started questioning themselves on the next decade evolutions. It seems rather obvious that future products must, at least, be able to provide what users consider as ”normal” services, i.e. broadband services. Several solutions have been envisaged:

- a new PMR standard, whose characteristics would place it in the family of broadband technology; however, creating a new standard is particularly cumbersome, expensive and time consuming;
- an evolved PMR standard, based on existent technologies; nevertheless, there are currently several versions of PMR technologies, from which some already propose several improved versions; upgrading to broadband an existent standard would engender considerable modifications, would also be time consuming, and would naturally privilege one of the existent technologies;
- choose an existent broadband technology, and perform minor changes to render it public safety operational.

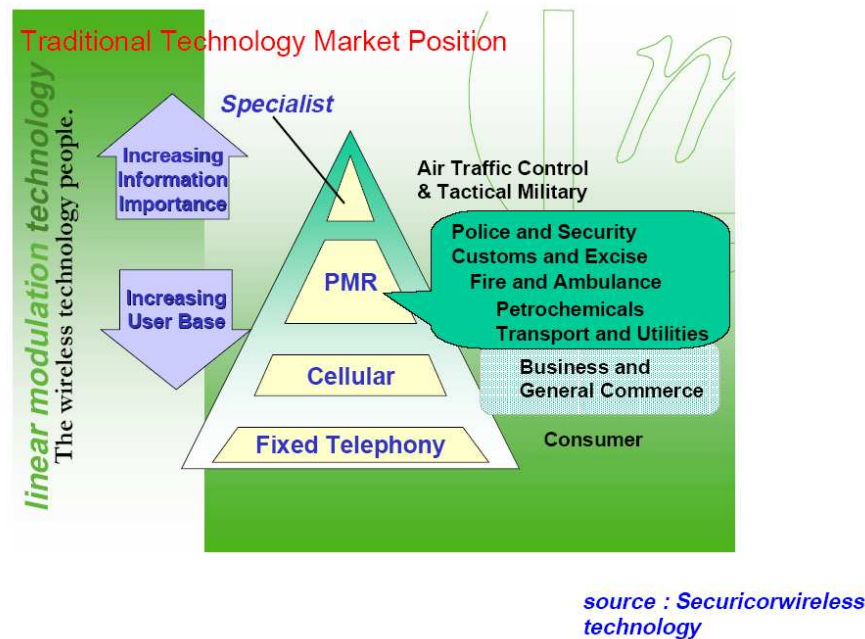


Figure 1.1. PMR networks' market position.

As the last option seems to be the cheapest and least time consuming, it is only obvious that industry contributors concentrated their efforts on the subject, as did Cassidian, part of the European Aeronautic Defence and Space Company (EADS) group. The work presented in this dissertation is part of the preliminary studies meant to contribute at the evolutions of PMR. We have focused on one broadband candidate: the Long Term Evolution (LTE), the Third Generation Partnership Project (3GPP) proposed standard, that seems to have been unanimously adopted by public operators in Europe and the United States.

1.2 Mission Critical Communications over LTE

LTE has been introduced by the 3GPP as a future milestone of incoming broadband technologies. Even though the mass-media often refers to LTE as the fourth generation (4G) radio standard, LTE is actually still a part of the third generation (3G) radio, with its Release 9. And it is LTE Advanced, starting with Release 10, that is considered a real 4G evolution.

However, the 3GPP proposed LTE standard is not mission critical. Its use with the PMR industry implies refinements of certain characteristics in order to address key requirements. The technology must be able to provide efficient voice and video communications. But using internet protocol (IP) and proposed physical layer technologies are not convincing for PMR specialists, who contest their possible misconception for more efficient radio technologies. IP packets seem particularly cumbersome for radio transmission, and the error correction techniques are not adapted to PMR constraints. The main difference between the public LTE and the mission critical LTE lies on the type of user applications. While the public operators privilege the high definition voice and video transmissions, independently of spectrum efficiency or the number of users having network access, the PMR solutions are based on the exact opposite. Public safety dedicated networks must privilege user access, network capacity in terms of number of users, network and service availability, therefore a maximum efficiency in spectrum use. In this context, low rate voice coders are particularly privileged, and, in the future, low rate video transmission is also envisaged. One of the most important specificities of PMR is network and service availability at 100% of the time, and this on all cell coverage. This becomes a necessity in times of emergencies, when emergency calls must have immediate network and service accessibility. Communications

must not only be accessible, but also stable. The design of the network must be performed considering worst case scenarios, like large scale disasters, when individuals and group-calls must be set up rapidly. The number of group members may vary up to several hundreds of users. And all users, even those placed at cell edge, must receive their voice and data communications in a reliable manner. Besides these essential requirements, in PMR technologies, all air interface transmitted data is encrypted, and point to multipoint communications are also possible between the members of a group.

Voice and video communications are therefore characterized by low throughput transmission, with a very robust channel protection, and are encrypted. While the target throughput for speech encoding is of 2400 bits/s, the video rate is estimated around 350 kbits/s. Voice communications are mainly established as group calls in downlink, and individual calls in uplink. On the contrary, video transmissions are supposed to be generated mainly as uplink individual communications, with a reduced refreshment rate.

For an optimal system design, with a maximum efficiency in spectrum use, one must therefore consider multi-layer characteristics, and especially the type of applications that are to be transmitted. Voice and video frames possess certain characteristics that can be exploited by the intermediate or physical layers. This can engender solutions that will not necessarily be optimal locally, but can propose an optimum use of available resources for the end-user provided quality.

This dissertation analyzes the PMR broadband perspectives, through the evaluation of the preferred candidate, LTE, and the proposal of a possible channel coding evolution, the patented solution of unequal error protection embedded turbo codes. A first study in chapter 2 focuses on the multi-layer analysis and the identification of key issues for professional-like LTE for voice and video communications. The voice and video capacities are estimated for both downlink and uplink LTE transmissions, and the downlink LTE voice system efficiency is compared with that of the PMR and Global System for Mobile Communications (GSM). This chapter helps highlighting some of the key points. If not resolved, the latter could lead to the LTE downfall as a candidate for the PMR evolution. One such key characteristic of PMR systems is the unequal error protection channel coding technique, which might be adapted to the LTE technology for its evolution to public safety requirements. Chapter 3 further introduces the proposed evolution patented ideas: the unequal error protection embedded turbo codes. We propose a new approach for the unequal error protection channel coding through the progressive hierarchical turbo codes. Both parallel and serial turbo configurations are closely studied. The unequal error protection mechanisms are embedded in the encoder's structure itself through the progressive and hierarchical insertion of new data. The turbo decoding is modified as to optimally exploit the progressive insertion of information in the encoding process and hierarchically estimate the corresponding data. Both parallel and serial configurations' properties are analyzed using an analogy with a pilot code behavior, as well as a zoom on the weight error functions coefficients. The virtual code rate and factor graph interpretations also provide a better insight on the code properties. The code possible gains are highlighted through computer simulations in both static and dynamic transmission environments, by using carefully chosen benchmarks. Finally, in chapter 4, the patented idea of parallel progressive hierarchical turbo codes (PPHTC) is evaluated over the LTE platform. A detailed description is given of the voice transmission bearer architecture over LTE, and its consequences are discussed. The new channel code is inserted and evaluated over this platform and its performances compared with the existent LTE transmission schemes. The voice quality results help concluding on the efficiency of the proposed solution in a real transmission scenario. However, even though the newly presented solution gives the best results, further system optimizations should be envisaged for obtaining better gains and exploit the parallel progressive hierarchical turbo codes potential. The dissertation concludes in chapter 5 and a short discussion is given on future research perspectives.

Chapter 2

PMR Broadband Perspectives

Abstract — This chapter proposes an overview of Private or Professional Mobile Radio (PMR) networks, followed by a thorough analysis of their broadband perspectives. We highlight key issues regarding voice and video transmission mechanisms for the second and third generation PMR technologies. While voice communications are performed using circuit switched-like mechanisms over narrowband radio, video transmission has lately become possible using Internet Protocol (IP) and advanced physical layer techniques over the wideband networks. But up-coming broadband public systems nurture the PMR evolution towards broadband technologies, from which the Long Term Evolution (LTE) seems a promising candidate. This chapter will analyze LTE's voice and video predictive capacity in a typical PMR use case: groups calls. The evaluation is performed considering a multi-layer realistic system configuration, including both radio frame and transmission protocols overheads. The LTE layer one voice transmission parameters are nevertheless normalized for a reasonable PMR configuration. The downlink LTE voice spectral efficiency is further compared with highly efficient second generation private and public mobile networks. LTE is not yet tailored for PMR services. The transmission protocols and the resource allocation parameters are not foreseen for low bit rate transmissions. Considering the proposed analysis, results show that this broadband candidate remains spectrally inefficient in the PMR context, most especially for voice communications.

2.1 Introduction

The Private or Professional Mobile Radio (PMR) and the Public Access Mobile Radio (PAMR) emerged in the USA as early as 1920s for public safety sectors. They became of large interest for different private sectors after the 1960s, because of their reliable equipment, with low complexity and acceptable costs.

The first generation (1G) PMR was based on analogue solutions, which are still used today in some parts of the world. PMR networks evolved towards the second generation (2G) in the 1990s and third generation (3G) systems after 2000. These systems have dedicated constraints and dimensioning issues, since they must address communication needs of public safety users like police forces, civil protection customs, firefighters, as well as business and industrial fields as utilities, transports, airports, private security, maintenance services (water, gas, electricity), petrochemicals, factories, ports, etc. With very specific requirements, PMR systems may be used for local networks, as well as for very complex regional or national multisite deployments.

This chapter proposes an overview of 2G to 3G currently most widely spread PMR networks, and an analysis of the PMR broadband perspectives. We shortly survey the voice transmission mechanisms considering the following 2G PMR technologies proposed in the 1990s:

- Association of Public Safety Communications Officials' Project 25 (APCO25), standardized by the Telecommunications Industry Association (TIA) in the USA;
- Terrestrial Trunked Radio (TETRA), standardized by the European Telecommunications Standards Institute (ETSI);
- TETRAPOL, proprietary solution of the European Aeronautic Defence and Space (EADS) company;

and the video transmission in TETRA Enhanced Data System (TEDS), currently the only PMR 3G system, an evolution of TETRA proposed by ETSI.

Once we have identified PMR key issues and existent mechanisms for voice and video transmission, we will analyze the PMR broadband perspectives. The possible candidates that have been identified for the PMR broadband evolution are the Worldwide Interoperability for Microwave Access (WIMAX) and the Long Term Evolution (LTE). However, even if WIMAX drew considerable attention up to 2009, recent developments show that it might only become a niche PMR technology. And, currently, it is LTE, the Third Generation Partnership Project (3GPP) proposed standard, that seems to have been seducing the PMR community.

In this chapter, we propose an objective evaluation of LTE as a possible PMR broadband perspective. Nevertheless, for a true PMR use case evaluation, we propose several adjustments to one specific 3GPP allocation algorithm. The latter defines the layer one transmission parameters: the transport block size, the coding rate and the radio resources. We model multi-layer realistic voice and video transmission systems, considering both the protocol stack and the air frame overheads. We further compute the realistic LTE voice and video capacity, for downlink (DL) and uplink (UL) connections, and evaluate the protocol overhead impact on the overall capacity. Although acceptable for video transmission, the protocol overhead remains consequential for PMR voice communications, as it demands up to 50% of the radio allocated resources even using protocol compression mechanisms. This is due to the very low bit rate voice codecs used in PMR. While high throughput video allocation is radio optimized, low rate voice and even low rate video capacities are further restricted by the layer one transmission strategy.

Voice transmission spectral efficiency seems particularly affected by the LTE configuration. For an objective evaluation, we evaluate the LTE DL voice spectral efficiency and compare it to 2G PMR and the Global System for Mobile (GSM) communications networks. LTE is not yet optimized for real-time voice communications, its spectral efficiency is not improved compared to GSM and PMR. Low throughput voice communications are not bandwidth efficient, which is not PMR favorable, because frequency bandwidths availability is very restrictive for these systems. The 3GPP proposed protocols and transmission parameters in LTE are optimized and basically restricted to high bit rate applications. This explains why LTE, in the form of Release 9 or the pre-fourth generation (pre-4G), is not properly efficient for the low rate applications of PMR, where one major problem is bandwidth availability, and where spectral efficiency is essential to system deployments.

This chapter is organized as follows. Section 2.2 identifies the PMR key issues for voice and video communications, from the end-user's perspective. In section 2.3 we overview the voice communications mechanisms in 2G PMR, which are based on circuit-switched transmission systems. The PMR network architecture evolution to 3G is presented in section 2.4. The PMR broadband perspectives are discussed in section 2.5, while the convergence possibility between PMR and the LTE candidate are analyzed in section 2.6. The results of the theoretical analysis are given in section 2.7. LTE voice and video capacity are given for the two smallest deployment bandwidths, for both DL and UL, and for one specific PMR use case: groups calls. The voice spectral efficiency is given for DL transmission only, comparing the LTE voice broadcasting capabilities with today's most efficient 2G technologies. We conclude in section 2.8.

2.2 PMR Key Issues

For a better apprehension of the issues prevailing in PMR systems, a short definition is necessary, as follows:

"PMR offers two-way radio communication carrying speech, data or mix of both in non-public networks tailored to the specific operational needs of professional mobile user groups for efficient and flexible communication within their area of daily operation" [1].

Their specificities include secured voice and data communications, individual and group calls, broadcast calls, multilevel priority calls, emergency and help calls, dispatcher functionalities, disaster relief services. Day to day field operations must benefit from fast call setup and high channel availability with end-to-end communication encryption. Direct communication between radio terminals must also be possible. PMR networks are mainly used today for voice communications and short text messaging, but narrowband data transfers are also possible, like automatic vehicle or person location using location tracking, or database inquiries for different kinds of medical or surveillance informations.

Spectral efficiency is a key factor in PMR networks, since they have limited frequency allocations. Service must be demand-oriented and reliable in any coverage area, since at any moment from any point an urgent call may arrive. The service must be designed for urban and rural areas as well, with robust communications and good reception unconditioned on the good or bad propagation channel. Typically, broadcast communications are frequently used in PMR, when short concise messages are instantly sent to a group or several groups of users. These communications are then naturally very robust using adequate modulation and coding techniques. Most PMR networks use the trunking technology, i.e. frequency channels are allocated and rapidly switched between users or groups of users for limited conversation periods.

PMR systems' frequency bands are allocated in the 400 MHz bandwidth in Europe and the 700 MHz bandwidth in the USA, but other bandwidths are possible world widely. These ultra high frequencies (UHF) provide wide cell coverage, which is cost efficient because a nationwide coverage can be obtained with less but wider cells than in the public networks. However, spectrum use is very restricted for PMR applications, and only narrowbands (from 6.25 to 25 kHz) have been provided by standardization organisms. Spectrum availability is one of the key issues of all PMR systems and, therefore, the spectral efficiency is of an utmost importance for designing these systems.

2.2.1 Voice Communications Constraints

"For many applications in the private land mobile sector, the uniqueness provided by voice communications (such as recognition of the speaker, and perception of voice inflection and emotional content) is quite unnecessary" [2]. This remark made in 1989, when the PMR standards were evolving from analogue to digital, remains true even today. Very short and concise communications are typical to the PMR use case, the receiver must only receive the message in an intelligible form. Therefore, there is no need of high-quality speech coders, the low bit-rate voice coders are good enough. The immediate consequence, compared to public networks, is that the number of communications per channel is increased because the data rate per communication is reduced. These low bit-rate voice coders are designed for PMR constraints, e.g. for some users, *"it is also particularly important that speech quality, or more precisely intelligibility, is preserved under conditions of high acoustic background noise"* [3].

Another voice transmission constraint in PMR networks is that "good quality speech", i.e. intelligible speech, must be maintained at high error rates. This requires very robust channel coding and modulation techniques. But error control strategies designed without any knowledge of the application using them would require considerable channel bandwidth. For example, particular applications, like voice and video, may tolerate errors on some bits, and none on other very important bits. Typically, PMR voice coders would transmit parameters like pitch amplitude, the position of formants and a codebook index [4]. Channel errors on the bits describing the pitch would be intolerable, but errors on the last formant would not even be noticed by the listener. For this reason, unequal error protection (UEP) techniques are used in all 2G PMR networks for voice transmission. The different importance bits are grouped in classes of bits that benefit of different channel protection techniques and ratios. *"This grouping is very efficient because it means that channel bandwidth can be saved by tailoring the amount of redundancy specifically to the perception of the user of this particular application"* [4].

2.2.2 Data and Video Transmissions Issues

In 2G PMR systems, low throughput data transfers are possible (1 to 10 kbps). But these data messages are limited to short text messages, status messages, database queries, alarm feedback, small still image transfers, geolocalization. The 3G evolution is meant to bring a wideband technology, which is TEDS, and larger possible bit rates. Interesting new data applications would then be possible, like mobile video or high quality resolution image transmission.

Some of the identified objectives for UL and DL connections in 3G, and later in broadband networks, would be:

- live and recorded video streaming for either mobile or fixed video systems, with the possibility of database transfers or queries;

- possibility of using advanced video analytics techniques, like for example object recognition or automatic movement detection;
- possibility of using video stream control for requesting better quality images or zoom on specified frames from the camera itself or the database, i.e. scalable video coding.

These new generation systems would help improve public safety and disaster relief systems by providing the necessary video information to the control room from the scene itself. Typically, immediate firefighting response would be given if real-time images were available from the scene of a fire or other type of emergency or natural disaster. In telemedicine, high quality images of patients would provide doctors with immediate feedback on their physical status. Real-time video would also be very useful when used with robotics, for cases such as critical situations nuclear disasters or underwater rescue operations, where the conditions would be too risky for human intervention.

As use cases might be quite extreme in some situations, PMR video coders would need an effective compromise between video quality and video throughput. High quality images must allow operators to identify movement and objects in critical scenes, e.g. a firefighter entering a building with considerable black smoke and falling debris. But the transmission channel must allow other incoming video streams from other field operators as well.

Nevertheless, real-time video transmission is still a subject under study in the PMR community and no decisions have been made yet on what video coder would be chosen for these systems. However, in the SAFECOM program document released by the USA Department of Homeland Security in 2006 [5], some of the parameters for video transmission in PMR systems are identified and use cases highlighted.

2.3 2G Narrowband Digital PMR

Nowadays, there are several existing PMR technologies all over the world, that have been either standardized, either proposed by private organisms. In this chapter, we will concentrate especially on the technologies dedicated to medium to large high-tier systems, that have gained importance over the years.

As a brief reminder, we note that the Digital Mobile Radio (DMR), standardized by ETSI in the years 2000, is destined to small and medium systems, with limited user densities. Created as a frequency division multiple access (FDMA) technology that can be used in all PMR bands from 30 to 500 MHz, the DMR became economically more reasonable than TETRA for the lower market segments.

The digital PMR standards have been developed after the 1990s for an enhanced and efficient usage of the available narrowbands. But the proposed data transfers are limited to:

- signaling messages, that occupy a small percentage of the radio frame;
- short data messages (equivalent to the public systems' short messaging system (SMS)), to which special radio slots are reserved;
- voice communications which benefit of an end-to-end established circuit, with an unique voice coder, at low bit rate.

Hereafter, we will overview voice transmission mechanisms over 2G PMR networks. Their system architecture for voice transmission is mostly similar to circuit-switched GSM. Fig. 2.1 gives a general overview of the voice PMR circuit, mainly composed of:

- the application layer, where one voice coder encodes the analogue speech signal and prepares the digital voice packet,
- the layer two, where signaling or control information can be added depending on the technology, but the generated overhead is insignificant (several bits),

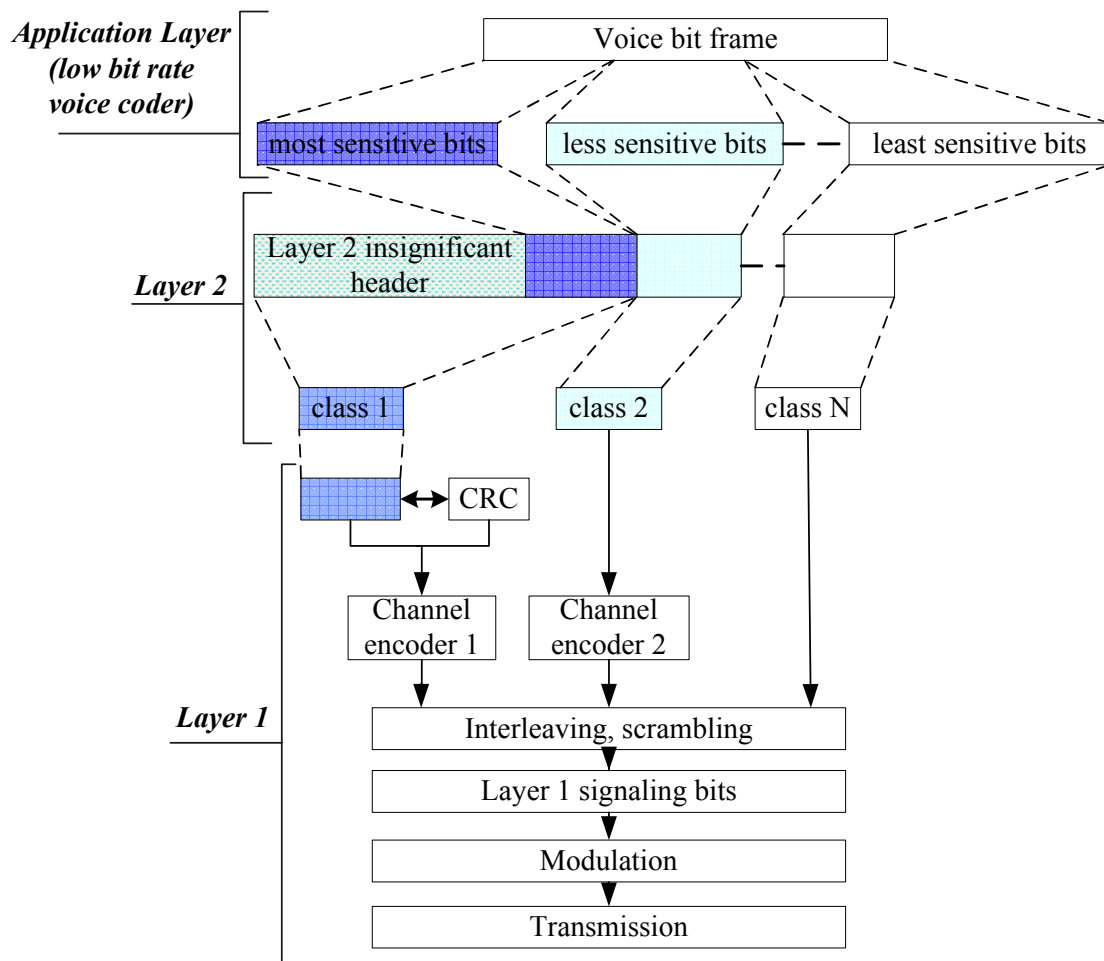


Figure 2.1. Circuit-switched like voice transmission mechanisms over PMR.

- the layer one or physical layer, which prepares the user frame through UEP channel encoding (the most sensitive bits are often cyclic redundancy checked (CRC) also), modulation and radio access; one radio frame may contain signaling together with voice or data messages.

These technologies can either use the single frequency allocation mode or the trunked mode. The latter is a more efficient method for radio resources allocation than the single frequency allocation, because it allows the rapid scheduling and switching of finite amounts of unused capacity between the different voice communications.

We note that the key features of PMR networks are: the low bit-rate voice coder (vocoder), the very small overhead and the reduced signaling, the UEP channel encoding, and the trunked transmission mode. Together, they play an essential role in designing very robust and spectrally efficient radio networks.

2.3.1 APCO25

Project 25 (P25) has been standardized by the TIA, in the USA. More commonly known today as APCO25, the system has been developed in two phases: Phase 1 (φ_1) and Phase 2 (φ_2). It can be run in both single frequency or trunked mode.

APCO 25 φ_1 is designed for 12.5 kHz frequency channels, in FDMA mode. The transmission is performed using data units, which can either transport voice or text messages, either control signaling messages. Half-

duplex¹ and full-duplex² modes are possible. The mechanisms behind voice transmission are similar to the circuit-switched GSM.

Improved MultiBand Excitation (IMBE) is the voice coder for this first phase, with a very low bit rate of 4.4 kbps. The voice bits are rated in three classes of bits and UEP encoded using Golay and Hamming codes, and modulated with a continuous four level frequency modulation (C4FM).

The air throughput reaches 9.6 kbps per voice communication, with 2.8 kbps of forward error correction coding (FEC) and 2.4 kbps of additional encryption and control information.

In $\varphi 2$, APCO25 radios use 6.25 kHz of bandwidth per voice channel. The access mode is time division multiple access (TDMA) half-duplex frequency division duplex (H-FDD).

$\varphi 2$ uses an improved voice coder version, the Advanced MultiBand Excitation (AMBE) at an even lower bit rate of only 2.45 kbps³. One voice frame is composed of only 49 bits. This frame is split in four classes of bits which are UEP channel encoded using Golay codes. The modulation types are specific: the harmonized continuous phase modulation (H-CPM) in UL and the harmonized differential quadrature phase shift keyed modulation (H-DQPSK) for DL.

The common air interface throughput is of 12 kbps in DL as well as in UL. With an improved configuration and lower bit-rate voice coder, APCO $\varphi 2$ registers three to four times more voice channels per cell and per MHz than $\varphi 1$. This means a considerably improved voice spectral efficiency.

2.3.2 TETRAPOL

TETRAPOL is an European PMR system, EADS proprietary. Operational since 1992, the TETRAPOL land mobile radio specification was defined by the TETRAPOL Forum. The TETRAPOL technology is based on packet transmission in connected or non-connected mode. The applicable band is very high frequencies (VHF) and UHF, below 1 GHz, with a channel spacing of 10 or 12.5 kHz. The access mode is FDMA.

Voice encoding is performed by a Regular Pulse Code-Excited Linear Prediction (RPELTP) type vocoder. Speech is digitized at 6 kbps and transmitted on a 8 kbps traffic channel. No echo cancelation techniques are used since the transmission is half-duplex.

Voice and data channels are fed to the physical layer where UEP channel encoding is performed, using CRC and convolutional codes, after which they are Gaussian minimum shift keying (GMSK) modulated. The transmission gross bit rate is therefore 8 kbps.

2.3.3 TETRA

TETRA was initially proposed in Europe to replace the old analogue PMR systems and to solve, together with the introduction of new services, the lack of security on voice and data calls. TETRA uses the trunking technology. It is also called a packet data optimized (PDO) technology, simulating the circuit-switched channels for the transmission of voice, as well as data. Every time slot can carry control signaling, speech or data calls, and the system uses the frequency division duplexing (FDD) with a TDMA of 4, that we will be denoting by TDMA4.

TETRA uses an Algebraic Code Excited Linear Prediction (ACELP) for speech compression. 30 ms of analogue signal are encoded into a packet of 216 bits. The speech frame packaging is performed at the low medium access control (MAC) layer, but with no significant overhead. At the physical layer, these frames undergo UEP encoding using a CRC and convolutional codes, before the $\Pi/4$ offset differential quaternary phase shift keying ($\Pi/4$ DQPSK) modulation.

¹The user is not capable of sending and receiving informations simultaneously, it has to transmit and receive alternatively using either one frequency channel or two different frequency channels for DL and UL (push-to-talk technology). This mode is also called simplex mode.

²The user terminal is capable of receiving and transmitting informations simultaneously, and two different frequency channels are used for DL and UL communications.

³AMBE is a registered trademark from DVSII. Further informations regarding AMBE can be found on the constructor's website: http://www.dvsinc.com/papers/eval_results.htm

Four speech channels may be successively transmitted on the full rate TETRA traffic channel (25 kHz), due to the TDMA⁴. TETRA circuit mode calls may be voice calls or circuit mode data calls. Depending on the channel slot partition and channel protection level, the data rates offered for circuit mode data are as follows:

- unprotected: 7,2 kbps; 14,4 kbps; 21,6 kbps; 28,8 kbps;
- low protection: 4,8 kbps; 9,6 kbps; 14,4 kbps; 19,2 kbps;
- high protection: 2,4 kbps; 4,8 kbps; 7,2 kbps; 9,6 kbps.

A circuit mode call may be an individual call (point-to-point), group call (point-to-multipoint), acknowledged group call (point-to-multipoint) or broadcast call (point-to-point). Individual calls may use either half-duplex or duplex operation. Group calls and broadcast calls use half-duplex operation (or push-to-talk technology).

2.4 3G Wideband Evolution: TEDS

TETRA is the only PMR technology that has evolved to a wideband architecture, TEDS, which became available in 2006. It is considered a 3G technology, since the frequency bandwidths envisaged by the standard are larger than 2G available ones. The Internet Protocol (IP) protocol is introduced for data services, and target throughput rates are of several hundreds of kbps, comparable to those of the enhanced data for GSM evolution (EDGE). Possible applications include e-mails, internet or intranet access, and low bit rate video transmissions [6].

TEDS or TETRA2 has been designed as an evolution which would provide customers with a backward compatibility to TETRA1. Therefore, it uses the TDMA4 channel access technique, same as TETRA, and the physical layer has been upgraded including advanced techniques like described hereafter:

- turbo coding (parallel concatenated convolutional codes) providing three possible transmission rates: 1/3, 1/2 and 1, alongside the existent convolutional encoding;
- three new quadrature amplitude modulation (QAM) schemes added to the existent $\pi/4$ and $\pi/8$ DQPSK: 4QAM, 16QAM, and 64QAM; these added modulations are similar to those of LTE;
- adaptive modulation and coding schemes, these help improving the user throughput according to the channel behavior;
- filter-bank multi-carrier modulation, similar to the orthogonal frequency division multiplexing (OFDM), with the exception that data symbols are pulse-shaped before sub-carrier mapping and no cyclic prefix is added;
- sectored antennas, which provide an improved channel coverage;
- wideband frequency channels have been considered: from 25kHz to 150 kHz.

At higher layers, IP has been introduced as an efficient data packet transmission protocol. The IP overhead is compressed at layer three using the sub-network dependent convergence protocol (SNDCP), which is also responsible for setting the quality of service (QoS) for one data stream. Three QoS classes are possible, one of which defines the parameters for voice and video real-time transmission, with scheduling and priority choice possibilities. These mechanisms are similar to the packet data convergence protocol (PDCP) defined context at layer three in LTE, which associates the different quality control information (QCI) to the specific bearers for each data stream respectively.

TEDS represents the next step for critical PMR data applications, believed to provide data services at speeds ten times higher than existent TETRA networks. While first TEDS networks are already being deployed, current standard working groups are concentrating on the development of voice services over TEDS. As we can see, TEDS tends to approach more broadband-like networks, but ensuring backwards compatibility with TETRA.

⁴One full rate channel (25 kHz) is divided in four time slots, therefore four independent voice communications may be transmitted.

2.5 Broadband Perspectives

The new broadband technologies have nurtured the evolution perspectives for PMR networks. The two standards considered as having the highest potential for delivering the next generation networks are WIMAX and LTE, which must comply with the International Telecommunications Union (ITU) International Mobile Telecommunications (IMT) Advanced requirements. WIMAX is an Institute of Electrical and Electronics Engineers (IEEE) specification also known as IEEE 802.16. Its most famous 3G releases are IEEE 802.16d (2004) and IEEE 802.16e (2005). The IEEE 802.16m (2009) is believed to be a part of the 4G networks. While 3GPP standard LTE is also considered a 3G evolution, its main characteristics are a prerequisite for the future 4G. And it is LTE-Advanced which represents the 4G evolution in the 3GPP family of standards.

Hereafter, we present the common LTE and WIMAX features that reveal the form of pre-4G standards or what are the 4G prerequisites.

- All IP architecture, which is meant to improve the core network performance by providing a flat architecture. Central management in a network is eased by its hierarchical structure. The trade-off is the reduced performance because of the increased number of nodes that the packets must traverse. Therefore, to reduce latency, a flat architecture with more direct routing from mobile device to end system is more effective.
- Intelligent base stations, capable of radio resource management and scheduling, thus the radio intelligence is centralized at the cell level.
- Multiple-input multiple-output (MIMO) and adaptive antenna systems have been adopted, improving the cell coverage.
- Performing FEC techniques, like turbo codes, are used for a very efficient protection against channel errors.
- OFDM and/or single carrier (SC) FDMA have been chosen as radio access technologies. In [7], it is highlighted that these two technologies present no inherent advantage over code division multiple access (CDMA) in 10 MHz or less bandwidths. The fundamental advantage of OFDM is that it solves the inter-symbol interference induced by multipath and therefore simplifies channel equalization. Also, the advantage of SC-FDMA over OFDM for UL is its lower peak average power ratio (PAPR).

With very few technical differences, namely regarding the air frame configuration and channel allocation strategy, WIMAX and LTE represent the first generation of broadband networks, the pre-4G or the milestones for the 4G evolution. Since the PMR networks growth has been very modest in the past decade, it is likely that the PMR world would adopt these new broadband technologies with some modifications to meet their specific constraints and requirements.

Another possibility would be the evolution of TEDS or TETRA2 towards TETRA3. TEDS is currently the only PMR technology that has 3G capabilities, first deployments being expected before the end of 2012. As shown in section 2.4, TEDS has already some common features with LTE, and the evolution of TEDS would be natural if the pre-4G features here highlighted were introduced. The main problem is that this standard does not exist yet. Therefore, as it is easier to adopt an existing standard than actually proposing a new one, currently the choice is between WIMAX and LTE.

Up to 2009, mobile WIMAX was world widely thought to become the broadband wireless technology of choice for evolving mobile networks. For several years, WIMAX had been considered as an interesting broadband perspective for the PMR world as well. This IEEE standard was technologically in advance compared to the not yet finalized 3GPP LTE standard. In [8] for example, the authors have studied the possibility of using WIMAX as a backbone for supporting critical communications and inter-connections with heterogeneous networks in a disaster management scenario. In [9], the convergence for network and terminal level functionalities between TETRA and different radio networks is investigated, among which WIMAX is also considered.

However, starting with 2010, LTE emerged as an alternative to WIMAX. New 3GPP LTE releases included interesting features of WIMAX. 3GPP LTE came as a natural upgrade of the former 3GPP standards such as

GSM, the universal mobile telecommunications system (UMTS) and the high speed packet access (HSPA), and currently emerges as the most popular pre-4G wireless technology. Even if these two standards, WIMAX and LTE, have similar technological features, LTE seems to become the preferred candidate for the broadband PMR evolution, whereas, WIMAX seems to remain only a niche technology [10].

Lately, LTE has been studied from different perspectives in view of its integration in the PMR world. An inter-system interface is presented in [11], which would enable smartphones to receive both TETRA and LTE communications. In [12], the very important problem of priority access calls by maximizing spectrum usage is addressed. The authors conclude that LTE is capable of including robust priority mechanisms for public safety users. Also, the use of LTE together with a public safety network as a heterogeneous network has its advantages: providing a wider coverage and the necessary spectrum to emergency calls.

Naturally, the first step of using LTE for the public safety will be in a heterogeneous context. A better adaptation to public safety needs is necessary for a full roll-over to only LTE-like coverage in the future. Currently, in the USA, the possibility of deploying APCO25 φ 2 together with LTE is envisaged. In coming years, in Europe also, LTE will be deployed alongside existent TETRA and TETRAPOL networks. The transition will be performed most likely similarly to public networks, starting with a co-existence of LTE and circuit-switched radio networks. LTE will provide high-rate coverage, while voice calls will continue using existent 2G systems. Today, it is a real need in identifying and correcting LTE weaknesses in view of its future use cases.

2.6 LTE and PMR Convergence Analysis

The LTE standard has been proposed by the 3GPP as the first step towards broadband technologies. It represents the radio network evolution, part of the evolved packet system (EPS) [13], which also includes the evolved packet core (EPC) network standardization. LTE is expected to provide smaller transmission and connection delays, increased bit rate even at cell edge, better spectral efficiency, transparent mobility towards any network and reasonable mobile power consumption.

In this section, we shortly overview the DL and UL LTE transmission systems. We further present the proposed multi-layer algorithm for the realistic evaluation of DL and UL LTE voice and video capacity. We point out one standard weakness, which is the inefficient transmission of reduced bit rate applications.

2.6.1 LTE Technical Overview

In this section, we will describe the realistic transmission system model and explain 3GPP LTE standard parameters for DL and UL.

The system model is represented in Fig. 2.2, as defined by the 3GPP standards.

The application layer codec emits compressed voice or video packets, P_{voice} or P_{video} respectively. These packets are consecutively prepared for transmission using: real-time transport protocol (RTP), user datagram protocol (UDP) and IP. At layer three, the PDCP context is negotiated and the robust header compression (ROHC) is performed. The PDCP header and the radio link control (RLC) header are added. At layer two, the MAC header is included. The newly obtained packet represents one MAC packet data unit (PDU) which can be processed by the physical layer using one or several transport blocks.

The system will define the number of transport blocks to be used for the transmission depending on the scheduled modulation and coding scheme (MCS) specific to each user. This MCS is computed based on the channel quality information (CQI) exchanged between the base station or eNodeB and user element (UE). The mechanisms for the choice of one MCS can become even more complex when the level of quality of service (QoS) class identifier (QCI) is considered.

In this chapter, we will not be considering the segmentation at the physical layer. Given the PMR context, the MAC PDUs will be considerably small compared to the transport block sizes (TBS) proposed by the standard. Therefore, we will be considering one TBS for the encapsulation of one MAC PDU for each call. We will be denoting by $TBS_{necessary}$ the minimum necessary TBS for the transmission of one MAC PDU. We will continue by searching the closest standardized TBS value that complies with the pre-defined system MCS.

For all accepted modulation orders, M , and for all possible radio allocations, N_{PRB} , the 3GPP standard defines all possible TBSs for which layer one mechanisms are configured [14]. These values must be determined using system defined parameters: the number of channel bits that can be used for the first transmission, N_{ch} , and the scheduled coding rate, $R_{scheduled}$. According to the 3GPP algorithm, the TBS must verify

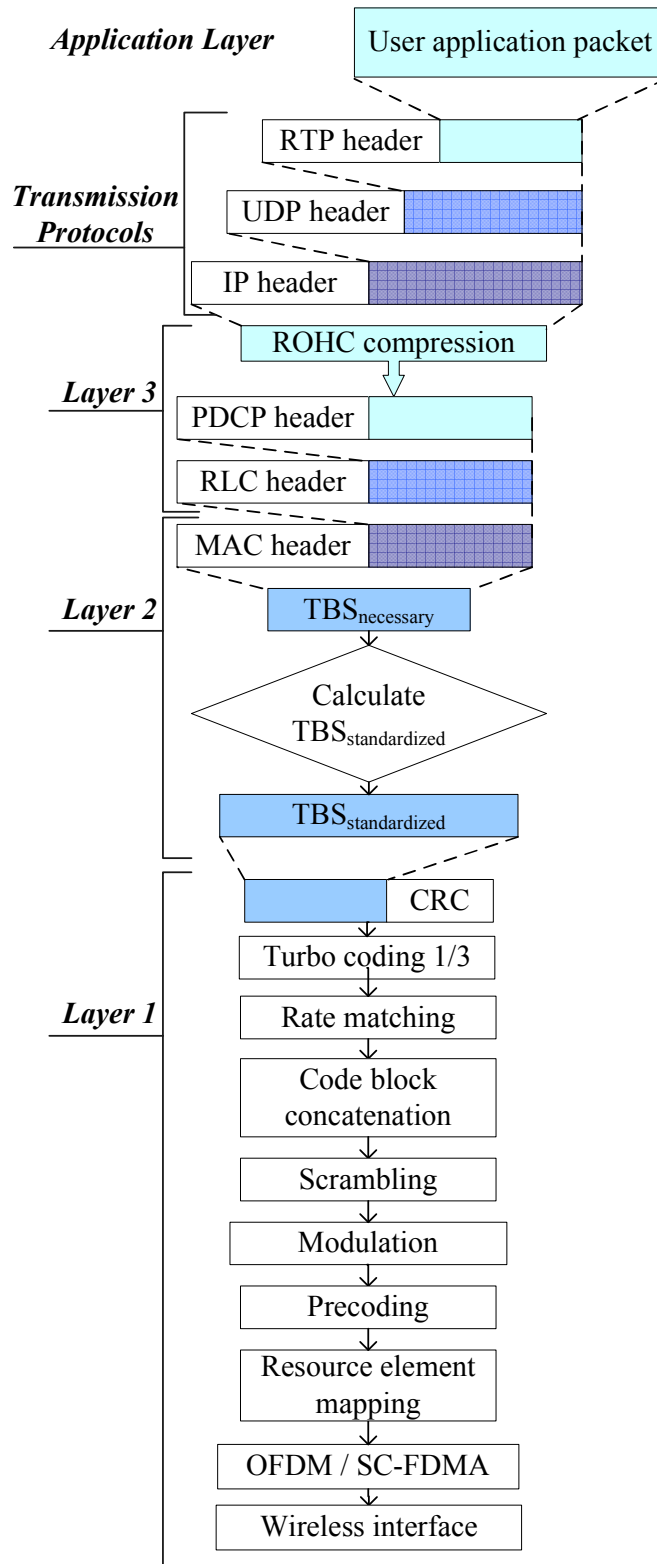


Figure 2.2. LTE transmission system model for voice and video packets.

$$\min |R_{\text{scheduled}} - \frac{TBS_{\text{standardized}} + N_{\text{CRC}}}{N_{\text{ch}}}|, \quad (2.1)$$

where $TBS_{\text{standardized}}$ denotes a valid TBS as standardized in [14] and N_{CRC} the size of the layer one CRC code in number of bits.

Thus, the layer one receives a valid TBS and, after CRC attachment, performs the specific mechanisms for wireless interface transmission: turbo encoding, rate matching, code block concatenation, scrambling, modulation and layer mapping, precoding and the corresponding symbol mapping to the air frame resources, before OFDM in DL or the SC-FDMA signal generation in UL.

The difference between DL and UL transmission systems is that, in UL, a multiplexing of control information (channel quality indicator (CQI), rank indicator (RI) and precoding matrix indicator (PMI)) with user data is possible in the physical shared channel⁵. This latter option has not been considered in this study, since the theoretical analysis shows that the bandwidth allocation per user would increase considerably because of the additional control information. This is not interesting for the moment as our purpose is to evaluate the maximum theoretical LTE user capacity. However, we consider that these control informations are transmitted by the UE to the eNodeB using the physical uplink control channel (PUCCH).

For each user, the air frame resource allocation has been defined by higher layers. One radio frame is 10 ms long, and counts 10 sub-frames. Thus, the time granularity emission is of one sub-frame. Each user radio allocation is measured as one sub-frame⁶ spanning the length of N_{PRB} physical resource blocks (PRBs) of frequency bandwidth⁷. We will denote by N_{PRB} the number of PRB pairs assigned to one user for the specific sub-frame⁸. Using one layer mapping, one quadrature phase shift keying (QPSK) symbol is mapped on one resource element (RE). One RE is defined as one time symbol on one sub-carrier frequency.

Fig. 2.3 gives the graphical representation of one time sub-frame spanning one frequency PRB in DL. Each DL sub-frame contains pilot resource elements (REs), physical downlink control channel (PDCCH) REs and the physical downlink shared channel (PDSCH) REs. The user data is transmitted only on PDSCH REs. The REs dedicated to PDCCH and pilots (or reference signals) are considered air frame overhead and represent an important percentage of the frame capacity, especially in the lower bandwidths. Here, we consider a fixed amount of control channel symbols for DL and UL respectively, that represent the maximum number of control symbols admitted by the network. It is outside the scope of this chapter to investigate their own influence on the network capacity. Detailed studies on the design and scheduled capacity for the PDCCH are given in [15] and [16]. Also, here, we have not counted the synchronization channels from the first and sixth sub-frames, nor the broadcast channel in the first sub-frame. These channels occupy the center 6 PRBs of the deployed LTE bandwidth (BW) of N_{BW} PRBs.

Fig. 2.4 gives the graphical representation of one UL sub-frame spanning the entire bandwidth. At both band edges, several PRBs may be allocated to the physical uplink control channel (PUCCH) and, in-between, the allocation is divided between the pilots or demodulation reference signal (DMRS), the data transmission channel, i.e. physical uplink shared channel (PUSCH), and the random access channel (RACH). The DMRS occupies 2 symbols per slot if the normal CP is used and 1 symbol per slot if the extended CP is used. For our study, we have not considered the PRACH allocated resources.

For a specific MCS, the number of channel bits necessary for each user data transmission, N_{ch} , is strictly derived from the modulation order, M , the scheduled radio bandwidth allocation, N_{PRB} , and the number of REs per PRB available in the PDSCH for DL and PUSCH for UL, $N_{\text{REs/PRB}}$, as

$$N_{\text{ch}} = N_{\text{REs/PRB}} \times N_{\text{PRB}} \times M. \quad (2.2)$$

⁵The physical downlink shared channel (PDSCH) is used only for user data transmission, e.g. voice and video, while the physical uplink shared channel (PUSCH) can be used either with user data only, or user data multiplexed with its corresponding control information.

⁶14 symbols if the short cyclic prefix (CP) is used and only 12 symbols if the extended CP is used.

⁷One PRB is defined as spanning 12 sub-carriers (SC) in the frequency domain and half of a sub-frame (or one slot) in the time domain.

⁸For simplicity, in the standard, a measure of $N_{\text{PRB}} = 1$ in the frequency domain will refer to 2 PRBs, since the 12 SCs are spanning 2 time slots.

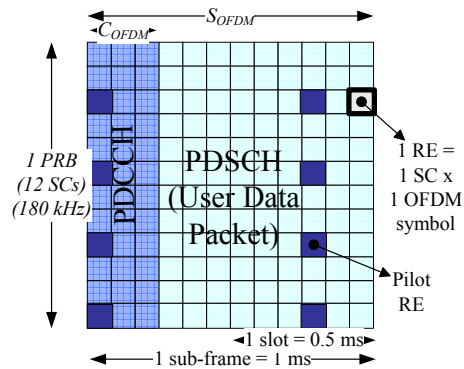


Figure 2.3. LTE DL radio frame configuration (1 ms spanning 1 PRB).

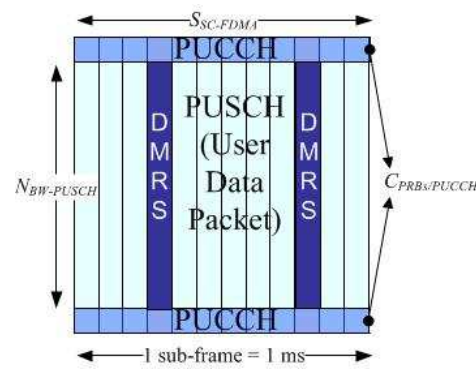


Figure 2.4. LTE UL radio frame configuration (1 ms spanning the allocated bandwidth).

2.6.2 Voice over LTE: a PMR use case

LTE represents an interesting broadband perspective for the PMR world. But optimized for high data rates, the technology does not provide any voice specific mechanism. Since one of its main characteristics is the end-to-end IP transmission, the envisaged solution for voice communications seems to be voice over IP (VoIP).

Consistent effort has been put in finding different results and proposals to answer the questions related to voice services over LTE, as what would the real LTE efficiency be for conversational voice transmission using the architecture defined by today's standard. In [17], the authors provide a thorough overview of the LTE protocol stack and their use with voice transmission. The RLC protocol must be used in unacknowledged mode (UM). Because some voice coders may tolerate high packet error rates, the MAC must allow the transmission of up to 10^{-2} packet error rates to higher layers. The LTE overheads for transport control protocol (TCP) used for data transmissions and VoIP services are estimated and compared. The ROHC protocol can compress up to 42 % of the overhead, as low as 3 bytes, for the adaptive multi-rate (AMR) voice coder with TCP acknowledgement. The impact of the IP/TCP overhead and the LTE protocol stack configuration are considered. However, their impact on the overall voice capacity is not investigated. In [18], the LTE radio interface and its options are discussed. The authors highlight the importance of the scheduler on the overall DL system performance. The chapter further analyses the LTE spectral efficiency and its improvement when key radio features are introduced. In a FDD configuration and a 10 MHz deployment BW, the target throughput numbers evolve from 1.07 bps/Hz/sector up to 1.73 bps/Hz/sector in DL and from 0.46 to 1.05 in UL. Nevertheless, these estimations are given considering only radio layer configuration and deployment parameters. Upper layers control overhead and voice coders configurations are not taken into account.

A second question on voice solutions over LTE is related to voice transmission architectures. VoIP is highly encouraged, but migration from existent radio networks to all-IP networks must also be envisaged. A series of proposals have emerged, a few of which have been considered by the 3GPP: circuit switched (CS) fallback [19], IP multimedia sub-system (IMS) telephony (MMTel) [20], and IMS telephony with handover to CS domain (SRVCC) [21]. The not 3GPP supported are the internet-based voice services and the voice over LTE generic access (VoLGA) [22]. In [23], these technologies are discussed, comparing the benefits for the operator and the end-user. The advantage of MMTel is its transparency for any kind of services whether the device is mobile or fixed and would represent a true IP solution for LTE. SRVCC and CS are based on the usage of existent circuit-switched radio networks. The internet-based services do not benefit from a standardized inter-operator interface and do not support CS handover and emergency numbers if needed. VoLGA proposes to connect existent technologies to LTE via one gateway, but the end-to-end call would not benefit from an all-IP architecture. The authors concentrate on the different solutions for voice transmission, but do not mention voice capacity. To the best of our knowledge, no objective and realistic study has been performed on VoIP transmission which consider both protocol stack and air frame configurations.

In this subsection, we present the scenario and the algorithm used for the voice evaluation capacity over LTE.

We consider a single PMR cell, where different users are receiving messages or accessing the network using group calls. In DL, one group call is defined as a multicast transmission, i.e. every user associated to the specific group will receive the message transmitted on the allocated channel. In UL, due to the trunked configuration, only one channel will be scheduled for response, every user accessing a time slot using PDO technology. Therefore, one group call corresponds to one DL and one UL allocated channels. Also, we note that, typically, in group call scenarios, there are no feedback mechanisms like automatic repeat request (ARQ) and hybrid ARQ (HARQ). The channel conditions are configured so that all users receive the message, i.e. the farthest user in the cell with the worst channel conditions must imperatively receive the call. Therefore, the scheduled MCS will be the most robust one corresponding to a coverage of 90% of the cell. We also suppose that all link control mechanisms have been performed by the network prior to the group calls' establishment. Link control mechanisms are essential for the network configuration and help defining the transmission MCSs. A complete overview on the impact of control channel limitations on the VoIP capacity is given in [24]. The authors conclude that the fullband CQI impact on user capacity is larger than that of the wideband CQI, and using the semi-persistent packet scheduling is 40 to 67 % more efficient than dynamic scheduling. A further discussion on the effect of channel or transmission control mechanisms on the user capacity is however outside the scope of this chapter.

Regarding the resource allocation strategy, the 3GPP defines a specific algorithm which computes the maximum TBS value that minimizes equation (2.1) given in sub-section 2.6.1. Considering the scheduled number of physical resource blocks, N_{PRB} , and the scheduled encoding ratio, $R_{scheduled}$, equation (2.1) computes the TBS value corresponding to the number of channel bits, N_{ch} , that can be transmitted using this radio block for the given system MCS. But, for a realistic voice capacity evaluation of LTE used with PMR constraints, one element is essential: the use of a **very low bit rate voice coder**. Using the standard given algorithm, we have concluded that the obtained TBS value, which would perfectly respect equation (2.1) and the specified MCS parameters, would be considerably larger than the voice packet. The problem with this algorithm, the given TBSs and possible allocations is that they are not optimized for small voice frames transmission, when considering robust low coding rates. The standard does simply not offer a reasonable choice between the transport blocks and radio allocations for robust coding rates, and, as a consequence, there are no interconnections defined for an optimal MCS necessary to a PMR use case. It is also obvious that there are no UEP mechanisms envisaged in LTE for voice transmission, therefore we will suppose in this study an equal error protection (EEP) channel coding.

Considering the standard proposed algorithm, we have performed several normalizations as to find a reasonable compromise between the chosen TBS and the transmission code rate. We describe hereafter the algorithm we have used, step by step. We will be referring to this algorithm as "**Algorithm for Voice**".

Step 1) Compute the voice packet bits length, P_{voice} , considering the voice coder bit rate, $R_{vocoder}$, and the voice frame time length, T_{voice} , as

$$P_{voice} = R_{vocoder} \times T_{voice}.$$

Step 2) Calculate the $TBS_{necessary}$ by adding the higher layer overhead, $H_{protocols}$,

$$TBS_{necessary} = P_{voice} + H_{protocols}.$$

Step 3) According to the scheduled MCS, set modulation order, M , and system required code rate, $R_{scheduled}$.

Step 4) If DL transmission, set air frame parameters as

- C_{OFDM} , number of OFDM symbols dedicated to control fields, PDCCH,
- N_{pilots} , number of REs dedicated to pilots,
- S_{OFDM} , number of OFDM symbols per sub-frame;

else if UL transmission, set air frame parameters as

- $C_{PRBs/PUCCH}$, number of PRBs dedicated to control fields, PUCCH,
- N_{pilots} , number of SC-FDMA symbols dedicated to DMRS per sub-frame,
- $S_{SC-FDMA}$, number of SC-FDMA symbols per sub-frame.

Step 5) If DL, compute the number of REs per PRB pair per sub-frame as

$$N_{REs/PRB} = 12 \times (S_{OFDM} - C_{OFDM}) - N_{pilots},$$

else if UL transmission, compute the number of REs per PUSCH per sub-frame as

$$N_{REs/PRB} = 12 \times (S_{SC-FDMA} - N_{pilots}),$$

and the available bandwidth for data transmission (PUSCH) as

$$N_{BW-PUSCH} = N_{BW} - C_{PRBs/PUCCH}.$$

Step 6) Load TBS_table valid values as given in 3GPP TS 36.213 V9.0, Table 7.1.7.2.1-1, pp. 28-34.

Step 7) For all possible allocation values, with i from 1 to N_{BW} , find $TBS(i)$ which verifies

$$\min(TBS(i) - TBS_{necessary}) > 0$$

where $TBS(i)$ spans column i in TBS_table ⁹.

Step 8) For each one of the computed TBS values, i.e. for i from 1 to N_{BW} ¹⁰, compute the corresponding number of channel bits and the value for equation (2.1)

$$N_{ch}(i) = N_{REs/PRB} \times i \times M,$$

$$\delta_{rate}(i) = |R_{scheduled} - \frac{TBS(i) + N_{CRC}}{N_{ch}(i)}|,$$

Step 9) Normalize δ_{rate} values as

$$\delta_{rate-normalized}(i) = \frac{\delta_{rate}(i)}{\max(\delta_{rate})}.$$

Step 10) For i from 1 to N_{BW} , normalize TBS values as

$$TBS_{normalized}(i) = \frac{TBS(i) - TBS_{necessary}}{TBS(i)},$$

$$TBS_{normalized}(i) = \frac{TBS_{normalized}(i)}{\max(TBS_{normalized})}.$$

Step 11) Compute the minimum TBS value closest to $TBS_{necessary}$, 3GPP standardized as

$$TBS_{standardized} = TBS(\text{index}(\min(\delta_{rate-normalized} + TBS_{normalized}))).$$

The proposed voice allocation algorithm considers all possible radio blocks allocations, from one to the maximum number of PRBs per bandwidth, N_{BW} . All possible radio allocations are envisaged for the closest values of TBSs that correspond to specific code rates. We choose the optimum standardized TBS as to minimize packet padding and obtain a code rate as close as possible to $R_{scheduled}$. Therefore, the TBS values are normalized together with their corresponding transmission rates, and their normalized minimums are finally chosen as optimum for transmission. The corresponding radio allocation, N_{PRB} , is chosen for user resource mapping.

2.6.3 Video over LTE: PMR Use Cases

Video transmission is foreseen as one of the key elements of the broadband radio mobile evolution. Transmission systems optimizations have been focusing on two aspects: either improving the network capacity through the use of advanced core network or radio technologies, or enhancing the end-user quality of experience through better scheduling and adaptive modulation and coding schemes, or improved video coders as the scalable video coder (SVC). In [25], an overview of unicast and multicast video options is given for LTE and WIMAX, as well as a comparative capacity evaluation. The authors find that LTE unicast control overhead is of 17% in DL and 9% in UL, while the WIMAX 802.16m presents 11.2 % and 9.23 % of control overhead respectively, but considering bandwidths of 80 MHz. With these estimated overheads, their system level evaluations show that the number of users per sector and the number of possible video channels are similar for both technologies.

We will hereafter concentrate on a more PMR oriented capacity analysis, considering video streams possible in PMR scenarios. The analysis is performed using only the smallest LTE bandwidths, that are suitable to PMR

⁹In the standard given table, i corresponds to N_{PRB} , i.e. the number of frequency PRBs allocated to that specific TBS.

¹⁰Here, N_{BW} denotes the maximum number of PRBs that can be allocated to the user, i.e. the BW size. For example, in LTE, the BW of 1.4 MHz corresponds to 6 PRBs in the frequency domain.

networks. For the evaluation of the video capacity of LTE, we have used the resource allocation algorithm as given in the 3GPP standard, without any modifications. We consider that no modifications are necessary since LTE is designed as a data transmission system. The standard algorithms and given numbers are believed to be favorable to high throughput applications. For the transmission scenario, the same assumptions as for the voice transmission will apply, i.e. all users are under a single PMR cell coverage and will receive and answer to video group calls. Also, all control channel parameters have been already negotiated and established by the network, and their influence on network capacity is outside the scope of this chapter's discussion.

We suppose that a SVC video coder is used here for video communications, e.g. H.264. The SVC characteristic refers to the possibility of transmitting the video layer by layer. In the case of a quality scalability, also assumed here, the first layer (called base layer) transmits the lowest quality images, containing essential information for the comprehension of the video message. The following layers enhance progressively the quality of the images, and thus, the quality of the video stream. In the scenario assumed here, the base layer will cover the entire PMR cell and will use the most robust MCS, and the next layers will cover users as they approach the eNodeB and less robust MCSs will be employed. Since the scenario supposes a group call (i.e. multicast), at least the base layer must be fully received by all users since there will be no retransmission mechanisms in case packets are lost. This most robust MCS will be configured so that the user having the worst channel conditions may receive it.

Hereafter, we describe the capacity estimation algorithm, step by step.

Step 1) Compute the packet length in number of bits per image, per transmission, P_{video} (one video image is transmitted per time transmission interval)¹¹. The video codec bit rate, R_{video} , is given in kbps and the frame rate is equal to $n_{images/s}$. P_{video} is equal to

$$P_{video} = 1000 \times R_{video} / n_{images/s}.$$

Step 2) Considering that one image is encapsulated in one IP packet and the header overhead has been compressed to the size of $H_{protocols}$, compute the percentage of useful video data as

$$p = \frac{P_{video}}{P_{video} + H_{protocols}}.$$

Step 3) Compute the video throughput (kbps), including video overhead as

$$T_{H+video} = \frac{R_{video}}{p}.$$

Step 4) Set modulation order, M , and system required code rate, $R_{scheduled}$, i.e. the system MCS as defined by the scheduler for the requested cell coverage and the desired video quality.

Step 5) Set air frame parameters as shown in "Algorithm for Voice": Steps 4 to 6.

Step 6) We suppose we are transmitting this video stream continuously for 1 second, i.e. in every sub-frame for 1000 sub-frames. The TBS is increased with the CRC bits. The new video bitrate (kbps) is computed at layer one output as

$$T_{layer-1} = \frac{T_{H+video}}{R_{scheduled}} + N_{CRC}.$$

Step 7) Compute the number of REs that would be occupied every second by this video stream as

$$N_{REs/video} = 1000 \times \frac{T_{layer-1}}{M}.$$

Step 8) Compute the occupied BW per second by this video stream as

$$N_{PRBs/s} = \text{roundSup}\left(\frac{N_{REs/video}}{1000 \times N_{REs/PRB}}\right).$$

Step 9) Compute the expected number of channel bits for this application

$$N_{ch} = N_{PRBs/s} \times M \times N_{REs/PRB}.$$

Step 10) Apply (2.1) as given in the 3GPP standard TS 36.101, Annex A.

¹¹This represents a simplified hypothesis, in real time transmission, the video throughput might fluctuate.

Step 11) With the newly obtained value of TBS, $TBS_{standardized}$, calculate what would be the new video bit rate if this $TBS_{standardized}$ is used as the constant packet size for video transmission for every sub-frame during 1 s,

$$R_{video}^{max} = p \times TBS_{standardized}.$$

This algorithm will compute the TBS value necessary for the continuous transmission of this video stream. R_{video}^{max} represents the maximum video codec rate achievable if the chosen TBS were fully used for video transmission, i.e. no padding bits employed. In other words, for the network scheduled transmission packet, this value indicates what is the optimum video codec rate to maximize spectral efficiency, or minimize resource loss. This algorithm will be used in section 2.7 for evaluating the video transmission and capacity over LTE.

2.7 Theoretical Analysis and Results

Considering the above explained algorithms and conditions, we have computed the realistic LTE voice and video capacity in two bandwidths of interest for the PMR: 1.4 MHz and 3 MHz, for both DL and UL. Further, we compared the computed LTE DL voice spectral efficiency in the smallest of the used bandwidths, 1.4 MHz, with PMR and GSM radio networks for an objective analysis.

2.7.1 LTE Voice Capacity Evaluation

The capacity is computed for two deployment bandwidths, N_{BW} : 1.4 MHz and 3 MHz, which are interesting for PMR. The chosen voice coder is the AMBE 2.45 kbps. For the same air frame overhead, we are comparing the obtained capacities using two possible protocols overheads: one realistic ROHC compressed overhead and one theoretical ideal overhead.

The realistic overhead is computed considering the minimal possible values given by the 3GPP standard:

- the ROHC protocol compresses the IP overhead as low as 3 bytes,
- the RLC layer is set in unacknowledged mode (UM), the minimal header value is of 1 byte,
- the PDCP header is equal to 1 byte; it does not contain any length indicator and the RLC is in UM,
- the MAC header is equal to 1 byte; we suppose that only one service data unit (SDU) is transmitted using one logical channel, and no supplementary control bits are considered.

The theoretical ideal overhead is defined as the minimum value that can be obtained if the voice transmission mechanisms were to simulate circuit-switched channels. The ROHC compressed overhead should descend to its minimum acceptable value (1 byte), and the PDCP, RLC and MAC headers would be unnecessary.

The TBS and radio allocations are computed as explained above for a necessary MCS identified as being QPSK 1/3. It has been shown in EADS Cassidian studies that, for LTE to match PMR cell coverage in voice broadcast, an MCS of QPSK 1/3 is necessary for a single-input single-output (SISO) antenna configuration, and a signal to noise ratio (SNR) equal to 2dB. We suppose a single cell configuration, with zero neighboring interferer. Users are mobile inside the pre-defined cell coverage.

The radio frame overhead does not include the following channels: the primary synchronization signal, the secondary synchronization signal and the physical broadcast channel in DL; and the physical random access channel in UL. We evaluate the capacity considering the extended cyclic prefix for the OFDM and SC-FDMA symbols.

The voice capacity evaluation is given in table 2.1 for DL and for UL, considering specific simulation configuration parameters. Table 2.1 also gives the effective speech code rate, defined as

$$R_{audio} = \frac{TBS_{necessary} - H_{protocols}}{N_{ch}}. \quad (2.3)$$

Layer one code rate is written as

$$R_{layer_1} = \frac{TBS_{standardized} + N_{CRC}}{N_{ch}}. \quad (2.4)$$

We note that LTE voice capacity is very sensitive to several elements:

- the large protocol stack overhead, as the higher layer's overhead and the physical layer's CRC may

Table 2.1
LTE PMR voice capacity in DL and UL.

System parameters	Computed values	Realistic values	Ideal values	
Voice encoder AMBE	$R_{vocoder}$ (bps)	2450		
	T_{voice} (ms)	20		
	P_{voice} (bits)	49		
Transmission protocols (bytes)	RTP + UDP + IP	40	40	
PDCP ROHC compression (bytes)		3	1	
PDCP header (bytes)		1	0	
RLC header (bytes)		1	0	
MAC header (bytes)		1	0	
Higher layer overhead (bytes)	$H_{protocols}$	6	1	
Necessary LTE TBS (bits)	$TBS_{necessary}$	97	57	
Overhead percentage	$H/TBS_{necessary}$	49.5 %	14%	
TBS for QPSK 1/3 (bits)	$TBS_{standardized}$	104	72	
PHY CRC (bits)	N_{CRC}	24	0	
LTE DL, $S_{OFDM} = 12$, $N_{pilots} = 12$.	1.4 MHz, $C_{OFDM} = 4$	N_{ch}	336	168
		R_{audio}	0.15	0.29
		$R_{layer-1}$	0.38	0.43
		N_{PRB}	2	1
		N_{BW}	6	
		Number users per sub-frame	3	6
	Number users per 20 ms sub-frame	60	120	
	BW > 1.4 MHz, $C_{OFDM} = 3$	N_{ch}	384	192
		R_{audio}	0.13	0.26
		$R_{layer-1}$	0.33	0.38
		N_{PRB}	2	1
	3 MHz	N_{BW}	15	
		Number users per sub-frame	7	15
		Number users per 20 ms sub-frame	140	300
	LTE UL, $N_{pilots} = 2$.	In every BW	N_{ch}	480
R_{audio}			0.10	0.20
$R_{layer-1}$			0.27	0.30
N_{PRB}			2	1
1.4 MHz, $C_{PRBs/PUCCH} = 1$		N_{BW} for data	5	
		Number users per sub-frame	2	5
		Number users per 20 ms sub-frame	40	100
3 MHz, $C_{PRBs/PUCCH} = 2$		N_{BW} for data	13	
		Number users per sub-frame	6	13
		Number users per 20 ms sub-frame	120	260

represent more than 50 % of the total frame size for an average ROHC compression,

- the reduced choice of small TBS, as the 3GPP proposes some few small TBSs for low bit rate applications,
- the radio allocation, as the standard imposes the allocation of a minimum of a PRB pair per user, which is large for low bit rate voice coders using a high order modulation, e.g. 64 QAM,
- the radio frame overhead, which is quite consistent in the smallest frequency bandwidths.

The 3GPP proposes the ROHC protocol for RTP/UDP/IP typical header compression for multimedia applications as video and speech. In public mobile systems, the speech packets are computed on high quality vocoders as AMR at 12,2 kbps, therefore the resulted speech frame will be equal to 32 bytes. The ROHC can compress the overhead, but it is a negotiation protocol, it will continuously change its status from very stable (3 bytes) to unstable (40 bytes). Using low bit rate vocoders, the PMR systems can not tolerate these large overheads. The usual voice bit rate is around 5 kbps, with a future target bit rate of 2,4 kbps. An overhead of 9 bytes (72 bits) will represent 59 % of the transport block size to be transmitted at the physical layer with only 52 bits of speech. The higher layer overhead clearly occupies a large percentage of the frame sent on the air interface and ROHC is not efficient enough as a header compression protocol. For PMR voice communications, the IP protocol, even though a desirable solution in the core network, it will not be efficient on the radio link.

LTE is not yet optimized for the usage of small voice packets, i.e. low bit rate voice coders. Our results show that it is difficult to choose the closest TBS value necessary for the small voice packet. This means that the closest TBS is considerably larger than the needed size for the useful voice bits. Important resources would be wasted if it were chosen for transmission on the air frame given the PMR context.

Radio resources allocation strategy is not optimized either, since a minimum of one PRB pair must be reserved for each user. Our results show that two PRB pairs are necessary for AMBE voice frames with protocol overhead. But even if we are considering a very robust MCS, as QPSK 1/3, these two PRBs contain a notable amount of dummy bits in this case. It would be even less suitable when considering higher order modulations. However, voice aggregation is possible¹² in order to try to enhance transmission efficiency, but it depends on system constraints and maximum tolerable audio delay.

Regarding the air frame overhead, the performances may be restrained because of a limited PDCCH capacity (2 to 6 users are addressed per control channel per sub-frame in the 1.4 MHz bandwidth). But using persistent or semi-persistent allocation allows one PDCCH field to reserve user resources for a certain number of incoming sub-frames, as shown in [24]. This may be interpreted as a "virtual voice circuit" establishment. Therefore, even though LTE capacity depends on the number of OFDM symbols assigned to control channels and also to pilot signals, we do not consider the air frame overhead as an obstacle for voice communications.

The theoretical analysis shows that by adjusting the protocol overhead only to lower values closer to "ideal" percentages, the LTE capacity can almost double in a PMR use case. Nevertheless, these values have been computed with some adjustments to the standard allocation algorithm. Therefore, it would be necessary for a future release to envisage a larger choice of TBSs dedicated to low bit rate applications and applicability to PMR use cases. Naturally, a more flexible allocations of air resources, i.e. PRBs, in a more trunked allocation perspective would also contribute to increasing the voice spectral efficiency. Of course, changing the values for TBSs and radio allocations would also mean defining new MCSs and eventually even UEP specific components for a more suitable and efficient voice transmission. The UEP perspective would allow a better partition of the channel protection between the different sensitivity layers of the voice packet.

2.7.2 LTE Video Capacity Evaluation

We are considering the transmission of one video stream during one second, and in each sub-frame. The total data stream buffered for 1 second's transmission is firstly split in the number of corresponding packets, with one packet corresponding to one video image. Each video image is transmitted per IP packet and per time transmission interval (1 ms). The higher layer overhead is considered for each packet, being quite insignificant due

¹²Voice aggregation means voice frames concatenation.

to the image large packet size. At the physical layer, this data unit is transmitted using one TBS corresponding to the scheduled MCS. Therefore, no segmentation is performed by the MAC layer. Table 2.2 gives an overview of the necessary static allocation for the transmission of different video bit streams for the three bandwidths of interest in DL and UL respectively.

Table 2.2
LTE PMR video capacity in DL and UL.

System parameters	Computed values	Stream 1	Stream 2	Stream 3		
Video bit-rate (kbps)	R_{video}	64	300	700		
Frame rate (images/s)	$n_{images/s}$	20	25	25		
Transmission protocols (bytes)	RTP+UDP+IP	40	40	40		
PDCP ROHC compression (bytes)		3	3	3		
PDCP header (bytes)		1	1	1		
RLC (UM) header (bytes)		1	1	1		
MAC header (bytes)		2	2	2		
Higher layer overhead (bytes)	$H_{protocols}$	7	7	7		
Modulation and coding scheme		QPSK 1/3	64 QAM 1/3	64 QAM 1/3		
PHY CRC (bits)	N_{CRC}	24	24	24		
LTE DL, $S_{OFDM} = 12$, $N_{pilots} = 12$.	1.4 MHz, $C_{OFDM} = 4$	$TBS_{standardized}$	72	600	1544	
		Padding bits %	19.64	2.98	13.57	
		$R_{layer-1}$	0.29	0.62	0.62	
		N_{PRB}	2	2	5	
		R_{video}^{max} (kbps)	70.76	597.21	1540.92	
		N_{BW} for data	6			
	BW > 1.4 MHz, $C_{OFDM} = 3$	$TBS_{standardized}$	104	600	1224	
		Padding bits %	29.69	15.10	5.47	
		$R_{layer-1}$	0.33	0.54	0.54	
		N_{PRB}	2	2	4	
		R_{video}^{max} (kbps)	102.21	597.21	1221.56	
	3 MHz	N_{BW} for data	15			
		Number users per sub-frame	3	3	1	
	LTE UL, $N_{pilots} = 2$.	In every BW	$TBS_{standardized}$	144	840	1736
			Padding bits %	43.75	32.08	24.38
$R_{layer-1}$			0.35	0.60	0.61	
N_{PRB}			2	2	4	
R_{video}^{max} (kbps)			141.52	836.10	1732.53	
1.4 MHz, $C_{PRBs/PUCCH} = 1$		N_{BW} for data	5			
		Number users per sub-frame	2	2	1	
3 MHz, $C_{PRBs/PUCCH} = 2$		N_{BW} for data	13			
		Number users per sub-frame	6	6	3	

Contrary to the speech transmission case, the video transmission is not affected by the overhead size. The higher layer protocols represent a small percentage of the video packet size. But, as can be seen for the lowest bandwidth transmissions, the number of users is still not important. This is a consequence of the LTE scarce resource availability in these small bandwidths, due to the radio control overhead. We also have to note that, if the useful data does not completely fit into the defined TBS considering the MCS, padding bits may be added

for the frame to correspond to the radio allocation. As we have considered a static video allocation, the video bit stream is uniformly split between the 1000 sub-frames (one video image per millisecond). We suppose that the video bit rate remains constant for at least 1s. This is a simplified theoretical hypothesis, since, for real transmissions, the video throughput fluctuates. The padding bits may vary up to 50% of the transport block in some cases precisely because the TBS is not filled with useful video bits.

We note that if the TBS is used at its maximum capacity, the number of necessary sub-frames might as well be reduced by half compared to the initial transmission, and the capacity in number of users may increase considerably. But this also means that video streams must be buffered and the video rate would become decorrelated with the physical layer rate, which should be further analyzed in real time PMR transmission systems. This is illustrated by the values of R_{video}^{max} in Table 2.2. This new maximum video rate is computed by taking the hypothesis that the $TBS_{standardized}$ is completely filled with video bits for every sub-frame, and no dummy bits are necessary. We note that the transmitted video rate may double. This highlights our previous remark concerning low bit rate applications, which is also validated here. LTE is designed for high rate applications where the MAC PDU segmentation is used for an efficient filling of TBSs, and when considering low throughput transmissions, the system becomes inefficient. This spectral inefficiency is not desirable in PMR systems, where bandwidths' availability is one of the key issues.

Of course, one may consider high video rate transmission over LTE. But a real mission critical LTE standard requires the flexibility of switching between the high rate perspective and the large number of users perspective. For example, in a disaster scenario, the system capacity in terms of number of users would be privileged over the high quality videos. Any user should be provided a network access for emergency calls. These emergency calls may come under the form of short real-time videos captured at the disaster scene. Therefore, a good control on the type and nature of video streams is necessary, and the manner in which the physical layer exploits their characteristics must be optimized for a very good system efficiency.

2.7.3 LTE Voice Spectral Efficiency

In this section, we compute the DL LTE voice spectral efficiency and compare it to existent PMR and GSM respective efficiencies. We evaluate the system maximum capacity and efficiency in terms of simultaneous calls or Erlangs per MHz and per cell. The evaluation in number of bits per Hz per cell is given as well, but this perspective applies mostly for data transmission systems. However, these numbers give an interesting insight on the radio resources allocations.

We are interested in evaluating the maximum number of simultaneous communications, since, in a PMR system, all users or groups of users may communicate simultaneously. Contrary to public systems, where the call arrival according to a Poisson distribution applies, public safety networks must be dimensioned for disaster situations. PMR users do not necessarily access the network progressively, but rather simultaneously. Also, in public networks, when a larger number of users than the network capacity try to access the network, the system is saturated and may shut down. On the contrary, the PMR system's shut down is not acceptable. In these public safety networks, call priority handling is applied. If the number of incoming calls is superior to the network capacity, the highest priority calls will be given network access, in the decreasing order of their respective priority.

Table 2.3 gives the PMR and GSM voice spectral efficiencies, calculated considering EADS Cassidian documents, theoretical numbers given in [26], and also the LTE spectral efficiency results obtained using the proposed algorithm. We suppose that we are comparing the performances of the different technologies during 1 second (1 call lasts 1 second). Also, for a fair comparison, all technologies are deployed in a bandwidth of $\Delta_{f-BW} = 1.4$ MHz. However, since it is unusual to compare circuit switched technologies performances with packet switched ones, we only consider special LTE cases, for which the hypotheses are clearly stated.

The common PMR, GSM and LTE hypotheses and parameters are the following:

- voice coders: AMBE 2.45 kbps, ACELP 4.6 kbps, RPELTP 6 kbps, AMR 12.2 kbps, as specified in Table 2.3,
- radio access: FDD for each of the presented technologies, with different possible TDMA slots, T_{TDMA} , per frequency carrier.

For PMR and GSM only, we suppose:

- one channel, δ_f , denotes the reserved frequency bandwidth per time slot during one communication (or one call),
- the air throughput remains constant in kbps independently of the communication because only one channel coding rate and one modulation are used.

For packet switched LTE, we consider:

- $H_{protocols}$ of 6 bytes and N_{CRC} of 24 bits,
- DL $\Delta_{f-BW} = 1.4$ MHz bandwidth configuration, i.e. $S_{OFDM} = 12$, $N_{pilots} = 12$ and $C_{OFDM} = 4$,
- QPSK modulation with 1/3 coding rate;
- one transmission channel bandwidth, δ_f , is represented by the reserved frequency blocks ($180 \times N_{PRB}$ kHz, with $N_{PRB} = 2, 4, 6$) per sub-frame for the duration of the communication (either dynamic or persistent allocation),
- even if LTE has 6 PRBs in 1.4 MHz, if one user needs N_{PRB} and N_{PRB} is not a divisor of 6, we suppose only 6 divided by N_{PRB} such users may be scheduled in this BW,
- each user transmits a new encoded voice frame after T_{voice} milliseconds, this periodicity is supposed to be equal to the TDMA transmission value for LTE, T_{TDMA} .

In Table 2.3, we first consider the absolute channels capacity per carrier, i.e. the number of maximum simultaneous calls or Erlangs per $\Delta_{f-BW} = 1.4$ MHz, as

$$\lambda = \frac{\Delta_{f-BW} \times T_{TDMA}}{\delta_f}. \quad (2.5)$$

The TETRA system can expect a number of 224 simultaneous calls in a 1.4 MHz bandwidth, compared to the TETRAPOL 112 to 140, 56 calls for GSM, and only 20 to 60 calls for LTE in the same 1.4 MHz bandwidth. The LTE capacity is significantly lower than GSM and PMR capacities. But these numbers represent the estimation of the maximum Erlang capacity per system if the entire bandwidth $\Delta_{f-BW} = 1.4$ MHz were used for one radio cell only.

In a real deployment scenario, the bandwidth $\Delta_{f-BW} = 1.4$ MHz is divided between a certain number of radio cells, which form a radio cluster. Every radio cell of the cluster uses a fraction of the bandwidth Δ_{f-BW} which is not re-used in another cell of the same cluster. This avoids significant interferences between neighboring cells. The number of radio cells from a cluster is quantified by the frequency reuse factor, which is specific to every radio system and can be computed using the minimum value of the carrier to interference ratio, C/I . In PMR systems, the minimum C/I value is obtained considering the minimum level of performances at cell edge. For speech communications, this is typically estimated as equal to 1 to 2 % of frame error rate (FER) for the first class bits, which have to be very well protected.

In the LTE case, the reuse factor is considered to be equal to 1 for data transmission. But for future speech communications, a larger reuse factor will be introduced in order to avoid considerable interferences between neighboring cells. For example, the reuse factor might be translated in a real deployment scenario in a fractional frequency reuse. The fractional frequency reuse would allow the allocation of different PRBs from the same radio channel to different users from neighboring cells. However, the radio dimensioning techniques are outside the scope of this chapter, and we will only perform a theoretical evaluation of the LTE reuse factor in order to evaluate its impact on the final voice capacity.

Following the recommendations of [26], we can evaluate the reuse factor for LTE if it were used as a PMR technology. The reuse factor, N_{RF} , is computed as

$$N_{RF} = \frac{1}{3} \left(6 \times N_{LI} \times \left(\frac{C}{I} \right)_D \right)^{2/\alpha}, \quad (2.6)$$

where α represents the propagation coefficient, N_{LI} denotes the system load, and $\left(\frac{C}{I}\right)_D$ the linear value of the estimated carrier to interference ratio in a dynamic environment. According to [26], the Okumura and Hata propagation model states that α varies between 3.34 and 3.57, for frequency ranges of 150 MHz to 900 MHz, and considering the mobile station antenna height of 1.5 m, for a base station antenna height of 30 to 50 m. Therefore, document [26] suggests $\alpha = 3.5$. The value of N_{LI} is estimated at 0.5. Also, the same document states that the fading degradation only can be estimated to 9 dB from the static C/I value.

But for real deployments, Cassidian studies also include the shadowing degradation. For a 90 % guaranteed service at cell edge, they estimate the shadowing margin to 10 dB. The same theoretical studies show that a SISO SNR of 2 dBs, i.e. $\left(\frac{C}{I}\right)_S$, is necessary for an LTE system to match the PMR radio coverage for speech transmission.

Therefore, the LTE reuse factor can be estimated as

$$N_{RF}^{(LTE)} = \begin{cases} \frac{1}{3} \left(6 \times 0.5 \times 10^{[(\frac{C}{I})_S + 9]/10}\right)^{2/3.5} = 2.65, \text{ including fading degradation,} \\ \frac{1}{3} \left(6 \times 0.5 \times 10^{[(\frac{C}{I})_S + 9 + 10]/10}\right)^{2/3.5} = 9.89, \text{ including fading and shadowing degradations.} \end{cases} \quad (2.7)$$

We can thus estimate the reuse factor of LTE for speech communications to almost 3, and in conditions with shadowing to almost 10.

For a fair comparison, the voice spectral efficiency of each of the different technologies can now be computed for the respective voice coders using their respective reuse factors, and reported in Table 2.3.

Table 2.3
LTE spectral efficiency comparison with PMR and GSM.

Technology	$R_{vocoder}$ (kbps)	δ_f (kHz)	T_{TDMA}	λ (Erlangs)	N_{RF}^a	Λ (Erlangs/MHz/cell)	SE_{voice} (bits/s/Hz/cell)
TETRA	ACELP 4,6	25	4	224	16	10	0.046
TETRAPOL 10kHz	RPCELP 6	10	1	140	12	8.32	0.05
TETRAPOL 12,5 kHz	RPCELP 6	12,5	1	112	12	6.66	0.04
GSM 900	AMR 12,2	200	8	56	9	4.44	0.054
LTE ^b	AMBE 2,45	2x180	20	60	1	42.58	0.104
					$3^{(F)}$	$14.28^{(F)}$	$0.035^{(F)}$
					$10^{(F+S)}$	$4.28^{(F+S)}$	$0.011^{(F+S)}$
LTE ^c	ACELP 4,6	4x180	30	30	1	21.43	0.1
					$3^{(F)}$	$7.14^{(F)}$	$0.033^{(F)}$
					$10^{(F+S)}$	$2.14^{(F+S)}$	$0.01^{(F+S)}$
LTE	RPCELP 6	4x180	20	20	1	14.28	0.086
					$3^{(F)}$	$4.76^{(F)}$	$0.03^{(F)}$
					$10^{(F+S)}$	$1.42^{(F+S)}$	$0.009^{(F+S)}$
LTE ^d	AMR 12,2	6x180	20	20	1	14.28	0.174
					$3^{(F)}$	$4.76^{(F)}$	$0.06^{(F)}$
					$10^{(F+S)}$	$1.42^{(F+S)}$	$0.017^{(F+S)}$

^aThe exponent F counts for fading only, while F+S count for both fading and shadowing.

^b2 PRBs per communication are assumed.

^c4 PRBs per communication are assumed.

^d6 PRBs per communication are assumed.

We compute the voice spectral efficiency in number of Erlangs per MHz and per cell as

$$\Lambda = \frac{\lambda}{N_{RF} \times \Delta_{f-BW}}. \quad (2.8)$$

The voice spectral efficiency, expressed in bits per second per Hz and per cell, i.e. from a pure data transmission perspective, can be estimated as well as

$$SE_{voice} = \frac{R_{vocoder} \times \lambda}{N_{RF} \times \Delta_{f-BW}} = R_{vocoder} \times \Lambda. \quad (2.9)$$

Table 2.3 presents the computed results in columns Λ and SE_{voice} respectively. The results show that the number of possible communications in LTE may be superior to those in PMR and GSM, but if a theoretical reuse factor of 1 is applied. Thus, for the same ACELP vocoder, we can expect 21.43 Erlangs/MHz/cell in LTE compared to the 10 Erlangs/MHz/cell in TETRA. The proportionality factor is also reported in the SE_{voice} column, with 0.1 bits/s/Hz/cell for LTE and 0.046 bits/s/Hz/cell for TETRA. LTE predicts the double of the TETRA capacity. The same factor can be roughly estimated when also compared to TETRAPOL for the RPELTP vocoder. The GSM capacity seems to be three times inferior to that expected in LTE for the same use of the AMR vocoder. We can regret however, that the use of a lower rate vocoder, i.e. AMBE 2.45 kbps, does not have a larger impact on the overall spectral efficiency. Even though its bitrate is almost six times smaller than that of AMR 12.2 kbps, the values of Λ and SE_{voice} do not improve by a factor of six. The voice throughput is too small for the LTE system to be efficient. This is visible especially in the δ_f column, where 2 PRBs are allocated for AMBE, and 6 PRBs are allocated for AMR. The factor of 6 between the vocoders' bitrates becomes a factor of 3 at the radio level, mainly due to the protocol overhead and the radio allocation granularity.

Even though LTE seems to present a rough capacity twice better than the PMR networks, the favorable reuse factor of 1 is predicted for system data transmissions only. For reliable voice calls, the real reuse factor must be used, and we have estimated this factor to 3 for normal fading conditions, and to 10 when shadowing is also considered. When using these new reuse factors, the spectral efficiency numbers from Table 2.3 change to a notably large extent. LTE becomes considerably less efficient compared to PMR and GSM.

For a reuse factor of 3, one can expect the LTE efficiency to be lower than that of TETRA and TETRAPOL 10, 12.5 kHz for their respective vocoders: 7.14 vs. 10 Erlangs/MHz/cell, and 4.76 vs 8.32, 6.66 Erlangs/MHz/cell respectively. LTE presents the same inferiority in spectral efficiency when measured in bits/s/Hz/cell. Only the use of AMBE might offer to LTE an efficiency equivalent to that of PMR. Nevertheless, the LTE 14.28 Erlangs/MHz/cell are disappointing compared to the already available 10 Erlangs/MHz/cell computed for TETRA. As for the AMR vocoder, the LTE presented efficiency of 4.76 Erlangs/MHz/cell seems quite equivalent to that of GSM of 4.44.

When considering the reuse factor of 10, the LTE spectral efficiency becomes catastrophic. The predicted LTE capacity is highly inefficient compared to either PMR or GSM. For an ACELP vocoder, the LTE efficiency is almost five times lower than that of TETRA. Even with the use of the very low rate AMBE vocoder, the LTE efficiency is lower than that of PMR systems. And compared to GSM, the LTE capacity seems almost four times lower.

Results from Table 2.3 show that, even if LTE seems optimized at a first glance, further investigations are required in order to conclude regarding its use with PMR networks. Already, by introducing the PMR vocoders and estimated reuse factors, the LTE behavior is surprisingly inefficient. Compared to existent PMR systems, its effectiveness is highly questionable and improvements must be included in future releases for the system to become more competitive.

2.8 Conclusion

This chapter has analyzed 2G and 3G PMR networks, as well as future broadband perspectives with a focus on the LTE candidate.

Both voice and video communications will become key features of future PMR networks. On one side, voice calls are the legacy of existent systems, essential to the professionals to which PMR networks are dedicated. And, on the other side, these systems are evolving to support new demands like video transmissions. Intended for professional use, in either public safety or industrial fields, the PMR must provide single and group-calls, in unicast and broadcast, and with priority handling. While low bit rate voice codecs are privileged as well as robust voice communications, video applications must comply with scalability issues and analytics techniques' requirements.

But one of the most important key issues for all of today's PMR systems is spectrum availability. Therefore, we have provided a thorough analysis of the LTE Release 9 possibilities regarding voice and video capacities, in both DL and UL. Although our analysis is only theoretical, we have proposed a multi-layer realistic system, considering the higher layer protocol overhead, the physical layer allocation parameters, as well as the radio frame overhead. We have also provided an objective comparison evaluation of the LTE DL voice spectral efficiency with existent PMR networks.

Our analysis shows that, in its current state, LTE is not a spectrally efficient candidate. Even though ROHC is an interesting compression protocol for video encapsulation, its generated overhead remains considerably large for PMR voice communications. Using IP does not seem as a plausible solution for the radio link transmission for these low bit rate applications. Moreover, the layer one packet allocation strategy, from the TBS choice to the radio PRB, together with their proposed MCSs, are highly inefficient and not adapted to small voice and video packets. LTE is not designed for neither low throughput voice calls nor low data rates video transmissions.

In the 3GPP proposed sphere of technologies, LTE is supposed to bring innovative and efficient solutions. Unfortunately, it is high throughput oriented only and it is not designed for low bit rate applications. In its current state, LTE is spectrally inefficient for small data rates and is not yet perfectly suitable to the PMR systems. An improved protocol stack would help reducing the current large overhead and improve the system raw capacity. Enhanced error protection techniques and modulation coding schemes, which consider voice and video characteristics, would allow a perfect compromise between the spectral efficiency and user perceived quality. And also, better radio allocation strategies, e.g. a lower granularity for the PRB allocation, would provide an increased flexibility for both small and large data transmission rates.

Bibliography

- [1] H. Ketterling, *Digital Professional Mobile Radio*. Artech. House. Inc, 2004.
- [2] J. C. D. Moore, "Projecting the technological evolution of the private land mobile radio services," in *IEEE 39th Vehicular Technology Conference*, vol. 1, May 1989, pp. 38–43.
- [3] T. Mousley and I. Wells, "Speech transmission in TETRA," in *IEEE Colloquium on Low Bit-Rate Speech Coding for Future Applications*, Dec. 1993, pp. 2/1 – 2/6.
- [4] E. Shearer, "TETRA - a platform for multimedia," in *IEEE Colloquium on Mobile Computing and its Applications*, Nov. 1995, pp. 5/1 – 5/4.
- [5] "Public safety statement of requirements for communications and interoperability, vol ii, v1.0," The SAFECOM Program Department of Homeland Security, Tech. Rep., Aug. 2006.
- [6] M. Nouri, V. Lotici, R. Reggiannini, D. Ball, and M. Rayne, "TEDS:a high speed digital mobile communication air interface for professional users," *IEEE Vehicular Technology Magazine*, vol. 1, pp. 32–42, Dec. 2006.
- [7] "EDGE, HSPA, LTE: Broadband innovation," 3G Americas, Tech. Rep., Sep. 2008.
- [8] F. Chiti, R. Fantacci, L. Maccari, D. Marabissi, and D. Tarchi, "A broadband wireless communications system for emergency management," *IEEE Communications Magazine*, vol. 15, pp. 8–14, Jun. 2008.
- [9] A. Durantini, M. Petracca, F. Vatalaro, A. Civardi, and F. Ananasso, "Integration of broadband wireless technologies and PMR systems for professional communications," in *IEEE Fourth International Conference On Networking and Services*, Mar. 2008, pp. 84–89.
- [10] "Mobile broadband in a mission critical environment - as seen from a TETRA perspective," TETRA Association, Tech. Rep., Feb. 2011.
- [11] S. Subik and C. Wietfeld, "Integrated PMR-broadband-IP network for secure realtime multimedia information sharing," in *IEEE International Conference on Technologies for Homeland Security*, Nov. 2011, pp. 20–25.
- [12] S. Borkar, D. Roberson, and K. Zdunek, "Priority access for public safety on shared commercial LTE networks," in *Technical Symposium at ITU Telecom World*, Oct. 2011, pp. 105–110.
- [13] "TS 22.278: 3GPP technical specification group services and system aspects, service requirements for the evolved packet system (EPS)," 3GPP, Tech. Rep., Sep. 2010.
- [14] "TS 36.213: 3GPP evolved universal terrestrial radio access (E-UTRA); physical layer procedures," 3GPP, Tech. Rep., Dec. 2009.
- [15] J. Liu, R. Love, K. Stewart, and M. Buckley, "Design and analysis of LTE physical downlink control channel," in *IEEE Vehicular Technology Conference*, Apr. 2009, pp. 1–5.
- [16] P. Hosein, "Resource allocation for the LTE physical downlink control channel," in *IEEE GLOBECOM Workshops*, Dec. 2009, pp. 1–5.
- [17] A. Larmo, M. Lindstrom, M. Meyer, G. Pelletier, J. Torsner, and H. Wiemann, "The LTE link-layer design," *IEEE Communications Magazine*, vol. 47, pp. 52–59, 2009.
- [18] D. Astely, E. Dahlman, A. Furuskar, Y. Jading, M. Lindstrom, and S. Parkvall, "LTE: the evolution of mobile broadband," *IEEE Communications Magazine*, vol. 47, pp. 44–51, Apr. 2009.
- [19] "TS 23.272: 3GPP technical specification group services and system aspects, circuit switched (CS) fall-back in evolved packet system (EPS), stage 2," 3GPP, Tech. Rep., Sep. 2011.

- [20] “TS 24.173: 3GPP technical specification group core network and terminals; IMS multimedia telephony communication service and supplementary services, stage 3,” 3GPP, Tech. Rep., Sep. 2011.
- [21] “TS 29.280: 3GPP technical specification group core network and terminals; evolved packet system (EPS); 3GPP Sv interface (MME to MSC, and SGSN to MSC) for SRVCC,” 3GPP, Tech. Rep., Sep. 2011.
- [22] “Voice over LTE via generic access; requirements specification; phase 1,” VoLGA Forum Technical Specification, Tech. Rep., Jun. 2009.
- [23] S. Gavrilovic, “Standard based solutions for voice and SMS services over LTE,” in *Proceedings of the 33rd International Convention MIPRO*, May 2010, pp. 334–339.
- [24] J. Puttonen, H. Puupponen, K. Aho, T. Henttonen, and M. Moisio, “Impact of control channel limitations on the LTE VoIP capacity,” in *IEEE Ninth International Conference on Networks*, Apr. 2010, pp. 77–82.
- [25] O. Oyman, J. Foerster, Y. Tcha, and S. Lee, “Toward enhanced mobile video services over WiMax and LTE,” *IEEE Communications Magazine*, vol. 48, pp. 68–76, Aug. 2010.
- [26] “Methodology for the assessment of PMR systems in terms of spectrum efficiency, operation and implementation,” European Radiocommunications Committee (ERC) Report 52, European Conference of Postal and Telecommunications Administrations (CEPT), Tech. Rep., Dec. 1997.

Chapter 3

Progressive Hierarchical Turbo Codes

Abstract — Private or Professional Mobile Radio (PMR) technologies are expected to migrate to broadband technologies in the near future. However, public standards, such as Long Term Evolution (LTE), do not comply with the harsh requirements of public safety, where the radio efficiency is an absolute necessity. While the need for higher data rates for higher definition voice or video are clearly expressed in the field, the network provider can not underestimate the importance of system capacity in critical situations. Thus, the number of communications must be maximized such as the spectral resources be fully exploited for an optimal user perceived voice/video quality. Channel coding can be considered as one solution that could provide an optimal compromise between channel capacity and source characteristics. In this chapter, we have thoroughly investigated channel coding techniques that can comply with both broadband technologies and PMR constraints. As such, turbo codes have been identified as next generation coding techniques. Already included in third generation radio networks, they are considered, undoubtedly, the milestones of broadband technologies. Combined with the PMR feature of unequal error protection, turbo codes might gain the potential to become an efficient PMR broadband milestone. Therefore, in this chapter, we propose a new turbo encoding perspective, which considers the prioritizations of information bits. We introduce a new mechanism for embedding unequal error protection into turbo codes, through the multi-level hierarchical encoding of source provided data. An overall embedded unequal error protection is obtained, where each family of bits is provided a level of redundancy proportional to its defined characteristics. The idea consists in inserting new raw streams of data progressively, in the encoding process, and at each new encoding level. The concept can be declined for both parallel and serial turbo codes, and existing techniques, e.g. puncturing, can even be envisaged as supplementary elements. The chapter firstly presents a detailed analysis of the encoder and decoder for the particular case of two families of bits, whose channel protection requirements are different. The maximum a posteriori (MAP) and maximum likelihood (ML) duality is investigated, and the Bahl-Cocke-Jelinek-Raviv (BCJR) algorithm is mathematically developed for a better comprehension of the existent hidden redundancy. Further, we present the straightforward generalization of this concept, to an infinite number of different codes and transmission rates for an infinite number of family bits. The code characteristics are graphically explained through factor graphs, mathematically detailed using weight error functions representations, and the virtual transmission rates and pilot insertion code relatedness are investigated. Finally, the code behavior is evaluated using several benchmark turbo codes over two different platforms. Each platform has its own advantages and disadvantages, and is based, in one case, on random elements, and, in the second case, on LTE specific elements. The results are given for both additive white Gaussian noise (AWGN) and Rayleigh channels and provide an effective overview of the code performances.

3.1 Turbo Codes & UEP Enhancements

For the last fifty years, significant effort has been made in improving coding schemes that could approach channel capacity, as defined by Claude Shannon in 1948. But with the discovery of turbo codes in the 1990's, the re-discovery of low-density parity-check (LDPC) codes, the invention of fountain codes, Shannon's channel capacity was finally achieved [1]. But in recent years, turbo codes have gained considerable notoriety and have been included in various telecommunications standards. They are currently used for channel coding in a large variety of networks, and are considered as key elements for the next generation broadband mobile networks as

well.

However, these next generation radio technologies are expected to deliver higher bit rates, and the number of subscribers is believed to increase. In this context, one must consider effective transmission mechanisms for an optimum use of the available radio spectrum. Although envisaged in public radio networks, the user quality perspective seems nevertheless privileged. On the contrary, in Private/Professional Mobile Radio (PMR) systems, spectrum efficient use becomes a critical requirement. Here, even though the end-user perceived quality is controlled, the network architecture engineering focuses especially on the network effectiveness.

Unequal error protection (UEP) mechanisms represent one interesting solution worth investigating. As it has been widely discussed in literature, UEP schemes have been long considered as the best compromise between the user perceived signal quality and the use of radio resources. The UEP philosophy is quite simple, yet very effective, and is based on the fact that every bit of every frame of either voice or video streams is different. This difference is quantified when the corresponding signal is reconstructed at the receiver. By measuring the impact of every single bit and its associated error on the end-user perceived quality, we may define what is commonly known as *bit sensitivity*. The higher the bit sensitivity to errors, the more important this bit becomes for the good reconstruction of the signal, since damaging it would imply irreversible reconstruction errors. Therefore, if we envisage to preserve the radio spectrum for an effective use, we can simply not afford using an uniform error protection, unrelated to sensitivity characteristics. It becomes only natural to provide a better channel protection to more sensitive bits than to their counterparts, the less sensitive ones.

The UEP concept is especially known for its effectiveness in the Global System for Mobile communications (GSM) speech transmission [2]. The voice coder incoming data is divided into several groups of bits called "classes". Each class has a different pre-defined importance in the reconstruction of the audio signal, and, therefore, a proportional sensitivity to channel errors. The voice frame bits are divided into three classes: 1a, 1b and 2. Class 1a regroups most important bits, essential for voice reconstruction. The bits in class 1b are defined as less important than those of class 1a. And class 2 is the least important class. New generation radio mobile technologies need not only UEP and good performance channel coding, but also flexible coding rates and real-time adaptable structures for system configurations. Designed to meet different throughput requirements, a flexible multirate encoder is presented in [3]. Multiple services with different quality requirements can be multiplexed in one frame, along with control information. Also, the rate is variable on frame by frame basis. The transmission system is modeled as a serial concatenation of codes and interleavers, but no turbo concepts are applied and UEP for a single user service is not discussed.

In this section, we will be investigating the UEP mechanisms used with turbo codes, but we will also survey the different architectures for multiple or hybrid turbo structures. These latter perspectives are interesting for their adaptability and flexibility to system constraints, e.g. a predefined number of classes of bits.

In 1967, Masnick and Wolf propose for the first time linear UEP codes and the theory of UEP codes [4]. They achieve UEP using one code only, rather than separate codes for each protection level. These linear UEP codes assign a different error protection level to each digit of the transmitted code words. At the receiver, the digits with a higher protection than the average are correctly decoded. The authors also highlight that computing the average probability of error for a code word is not satisfactory in this situation since all errors are weighted equally; therefore the errors must be computed on individually UEP coded digits. Later on, an information theoretic perspective on UEP is developed in [5], where the differences between bit-wise and message-wise UEP are highlighted. The "bit-wise" UEP provides a better protection to only a subset of bits from the data frame. Thus, the probability of one of these bits being false is smaller than in other subsets of bits. "Message-wise" UEP refers to protecting one particular set of bits. Their bad decoding would engender the transmission of some other bit sequence.

UEP can become a very powerful tool when used with powerful codes. Embedding UEP in the excellent turbo codes can prove very performing for future mobile technologies for both end-user and network operator. An appropriate design and use of turbo UEP may translate into better spectral efficiency. The consequences can be materialized into higher bit rates, or a larger user capacity, or even an improved end-user perceived quality.

Turbo codes have firstly been investigated by Berrou et al. [6], as parallel concatenated convolutional codes (PCCC). Benedetto et al. introduced serial concatenated convolutional codes (SCCC) [7]. Turbo codes' behavior and performances have been abundantly analyzed in the scientific literature [8], [9]. A careful overview

on parallel and serial encoding and decoding is given in [8], and the soft-input soft-output (SISO) theoretical aspects are discussed. Forney is reminded as the father of concatenated codes. In the mid 1960's, he proposed concatenating short codes to obtain long codes. Their decoding complexity is solved "by breaking the required computation into manageable segments according to the divide and conquer strategy", concept very much proven by the turbo decoding algorithm performances. P. A. Regalia and J. MacLaren Walsh identify in [10] the mathematical duality between two characterizations of the turbo decoder, one related to the Bethe approximation, the second involving constrained likelihood estimation. Both methods highlight the existence of the dependence and correlation between the different quantities turbo decoded. This becomes mostly obvious when analyzing the forward and backward recursions from the Bahl-Cocke-Jelinek-Raviv (BCJR) algorithm. In [9], H. Jin and R.J. McEliece prove the goodness of turbo code ensembles. They find that the average maximum-likelihood decoder block error probability approaches zero at least as fast as $n^{-\beta}$, where n is related to the size of the encoded frame, and β refers to the interleaver gain exponent, firstly defined by Benedetto et al. in 1996 [11]. It is widely accepted that the interleaver size is a key element in the turbo decoder convergence behavior.

In [12], the SCCC has been proven to often yield superior performances to those of PCCC, particularly for low bit error probabilities where the error floor is absent. The iterative maximum a posteriori (MAP) decoding for two SCCC types is analyzed in [13]. In one case, only the parity bits of the outer encoder are fed to the inner encoder. And, in the second case, both the systematic and parity bits are encoded a second time by the inner encoder. Through this second test, authors prove the benefits of having concatenated the overall information before interleaving and encoding by the inner encoder. The sequence minimum weight is increased and the interleaver gain is improved. Therefore, it is proven that it is better to interleave all encoded or external incoming information before the inner encoding. It thus becomes clear that a large incoming code block and a larger interleaver will benefit the turbo decoding convergence behavior.

The use of UEP with turbo codes has been intensively discussed in literature, although it rarely supposed modifying the encoder's structure. We have identified several families of turbo codes, which employ the concepts of UEP.

The first family of UEP turbo codes is represented by turbo codes using pruning, puncturing and interleaving techniques to achieve UEP. Many works have considered UEP PCCC structures [14–18], or UEP SCCC structures [19–22]. SCCC using puncturing techniques are mostly referred to as rate compatible punctured SCCC. Puncturing is used as a supplementary element which modifies the default SCCC transmission rates. In [14–16], pruning or puncturing are used to obtain UEP. In [17], interleaving and puncturing together are proposed. The authors develop interleavers that permute the bits within the same protection level. UEP is necessarily obtained with three types of puncturing in [17] and with non-uniform puncturing patterns in [15], [18]. This first family's main characteristic is that additional techniques, like pruning and puncturing, are used to modify the encoder's output rate and thus to obtain UEP. The turbo code itself is only an equal error protection (EEP) code.

The second family of UEP turbo codes is represented by the hybrid architectures. In [23], an interesting code design is proposed, even though the performed decoding is not turbo. Multilevel coset or superimposed codes with UEP and multistage Viterbi decoding are discussed. The two levels convolutional codes (CC) based on the $|u|u+v|$ construction are shown to be a special case of the generalized concatenated (GC) codes. Two and three stage Viterbi decoding are detailed. After each stage, different importance bits are recovered. Nevertheless, this solution is not an embedded UEP solution. The different priority bits, u and v , are encoded using independent encoding branches. UEP is achieved for the most important bits, u , through their double transmission only after encoding, i.e. u is transmitted alone and together with v as $u+v$. Frey and MacKay introduce irregular turbo codes in [24], but only by using PCCC. The SCCC case was not considered. In [24], all bits are encoded by the upper encoder, then each subframe of degree of importance, d , is repeated d times before being interleaved and lower encoded. The overall encoding rate is proportional to the average degree of importance of the respective bits. Irregular turbo codes give better performance than classical turbo codes. The authors observe that the more protected bits can improve the decoding of the remaining bits. This concept is adapted to UEP in [25]. All bits are repeated proportionally to their degree of importance, before being interleaved together and fed to a PCCC. Thus, for these irregular turbo codes, UEP is obtained only by repeating the bits an integer number of times before the inner turbo encoding. The higher level importance bits benefit of only an additional repetition code, compared to the less important bits.

Multiple turbo codes, defined as PCCCs [26] or SCCCs [27] with multiple constituent codes, form a different family of turbo codes. The main advantage of multiple codes is the use of two or more interleavers between constituent codes. The probability of breaking the error blocks is thus increased. In addition, various decoding strategies are possible allowing a better adaptability to the encoder's design and to system constraints. Multiple extrinsic information streams may be differently combined. In [28], authors have shown that the simultaneous transferring of information to the other two MAPs out of the three is the optimum method for more efficient turbo decoding. The authors called this extended serial decoding. But in all [26]- [28], no UEP has been designed.

Fully exploiting the multiple turbo codes concept, woven convolutional codes come closer to embedding UEP in turbo codes. Jordan et al. propose a two level serial concatenation of codes [29]. Both inner and outer encoders, i.e. outer-inner warp, are multiple parallel codes. The data is first reorganized into several strictly equal sized subblocks. Each subblock is encoded by a parallel constituent outer encoder. Then, the whole frame is interleaved, before being split into strictly equal sized subblocks again. Each subblock is further encoded by a parallel constituent inner encoder. The decoding is performed using a windowed turbo algorithm [30]. Each subblock of data is thus decoded by a two levels turbo only. UEP is considered in [31–33]. In [31], different rates are assessed to different parallel constituent outer encoders. The UEP encoded frame is interleaved and encoded by only one inner constituent encoder. In [32], a simplified woven structure performs UEP on both information and code symbols. The input active-distance slopes are compared for non-encoded and encoded data in the outer warp. The output active-distance slopes are given for two different parallel constituent encoders of the inner warp. The authors conclude that a larger free input or output distance is obtained when using stronger codes. UEP simulation results are presented in [33]. UEP is obtained in the outer warp with two different rates parallel constituent encoders.

Multifold coding discussed in [34] presents improved error performance results for a three level PCCC. The original data frame is split into three subframes which are concatenated two by two and each combination encoded by one recursive systematic convolutional (RSC) encoder after a possible pseudorandom interleaving. The multiple estimates of information bits give more reliable decoding decisions, by using three independent decoding branches which exchange extrinsic information regarding common decoded data. The concept is cleverly adapted for UEP in [35] for image transmission. The most important data segment is encoded not only two times, but also concatenated to the third segment's combination before RSC encoding. This provides a partly embedded UEP to the encoded data frame. However, since the classes are decoded on separate branches, the advantages of an embedded UEP are not fully exploited.

Even though not applied to UEP, an interesting concept of 3D turbo codes is discussed in [36] by Berrou et al. They are trying to increase the minimum distance of a turbo code by adding a partial rate-1 third dimension in the form of a concatenated post-encoder to the PCCC structure. The PCCC itself has two encoding dimensions. The third component encodes only a variable fraction λ of the output parity bits. Even though the versatility of λ may lead to higher minimum distances, the convergence performance is disadvantaged. Since the post-encoder associated decoder does not profit from redundancy information at the first iteration, the induced errors are increased for this first processing. This hybrid structure highlights the advantages and disadvantages of partial turbo encoding. Although the code minimum distances become larger as a function of the size of the re-encoded information, the absence of extrinsic informations damages the turbo performances.

The above discussed works allow us to identify several characteristics of turbo codes, that must be considered for the design of new turbo architectures. In a first place, the size of the encoded frame has a direct influence on the convergence behavior. It is a well known truth that the turbo codes convergence waterfall becomes steeper with the code block length. Even though video code blocks can reach several thousands of bits, voice transmission over PMR networks implies the use of very low rate voice coders. Therefore, as expected, these voice frames will generate small lengths code blocks. Therefore, if turbo codes were to be used for voice radio transmission, we must consider the performances of the scheme compared with existent mechanisms. Currently, in both circuit switched PMR and GSM, mostly convolutional codes are used for voice channel encoding. Secondly, the interleaver is an essential element of turbo structures. Its effectiveness becomes visible with an increasing code block length, since the probability of breaking existent error blocks is greater. Even though the design of the interleaver itself plays an important role in the turbo convergence behavior, it has been proven that we must firstly consider its length before speaking of design. In [37], authors observe that "careful

interleaver design is required for long block lengths, while for short block lengths, or regarding bit error rates, random interleavers are fully sufficient, in achieving extremely small bit error rates even if operated very close to capacity". This frontier between length and design effectiveness seems to be close to a size of 2000 bits. Further, the multiple turbo codes concept appears interesting in an UEP encoding case. For both voice and video transmission, an UEP channel code must be flexible enough to adapt itself to a different number of classes of bits. Multiple codes may offer a wide range of error protection rates. As for the puncturing mechanisms, they seem a rather complex method for achieving UEP. For one type of channel code, multiple classes of bits would require multiple puncturing patterns. But in today's standards, e.g. LTE, only a single puncturing method is proposed, called rate matching, providing only EEP puncturing. Therefore, the puncturing mechanism should only modify the channel transmission rate uniformly for all data streams, and the encoder structure itself embed the UEP concepts. Berrou et al. have proven through their 3D turbo codes that it is possible to partially change the protection for a code block. In their structure, the fraction of the output parity bits can be even controlled. But as they observe, this method has both an advantage and a disadvantage. The advantage is measured through the increase of code minimum distances with the secondly encoded frame fraction. But, the disadvantage is measured in turbo decoding performance, due to the absence of the corresponding fraction of extrinsic data. As we have noticed, the BCJR algorithm works through a forward and backward recursion, due to which a high correlation and dependence between the turbo decoded quantities has been observed. It is only natural that the missing fraction of data influences the decoder performances. Nevertheless, the different dimension encoding and decoding can prove very interesting for UEP transmission, where, often, the protection must be cleverly divided between most important bits and less important bits.

In this chapter, we propose the evolution of turbo codes through the embedding of UEP concepts in their turbo structures themselves. The new ideas presented here have been patented and have given birth to the progressive hierarchical turbo codes. These progressive hierarchical turbo codes present a simple, yet very effective solution to an embedded UEP turbo evolution.

Following the principles of the basic turbo code, the proposed solution is constructed using the concatenation of RSC codes separated by interleavers. The difference between the progressive hierarchical turbo codes and their classical counterparts is the information encoding perspective. In the classical turbo encoder, the entire code block of information is fed to all constituent RSCs, and thus equally protected. On the contrary, the here proposed encoder progressively encodes sub-blocks of data using a hierarchical approach. Thus, the concatenation of several RSCs and interleavers becomes not only a means to provide a different encoding version of the same data, but also a way to enhance the protection of a sub-block of that data. The innovation of the solution consists in feeding a new sub-block of raw data to every next encoding level, and before the interleaving. The interleaver helps in spreading the newly introduced information throughout the encoder existent stream. And, since it is the structure of the code itself that provides different levels of protection for one block of data alone, we have called this solution an embedded UEP solution.

The embedded UEP progressive hierarchical turbo encoder can be declined in two different versions: parallel and serial. Both versions are based on the well known parallel and serial turbo codes, or, what one might call, the PCCC and the SCCC. The embedded UEP parallel solution based on the PCCC has been called the parallel progressive hierarchical turbo code (PPHTC), while the serial counterpart is based on the SCCC and has been called the serial progressive hierarchical turbo code (SPHTC).

This chapter is organized as follows. Section 3.2 provides a detailed description of the PPHTC and SPHTC encoders and decoders, for the particular case of two dimensions encoding (2-D), as well as for the general case or n dimensions encoding (n -D). Further, the code's properties and characteristics are analyzed in section 3.3. And finally, in section 3.4, we evaluate the performances of these proposed structures using two different platforms. One platform supposes random characteristics elements, while the second one introduces LTE standard elements. The embedded UEP code behavior is highlighted using two opposite UEP scenarios configurations. Also, the obtained results are compared with benchmark turbo codes. We conclude in section 3.5.

3.2 PPHTC & SPHTC: Enabling UEP Turbo Adaptation

As most common turbo codes structures present only two levels of encoding, i.e. two RSCs, we begin by introducing the two levels PPHTC and SPHTC in subsection 3.2.1. We denote these two levels encoding versions as two-dimensional or 2-D encoding. A detailed analysis of the 2-D encoder and decoder architectures is given, and the duality between the MAP and maximum likelihood (ML) decodings is explained. We extend the embedded UEP solution to multiple turbo codes in subsection 3.2.2. Thus, through the concatenation of n RSCs, an n dimension encoding or n -D decoding is performed.

3.2.1 2-D Architecture Design

The code architecture designs and transmission systems are represented in Fig. 3.1 and 3.2 for PPHTC and SPHTC respectively. The figures present the code architecture corresponding to two UEP levels, i.e. two different classes of bits predefined at higher layers, which are encoded using two dimensions.

Thus, the data frame or code block, A , is split into 2 sub-blocks called classes as $A = \{A_1, A_2\}$. Here, $A_1 = \{a_1^{(1)}, a_2^{(1)}, \dots, a_{N_1}^{(1)}\}$ denotes the first sub-block of symbols of size N_1 , and $A_2 = \{a_1^{(2)}, a_2^{(2)}, \dots, a_{N_2}^{(2)}\}$ denotes the second sub-block of symbols of size N_2 . A_1 represents the data segment with the higher level sensitivity bits, while A_2 consists of lower level importance bits.

The code block, A , is fed to the turbo encoder. Each PPHTC and SPHTC encoder is composed of two RSCs, concatenated in parallel and serial respectively, and separated by an interleaver. For simplicity, we consider here the two constituent RSCs as identical for both PPHTC and SPHTC structures. The designs of the encoders themselves are naturally based on the well known structures of PCCC and SCCC. The fundamental difference between these proposed structures and the classical structures is the insertion of new raw data before the interleaving and the second RSC encoding. Thus, we identify two different streams at the input of the embedded UEP structures. In an UEP environment, it is only natural to envisage the reception of multimedia specific information, where the bit sensitivity to channel errors must be considered. In consequence, the channel coding has to be defined to comply with the error protection requirements. For this particular use case, we suppose the reception of one code block of bits where two different sensitivities have been defined by the higher layers. Therefore, two levels of error protection will be proposed for both PPHTC and SPHTC. The first class, A_1 , must benefit of higher error protection than the second class, A_2 . Therefore, A_1 will be encoded twice by both constituent RSCs, while A_2 will only benefit of a single's RSC redundancy. The interleaver remains an important element of the turbo structures, as it will not only provide a different encoded version of A_1 , but will also help spread the bits of A_2 throughout the first class data.

3.2.1.1 UEP Encoder Description

Each constituent RSC is characterized by a generator polynomial G expressed in delay algebra D as

$$G(D) = \left\{ 1, \frac{\sum_{k=1}^m g_k D^k}{\sum_{k'=1}^{m'} g_{k'} D^{k'}} \right\}, \quad (3.1)$$

where m and m' the positive integers degrees of the feed forward and feed backward polynomial respectively, g_k and $g_{k'}$ the k th and k' th coefficient of the polynomial expressed in GF(2). The interleavers are denoted by π , although the length of the constituent interleavers for PPHTC and SPHTC are different.

Classes A_1 and A_2 are encoded as

$$\{S_i, P_i\}(D) = G(D) \times c_i(D), \quad (3.2)$$

where c_i represents the RSC input at level i , either first or second level.

The PPHTC and SPHTC encoders' characteristics are presented hereafter.

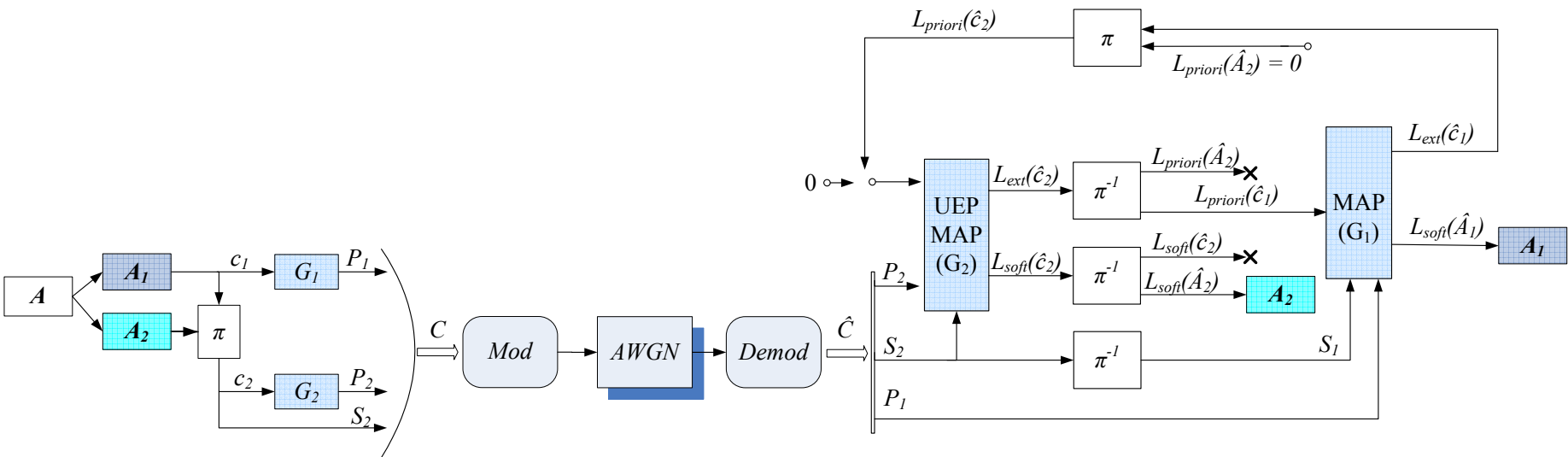


Figure 3.1. Transmission system for PPHTC $n = 2$.

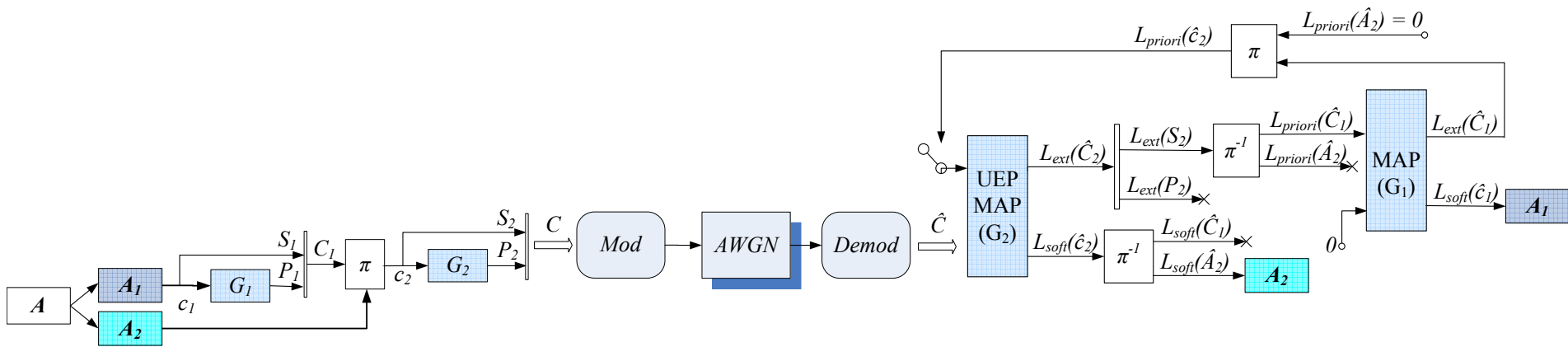


Figure 3.2. Transmission system for SPHTC $n = 2$.

PPHTC

In Fig. 3.1, the PPHTC encoder is represented. c_1 is considered equal to A_1 , while c_2 denotes the interleaved concatenated class A_1 with A_2 respectively. Each RSC's output is composed of the systematic output, S_i , and the parity output, P_i . However, only one of the two systematic informations will be transmitted, i.e. S_2 , since S_2 contains the sub-blocks of data for both classes.

The transmission code rate, r_{A_1} , for class A_1 , is thus

$$r_{A_1} = \frac{1}{\frac{1}{r_1} + \frac{1}{r_2}}, \quad (3.3)$$

and the transmission code rate, r_{A_2} , for class A_2 , is

$$r_{A_2} = r_2, \quad (3.4)$$

where r_1, r_2 represent the individual code rates per level of RSC encoding.

The overall code block transmission rate is then calculated as

$$r_A = \frac{A}{\frac{A_1}{r_{A_1}} + \frac{A_2}{r_{A_2}}} = \frac{A}{\frac{x_1 \times A}{r_1 \times r_2} + \frac{x_2 \times A}{r_2}} = \frac{r_1 \times r_2}{x_1 \times (r_1 + r_2) + x_2 \times r_1}, \quad (3.5)$$

with x_1 and x_2 the percentages of each one of the classes of bits in the code block A .

SPHTC

The SPHTC encoder is represented in Fig. 3.2. In serial terms, the first level of encoding is often denoted as the outer encoder, while the second level of encoding is called the inner encoder. Each RSC's output is composed of the systematic output, S_i , and the parity output, P_i . But while c_1 is considered equal to A_1 , c_2 refers to the interleaved concatenated class A_2 with the already encoded A_1 respectively. This encoded information corresponding to A_1 is referenced in Fig. 3.2 by C_1 , which is obtained through the multiplexing of S_1 and P_1 .

The transmission code rates for each one of the two classes, i.e. r_{A_1} and r_{A_2} , are computed as

$$r_{A_1} = r_1 \times r_2, \quad (3.6)$$

$$r_{A_2} = r_2, \quad (3.7)$$

where r_1 and r_2 are the outer and inner RSC rates.

The overall code block transmission rate becomes

$$r_A = \frac{A}{\frac{A_1}{r_{A_1}} + \frac{A_2}{r_{A_2}}} = \frac{A}{\frac{x_1 \times A}{r_1 \times r_2} + \frac{x_2 \times A}{r_2}} = \frac{r_1 \times r_2}{x_1 + x_2 \times r_1}, \quad (3.8)$$

with x_1 and x_2 the percentages of each one of the classes of bits in the code block A .

3.2.1.2 UEP Decoder Description

At the turbo decoders, the received signal, R , can be written as

$$R = \Phi E + N, \quad (3.9)$$

where E denotes the modulated emitted signal, Φ the transmission channel and N is the channel noise component characterized by zero-mean complex valued Gaussian variable having variance N_0/T_c (N_0 is the single sided AWGN power spectrum density and T_c denotes the fast Fourier transform (FFT) sampling period). R is demodulated and \hat{C} is estimated as the soft values frame to be decoded.

The decoders are shown in Fig. 3.1 and 3.2 for PPHTC and SPHTC respectively, as part of the transmission systems. The decoding is performed using the MAP criteria, but implemented in its simplified form. The latter

refers to the log likelihood ratios (LLRs) mathematics using the MAP criteria itself, i.e. the Log MAP algorithm. The symbol L used for identifying the quantities exchanged between the MAP decoders thus refers to LLR expressions concerning classes A_1 and A_2 .

Hereafter, we shortly describe the decoding philosophies presented in Fig. 3.1 and 3.2. But for a good comprehension of the PPHTC and SPHTC behaviors, we further present a detailed discussion regarding the mathematics behind these decoding procedures. We begin by the theoretical analysis of the MAP criteria decoding in subsection 3.2.1.3, followed by its computation using the BCJR algorithm in section 3.2.1.4. And finally, the LLR expressions are directly derived from the BCJR equations in section 3.2.1.5.

In Fig. 3.1 and 3.2, we note that the first class, A_1 , has been encoded by two concatenated RSCs, whilst class A_2 has been encoded only once by a single RSC. Thus, the UEP iterative decoding for two classes of bits presents itself as the concatenation of two MAP decoders.

During the iterative decoding, several iterations are established until the decoders converge, i.e. the estimated decoded values are reliable. For the first turbo iteration, the decoders receive only channel information and there are no existent priori information. This priori information is then set to zero for both PPHTC and SPHTC decodings, i.e. $L_{\text{priori}}(\hat{c}_2) = 0$.

After one iteration only, we can estimate the first information values, $L_{\text{soft}}(\hat{c}_2)$, which provides $L_{\text{soft}}(\hat{A}_2)$ after deinterleaving and demultiplexing. We also obtain the extrinsic information, $L_{\text{ext}}(\hat{c}_2)$ for PPHTC and $L_{\text{ext}}(\hat{C}_2)$ for SPHTC. This extrinsic information is defined as the supplementary data conveyed by the decoder itself regarding the symbols' reliability. Through deinterleaving, we obtain priori informations for both classes, A_1 and A_2 .

Class A_1 is decoded by both concatenated MAPs. Extrinsic information regarding it is obtained from both MAP decoders, and can be therefore exchanged between the two for the improvement of data estimation. But while the G_1 MAP is concerned by the presence of class A_1 alone, the G_2 MAP must estimate both classes, A_1 and A_2 .

But the priori regarding class A_2 , $L_{\text{priori}}(\hat{A}_2)$, is not reused in the iterative decoding process, since it is the result of the first MAP decoder only, the MAP corresponding to G_2 . The obtained extrinsic information can not be reused in the iterative exchange process, since its reuse on the same MAP would engender a divergence, i.e. worsened results. The immediate consequence of this absence of extrinsic information in the iterative decoding is the absence of priori information regarding class A_2 . To compensate this absence, the LLR priori of class A_2 are set to 0, which in probability terms is equivalent with equally likely probabilities. The multiplexed priori values for classes A_1 and A_2 are thus used for the following iteration. But, this effect of the embedded UEP is restricted to the first MAP decoder only (for RSC G_2). Therefore, we have denoted the first decoder as UEP-MAP. Its behavior is carefully analysed in the following sections.

The second MAP decoder, corresponding to G_1 , remains equivalent to a well known classical MAP, since it is concerned by only one type of information. Thus for both PPHTC and SPHTC, the first decoder receiving the channel information is the UEP-MAP decoder. It performs the estimation of the second class, A_2 , and feeds forward the extrinsic information regarding the remaining data, A_1 for the PPHTC, and the encoded A_1 for the SPHTC. Further on, the second decoder handles only information and redundancy bits regarding class A_1 .

3.2.1.3 UEP MAP Decoding Analysis

The progressive hierarchical turbo decoding is based on the well known turbo decoder structure, which uses the MAP criteria. As a matter of fact, the MAP decoding is generally associated to the iterative turbo decoding and the computation of a posteriori probability (APP). However, a second criteria which is globally used for convolutional decoding is the ML criteria. As we will discuss hereafter, these two strategies have a fundamental difference, whose influence in the UEP case is non negligible.

The symbol-by-symbol MAP criteria may be written as

$$\hat{a}_t = \underset{a_t}{\operatorname{argmax}} P(a_t | \hat{C}), \quad (3.10)$$

where \hat{a}_t denotes the received estimated symbol for the sent symbol a_t , knowing the entire received frame \hat{C} . The MAP rule exploits existent a priori distribution over the information symbols as to enhance the probability

of a good reception for symbol a_t .

The symbol-by-symbol ML criteria is expressed as

$$\hat{a}_t = \operatorname{argmax}_{a_t} P(\hat{C}|a_t), \quad (3.11)$$

where \hat{a}_t denotes the received estimated symbol for the sent symbol a_t , enhancing the probability of good reception for the received frame \hat{C} . The ML decoding assumes equally likely information symbols, i.e. this rule implies that a priori distribution over the information bits is equal to one or non-existent.

As stated in [38] and [39], and as expected from the equations above, the MAP criteria becomes equivalent to the ML criteria if no a priori informations are available in any iterative decoding algorithm. This information becomes particularly valuable, since, for the second UEP encoded class, there is no available a priori information in the decoder, as discussed.

In the following paragraphs, we investigate the influence of UEP concepts in the decoding process.

UEP MAP Estimation

In the MAP criteria expression written as

$$\hat{a}_t = \operatorname{argmax}_{a_t} P(a_t|\hat{C}), \quad (3.12)$$

$P(a_t|\hat{C})$ can be calculated from the APP $P(C|\hat{C})$ of all code sequences C which correspond to an information symbol a_t at position t as

$$P(a_t|\hat{C}) = \sum_{C \in \Omega|a_t} P(C|\hat{C}), \quad (3.13)$$

where $\Omega|a_t$ is the set of all possible sequences C such as the t th symbol is equal to a_t .

Assuming memoryless channel and statistically independent information bits

$$P(C|\hat{C}) = \frac{P(\hat{C}|C)P(C)}{P(\hat{C})} = \prod_{j=1}^{N_1+N_2} \frac{P(\hat{C}_j|C_j)P(C_j)}{P(\hat{C}_j)}, \quad (3.14)$$

where N_1 denotes the length of class A_1 and N_2 the length of class A_2 in number of information symbols, C_j and \hat{C}_j represent the sent and received symbols respectively. But in the decoding trellis, the transition corresponding to the sent symbol C_j corresponds to the sent information symbol a_j of frame A .

For any sent symbol a_t , we may write the MAP criteria which exploits a priori distribution over the information symbols as

$$P(a_t|\hat{C}) = \sum_{C \in \Omega|a_t} \prod_{j=1}^{N_1+N_2} \frac{P(\hat{C}_j|a_j)P(a_j)}{P(\hat{C}_j)}, \quad (3.15)$$

where $P(a_j)$ represents the existent a priori information on symbol a_j . This gives

$$P(a_t|\hat{C}) = \frac{1}{P(\hat{C})} \sum_{C \in \Omega|a_t} \prod_{j=1}^{N_1+N_2} P(\hat{C}_j|a_j) \prod_{j=1}^{N_1+N_2} P(a_j). \quad (3.16)$$

If a_j belongs to A_1 , then $P(a_j)$ is a valid a priori information computed by the other MAP decoder. If a_j belongs to A_2 , then $P(a_j)$ contains no information over symbols of A_2 , and we assume equally likely information symbols for any A_2 symbols. This is mathematically equivalent to $P(a_j) = 1$.

The interleaving of priori independent probabilities of A_1 and A_2 does not change their values, but only their indexing in the code block A . Therefore, the result of the product of all priori probabilities of A is mathematically equal to the product of the two sub-products of the independent probabilities of class A_1 and class A_2 .

$$\prod_{j=1}^{N_1+N_2} P(a_j) = \underbrace{\prod_{k_1=1}^{N_1} P(a_{k_1}|a_{k_1} \in A_1)}_{\text{Priori}(A_1)} \underbrace{\prod_{k_2=1}^{N_2} P(a_{k_2}|a_{k_2} \in A_2)}_{\text{Priori}(A_2)}, \quad (3.17)$$

with the observation that $\pi(P(a_j)) = P(a_k|k = \pi^{-1}(j))$, i.e. the interleaving π changes only the indexing of the probabilities, and not their values.

The expression (3.16) becomes then in the UEP-MAP case

$$P^{(UEP-MAP)}(a_t|\hat{C}) = \frac{1}{P(\hat{C})} \sum_{C \in \Omega|a_t} \prod_{j=1}^{N_1+N_2} P(\hat{C}_j|a_j \in A) \prod_{k_1=1}^{N_1} P(a_{k_1}|a_{k_1} \in A_1), \quad (3.18)$$

since the product corresponding to priori informations for class A_2 is equal to one, i.e. $\prod_{k_2=1}^{N_2} P(a_{k_2}|a_{k_2} \in A_2) = 1$.

This UEP-MAP can be interpreted as a partial MAP decoding, since the priori information is exploited only for a fraction of the code block A . This partial MAP expression has two innate boundaries.

One upper absolute bound is the classical MAP criteria decoding. If all symbols are of class A_1 , i.e. there exists one valid priori probability $P(a_j)$ for every symbol a_j . This expression is equivalent with the classical turbo decoding MAP written as

$$P^{(MAP)}(a_t|\hat{C}) = \frac{1}{P(\hat{C})} \sum_{C \in \Omega|a_t} \prod_{j=1}^{N_1+N_2} P(\hat{C}_j|a_j) \prod_{j=1}^{N_1+N_2} P(a_j). \quad (3.19)$$

This expression is used in the turbo iterative decoding and exploits the priori information over all the symbols of the code block.

The second bound or lower bound is represented by the ML decoding. If all symbols were of class A_2 , i.e. there would be no valid priori probability $P(a_j)$ for every symbol a_j , and we would assume equally likely information symbols for all symbols. This second expression may thus be written as

$$P^{(ML)}(a_t|\hat{C}) = \frac{1}{P(\hat{C})} \sum_{C \in \Omega|a_t} \prod_{j=1}^{N_1+N_2} P(\hat{C}_j|a_j). \quad (3.20)$$

The ML criteria recalls the soft Viterbi convolutional codes (CC) decoding. The Viterbi algorithm is known as being an algorithm which computes a maximum likelihood estimation. In fact, the soft Viterbi does not manipulate probability expressions, but directly soft LLRs, and decides of the optimum likelihood by minimizing the code word distance (equivalent to maximizing the code word weight). This behavior will be easily noted in the decoding performances, where, after the first iteration, the estimation of the second class A_2 closely approaches the CC soft Viterbi decoding.

Therefore, in the particular case of all symbols of frame A being symbols of A_1 , the UEP-MAP becomes exactly equal to the turbo decoding. The overall decoding composed of the concatenation of the first and second decoder will be equivalent to a classical turbo decoder. In the opposite case, where all A frame symbols are composed of only symbols of A_2 , then the expression of the output of the UEP-MAP (equation (3.18)) is highly similar to the classical soft convolutional decoding (equation (3.20)).

By considering $P^{(UEP-MAP)}$, we can therefore resume the performances to

- when class A_1 length is larger than class A_2 length, the UEP MAP decoding performance closely approaches the turbo performance, since large size extrinsic information is considered,

$$\lim_{A_2 \rightarrow 0} P^{(UEP-MAP)} = P^{(MAP)}, \quad (3.21)$$

- when class A_1 size is much smaller than that of the class A_2 , theoretically, the results should approach the convolutional decoding performance, since fewer extrinsic information are considered.

$$\lim_{A_1 \rightarrow 0} P^{(UEP-MAP)} = P^{(ML)}. \quad (3.22)$$

Therefore, the first decoding of both classes A_1 and A_2 is performed by a partial MAP or UEP-MAP, as shown in equation 3.18. The estimation of class A_2 is performed after one MAP decoding only.

Single Class MAP Decoding

As for the first class estimation, A_1 , its estimation is performed after the second MAP decoding, i.e. A_1 has been doubly encoded and it is doubly MAP decoded. The second MAP expression is written as a classical MAP since only a single stream is decoded here

$$P^{(MAP)}(a_t|\hat{C}) = \frac{1}{P(\hat{C})} \sum_{C \in \Omega|a_t} \prod_{j=1}^{N_1} P(\hat{C}_j|a_j) \prod_{j=1}^{N_1} P(a_j). \quad (3.23)$$

Bit or Symbol MAP Decoding

Also, as expected, the MAP decodings for the PPHTC and SPHTC are similar, yet we must highlight their differences. Already, comparing Fig. 3.1 and Fig. 3.2, we note that the extrinsic information exchanged between the two MAPs for the parallel and serial structures are of different nature.

In Fig. 3.1, the PPHTC uses the **bit MAP** criteria for estimating the soft and extrinsic information regarding information or systematic bits only. Regarding the symbol a_t in the mathematical expressions above, this symbol refers to systematic bits only, i.e. only one bit is estimated. This is due to the fact that, in the PCCC configuration, it is only the systematic stream of bits that is doubly encoded by the upper and the lower RSC. Thus, in the decoding process, only systematic related data needs to be fed forward and backward between the two MAP decoders.

For the SPHTC decoding from Fig. 3.2, the estimations of two types of bits are done in the **symbol MAP** decoding, i.e. both systematic and parity bits. Thus, the symbol a_t in the expressions above may refer to either a systematic bit, either a parity bit, i.e. the encoded symbol. This is a direct consequence of the SCCC legacy. In this serial configuration, the inner or second RSC encodes both systematic and parity data coming from the outer of first RSC. In the decoder, this translates in the necessity of feeding forward and backwards both systematic and parity related extrinsic information. Therefore, in the above equations, the length of A_1 would become $2N_1$ instead of N_1 .

3.2.1.4 BCJR Algorithm UEP Characteristics

In this subsection, we analyze the influence of UEP concepts on the classical BCJR algorithm. As mentioned before, we consider that the transmitted information symbol is composed of only one bit of information, therefore a_t denotes one transmitted bit of information while \hat{a}_t represents the estimated received bit of information.

In the decoder trellis, the APP of one transition from state $\Psi_t = p$, at time instant t , to state $\Psi_{t+1} = q$, at time instant $t + 1$, given the observed received sequence \hat{C} may be expressed as

$$P(\Psi_t = p, \Psi_{t+1} = q|\hat{C}) = \frac{1}{P(\hat{C})} \alpha_t(p) \gamma_t(p, q) \beta_{t+1}(q), \quad (3.24)$$

where

$$\alpha_t(p) = p(\Psi_t = p, \hat{C}_{<t}), \quad (3.25)$$

$$\gamma_t(p, q) = p(\Psi_{t+1} = q, \hat{C}_t | \Psi_t = p), \quad (3.26)$$

$$\beta_{t+1}(q) = p(\hat{C}_{>t} | \Psi_{t+1} = q). \quad (3.27)$$

The APP of receiving bit \hat{a}_t at time t is

$$P(\hat{a}_t|\hat{C}) = \sum_{(p,q) \in T} P(\Psi_t = p, \Psi_{t+1} = q|\hat{C}) = \frac{1}{P(\hat{C})} \sum_{(p,q) \in T} \alpha_t(p) \gamma_t(p, q) \beta_{t+1}(q), \quad (3.28)$$

where T denotes the set of possible transitions (p, q) corresponding to bit \hat{a}_t . We can replace α, γ, β with their trellis computed expressions

$$\alpha_t(p) = \sum_{m=0}^{Q-1} \alpha_{t-1}(m) \gamma_{t-1}(m, p), \quad (3.29)$$

$$\beta_{t+1}(q) = \sum_{r=0}^{Q-1} \gamma_{t+1}(q, r) \beta_{t+2}(r), \quad (3.30)$$

where m and r denote previous and following trellis states respectively.

However, here, in the expression of γ , the UEP characteristics are visible through the priori probabilities as

$$\gamma_t(p, q) = p(\hat{C}_t^{(0)} | C_t^{(0)} = C_t^{(0,p,q)}) p(\hat{C}_t^{(1)} | C_t^{(1)} = C_t^{(1,p,q)}) P(\hat{a}_t = a^{(p,q)}), \quad (3.31)$$

where the value of $P(\hat{a}_t = a^{(p,q)})$ is equal to one if $\hat{a}_t \in A_2$, and

- $\hat{C}_t^{(0)}$ and $\hat{C}_t^{(1)}$ denote the estimated received systematic and parity bits respectively at time instant t of received symbol \hat{C}_t ,
- $C_t^{(0)}$ denotes the transmitted systematic bit whose value, $C_t^{(0,p,q)}$, corresponds to the trellis transition $p - q$,
- $C_t^{(1)}$ denotes the transmitted parity bit whose value, $C_t^{(1,p,q)}$, corresponds to the $p - q$ transition,
- $C_t^{(0,p,q)}$ equals the value $a^{(p,q)}$ of the received bit \hat{a}_t if the APP is computed for a systematic bit
- $C_t^{(1,p,q)}$ equals the value $a^{(p,q)}$ of the received bit \hat{a}_t if the APP is computed for a parity bit.

The forward recursion for α is developed as

$$\begin{aligned} \alpha_t(p) &= \sum_{m=0}^{Q-1} p(\hat{C}_{t-1}^{(0)} | C_{t-1}^{(0)} = C_{t-1}^{(0,m,p)}) p(\hat{C}_{t-1}^{(1)} | C_{t-1}^{(1)} = C_{t-1}^{(1,m,p)}) P(\hat{a}_{t-1} = a^{(m,p)}) \times \\ &\quad \sum_{k=0}^{Q-1} p(\hat{C}_{t-2}^{(0)} | C_{t-2}^{(0)} = C_{t-2}^{(0,k,m)}) p(\hat{C}_{t-2}^{(1)} | C_{t-2}^{(1)} = C_{t-2}^{(1,k,m)}) P(\hat{a}_{t-2} = a^{(k,m)}) \alpha_{t-2}(k) \\ &= \sum_{m=0}^{Q-1} \sum_{k=0}^{Q-1} \dots \sum_{b=0}^{Q-1} \alpha_0(b) \prod_{i=0}^{t-1} p(\hat{C}_i^{(0)} | C_i^{(0)}) p(\hat{C}_i^{(1)} | C_i^{(1)}) P(\hat{a}_i), \end{aligned} \quad (3.32)$$

where k denotes one of the previous trellis states and b denotes the first trellis state.

The backward recursion, β , is computed on the given trellis as

$$\begin{aligned} \beta_{t+1}(q) &= \sum_{r=0}^{Q-1} p(\hat{C}_{t+1}^{(0)} | C_{t+1}^{(0)} = C_{t+1}^{(0,q,r)}) p(\hat{C}_{t+1}^{(1)} | C_{t+1}^{(1)} = C_{t+1}^{(1,q,r)}) P(\hat{a}_{t+1} = a^{(q,r)}) \times \\ &\quad \sum_{s=0}^{Q-1} p(\hat{C}_{t+2}^{(0)} | C_{t+2}^{(0)} = C_{t+2}^{(0,r,s)}) p(\hat{C}_{t+2}^{(1)} | C_{t+2}^{(1)} = C_{t+2}^{(1,r,s)}) P(\hat{a}_{t+2} = a^{(r,s)}) \beta_{t+2}(s) \\ &= \sum_{r=0}^{Q-1} \sum_{s=0}^{Q-1} \dots \sum_{v=0}^{Q-1} \beta_N(v) \prod_{j=t+1}^N p(\hat{C}_j^{(0)} | C_j^{(0)}) p(\hat{C}_j^{(1)} | C_j^{(1)}) P(\hat{a}_j), \end{aligned} \quad (3.33)$$

where s denotes a future trellis state and v refers to the last trellis state.

Considering the two transition states (p, q) in the decoding trellis for bit value $a^{(p,q)}$ respectively, with p the departing state and q the arrival state, we develop (3.28) as follows

$$P(\hat{a}_t | \hat{C}) = \frac{1}{P(\hat{C})} \sum_{(p,q) \in T} \alpha_t(p) \beta_{t+1}(q) p(\hat{C}_t^{(0)} | C_t^{(0)} = C_t^{(0,p,q)}) p(\hat{C}_t^{(1)} | C_t^{(1)} = C_t^{(1,p,q)}) P(\hat{a}_t = a^{(p,q)}). \quad (3.34)$$

As proven, $\alpha_t(p)$ performs the forward recursion considering the systematic and parity bits transition probabilities, as well as existent priori values, over all states from 0 to t . The priori values of the interleaved bits count for both A_1 and A_2 specific priori information. The interleaved priori values for both A_1 and A_2 are also considered in the backward recursion through the computation of $\beta_{t+1}(q)$. Thus, the existence or non-existence of priori information regarding a part of the frame has immediate consequences over the value of APP $P(\hat{a}_t|\hat{C})$.

If Ω represents all possible trellis transitions, and $\Omega|_{a_t}$ is the set of all possible sequences C such as the t th symbol is equal to a_t then

$$P(\hat{a}_t|\hat{C}) = \frac{1}{P(\hat{C})} \sum_{C \in \Omega|_{a_t}} \alpha_0(b)\beta_N(v) \prod_{j=0}^N \left\{ p(\hat{C}_j^{(0)}|C_j^{(0)})p(\hat{C}_j^{(1)}|C_j^{(1)})P(\hat{a}_j) \right\}, \quad (3.35)$$

with b and v the initial and final states of the trellis, which are equal to zero. But the code block size N can be split in two sub-block size N_1 and N_2 , with $N = N_1 + N_2$, since the code block A is constructed with classes A_1 and A_2 .

$$P(\hat{a}_t|\hat{C}) = \frac{1}{P(\hat{C})} \sum_{C \in \Omega|_{a_t}} \alpha_0(b)\beta_N(v) \prod_{j=0}^{N_1+N_2} \left\{ p(\hat{C}_j^{(0)}|C_j^{(0)} \in A)p(\hat{C}_j^{(1)}|C_j^{(1)} \in A)P(\hat{a}_j|a_j \in A) \right\}. \quad (3.36)$$

But considering that the informations regarding the two classes are not correlated and the interleaving does not change the values of individual probabilities, the previous product can be split in two sub-products as

$$P(\hat{a}_t|\hat{C}) = \frac{1}{P(\hat{C})} \sum_{C \in \Omega|_{a_t}} \alpha_0(b)\beta_N(v) \prod_{k_1=0}^{N_1} \left\{ p(\hat{C}_{k_1}^{(0)}|C_{k_1}^{(0)} \in A_1)p(\hat{C}_{k_1}^{(1)}|C_{k_1}^{(1)} \in A_1)P(\hat{a}_{k_1}|a_{k_1} \in A_1) \right\} \prod_{k_2=0}^{N_2} \left\{ p(\hat{C}_{k_2}^{(0)}|C_{k_2}^{(0)} \in A_2)p(\hat{C}_{k_2}^{(1)}|C_{k_2}^{(1)} \in A_2)P(\hat{a}_{k_2}|a_{k_2} \in A_2) \right\}. \quad (3.37)$$

The value of $P(\hat{C})$ is stable and can be considered as a constant, that we denote by N_c . If we consider the bit a_t as a systematic bit of either class one or class two, denoted by $a_t^{(s)}$, than its corresponding channel probability and priori information are independent of the trellis state. The equation (3.37) can be rewritten as

$$P(\hat{a}_t^{(s)}|\hat{C}) = N_c p(\hat{C}_t^{(0)}|C_t^{(0)} \in A)P(\hat{a}_t^{(s)}|a_t^{(s)} \in A) \sum_{C \in \Omega|_{a_t}} \alpha_0(b)\beta_N(v) \prod_{k_1=0}^{N_1} p(\hat{C}_{k_1}^{(0)}|C_{k_1}^{(0)} \in A_1, k_1 \neq \pi^{-1}(t))p(\hat{C}_{k_1}^{(1)}|C_{k_1}^{(1)} \in A_1)P(\hat{a}_{k_1}|a_{k_1} \in A_1, k_1 \neq \pi^{-1}(t)) \times \prod_{k_2=0}^{N_2} p(\hat{C}_{k_2}^{(0)}|C_{k_2}^{(0)} \in A_2, k_2 \neq \pi^{-1}(t))p(\hat{C}_{k_2}^{(1)}|C_{k_2}^{(1)} \in A_2)P(\hat{a}_{k_2}|a_{k_2} \in A_2, k_2 \neq \pi^{-1}(t)), \quad (3.38)$$

where $\pi^{-1}(t)$ denotes the inverse interleaving transformation of index t .

The equation above is generally used in the PCCC case, therefore we have employed it in the PPHTC MAP decoding. For the SPHTC decoding, the MAP structure is related to the SCCC decoding. Therefore, the equation above is employed for computing the APP of the systematic bit. For the APP of the parity bit, on the other hand, we have to consider bit a_t as a parity bit, i.e. $a_t^{(p)}$. Thus, the channel and priori probabilities of the parity bit become independent of trellis transitions and can be factorized out of the sum.

However, as expected, the PPHTC and SPHTC decoding does not provide valid priori information for class A_2 . The only available extrinsic data related to A_2 is obtained from a single MAP, and can not be used in the

iterative decoding. Therefore, we have set the priori probabilities regarding A_2 to 1, i.e. we assume equally likely information symbols. For a systematic A_1 bit, the BCJR APP becomes

$$\begin{aligned}
P(\hat{a}_t^{(s)} | \hat{C}, a_k^{(s)} \in A_1, k = \pi^{-1}(t)) &= N_c \underbrace{p(\hat{C}_t^{(0)} | C_t^{(0)} \in A_1)}_{\text{Systematic}(a_k^{(s)})} \underbrace{P(\hat{a}_t^{(s)} | a_t^{(s)} \in A_1)}_{\text{Priori}(a_k^{(s)})} \times \\
\sum_{C \in \Omega | a_t} \alpha_0(b) \beta_N(v) \prod_{k_2=0}^{N_2} p(\hat{C}_{k_2}^{(0)} | C_{k_2}^{(0)} \in A_2) p(\hat{C}_{k_2}^{(1)} | C_{k_2}^{(1)} \in A_2) &\times \\
\prod_{k_1=0}^{N_1} p(\hat{C}_{k_1}^{(0)} | C_{k_1}^{(0)} \in A_1, k_1 \neq \pi^{-1}(t)) p(\hat{C}_{k_1}^{(1)} | C_{k_1}^{(1)} \in A_1) P(\hat{a}_{k_1} | a_{k_1} \in A_1, k_1 \neq \pi^{-1}(t)). & \quad (3.39)
\end{aligned}$$

For a systematic A_2 bit, the BCJR APP becomes

$$\begin{aligned}
P(\hat{a}_t^{(s)} | \hat{C}, a_k^{(s)} \in A_2, k = \pi^{-1}(t)) &= N_c \underbrace{p(\hat{C}_t^{(0)} | C_t^{(0)} \in A_2)}_{\text{Systematic}(a_k^{(s)})} \times \\
\sum_{C \in \Omega | a_t} \alpha_0(b) \beta_N(v) \prod_{k_1=0}^{N_1} p(\hat{C}_{k_1}^{(0)} | C_{k_1}^{(0)} \in A_1) p(\hat{C}_{k_1}^{(1)} | C_{k_1}^{(1)} \in A_1) P(\hat{a}_{k_1} | a_{k_1} \in A_1) &\times \\
\prod_{k_2=0}^{N_2} p(\hat{C}_{k_2}^{(0)} | C_{k_2}^{(0)} \in A_2, k_2 \neq \pi^{-1}(t)) p(\hat{C}_{k_2}^{(1)} | C_{k_2}^{(1)} \in A_2). & \quad (3.40)
\end{aligned}$$

These equations, (3.39) with (3.40), prove that the APP of each bit is computed on the entire trellis, considering all available channel and priori information.

We note that the priori probability of bit $a_t \in A_1$ appears in (3.39) as $P(\hat{a}_t | a_t \in A_1)$, along with its own systematic channel estimation $p(\hat{C}_t^{(0)} | C_t^{(0)} \in A_1)$, and the extrinsic information composed of the remaining channel information of both classes and the remaining priori of only A_1 . Therefore, we can expect a turbo behavior from class A_1 , since, with every iteration, new priori A_1 information will be used for improving the results. However, these turbo results will be influenced not only by their own channel errors, but also by the existent channel errors of the other class, i.e. A_2 .

On the contrary, in (3.40), we only identify the systematic channel information $p(\hat{C}_t^{(0)} | C_t^{(0)} \in A_2)$ and the extrinsic data. The latter is composed of the channel information of both classes, A_1 and A_2 , and the priori information on class A_1 only. There is no direct influence of a priori A_2 data. Nevertheless, there exists one priori data stream which will help improving the estimation of A_2 with every iteration, i.e. $P(\hat{a}_{k_1} | a_{k_1} \in A_1)$, the priori regarding class A_1 . This is the consequence of the forward and backward trellis consideration. Thus, we can only expect the performances of A_2 to improve with every new turbo iteration. But the interesting questions are the following. How much will the priori probabilities of A_1 contribute in the improvement of A_2 ? How will the absence of the A_2 priors affect the decoding behavior? And how is quantified the turbo correlation and dependence between these turbo decoded quantities? We will address these questions further on through computer simulations.

3.2.1.5 Log Likelihood UEP Adaptation

In Fig. 3.1 and Fig. 3.2, we have been using LLRs expressions in the decoding process. Their mathematical expressions are derived hereafter.

For simplicity, we choose notations

$$\varphi_{0,t,A} = p(\hat{C}_t^{(0)} | C_t^{(0)} \in A), \text{ refers to the channel systematic probability,} \quad (3.41)$$

$$\varphi_{1,t,A} = p(\hat{C}_t^{(1)} | C_t^{(1)} \in A), \text{ refers to the channel parity probability} \quad (3.42)$$

$$\delta_{t,A} = P(\hat{a}_t | a_t \in A), \text{ refers to the priori probability.} \quad (3.43)$$

Hereafter, we denote the LLR probabilities by the symbol L , defined as

$$L(\hat{a}_t | \hat{C}) = \log \frac{P(\hat{a}_t = 1 | \hat{C})}{P(\hat{a}_t = 0 | \hat{C})} \quad (3.44)$$

where the sign of L is used for hard bit decision, i.e. $+1$ determines $\hat{a}_t = 0$ and -1 determines $\hat{a}_t = 1$ and its absolute value measures the degree of reliability. We use L_{soft} and $L_{channel}$ to reference the soft and channel LLRs respectively.

The equation (3.37) is written as an LLR probability for one systematic bit $\hat{a}_t^{(s)}$ as

$$L(\hat{a}_t^{(s)} | \hat{C}) = \log \frac{\varphi_{0,t,A} \delta_{t,A} \sum_{(p,q) \in T_1} \varphi_{1,t,A} \alpha_t(p) \beta_{t+1}(q)}{\varphi_{0,t,A} \delta_{t,A} \sum_{(p,q) \in T_0} \varphi_{1,t,A} \alpha_t(p) \beta_{t+1}(q)}, \quad (3.45)$$

where the summation is performed over the transitions for which the bit is equal to 1 for the numerator, i.e. T_1 , and 0 the denominator, i.e. T_0 .

$\delta_{t,A}$ and the systematic channel information regarding bit $a_t^{(s)}$ do not depend of the trellis transition's values, but only of the value 1 or 0 of $a_t^{(s)}$, and can be written outside the sum.¹

$$\begin{aligned} L_{soft}(\hat{a}_t^{(s)} | \hat{C}) &= \log \frac{\varphi_{0,t,A} |_{a_t^{(s)}=1}}{\varphi_{0,t,A} |_{a_t^{(s)}=0}} + \log \frac{\delta_{t,A} |_{a_t^{(s)}=1}}{\delta_{t,A} |_{a_t^{(s)}=0}} + \log \frac{\sum_{(p,q) \in T_1} \varphi_{1,t,A} \alpha_t(p) \beta_{t+1}(q)}{\sum_{(p,q) \in T_0} \varphi_{1,t,A} \alpha_t(p) \beta_{t+1}(q)} \\ &= L_{channel}(\hat{C}_t^{(0)}) + L_{priori}(a_t^{(s)}) + L_{ext}(a_t^{(s)}). \end{aligned} \quad (3.46)$$

Considering the different classes, A_1 and A_2 , (3.46) becomes

$$L_{soft}(a_t^{(s)} | \hat{C}) = \begin{cases} L_{channel}(\hat{C}_t^{(0)}) + L_{ext}(a_t^{(s)}), & \text{if } a_t^{(s)} \in A_2, \\ L_{channel}(\hat{C}_t^{(0)}) + L_{priori}(a_t^{(s)}) + L_{ext}(a_t^{(s)}), & \text{if } a_t^{(s)} \in A_1. \end{cases} \quad (3.47)$$

Extending the above expression to the entire code block for the UEP MAP decoding gives

$$L_{soft}(A_i | \hat{C}) = \begin{cases} L_{channel}(S_i) + L_{ext}(A_i), & \text{if } i = 2, \\ L_{channel}(S_i) + L_{priori}(A_i) + L_{ext}(A_i), & \text{if } i = 1, \end{cases} \quad (3.48)$$

where the different LLRs are obtained through demultiplexing and deinterleaving.

3.2.2 n -D Extended UEP Architecture

The PPHTC and the SPHTC structures can be easily extended to n levels of encoding. Thus, n RSCs are concatenated, and separated by interleavers. At each encoding level, and before the interleaving, a new sub-block of raw data is introduced in the encoding process. The decoding is performed through the concatenation of n MAPs, from which the first $n - 1$ UEP-MAPs would decode several different data streams corresponding to $n - 1$ different classes of bits.

Fig. 3.3 and Fig. 3.4 present the generalized designs for the PPHTC and SPHTC respectively. If every constituent RSC and every separating interleaver is unique, then the number of UEP possibilities are infinite. The proposed solution provides embedded UEP structures having a large flexibility in terms of number of constituent codes, interleaver types and possible code rates. The advantage of such a structure is its adaptability to any constraints regarding multimedia transmission. A channel codec structure is rarely designed to fit a flexible error protection.

¹In the SPHTC case, we perform decoding for the serial codes' concatenation, and extrinsic information is computed on both systematic and parity bits. If a_t is a parity bit, then $\varphi_{1,t,A}$ value becomes independent of trellis transitions.

3.2.2.1 UEP Turbo Multiple Encoding

Each i th RSC is characterized by a generator polynomial G_i written as

$$G_i(D) = \left\{ 1, \frac{\sum_{k=1}^m g_k^{(i)} D^k}{\sum_{k'=1}^{m'} g_{k'}^{(i)} D^{k'}} \right\}, \quad (3.49)$$

where $i = 1 \dots n$, n the number of concatenated codes, m and m' the positive integers degrees of the feed forward and feed backward polynomial respectively, $g_k^{(i)}$ and $g_{k'}^{(i)}$ the k th and k' th coefficient of the i th polynomial expressed in GF(2). Each interleaver is denoted by Π_j , with $j = 1 \dots n - 1$.

The multimedia code block data, A , can be split into n different segments, each one having its own characteristics and channel sensitivities. Thus, we have designed the encoder structure to fit the number of different error protection levels. The data classes are defined as $A = \{A_i\}_{i=1 \dots n}$ with $A_i = \{a_1^{(i)}, a_2^{(i)}, \dots, a_{N_i}^{(i)}\}$ denoting one segment of symbols of size N_i . All symbols of class A_i have the same importance degree and benefit of the same level of protection. A_1 is considered as most important class and A_n as less important one. Each class A_i is thus fed to the i th level of encoding, but before interleaving. Thus, at each encoding level, the interleaver receives new non-encoded information that is spread throughout the existent encoder stream. Each sub-block experiences a cascaded interleaving. The error vectors are projected in consecutively independent and greater spaces by ever higher length interleavers, as $\pi_1 < \pi_2 < \dots < \pi_{n-1}$.

The classes are time progressive and hierarchically encoded at n encoding steps. Each encoding process, i , is described as

$$C_i(D) = \{S_i, P_i\} = G_i(D) \times c_i(D). \quad (3.50)$$

Extended PPHTC Encoding

In the extended PPHTC case, c_i represents the encoder input and C_i the corresponding encoded data, comprising the systematic S_i and the parity output P_i . c_1 represents the first encoder input, A_1 , while the following c_i , with $i = 2 \dots n$, depict the interleaved concatenated class A_i with $\{A_j\}_{j=1 \dots i-1}$ respectively. At each encoding level i , a new raw sub-block of data is fed to the encoder and mixed to the encoder existent stream. This existent stream is composed of classes of higher level sensitivity, $\{A_j\}_{j=1 \dots i-1}$, which must benefit of an increased channel error protection.

Each class's A_i transmission code rate, r_{A_i} , becomes

$$r_{A_i} = \frac{1}{\sum_{k=i}^n \frac{1}{r_k}}, \quad (3.51)$$

where r_k denotes the RSC encoding rate of level k , and $i = 1 \dots n$.

The overall code block transmission rate is therefore equal to

$$r_A = \frac{A}{\sum_{k=1}^n \frac{A_k}{r_{A_k}}} = \frac{1}{\sum_{k=1}^n \frac{x_k}{r_{A_k}}}. \quad (3.52)$$

Extended SPHTC Encoding

In the SPHTC case, the general equation is written similarly to (3.50), but with a different interpretation. Thus, in the general encoding equation, (3.50), c_i represents the encoder input and C_i the corresponding encoded data, comprising

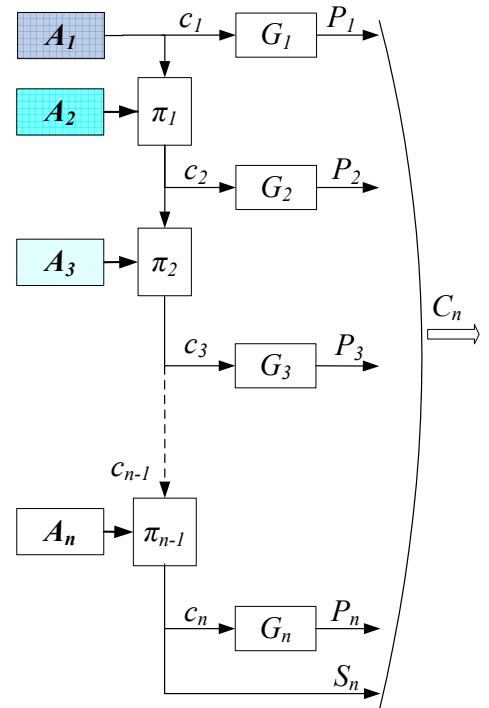


Figure 3.3. General form for the PPHTC encoder.

the systematic output S_i and the parity bits output P_i . c_1 is considered equal to A_1 while the following c_i , with $i = 2 \dots n$, depict the interleaved concatenated class A_i with C_{i-1} respectively.

The proposed SPHTC encoder naturally provides a progressive hierarchical protection to classes A_1, A_2, \dots, A_n , by adding new redundancy symbols to higher level data. At each encoding level, new non-protected data is introduced. Considering r_i the constituent code rate at level i , class A_i benefits of the overall code rate r_{A_i}

$$r_{A_i} = \prod_{k=i}^n r_k. \quad (3.53)$$

The code block A transmission rate becomes

$$r_A = \frac{A}{\sum_{k=1}^n \frac{A_k}{r_{A_k}}} = \frac{1}{\sum_{k=1}^n \frac{x_k}{\prod_{j=k}^n r_j}}. \quad (3.54)$$

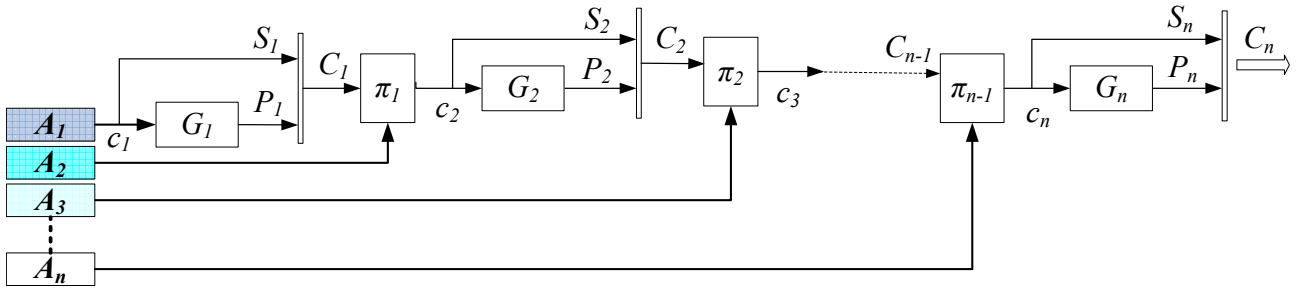


Figure 3.4. General form for the SPHTC encoder.

3.2.2.2 UEP Multiple Decoding Description

The n levels decoding is shown in Fig. 3.5 for the PPHTC, and in Fig. 3.6 for the SPHTC case. The generalization of the decoding principles is intuitive when having considered the case $n = 2$.

At encoding level n , the encoded frame C_n is emitted on an AWGN channel and the received signal, R_n , can be written as

$$R_n = \Phi E_n + N, \quad (3.55)$$

where E_n denotes the modulated emitted signal, Φ designates the transmission channel and N is the channel noise component characterized by zero-mean complex valued Gaussian variable having variance N_0/T_c . R_n is demodulated and \hat{C}_n is estimated as the soft values frame to be decoded.

PPHTC Decoder Description

Fig. 3.5 gives a detailed and general representation of the modified iterative decoding algorithm. $n - 1$ UEP-MAPs are concatenated and followed by a single MAP decoding. In the parallel structure decoding, it is commonly acknowledged that only the information bit is estimated. Therefore, the PCCC used MAPs are often referred to as bit MAPs.

The decoder receives the estimated soft information \hat{C}_n from the channel demodulator. The bit MAP decoders compute the data in the reverse order of encoding. Each bit MAP block number i performs the decoding on the trellis corresponding to encoder G_i , receives channel systematic S_i and parity P_i soft values, and outputs $L_{ext}(\hat{c}_i)$ and $L_{soft}(\hat{c}_i)$, where $i = 1 \dots n$. $L_{ext}(\hat{c}_i)$ and $L_{soft}(\hat{c}_i)$ denote the extrinsic and soft information referring to the encoded data \hat{c}_i . The forward transmission and estimation of the extrinsic and soft information may be described as:

- de-interleave $L_{ext}(\hat{c}_i)$ with π_{i-1}^{-1} and forward $L_{priori}(\hat{c}_{i-1})$,

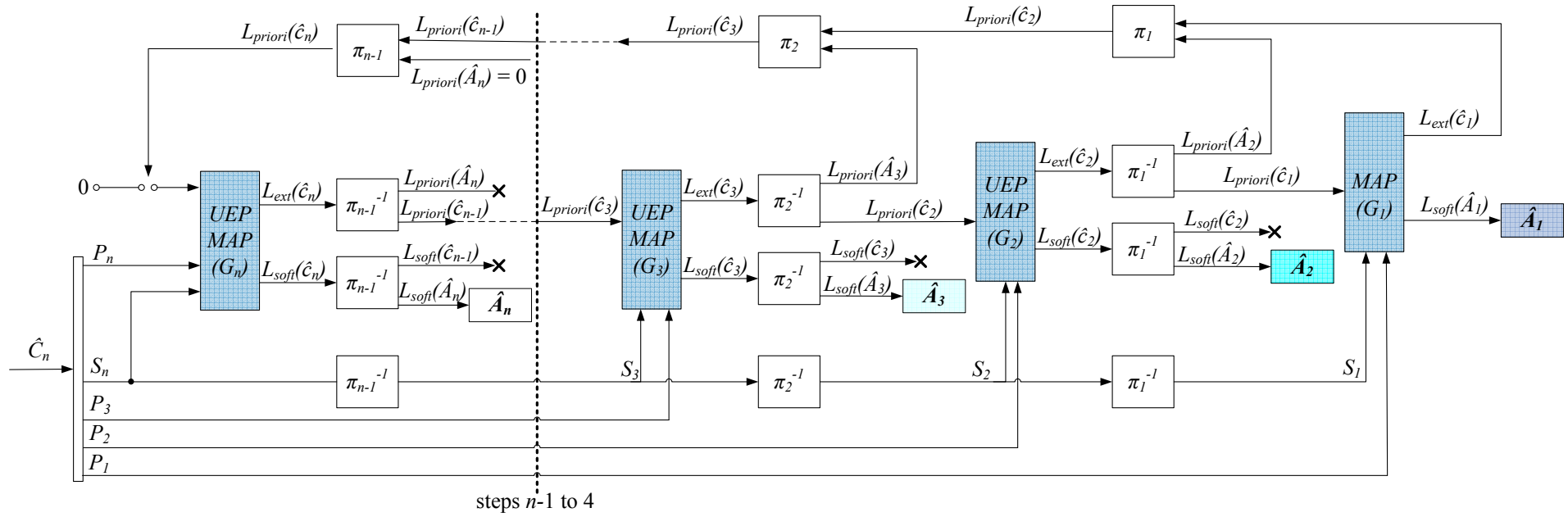


Figure 3.5. General form for the PPHTC decoder.

- de-interleave $L_{soft}(\hat{c}_i)$ using π_{i-1}^{-1} and estimate $L_{soft}(A_i)$, do not use $L_{soft}(\hat{c}_{i-1})$,

where $i = n \dots 2$. We note that $L_{priori}(\hat{A}_n)$ is not used since this last class is only decoded by UEP-MAP number n , i.e. corresponding to encoder G_n . The hard estimation value for the classes is denoted by \hat{A}_i with $1 \leq i \leq n$.

$L_{ext}(\hat{c}_1)$ is transmitted to the backward looping. Except for $L_{priori}(\hat{A}_n)$, every other supplementary priori information $L_{priori}(\hat{A}_i)$, with $2 \leq i \leq n$, is used as valuable information when iterating backwards, i.e. from MAP block G_1 to MAP block G_n . As shown in Fig. 3.5, during the backward looping, all available priori information is progressively reassembled and interleaved. Step $(n - 1)$ th output, $L_{priori}(\hat{c}_{n-1})$, is interleaved with one vector the size of class \hat{A}_n whose values are set to zero. This choice is made to avoid the divergence of MAP decoder G_n by neither inserting errors, nor its own extrinsic information. $L_{priori}(\hat{c}_n)$ is further used as a priori information for this n th decoding block.

The forward and backward looping is continued until convergence is established. After the last iteration, the hard estimations $\hat{A}_1, \dots, \hat{A}_n$ of the n different classes are obtained.

As detailed in Fig. 3.5, each class except the n th one experiences a "full turbo" decoding process whose number of dimensions coincide with the class priority. Through backward looping, we gather all remaining extrinsic information which we reuse as to not loose any existent error corrections. The performance gains are comparable to turbo quality in certain use cases. The n th class does not benefit from the reuse of it's priori information since only projected in one dimension space by one rate-1/2 RSC. Nevertheless, in some use cases, the exchange of large size extrinsic information helps in computing more reliable probabilities in this n th trellis, thus contaminating the n th class bits also.

SPHTC Decoder Description

The proposed decoder structure is presented in Fig. 3.6. The iterative algorithm is based on the classical turbo decoding, using the soft-input soft-output (SISO) or symbol by symbol Maximum A Posteriori (MAP) algorithm. Here, the MAP estimation is performed on both information (or systematic) and redundancy (or parity) bits. Therefore, one can say that the estimation is performed on the overall symbol.

The decoder receives the estimated soft information \hat{C}_n from the channel demodulator. The SISO decoders compute the data in the reverse order of encoding. Each symbol MAP block represented in Fig. 3.6 performs the decoding on the trellis corresponding to encoder G_i and outputs $L_{ext}(\hat{C}_i)$ and $L_{soft}(\hat{c}_i)$, where $i = 1 \dots n$. $L_{ext}(\hat{C}_i)$ and $L_{soft}(\hat{c}_i)$ denote the extrinsic information referring to the encoded data C_i and the log likelihood soft information relative to c_i , respectively. π_j refers to the interleaver matrix, as defined for the encoder's structure, and π_j^{-1} its corresponding inverse interleaver matrix, with $j = 1 \dots n - 1$.

The soft information, $L_{soft}(\hat{c}_i)$, is de-interleaved and split at each level of decoding, except the first one, to obtain soft values: $L_{soft}(\hat{C}_{i-1})$ and $L_{soft}(\hat{A}_i)$. $L_{soft}(\hat{C}_{i-1})$ is not used, but contains information on classes A_1, \dots, A_n . $L_{soft}(\hat{A}_i)$ data allows the estimation of the i th level class. The hard estimation value is denoted by \hat{A}_i .

Analysing the MAP decoders from n to 2, the extrinsic likelihood, $L_{ext}(\hat{C}_i)$, is de-multiplexed into extrinsic data relative to the systematic and parity bits of \hat{C}_i , that we call $L_{ext}(S_i)$ and $L_{ext}(P_i)$. These two quantities are essential for the hierarchical UEP decoding structure, as they contain all extrinsic information relative to all levels classes. Their circulation through the decoding process ensures no loss in supplementary information essential to good and fast decoding. We choose to transmit $L_{ext}(S_i)$ forward; it is de-interleaved and split into $L_{priori}(\hat{C}_{i-1})$ and $L_{priori}(\hat{A}_i)$. $L_{priori}(\hat{C}_{i-1})$ is used as a priori information for the next $(i - 1)$ th MAPs.

$L_{ext}(P_i)$ and $L_{priori}(\hat{A}_i)$ will be used as supplementary information when iterating backwards, i.e. from MAP G_1 to MAP G_n . As shown in Fig. 3.6, during the backward iteration, the extrinsic output of G_1 , $L_{ext}(\hat{C}_1)$, is interleaved together with $L_{priori}(\hat{A}_2)$. The result is equivalent to a priori information for c_1 , called $L_{priori}(\hat{c}_1)$. This soft value quantity is further multiplexed with the extrinsic information corresponding to the parity bits of \hat{C}_2 , $L_{ext}(P_2)$, as to obtain its complete extrinsic information, called $L'_{ext}(\hat{C}_2)$.

With $i = 1 \dots n - 2$, the next looping steps may be described similarly:

- interleave $L_{ext}(\hat{C}_i)$ with $L_{priori}(\hat{A}_{i+1})$,

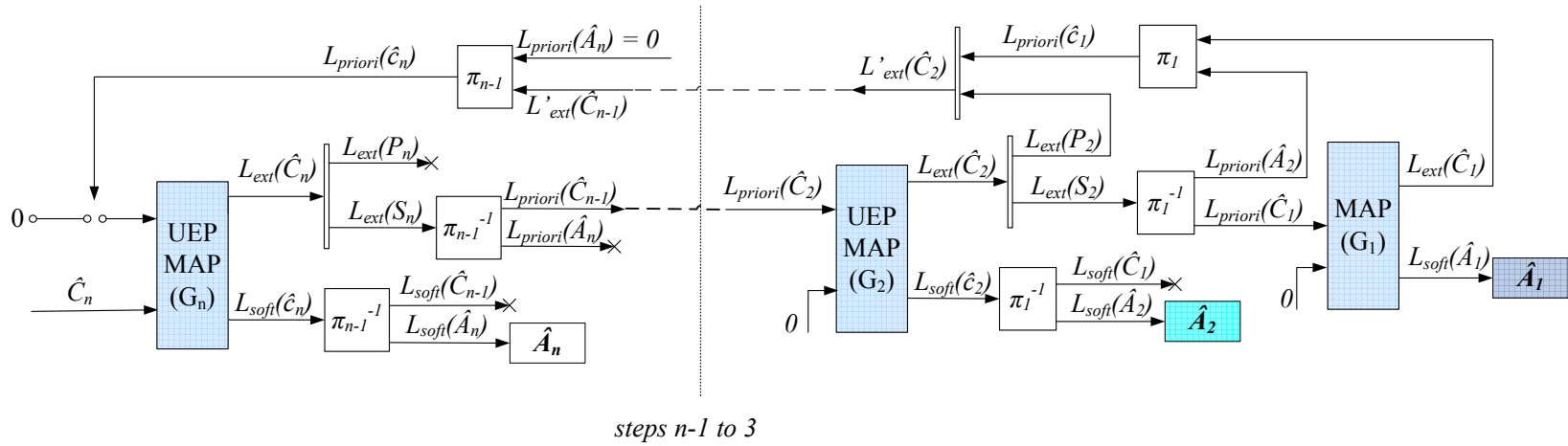


Figure 3.6. General form for the SPHTC decoder.

- multiplex the resulting $L_{priori}(\hat{c}_i)$ with the parity extrinsic information, $L_{ext}(P_{i+1})$,
- feed backward the extrinsic information $L'_{ext}(\hat{C}_{i+1})$.

Step $(n - 1)$ th output, $L'_{ext}(\hat{C}_{n-1})$, is interleaved with one vector the size of class A_n whose values are set to zero, choice made to avoid the divergence of MAP decoder G_n by neither inserting errors, nor its own extrinsic information. $L_{priori}(\hat{c}_n)$ is further used as a priori information for this n th decoding block.

The forward and backward looping is continued until convergence is established. After the last iteration, the hard estimations $\hat{A}_1, \dots, \hat{A}_n$ of the n different classes are obtained. They are regrouped to form the final estimated frame \hat{A} .

The proposed decoder's particularities consist in the ability to extract class A_i from UEP-MAP decoder number i . Forward and backward looping are using all available extrinsic information on each and every class and at all decoding levels. All classes benefit from the progressive error correction process. Each decoding step benefits from a different size trellis that recomputes the soft values differently from neighboring decoders, but considering their respective gains. The interleaver plays a key role. In forward decoding, it splits the frame's information, thus reducing code words distance properties for the next decoder and breaking existing error blocks. In backward looping, it reassembles all available extrinsic information by re-breaking created error blocks and continuously enlarging the existent low weight code words. The interleaver helps use the inter-class contamination and inter-dependence obtained through the hierarchical encoding.

3.2.2.3 n -D Progressive UEP MAP

The decoding is performed by n concatenated MAPs. Within these n MAPs, only a single MAP is decoding a single type of information, i.e. A_1 . As shown in Fig. 3.5 and Fig. 3.6, A_1 is decoded last. Thus, it is the single class for which the priori and channel informations of other classes do not interfere. The remaining $n - 1$ MAPs can be considered UEP-MAPs, since they handle several types of UEP data streams.

The expression (3.18) can be generalized to n UEP classes as

$$P^{(UEP-MAP)}(a_t|\hat{C}) = \frac{1}{P(\hat{C})} \sum_{C \in \Omega|a_t} \prod_{j=1}^{N_1+N_2+\dots+N_n} P(\hat{C}_j|a_j \in A) \prod_{k_1=1}^{N_1} P(a_{k_1}|a_{k_1} \in A_1) \dots \prod_{k_n=1}^{N_n} P(a_{k_n}|a_{k_n} \in A_n). \quad (3.56)$$

However, in the proposed decoding structure, each G_{n-i+1} MAP receives $n - i + 1$ classes. Therefore, the above equation is restricted for only $n - i + 1$ different channel data streams and $n - i + 1$ different priori data streams. Each class benefits of its own and the others' channel and priori information, with the exception of A_n . The latter priori probabilities are supposed equally likely, and its turbo behavior is due to the surrounding priori data only, regarding the remaining $n - 1$ classes.

3.2.2.4 BCJR Algorithm n -D Extension

The APP expression for n UEP classes is easily generalized from (3.37) as

$$\begin{aligned}
P(\hat{a}_t | \hat{C}_i) &= \frac{1}{P(\hat{C})} \sum_{C \in \Omega | a_t} \alpha_0(b) \beta_N(v) \\
&\quad \prod_{k_1=0}^{N_1} \left\{ p(\hat{C}_{k_1}^{(0)} | C_{k_1}^{(0)} \in A_1) p(\hat{C}_{k_1}^{(1)} | C_{k_1}^{(1)} \in A_1) P(\hat{a}_{k_1} | a_{k_1} \in A_1) \right\} \\
&\quad \prod_{k_2=0}^{N_2} \left\{ p(\hat{C}_{k_2}^{(0)} | C_{k_2}^{(0)} \in A_2) p(\hat{C}_{k_2}^{(1)} | C_{k_2}^{(1)} \in A_2) P(\hat{a}_{k_2} | a_{k_2} \in A_2) \right\} \\
&\quad \dots \\
&\quad \prod_{k_n=0}^{N_n} \left\{ p(\hat{C}_{k_n}^{(0)} | C_{k_n}^{(0)} \in A_n) p(\hat{C}_{k_n}^{(1)} | C_{k_n}^{(1)} \in A_n) P(\hat{a}_{k_n} | a_{k_n} \in A_n) \right\}.
\end{aligned} \tag{3.57}$$

But every MAP decoding at level i is based on the BCJR algorithm computed on a different size trellis corresponding to encoder G_i , with $i = 1 \dots n$. For simplicity reasons, we will always denote by t the observation time and by \hat{a}_t the received bit value at time instant t in all trellis.

In every i th trellis, the APP of one transition from state $\Psi_{i,t} = p_i$, at time instant t , to state $\Psi_{i,t+1} = q_i$, at time instant $t + 1$, given the observed received sequence \hat{C}_i may be expressed as APP of receiving bit \hat{a}_t at time t

$$\begin{aligned}
P^{(i)}(\hat{a}_t | \hat{C}_i) &= \sum_{(p_i, q_i) \in T^{(i)}} P(\Psi_{i,t} = p_i, \Psi_{i,t+1} = q_i | \hat{C}_i) \\
&= \frac{1}{P(\hat{C}_i)} \sum_{(p_i, q_i) \in T^{(i)}} \alpha_t^{(i)}(p_i) \gamma_t^{(i)}(p_i, q_i) \beta_{t+1}^{(i)}(q_i),
\end{aligned} \tag{3.58}$$

where $T^{(i)}$ denotes the set of possible transitions (p_i, q_i) corresponding to bit a_t . We can replace α, γ, β with their trellis computed expressions as shown in section 3.2.1.4.

3.2.2.5 Log Likelihood Extended Interpretation

Hereafter, we denote the LLR probabilities at decoding level i by the symbol $L^{(i)}$, defined as

$$L^{(i)}(\hat{a}_t | \hat{C}_i) = \log \frac{P^{(i)}(\hat{a}_t = 1 | \hat{C}_i)}{P^{(i)}(\hat{a}_t = 0 | \hat{C}_i)}. \tag{3.59}$$

We use $L_{ext}^{(i)}, L_{soft}^{(i)}, L_{priori}^{(i)}$ and $L_{channel}^{(i)}$ to reference the extrinsic, soft, a priori and channel information at level i respectively.

The detailed expressions of the LLRs for the systematic and parity bits may therefore be written as

$$L_{channel}^{(i)}(\hat{C}_{i,t}^{(0)} | \hat{a}_t) = \log \frac{P^{(i)}(\hat{C}_{i,t}^{(0)} | \hat{a}_t = 1)}{P^{(i)}(\hat{C}_{i,t}^{(0)} | \hat{a}_t = 0)}, \tag{3.60}$$

where bit a_t can denote a systematic bit only in the PPHTC case, but might refer to either systematic or parity bit in the SPHTC case.

$$L_{priori}^{(i)}(\hat{a}_t) = \log \frac{P^{(i)}(\hat{a}_t = 1)}{P^{(i)}(\hat{a}_t = 0)} \tag{3.61}$$

$$L_{ext}^{(i)}(\hat{a}_t) = \log \frac{\sum_{(p_i, q_i) \in T_1^{(i)}} p(\hat{C}_{i,t}^{(1)} | C_{i,t}^{(1)} = C_{i,t}^{(1,p_i, q_i)}) \alpha_t^{(i)}(p_i) \beta_{t+1}^{(i)}(q_i)}{\sum_{(p_i, q_i) \in T_0^{(i)}} p(\hat{C}_{i,t}^{(1)} | C_{i,t}^{(1)} = C_{i,t}^{(1,p_i, q_i)}) \alpha_t^{(i)}(p_i) \beta_{t+1}^{(i)}(q_i)}, \quad (3.62)$$

where the summation is performed over the transitions for which the systematic bit, or the parity bit, is equal to 1 or 0. $T_0^{(i)}$ and $T_1^{(i)}$ denote the set of transitions (p_i, q_i) which correspond to the input equal to 0 and 1 respectively on trellis number i (MAP G_i).

Ignoring the superscript for simplicity and extending to the entire code block of data, the general LLR expression becomes

$$L_{soft}(A_i | \hat{C}_i) = \begin{cases} L_{channel}(S_i) + L_{ext}(A_i), & \text{if } i = n, \\ L_{channel}(S_i) + L_{priori}(A_i) + L_{ext}(A_i), & \text{if } i < n. \end{cases} \quad (3.63)$$

In serial turbo decoding, only the G_n MAP decoder receives direct channel information. The $n - 1$ following MAP decoders receive only priori information that is considered in the BCJR algorithm as channel information, since it contains extrinsic values of systematic and parity bits from the previous decoding step. Thus, the priori corresponding branch is set to zero. In the parallel decoding, every constituent MAP receives channel information, and the priori data is originally calculated by another existent MAP.

After every step's BCJR algorithm, one corresponding class is estimated. Even though classes $A_1 \dots A_{n-1}$ go through different size trellis, they benefit of a full turbo decoding. Extrinsic information is available, priori computed by every G_1 to G_{n-1} MAP. Only the n th class is decoded by a single UEP-MAP. Therefore, no additional extrinsic information is available for the n th class. However, $\alpha^{(n)}$ and $\beta^{(n)}$ are computed on this n th trellis using all priori information. For every bit \hat{a}_t of class A_n , $\alpha^{(n)}$ and $\beta^{(n)}$ consider all adjacent bits of A_1, \dots, A_{n-1} , for which valid priori values exist and have been calculated by the remaining $(n - 1)$ th trellis.

3.3 Code Properties Analysis

In this section, we focus on different PPHTC and SPHTC properties. Progressively inserting data in the encoding process modifies turbo code characteristics. Therefore, we shortly overview these characteristics and their influence on the code behavior. However, we restrain the analysis only to the 2-D UEP progressive encoding for simplicity reasons. The extension to the n -D structure is straightforward.

3.3.1 Factor Graph

Factor graphs denote a Forney style graphical interpretation of the encoding process. They provide a visual representation of the turbo encoder.

Fig. 3.7 presents the factor graph interpretation for the **PPHTC**. The upper graph represents the upper RSC encoding process, where class A_1 is encoded and only parity bits P_1 are fed to the encoder's output. The series of bits $a^{(1)} \in A_1$ are forwarded to the interleaver of size $N_1 + N_2$, which also receives the series of bits $a^{(2)} \in A_2$. The latter are spread by the interleaver in-between the first class bits, and therefore the interleaved output is composed of both A_1 and A_2 bits. This series is denoted by S_2 and represents the systematic output of the lower RSC. The series of length $N_1 + N_2$ is equally protected by this lower RSC and the output is denoted by the parity P_2 .

This factor graph give a visual interpretation of the PPHTC encoding behavior. Its purpose is thus highlighted: each class is encoded at a level proportionally to its channel sensitivity. The lower level classes are spread between the higher level better protected bits. Even though the first class, A_1 , remains turbo encoded, the second class, A_2 , is basically only convolutionally encoded. However, the series of bits of the second class are spread in-between those of class A_1 , and, channel errors do not have the same influence on performances compared to the case where class A_2 has been encoded alone. This is explained by the fact that we have proposed a turbo-like decoding of class A_2 . We have introduced the perspective of decoding class A_2 in a turbo fashion, by exploiting the properties of the MAP decoding in the UEP context. Thus, in the decoding trellis, when a bit

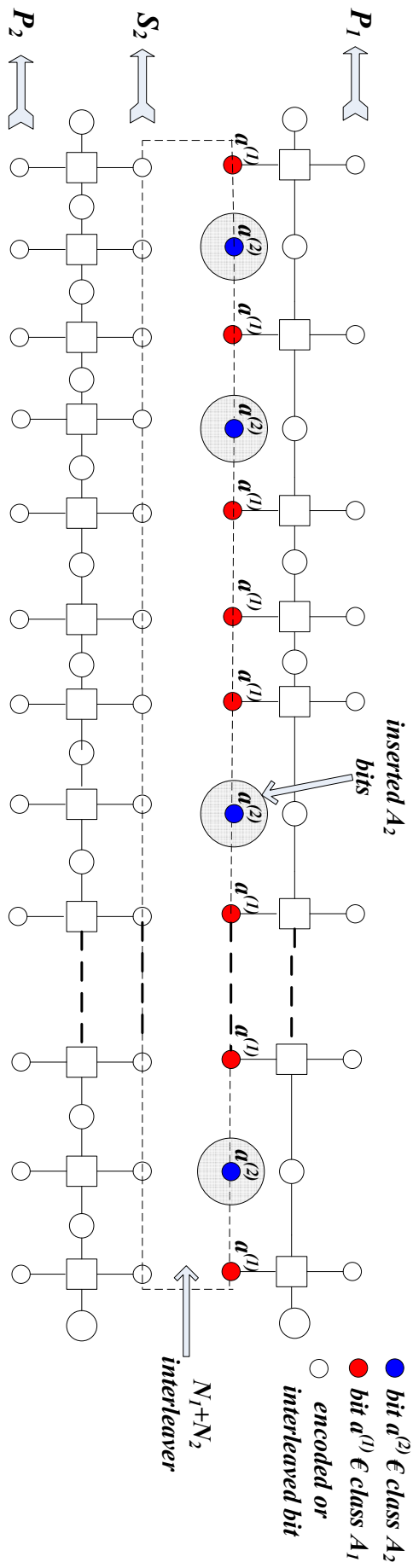


Figure 3.7. PPHTC factor graph representation.

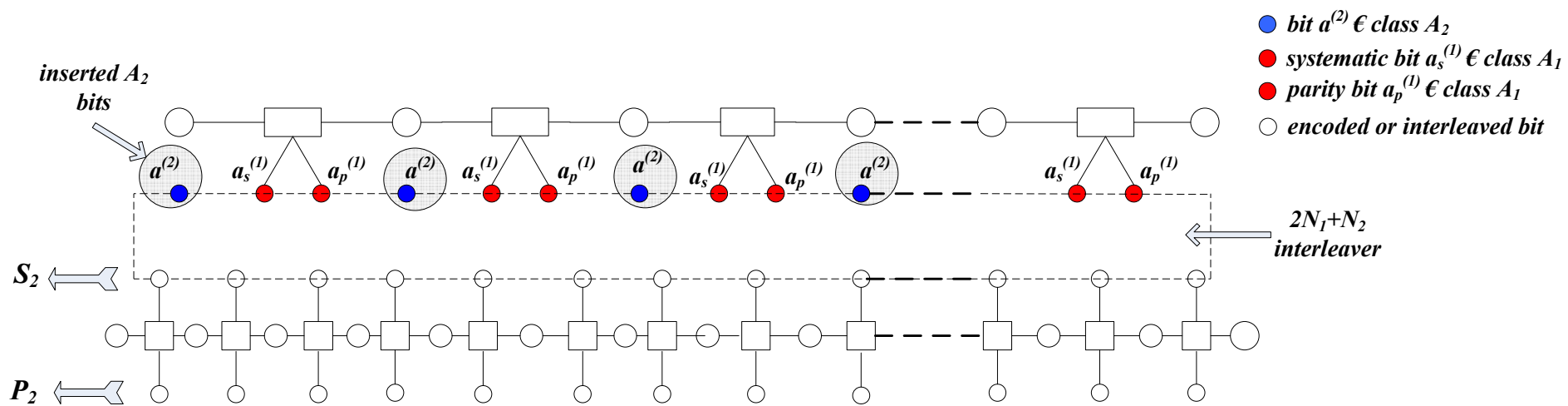


Figure 3.8. SPHTC factor graph representation.

$a^{(2)}$ is estimated, its probability is calculated considering the priori probabilities of all class A_1 as well, i.e. of bits $a^{(1)}$. The PPHTC decoding exploits the hidden redundancy, i.e. the redundancy not directly related to the decoded information A_2 , but hidden in the bits of A_1 .

Fig. 3.8 gives the representation of the **SPHTC** using this factor graph interpretation. The upper structure from this figure shows the outer encoder state with its outputs: systematic bits, $a_s^{(1)}$, and parity bits, $a_p^{(1)}$, of class A_1 . These bits are multiplexed with class A_2 bits, denoted by $a^{(2)}$, and interleaved by a $2N_1 + N_2$ interleaver depth². The lower structure shows the inner code which encodes the interleaver output and outputs systematic and parity bits, S_2 and P_2 .

Fig. 3.8 highlights the purpose of the interleaver. The latter must distribute the second class bits between the first class bits. It becomes obvious that, the larger the class A_1 length is, the more spread the bits of class A_2 can become. Thus, the systematic and redundancy bits of class A_1 at the output of the outer encoder will experience a different transmission channel than the inner encoder's output. The latter benefits not only from a different channel view due to the interleaver, but also from a larger channel data spreading because of the presence of A_2 and vice-versa. Compared to the PPHTC case, for equal sized classes, the series of bits $a^{(2)}$ are spread over a larger dimension. This is due to the fact that class A_1 both systematic and parity outputs of the outer encoder, S_1 and P_1 , are fed to the inner encoder. The UEP iterative decoding will benefit of a larger size hidden redundancy priori probabilities.

3.3.2 Pilot Insertion Codes

The here proposed PPHTC and SPHTC structures can be considered as a global generalization and evolution of pilot insertion codes. The idea behind pilot insertion codes is the improvement of the decoding performances using pilot sequences. The concept is derived from the well known channel estimation algorithms, where pilot symbols are used for predicting the current channel state. Similarly, the encoder and decoder can use pilot sequences for improving the estimation of the decoded signal in, what is called, "pilot symbol assisted coding schemes". Dummy bits or known sequences of bits are multiplexed with the code block data before turbo encoding. While some authors simply use an interleaver for spreading the pilot bits between the information symbols, others actually perform an optimization of the pilot insertion. In both approaches, it has been proved that these perfect bits support the decoding decision and result in an improved quality of the received signal.

In [40], [41], and [42] is given an interesting analysis of pilot insertion codes. The technique of inserting known sequences of bits in the encoding process is referred to as "trace bit injection", "pilot insertion code" or "insertion convolutional code". In [40], the authors note that the idea of injecting known bits in the input data stream has generally been used to accelerate convergence and reduce the error floor of turbo codes. This characteristic is particularly important for delay constrained applications using short interleavers. But through their work, the authors propose the code optimization using trace bit injection, followed by selective puncturing. While the pilot insertion improves the subcodes distance spectra, the puncturing helps maintaining a constant code rate. In [41], pilot insertion codes are also introduced as a means to improve the turbo distance spectra, but with a rate adaptation capability. Pilots are spread through the source data bits as to reduce or eliminate low weight codewords. The technique helps increasing the code minimum distance effectively. The code weight spectrum is improved and thus the results over multipath fading channels also. Low Hamming weight codewords manifest themselves particularly in the error floor region at high signal to noise ratios (SNR) values. The author's main contribution is the pilot insertion optimal pattern algorithm. This pattern is computed considering the weight spectral lines inferior to a pre-defined threshold for the code distance spectrum. In [42], extrinsic information transfer charts are computed for insertion convolutional codes. This theoretical approach is used to quantify the expected turbo decoding gain, which depends on the fraction of inserted pilot bits.

The here proposed patented codes go beyond these concepts. Instead of inserting dummy bits, we propose the progressive insertion of information data during the encoding process. The difference between pilot codes and the PPHTC and SPHTC concepts is the nature of the inserted data in the encoder. Pilot codes use infinite reliability bits that are bound to improve the decoding performances. On the contrary, PPHTC and SPHTC use

²For the simplicity of notations and graphical representations, we do not consider tail bits, even though they are included in computer simulations.

unknown receiver data. Every single data sequence, inserted progressively in the encoding progress, belongs to the application higher layer. The inserted data is not meant for decoding regulation, but represents effective estimated information. The difficulty of the proposed UEP turbo evolution consists in predicting the decoder performances. The code minimum distance is affected with each newly introduced coding dimension. And, similarly to the pilot case, the turbo iterative decoder uses the probabilities of the inserted data in estimating neighboring bits and vice-versa. Each class has been encoded using a different number of dimensions, therefore its corresponding extrinsic and priori probabilities have a different reliability level in the turbo iterative decoding.

Interesting performance results are given in section 3.4, where the pilot behavior is also analyzed for a better comprehension of the code properties.

3.3.3 Virtual Code Rate

The code structure has an interesting characteristic. By progressively inserting data in the encoder structure, each encoded class data will benefit of additional channel redundancy than if it were encoded by itself. This may be interpreted as a virtual class rate. The factor graphs representations give a good visual background for this new transmission rate.

The **PPHTC** exploits the UEP properties of classes A_1 and A_2 by hierarchically encoding them. The interleaving depth becomes $N_1 + N_2$, and the encoder's output is larger than the case where the classes would have been encoded independently of each other.

In the **SPHTC** case, A_2 bits are also inserted before the interleaving process. Therefore, the interleaving depth is of $2N_1 + N_2$ and the inner code encodes a larger frame than the outer code. Elements of class A_1 , as well as elements of class A_2 , benefit of an increased channel redundancy then by being encoded by themselves.

The virtual rate for class A_i , denoted by $r_{A_i}^{(v)}$, is written as

$$r_{A_i}^{(v)} = \frac{A_i}{\sum_{j=1}^n \frac{A_j}{r_{A_j}}} = \frac{x_i A}{\sum_{j=1}^n \frac{x_j A}{r_{A_j}}} = \frac{x_i}{\sum_{j=1}^n \frac{x_j}{r_{A_j}}}, \quad (3.64)$$

where $i \in \{1, 2\}$, and r_{A_j} the code mother rate for the respective class. Therefore, each class of bits A_i is transmitted on the wireless channel with $\Delta_{i,r}^{(v)}$ more redundancy than provided by the code itself. $\Delta_{i,r}^{(v)}$ may be written as

$$\Delta_{i,r}^{(v)} = A_i (r_{A_i}^{(v)} - r_{A_i}), \quad (3.65)$$

and refers to the other class redundancies than itself.

The technique of introducing additional channel redundancy in the encoding structure other than useful data in order to only modify transmission rate is known in literature as pruning. Pruning can refer to only dummy bits, whose main goal is to spread the channel errors in a larger dimension. This technique can improve performances, but less than the use of pilots. If pilots were introduced in the encoding process, their purpose would mainly be of improving the turbo decoding with the cost of additional redundancy. The difference with the PPHTC and SPHTC structures is that actual useful information is used to virtually increase rates.

3.3.4 Weight Characteristics

The convolutional code error detection and error correction capabilities are related to the encoded sequence distance properties. The performance of turbo codes themselves is known to be bounded by the error floor, especially in the parallel structure case. This error floor is a direct consequence of the code low free distance. The theoretical performances of turbo codes have been largely investigated based on their free distance and spectrum properties. The free distance is defined as the minimum Hamming distance calculated between all possible codewords. The Hamming weight refers to the Hamming distance of a codeword to the all-zero codeword. The code free distance is an important characteristic, which determines the code error correction performance. Thus, the performance improves with an increasing free distance.

But these theoretical results are mainly related to very low error rates, e.g. 10^{-5} , which are not of particular interest for voice communications, especially in the PMR context. However, they might become useful for future video transmission, and we provide a short study of the PPHTC and SPHTC weight characteristics. Moreover, an analysis of the weight influence on the encoded sequence of bits offers an enhanced comprehension of the decoding performances.

But in order to provide a description of the turbo code through its distance characteristics, we must firstly present the RSC weight error function computation. Weight error functions denote mathematical series which describe the distance properties of a code. Thus, they enumerate an infinity of input and output possible distances, together with their multiplicities or number of appearances in the encoded sequence. These weight enumerator functions are essential ingredients in all expressions estimating error probabilities, since their first factor is a direct reference to the code free distance. The series is called *input output weight error function* or IOWEF when both input and output weights are expressed.

The IOWEF is specific to each type of code. We must therefore compute it for the RSC used with the PPHTC and SPHTC. For simplicity, we have been supposing identical RSCs for 2-D UEP structures. One simple method for computing the IOWEF consists in analyzing the state diagram of the RSC. It is a practical method from which the generator polynomial of the IOWEF is determined.

For computer simulations, we have been using an RSC specific to LTE, an 8 state recursive encoder. Its generator matrix may be written as:

$$G(D) = \left[1, \frac{g_1(D)}{g_0(D)} \right] \quad (3.66)$$

where $g_1(D) = 1 + D + D^3$ also written as $(1101)_2$ or $(15)_8$, and $g_0(D) = 1 + D^2 + D^3$ also written as $(1011)_2$ or $(13)_8$.

In order to compute the IOWEF, the state diagram of the RSC must be redrawn with some modifications:

- the edges must be labeled with a variable H that denotes the output sequence, with the exponent of h representing the weight for that output sequence (computed Hamming distance from the all-zero sequence), e.g. for an output sequence of 11, the edge will be labeled H^2 ;
- the state S_1 is eliminated, because its loop is equal to 0 and this does not contribute to the weight of a sequence;
- the state S_1 is split into two states: input state and output state.

For each edge, its label is computed as the product of input and output sequence labels. If the H variable is used for output sequences, the W variable is used for input sequences with the same principles.

The modified state diagram of the code is represented in Fig. 3.9.

We further write the system of equations which will determine the IOWEF generating function. In the following equations, X_i stand for dummy variables corresponding to the diagram states. X_{in} and X_{out} denote the input and output states, i.e. S_0 .

$$\begin{aligned} X_4 &= WH^2X_{in} + WX_1, \\ X_2 &= HX_4 + HX_5, \\ X_6 &= WHX_4 + WHX_5, \\ X_7 &= WH^2X_7 + WX_6, \\ X_3 &= X_7 + H^2X_6, \\ X_5 &= WHX_3 + WHX_2, \\ X_1 &= HX_2 + HX_3, \\ X_{out} &= H^2X_1. \end{aligned} \quad (3.67)$$

We will denote the IOWEF by $T^G(W, H)$, and this function is determined by computing

$$T^G(W, H) = \frac{X_{out}}{X_{in}}. \quad (3.68)$$

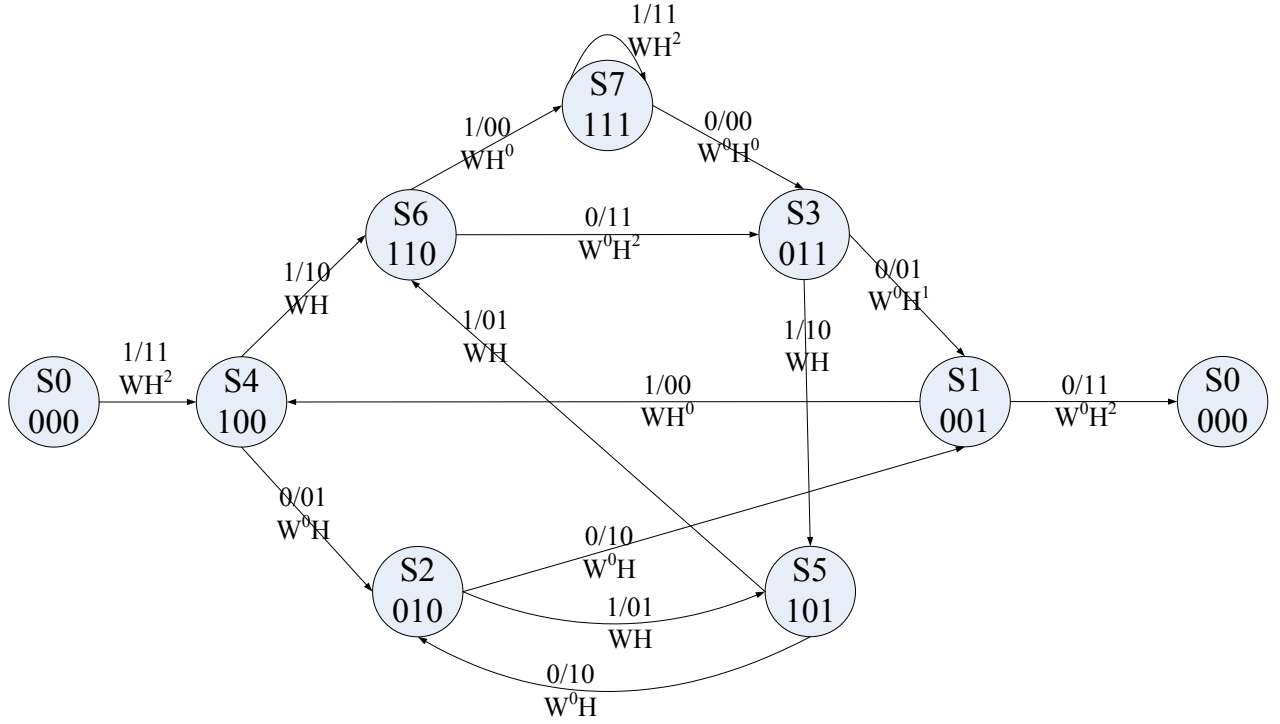


Figure 3.9. The state diagram for the 8 state RSC.

After computing the X_{out} and X_{in} values from the system of equation, the value of the IOWEF becomes:

$$T(W, H) = \frac{WH^6(1 + W^2 - W^2H^4)}{1 - WH^2(3 + 2W^2 - 2W^2H^4)}. \quad (3.69)$$

This $T^G(W, H)$ function must be written under the form

$$T^G(W, H) = \sum_{h=0}^{\infty} \sum_{w=0}^{\infty} A_{w,h} W^w H^h, \quad (3.70)$$

where $A_{w,h}$ represents the number of codewords of input weight w generating the output weight h .

Therefore, we must develop the equation obtained from the system as:

$$T^G(W, H) = WH^6(1+W^2-W^2H^4) \times \sum_{k=0}^{+\infty} 3^k W^k H^{2k} \sum_{p=0}^k \left(C_p^k (2/3)^p W^{2p} \times \sum_{t=0}^p \left(C_t^p (-1)^t H^{4t} \right) \right). \quad (3.71)$$

This gives:

$$T^G(W, H) = \sum_{k=0}^{\infty} \sum_{p=0}^k \sum_{t=0}^p (WH^6 + W^3H^6 - W^3H^{10}) 3^k C_p^k \left(\frac{2}{3} \right)^p C_t^p (-1)^t W^{k+2p} H^{2k+4t}. \quad (3.72)$$

This formula can be developed through computer simulation and the coefficients $A_{w,h}$ automatically calculated. In expression (3.70), the output weight h refers to both systematic and parity bits, i.e. the output encoded symbol. The obtained results represent the coefficients of the IOWEF for this specific RSC.

For computing the IOWEF coefficients of turbo codes, we must take into consideration that two RSCs are concatenated, separated by an interleaver. But, for any interleaver type, it is complicated to estimate the WEF of a turbo code. Therefore, the concept of uniform interleaver has been introduced. The property of the uniform interleaver is that it maps an input sequence of length N into all distinct C_i^N permutations with equal probability $1/C_i^N$. Each of the C_i^N inputs of weight i lead to one distinct codeword at the encoder's output,

therefore the factor $1/C_i^N$ is used for a proper normalization when computing the IOWEF coefficients for a turbo code. (With increasing block length, the expected number of codewords of fixed weight converges to a limit.)

PPHTC

The IOWEF for the PPHTC is written as follows (see Fig 3.10):

$$T^{C_p}(W, H) = \sum_{\omega_1=0}^{N_1} \sum_{\omega_2=0}^{N_2} \sum_{h=0}^{2(N_1+N_2)+N_1} A_{\omega_1, \omega_2, h}^{(C_p)} W^{\omega_1} W^{\omega_2} H^h, \quad (3.73)$$

where $A_{\omega_1, \omega_2, h}^{(C_p)}$ denotes the average number of codewords with input weights ω_1 and ω_2 for classes A_1 and A_2 respectively, that generate an output encoded codeword weight of h . The C_p superscript refers to the parallel code structure. But the number of input codewords can be split between the two classes as

$$A_{\omega_1, \omega_2, h}^{(C_p)} = A_{\omega_1, h_1, h_2}^{(A_1)} \times A_{\omega_2, h_2}^{(A_2)}, \quad (3.74)$$

where $A_{\omega_1, h_1, h_2}^{(A_1)}$ gives the average number of codewords of class A_1 with input weight ω_1 , that will contribute to the output weight h through h_1 and h_2 . And $A_{\omega_2, h_2}^{(A_2)}$ refers to the average number of codewords of class A_2 with input weight ω_2 , that will contribute to the same output weight h through h_2 only. h_1 and h_2 measure the weights of the parity output of each constituent RSC respectively, as shown in Fig. 3.10. We note that $h = h_1 + h_2 + \omega_1 + \omega_2$.

Each class number of average codewords can be estimated. However, given the code structure, the specific average of codewords per constituent code must be considered as follows.

- Class A_1 is turbo encoded, i.e. is encoded by the concatenation of two RSCs, therefore its average IOWEF coefficients are computed similarly to a classical PCCC. The PPHTC coefficient corresponding to A_1 influence is calculated as the multiplication of the coefficients of the constituent codes, multiplied by the equally likely probability of that specific combination introduced by the interleaver, $\frac{1}{C_{\omega_1+\omega_2}^{N_1+N_2}}$, which also acts as a normalization factor.

$$A_{\omega_1, h_1, h_2}^{(A_1)} = \frac{A_{\omega_1, h_1}^{(G_1)} A_{\omega_1+\omega_2, h_2}^{(G_2)}}{C_{\omega_1+\omega_2}^{N_1+N_2}}, \quad (3.75)$$

where $A_{\omega_1, h_1}^{(G_1)}$ and $A_{\omega_1+\omega_2, h_2}^{(G_2)}$ represent the IOWEF coefficients for the constituent RSCs respectively. Since we have supposed identical RSCs, i.e. $G_1 = G_2 = G$, the values of this coefficients are derived from the above developed transfer function $T^G(W, D)$. The factor $C_{\omega_1+\omega_2}^{N_1+N_2}$ is written as such and not as $C_{\omega_1}^{N_1} C_{\omega_2}^{N_2}$, because the interleaver is supposed uniform and not making a difference between the two UEP classes.

- IOWEF coefficients for class A_2 bits can not be computed as the concatenation of two codes, since A_2 has been encoded only by a single RSC. Therefore

$$A_{\omega_2, h_2}^{(A_2)} = \frac{A_{\omega_1+\omega_2, h_2}^{(G_2)}}{C_{\omega_1+\omega_2}^{N_1+N_2}}. \quad (3.76)$$

Here, we consider the fact that class A_2 has been encoded a single time, and by a single RSC, i.e. G_2 . Thus, from the perspective of A_2 , its average number of codewords of weight ω_2 , that will impact output weight h_2 , is affected by the presence of A_1 and of the interleaver. G_2 encodes both classes A_1 and class A_2 , that have been previously interleaved. The number of A_2 codewords that generate h_2 considering the influence of ω_2 is equal to the global number of codewords corresponding to both input classes multiplied by the probability of having that specific combination, $\frac{1}{C_{\omega_1+\omega_2}^{N_1+N_2}}$.

The PPHTC weight spectral lines are computed as the set of all pairs $(h_i, \varphi_{h_i}^{(C_p)})$, where h_i is the Hamming distance and $\varphi_{h_i}^{(C_p)}$ the error coefficient determining the contribution of the codeword with weight h_i to the bit error probability,

$$\varphi_{h_i}^{(C_p)} = \sum_{w_i=1}^{N_i} \frac{w_i}{N_i} A_{\omega_i, h}^{(A_i)}. \quad (3.77)$$

The weight spectrum of the code is an important tool in estimating code performance bounds. The upper bounds on the error probability can give good estimation of the code results in the very low error rates region. A short overview of theoretical ML decoding limits for the PPHTC decoding of classes A_1 and A_2 is given in Appendix C.

SPHTC

The IOWEF for the SPHTC is written as follows

$$T^{C_s}(W, H) = \sum_{\omega_1=0}^{N_1} \sum_{\omega_2=0}^{N_2} \sum_{h=0}^{2(2N_1+N_2)} A_{\omega_1, \omega_2, h}^{(C_s)} W^{\omega_1} W^{\omega_2} H^h, \quad (3.78)$$

where $A_{\omega_1, \omega_2, h}^{(C_s)}$ denotes the average number of codewords with input weights ω_1 and ω_2 for classes A_1 and A_2 respectively, that generate an output encoded codeword weight of h . The (C_s) exponent refers to the serial code structure. Considering the influences of the weights of the two classes independently, the transfer function coefficient is written as

$$A_{\omega_1, \omega_2, h}^{(C_s)} = A_{\omega_1, h}^{(A_1)} \times A_{\omega_2, h}^{(A_2)}, \quad (3.79)$$

where $A_{\omega_1, h}^{(A_1)}$ and $A_{\omega_2, h}^{(A_2)}$ give the average number of codewords of class A_1 and A_2 with input weight ω_1 and ω_2 respectively, that contribute to the global output weight h . A_1 is firstly encoded by the outer RSC, and the input weight ω_1 generates the output code word of weight $\omega_1 + h_1$. The latter is fed to the interleaver, where the weight ω_2 of class A_2 is also introduced. The inner RSC thus receives a code word of weight $\omega_1 + h_1 + \omega_2$ and encodes it into a parity weight h_2 . The SPHTC output code word weight, h , becomes equal to $\omega_1 + h_1 + \omega_2 + h_2$. Fig 3.11 provides a comprehensive architecture of the weight interpretation.

As in the PPHTC case, the IOWEF coefficients for class A_1 must be computed considering the turbo-like structure of the encoder, i.e. the concatenation of two RSCs. But the IOWEF coefficients corresponding to class A_2 benefit of only the presence of the interleaver and the single RSC encoding.

- The IOWEF coefficients for class A_1 become:

$$A_{\omega_1, h}^{(A_1)} = \frac{A_{\omega_1, \omega_1+h_1}^{(G_1)} A_{\omega_1+h_1+\omega_2, h}^{(G_2)}}{C_{\omega_1+h_1+\omega_2}^{2N_1+N_2}}. \quad (3.80)$$

- The IOWEF coefficients for class A_2 become:

$$A_{\omega_2, h}^{(A_2)} = \frac{A_{\omega_1+h_1+\omega_2, h}^{(G_2)}}{C_{\omega_1+h_1+\omega_2}^{2N_1+N_2}}. \quad (3.81)$$

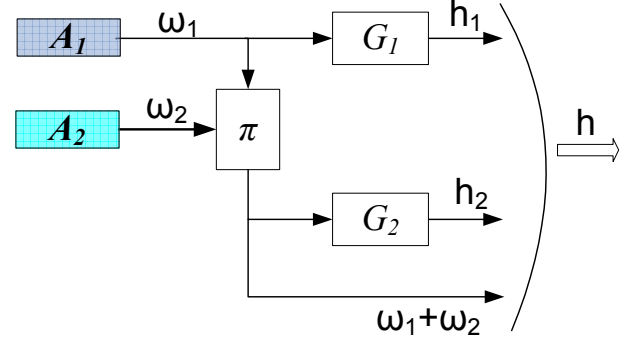


Figure 3.10. Input output weight representations for PPHTC.

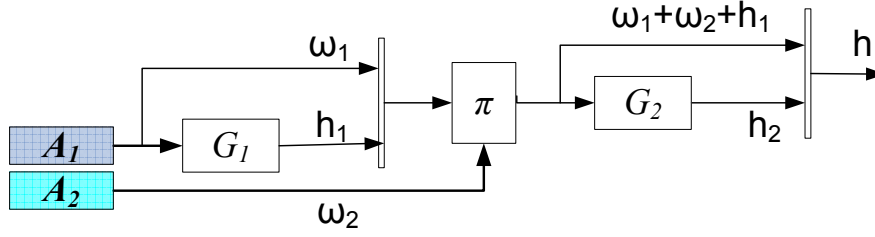


Figure 3.11. Input output weight representations for SPHTC.

The weight spectral lines can also be computed as the set of all pairs $(h_i, \varphi_{h(i)}^{(C_s)})$, where h_i is the Hamming distance and $\varphi_{h(i)}^{(C_s)}$ the error coefficient determining the contribution of the codeword with weight h_i to the bit error probability,

$$\varphi_{h(i)}^{(C_s)} = \sum_{w_i=1}^{N_i} \frac{w_i}{N_i} A_{\omega_i, h}^{(i)}. \quad (3.82)$$

The SPHTC computed IOWEF may be used for the theoretical analysis of the ML theoretical decoding performance bounds. A short overview of the bounds significance and complexity is given in Appendix C.

3.4 Performance Analysis: Methods and Results

The transmission system model is presented in Fig. 3.12. Two evaluation platforms in two different environments have been used for an objective analysis of the code performances. The two platforms denote the different constituent elements that have been adopted for the construction of the channel codes, i.e. the interleaver and puncturing types. One platform adopts elements of a random nature, while the second platform integrates standardized elements of LTE. The PPHTC and SPHTC performances are compared with convolutional and turbo codes. Each chosen benchmark offers a different evaluation perspective through given results. The two different environments refer to two transmission channels: AWGN and Rayleigh. Thus, we can estimate both theoretical and real propagation behaviors. Code properties are also highlighted based on these platforms and computer simulations.

Random binary values are generated by the source, and distributed between the UEP classes. For simplicity, in Fig. 3.12, as well as most of the results presented here, suppose two UEP classes. Source packet A is thus split between the two classes A_1 and A_2 . The classes are encoded by one of the channel codes, and quadrature phase shift keying (QPSK) modulated before orthogonal frequency division multiplexing (OFDM). The OFDM symbols are mapped on an LTE-like radio frame for the transmission on the channel.

Depending on the propagation channel, the transmission/reception antenna characteristics of the evaluation platform differ as follows:

- for the AWGN channel, the transmission/reception is performed using a single antenna,
- for the Rayleigh environment, the transmitter uses a single antenna, while the receiver has two configured antennas. Maximum ratio combining (MRC) is performed after OFDM demodulation. The decoder benefits from the channel diversity enhanced by the two reception antennas.

3.4.1 Evaluation Platforms & Benchmarks Description

The two evaluation platforms are denoted in Fig. 3.12 by the terms *random* and *LTE*. Our purpose is to evaluate the code performances, and not particularly optimize their constituent elements.

Both platforms radio layer simulate a simplified LTE radio configuration. The encoded and modulated data are mapped over the considered bandwidth size, N_{BW} , and the number of OFDM symbols are expanded in the time domain proportionally to the data frame size. We suppose that no control elements specific to LTE are

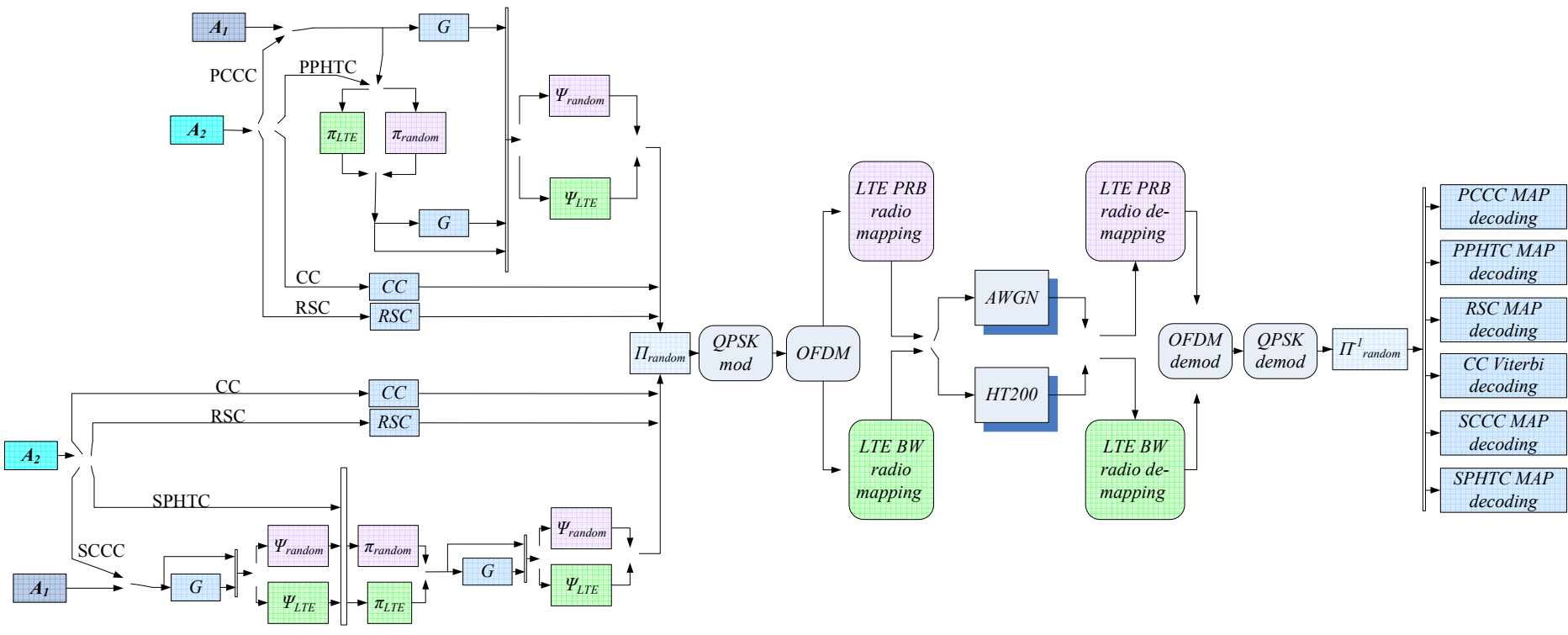


Figure 3.12. Simulation platform.

used in this radio frame. Also, the radio mapping of OFDM symbols has been performed differently on each of the random or LTE platforms, as explained hereafter.

The random platform elements are characterized as:

- the turbo codes internal interleaver, π , is of random nature, performs random generated interleaving on the exact input data;
- the puncturer, denoted by ψ , placed at the turbo code's output for rate control, is also of random nature, performing puncturing only on parity bits;
- the OFDM mapping is performed frequency first, i.e. every OFDM symbol information is spread over the entire bandwidth (BW), N_{BW} .

The LTE platform elements are:

- the turbo codes internal interleaver, π , is of LTE nature, and only standardized values can be initialized (the input data size has been slightly modified as to avoid dummy bits in the interleaving process, e.g. the size of A becomes 1008 bits instead of 1000 bits);
- the puncturer, denoted by ψ , placed at the turbo code's output for rate control represents the LTE rate matching system;
- the OFDM mapping is performed per physical resource block (PRB), or PRB first, i.e. every OFDM symbol information is spread over one PRB³, frequency first, followed by time filling, before the next PRB.

The LTE interleaving and rate matching are complex mechanisms well defined by the 3GPP standard [43]. The interleaver is a contention free interleaver, based on a quadratic permutation polynomial (QPP). Its structure is designed to facilitate efficient high speed turbo decoding. Three sub-block interleavers receive the first parity, second parity and the systematic information. Here, dummy bits are introduced in the system. This is due to the sub-block design, whose size is a multiple of 32 columns. After interleaving, the data streams are fed to a circular buffer, who picks out the bits following a standard formula. The buffer is firstly filled with systematic bits, followed by the bit-by-bit interlaced parity bits. The intriguing characteristic of the LTE rate matcher is that it performs a puncturing of 6% of the systematic bits. This small amount of punctured systematic bits enhances the performances for high coding rates. We have kept this rate matching philosophy for the PCCC benchmarks, but we have modified it for the SCCC structures, as the LTE standard does not use serial turbo codes. Thus, in the SCCC case, the rate matcher receives only one systematic stream and one parity stream. Each one of these streams is fed to one sub-block interleaver, followed by the circular buffer. The buffer is firstly filled with systematic bits, followed by only one parity stream. When the puncturing formula is applied, 6% of the systematic bits are deleted. The remaining quantity of bits that must be deleted is uniformly applied to the parity stream only.

The chosen benchmarks consist of turbo and convolutional codes, which offer a global perspective on the embedded UEP code performances. We will be evaluating the global performances of A_1 and A_2 by comparing them to benchmark codes applied to both classes, and from different UEP transmission perspectives.

The convolutional code perspective for class A_2 :

- CC 1/2, of high complexity, and decoded with the soft-input soft-output Viterbi decoder;
- RSC 1/2, identical to the turbo constituent RSC, decoded by a single MAP.

The convolutional perspective is given as the lower bound for the PPHTC/SPHTC performances of class A_2 . The RSC highlights the behavior of A_2 if it were coded and transmitted alone. The CC provides the same perspective, but its higher complexity offers better performances. Typically, this CC is well known for its excellent performance. Thus, the optimal class A_2 performances, when convolutionally encoded alone, can not

³Here, we denote by PRB only the frequency bandwidth length from LTE, i.e. 12 sub-carriers.

surpass those of the CC code. Compared to these "only convolutional" results, we evaluate the gain of the embedded UEP encoding of A_2 . In the UEP structures, A_2 has been encoded only by one of the RSCs and its mother code rate is $1/2$.

The turbo code perspective for both A_1 and A_2 , as well as for the code block A , in the case of **PPHTC**:

- PCCC $1/3$, composed of two parallel concatenated RSCs, separated by an interleaver, and followed by the puncturing mechanism; the puncturer is almost transparent for the transmission system, since the default code rate of $1/3$ is respected;
- PCCC $1/2$, composed of two parallel concatenated RSCs, separated by an interleaver, and followed by the puncturing mechanism; the turbo encoded data is punctured from the rate of $1/3$ to the rate of $1/2$;
- PCCC x , composed of two parallel concatenated RSCs, separated by an interleaver, and followed by the puncturing mechanism; the turbo encoded data is punctured from the rate of $1/3$ to the rate of x ; x represents the PPHTC equivalent code rate for frame A .

The PCCC $1/3$ performance is evaluated for A_1 , and is given as a benchmark for the $PPHTC(A_1)$. The PCCC $1/2$ performance is evaluated for A_2 , and is given as a benchmark for the $PPHTC(A_2)$. The PCCC x performance is evaluated for A , and is given as a benchmark for the $PPHTC(A)$. These benchmarks represent the turbo PCCC reference, since they provide the turbo convergence for each of the considered block codes if it were EEP encoded, at equivalent rate, and transmitted encoded alone over the radio channel.

The codes chosen as reference for the **SPHTC** for both classes A_1 and A_2 are:

- SCCC $1/4$, composed of two serial concatenated RSCs, separated by an interleaver; each of the RSCs is followed by the puncturing mechanism; the puncturer is almost transparent for the transmission system, since the default code rate of $1/4$ is respected;
- SCCC $1/2$, composed of two serial concatenated RSCs, separated by an interleaver; each RSC is followed by the puncturing mechanism; the turbo encoded data is punctured from the rate of $1/4$ to the rate of $1/2$; the punctured data is equally distributed between the outer and inner puncturer;
- SCCC x , composed of two serial concatenated RSCs, separated by an interleaver; each RSC is followed by the puncturing mechanism; the turbo encoded data is punctured from the rate of $1/4$ to the rate of x ; x represents the SPHTC equivalent code rate for frame A ; and the punctured data is equally distributed between the outer and inner puncturer.

The SCCC $1/4$ performance is evaluated for A_1 , and is given as a benchmark for the $SPHTC(A_1)$. The SCCC $1/2$ performance is evaluated for A_2 , and is given as a benchmark for the $SPHTC(A_2)$. The SCCC x performance is evaluated for A , and is given as a benchmark for the $SPHTC(A)$. These benchmarks represent the turbo SCCC reference, since they provide the turbo convergence for each of the considered block codes if it were EEP encoded, at equivalent rate, and transmitted alone over the radio channel.

Both platforms propose the AWGN and the Rayleigh transmission environments, and the receiver performs the corresponding decoding process for the estimation of classes A_1 and A_2 .

3.4.2 Simulation Parameters and Complexity Issues

The simulation parameters for the different encoding scenarios are given in Table 3.1. The complexity estimation of each one of the used structures is also indicated.

All encoding structures use one RSC type, characterized by $G = [1, g_1/g_2]$, where $g_1 = [1101]$ and $g_2 = [1011]$, with trellis termination. The considered CC has the generator vector $G' = [g'_1, g'_2]$, with $g'_1 = [1001111]$, $g'_2 = [1101101]$. Interleavers and puncturing mechanisms are generated considering the different input sizes. For computer simulation convenience, the soft input soft output (SISO) decoding blocks use the Max Log MAP algorithm. The number of maximum decoding iterations is set to 8 for turbo structures, and 1 for RSC single decoding. The QPSK modulated data is fast Fourier transformed (FFT) using $N_c = 128$ points to generate the

OFDM signal (T_c considered to be the OFDM FFT sampling period). A $N_g = 1/4 \times N_c$ length guard interval is added to the N_c length OFDM symbol. The data are transmitted using the necessary number of OFDM symbols on the time axis, and $N_{SC} = 72$ subcarriers separated by $\Delta_f = 15$ kHz frequency difference on the frequency axis. The simulations are computed on 100 000 data frames.

The Rayleigh channel type has the characteristics of a hilly terrain (HT) environment with the Doppler spread associated with the speed of 200 km per hour. We will be denoting this by HT200. The Rayleigh fading simulator follows the model given in [44]. The carrier frequency is of 450 MHz, typically used for European PMR deployments. This configuration is meant to evaluate the LTE system for a PMR radio configuration.

In both AWGN and Rayleigh channel transmission, the BER results are represented as a function of the average channel encoded bit energy to AWGN power spectrum density ratio, E_b/N_0 , as

$$E_b/N_0 = E_s/N_0 - 10\log_{10}(\log_2 M), \quad (3.83)$$

where M denotes the quadrature amplitude modulation (QAM) order, and E_s/N_0 refers to the QAM symbol energy to noise ratio. The QAM symbol energy is spread over the entire OFDM symbol, including its guard interval as

$$SNR = E_s/N_0 - 10\log_{10} \left(\frac{N_c + N_g}{N_{SC}} \right), \quad (3.84)$$

where SNR refers to the channel signal to noise ratio. This formula supposes that each of the QAM symbols is mapped on each of the available sub-carriers, therefore the energy of a QAM symbol is constant and applied to all sub-carriers, N_{SC} . The noise, N_0 , is considered spread over the extended OFDM symbol, i.e. $N_c + N_g$.

The computational complexity of the proposed UEP decoding algorithm is also presented in Table 3.1. The decoding computational complexity of turbo codes is obtained considering the number of iterations, the trellis size and the number of operations on a trellis section. In fact, the computational complexity issue becomes a simple problem once we have identified the complexity of estimating the maximum a posteriori values for a single trellis section.

In our analysis, we have considered that all turbo codes use the same constituent RSCs, characterized by a memory length $m = 3$. The number of operations for a trellis section is derived directly from the BCJR equations for α , β , γ and the APP. The complexity of computing their respective values at a trellis state t depends on the RSC memory length as follows:

- for each α_t , there are $2^m = 8$ additions for each departing state p ; but as we consider all possible states p , and from each state p there are 2 possible branches, we count $2^m \times 2 = 16$ multiplications;
- the β_t complexity is the same as α_t ;
- each γ_t is computed considering systematic, parity and/or priori bits, therefore either 2 or 1 elementary multiplications; but due to the fact that each of the state p and q outputs and receives 2 branches, γ_t can have $2^2 = 4$ values; there will be a total of $2^2 \times 2 = 8$ multiplications if priori probabilities are considered, and a total of $2^2 \times 1 = 4$ if only channel probabilities are considered.

For each of the a posteriori values, $2^m \times 2 = 16$ multiplications are necessary and a sum over $2^m/2 = 4$ possible transitions. But for each bit, two values are estimated for the APP, 1 and 0, therefore the reliability of a bit needs $2 \times (2^m \times 2) = 32$ multiplications and $2 \times 2^{m-1} = 8$ additions. Therefore, for a trellis section, the computation complexity in number of elementary operations is of

$$\begin{aligned} C_{section}^{MAP} &= (24 \times 2)_{\alpha_t, \beta_t} + 8_{\gamma_t} + 40_{APP} = 96, \text{ with priori values,} \\ C_{section}^{MAP} &= (24 \times 2)_{\alpha_t, \beta_t} + 4_{\gamma_t} + 40_{APP} = 92, \text{ without priori values.} \end{aligned} \quad (3.85)$$

Since this computation complexity is considered for a trellis section, the MAP decoder overall complexity is obtained by multiplying with the length of the input code word and the number of iterations.

The Viterbi complexity is computed in a simpler manner. If k represents the memory length of the CC 1/2, then its trellis possesses 2^k states. Due to the binary code structure, there are two branches out of each state, and two additions and a comparison can be estimated per branch. This results in $2^k \times 5$ operations per trellis section.

Table 3.1
UEP scenarios code parameters & respective complexities.

UEP scenarios	Code structure	Input code block size (bits)	Code rates	Complexity (operations)
Serial scenario 1 (S1)	$SPHTC^{(1)}$	$A_1=700, A_2=300$	$R_{A_1}=0.25, R_{A_2}=0.5$	3667200
	$SCCC(A)$	$A=1000$	$R_A=0.29$	4147200
	$SCCC(A_1)$	$A_1=700$	$R_{A_1}=0.25$	3225600
	$SCCC(A_2)$	$A_2=300$	$R_{A_1}=0.5$	921600
	$RSC^{(1)}$	$A_2=300$	$R_{A_2}=0.5$	28800
	$CC^{(1)}$	$A_2=300$	$R_{A_2}=0.5$	96000
Serial scenario 2 (S2)	$SPHTC^{(2)}$	$A_1=300, A_2=700$	$R_{A_1}=0.25, R_{A_2}=0.5$	1897600
	$SCCC(A)$	$A=1000$	$R_A=0.38$	3532800
	$SCCC(A_1)$	$A_1=300$	$R_{A_1}=0.25$	1382400
	$SCCC(A_2)$	$A_2=700$	$R_{A_2}=0.5$	2150400
	$RSC^{(2)}$	$A_2=700$	$R_{A_2}=0.5$	67200
	$CC^{(2)}$	$A_2=700$	$R_{A_2}=0.5$	224000
Parallel scenario 1 (P1)	$PPHTC^{(1)}$	$A_1=700, A_2=300$	$R_{A_1}=0.33, R_{A_2}=0.5$	1296000
	$PCCC(A)$	$A=1000$	$R_A=0.37$	1536000
	$PCCC(A_1)$	$A_1=700$	$R_{A_1}=0.33$	1075200
	$PCCC(A_2)$	$A_2=300$	$R_{A_2}=0.5$	460800
	$RSC(A_2)$	$A_2=300$	$R_{A_2}=0.5$	28800
	$CC(A_2)$	$A_2=300$	$R_{A_2}=0.5$	96000
Parallel scenario 2 (P2)	$PPHTC^{(2)}$	$A_1=300, A_2=700$	$R_{A_1}=0.33, R_{A_2}=0.5$	976000
	$PCCC(A)$	$A=1000$	$R_A=0.43$	1536000
	$PCCC(A_1)$	$A_1=300$	$R_{A_1}=0.33$	460800
	$PCCC(A_2)$	$A_2=700$	$R_{A_2}=0.5$	1075200
	$RSC(A_2)$	$A_2=700$	$R_{A_2}=0.5$	67200
	$CC(A_2)$	$A_2=700$	$R_{A_2}=0.5$	224000

But as mentioned in the simulation parameters paragraph, we have considered a CC of memory length $k = 6$, which engenders 320 elementary operations.

$$C_{section}^{Viterbi} = 2^6 \times 5 = 320. \quad (3.86)$$

For each one of the turbo structures, we evaluate the complexity order. For the $SPHTC^{(1)}$, the outer RSC encodes only class $A_1 = 700$ bits, therefore its corresponding MAP performs operations over $2 \times 700 = 1400$ trellis sections (the APP is estimated on both systematic and parity bits). Considering the number of iterations, the overall complexity is computed over $8 \times 1400 = 11200$ trellis sections. Including the $C_{section}^{MAP}$ value with priori values, the outer MAP complexity becomes $96 \times 11200 = 1075200$ number of elementary operations. The inner RSC receives the encoded class A_1 , which is $C_1 = 2 \times 700 = 1400$ bits, and $A_2 = 300$ bits. This gives an input code block of 1700 bits. The number of trellis sections for its corresponding MAP is of $8 \times 2 \times 1700 = 27200$. From a UEP-MAP perspective, a part of these trellis sections corresponding to A_1 bits consider priori values, and the remaining trellis sections evaluating the bits for A_2 do not consider priori values. This would mean $8 \times 2 \times 1400$ trellis sections for A_1 , giving 2150400 overall operations with priori values. Without considering the priori values, the number of operations for A_2 is of $8 \times 2 \times 300 \times 92 = 441600$. The overall number of iterations for the inner RSC decoding becomes $2150400 + 441600 = 2592000$. The $SPHTC^{(1)}$ decoding estimated number of operations is of $1075200 + 2592000 = 3667200$ for both constituent MAPs.

The chosen benchmark $SCCC(A)$, from serial scenario 1, has an equivalent transmission rate of 0.29. Puncturing has been applied in the encoding process and 600 bits are deleted. These bits are distributed equiv-

alently between the outer and inner RSC. Thus, the outer RSC encodes 1000 bits, and the corresponding trellis has 2×1000 trellis sections. But after the outer RSC, 300 bits are deleted, and the inner RSC receives only 1700 bits. Therefore, its corresponding decoding trellis has 2×1700 sections. The overall complexity is estimated as $8 \times 5400 \times 96 = 4147200$.

The complexities for the remaining serial scenarios' benchmarks are estimated similarly.

As for the $PPHTC^{(1)}$, the upper RSC encodes only class $A_1 = 700$ bits. Its corresponding MAP estimates A_1 soft values over 700 trellis sections (only systematic bits are estimated). The complexity becomes approximatively equal to $8 \times 700 \times 96 = 537600$ operations. The lower RSC encodes both classes A_1 and A_2 , and the MAP decoding is performed over 1000 trellis sections. Considering the existence of a priori values for class A_1 , the number of operations is estimated as $8 \times 700 \times 96 = 537600$. The number of operations for A_2 is then limited to $8 \times 300 \times 92 = 220800$. The lower RSC decoding complexity for both classes becomes $537600 + 220800 = 758400$. The overall decoding complexity for the $PPHTC^{(1)}$ is therefore close to $537600 + 758400 = 1296000$ operations.

We observe that, contrary to serial structure, the parallel structure's decoding complexity is not affected by the puncturing mechanisms. This is due to the fact that the puncturing is performed at the output of the encoder. Thus, when computing the trellis lengths, we consider the overall encoded block. For example, for the parallel scenario 1, the number of operations for $PCCC(A)$ is approximated as $2 \times 8 \times 96 \times 1000 = 1536000$, for 2 corresponding MAPs, 8 iterations each, 96 operations per sections, and of length 1000 sections each. Similarly, we perform the estimations regarding the complexities of the remaining code structures.

The computational complexity analysis shows that, generally, the SPHTC and PPHTC complexities are lower than their equivalent rate EEP turbo codes, $SCCC(A)$ and $PCCC(A)$. Therefore, at equivalent input and output, the estimated complexities of UEP structures are lower than their turbo EEP benchmarks. Also, it is proved that the turbo UEP encoding/decoding of both classes A_1 and A_2 is generally less complex than if they were separately turbo encoded/decoded. By observing the serial scenario 1, the complexity for the $SPHTC^{(1)}$ remains lower than the sum of complexities of $SCCC(A_1)$ and $SCCC(A_2)$. The only case when the independent encoding/decoding of the two classes presents a lower complexity is the case where class A_1 is turbo encoded/decoded and class A_2 is RSC or CC encoded and single MAP or Viterbi decoded respectively.

Based on these obtained complexity estimations, we will discuss in this next section on the performance-complexity trade-off of PPHTC and SPHTC structures compared with respective benchmark codes.

3.4.3 Code Performance Results

In this section, the code performance results are given only for the average bit error rates (BER), and from several perspectives. The frame error rate (FER) results are presented in Appendix D, section D.1. We start in subsection 3.4.3.1 by analysing the code iterative behavior. The figures present the iterative gains through turbo iterations for both classes, A_1 and A_2 . The UEP MAP decoding's direct influence on these performances is illustrated in both AWGN and HT200 environments. In subsection 3.4.3.2, we propose the analysis of these performances from the pilot code perspective. Thus, the PPHTC and SPHTC results are compared to their pilot counterparts, but only the AWGN performances are given here. Their corresponding HT200 results are given in Appendix D, subsection D.1.3. Finally, the two codes own performances are compared to respective benchmark codes in subsection 3.4.3.3 for AWGN channel and in subsection 3.4.3.4 for the HT200 transmission environment.

3.4.3.1 UEP Turbo Behavior

The UEP iterative decoding behavior is highlighted through two opposite scenarios for both PPHTC and SPHTC. Each scenarios refers to the input code block size of classes A_1 and A_2 , as given in Table 3.1. The analysis of the turbo convergence provides an insight on the UEP turbo decoder performances, which are highly correlated to the input UEP class lengths. The differences between the two opposite scenarios are easily observed and prove the existence of the two theoretical boundaries, i.e. MAP and ML decoding. The full MAP or turbo decoding performances are approached as the size of class A_1 increases, while the ML performances are

approached for class A_2 when its own length is preponderant. Only the average BER results are given here, the performances in FER are given in Appendix D, subsections D.1.1 and D.1.2.

PPHTC

The AWGN iterative behavior for the first parallel scenario, $P1$, or $PPHTC^{(1)}$, is presented in Fig. 3.13 and Fig. 3.14, considering LTE and random elements respectively. Their respective behaviors in HT200 are illustrated in Fig. 3.15 and Fig. 3.16. We particularly note that both classes present important turbo iterative gains between their first and eighth iterations. Very important in AWGN, these gains are considerably flattened in HT200 case. Also, the results obtained over the two platforms, random and LTE, are similar to each other.

In AWGN channel, while the last iteration of A_1 shows a steep waterfall, class A_2 presents a hybrid, interesting convergence. The UEP-MAP decoding influence on A_2 is remarkable, since approximately 2.2 dB

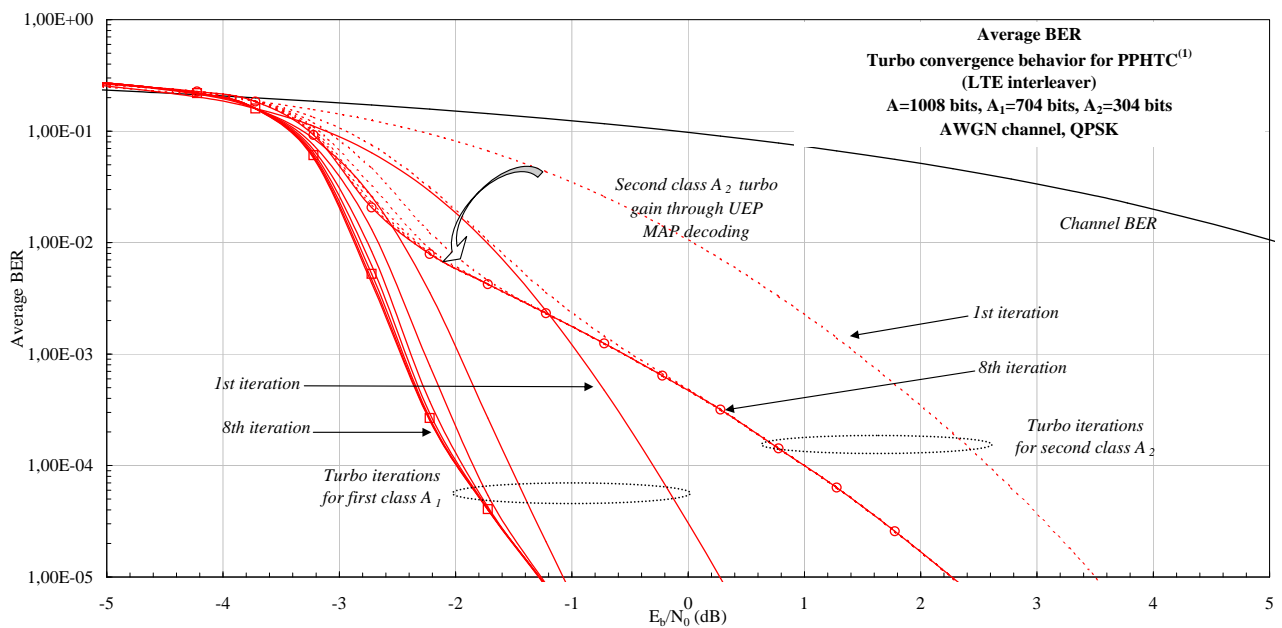


Figure 3.13. AWGN $PPHTC^{(1)}$ turbo iterative behavior, LTE platform.

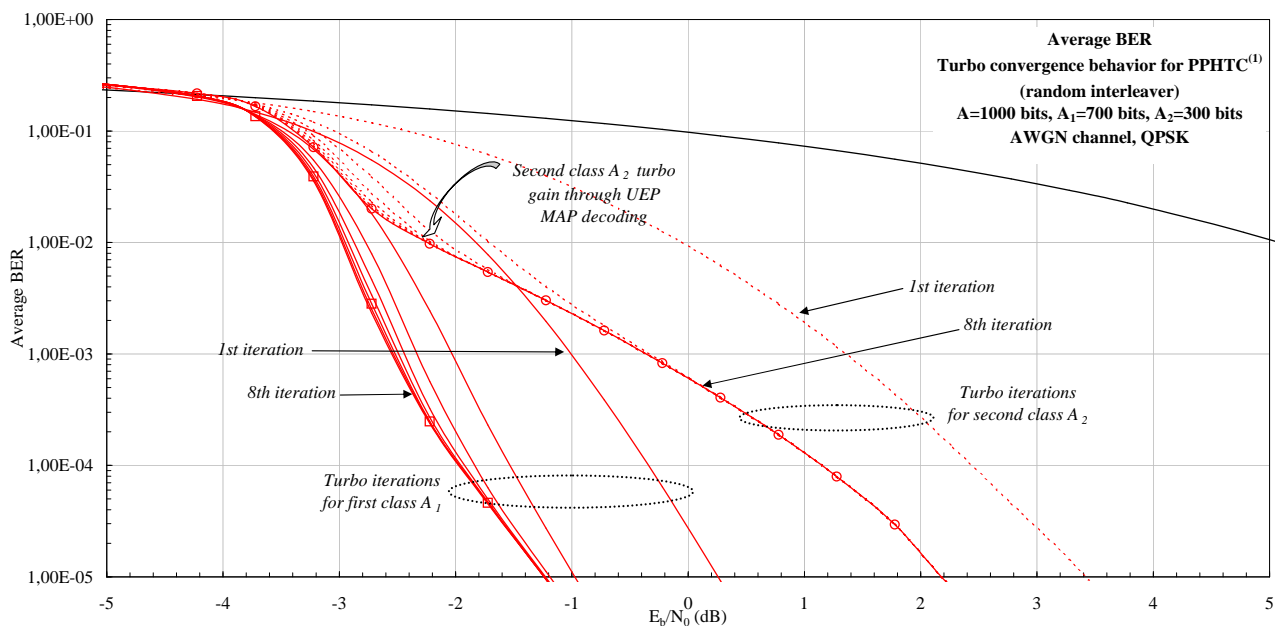


Figure 3.14. AWGN $PPHTC^{(1)}$ turbo iterative behavior, random platform.

are gained between the first and eighth iterations. The performance differences between the two platforms are quite small, yet visible. The LTE platform proves to be more efficient for class A_2 , where the latter gains 0.2 dB at 10^{-2} compared to its random version. Class A_1 on the other hand gains 0.1 dB at 10^{-2} on the random platform compared to the LTE case.

In HT200, A_1 iterations are particularly flattened, while an important gain between the first and eighth iterations is still visible for class A_2 . An iterative gain of 1.4 dB at 10^{-2} is registered for this second class on both platforms. We note that the LTE platform performances are improved compared to the random platform, the gains are mostly visible for class A_2 . At a BER of 10^{-5} , the gain differences between the last iterations of the two classes is of 0.8 dB over LTE, and of 1 dB over the random platform. Thus, the 0.2 dB gain for A_2 from the AWGN case are well represented in the HT200 case as well, while the difference for A_1 over the two platforms is less visible.

The opposite case scenario, the ($PPHTC^{(2)}$) turbo LTE and random convergence is given in Fig. 3.17

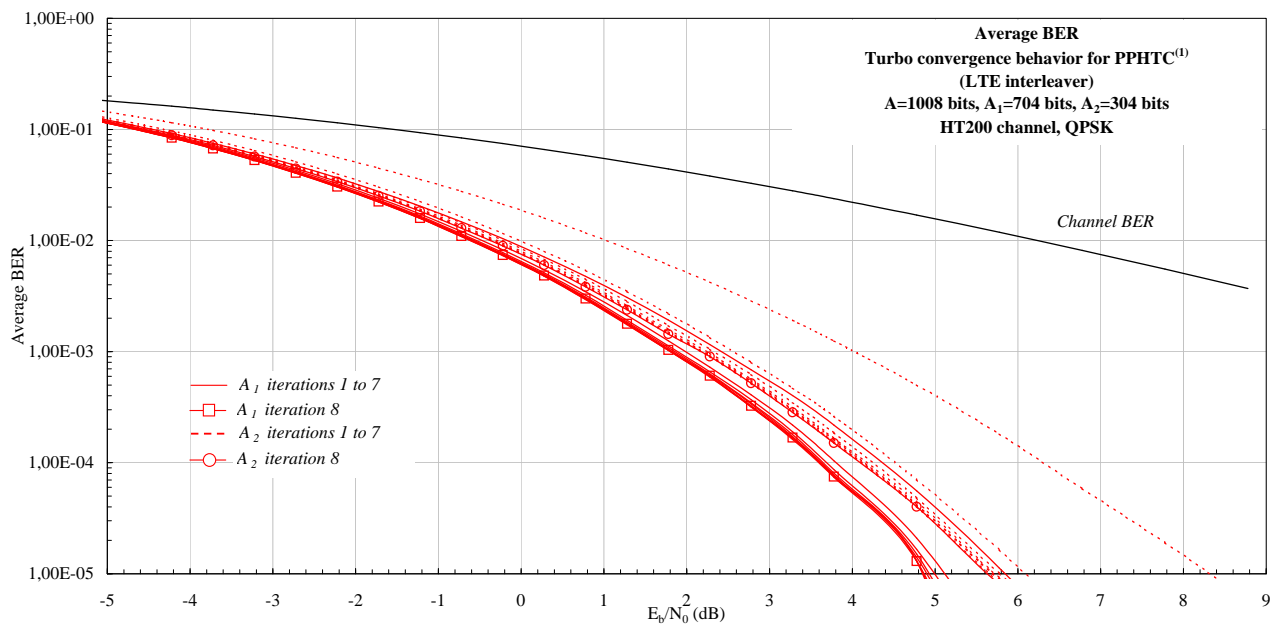


Figure 3.15. HT200 $PPHTC^{(1)}$ turbo iterative behavior, LTE platform.

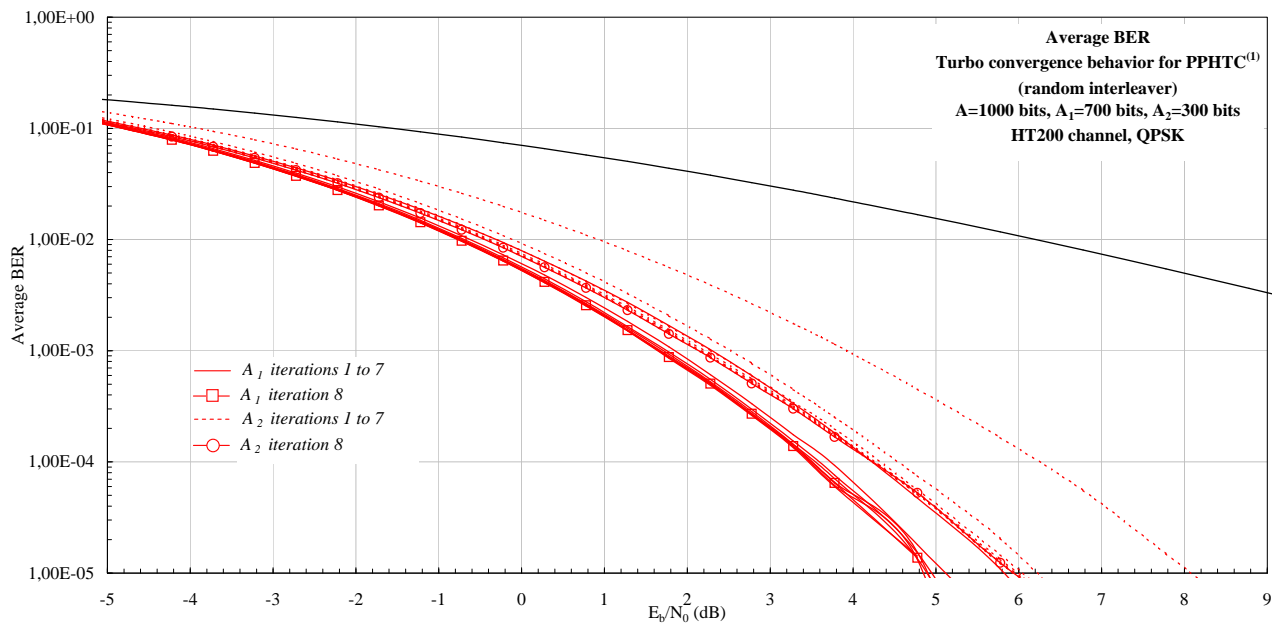


Figure 3.16. HT200 $PPHTC^{(1)}$ turbo iterative behavior, random platform.

and Fig. 3.18 respectively for the AWGN channel. The HT200 results are shown in Fig. 3.19 and Fig. 3.20. Compared to the first scenario, the second scenario uses the opposite ratios for each one of the two classes. Thus, $A_1 < A_2$, and the code behavior changes considerably. The input code block is composed mainly of class A_2 bits, and therefore the PPHTC encoding is mostly of a convolutional nature. The iterative decoding of class A_2 tends to resemble the ML decoding of a convolutional code. But the presence of A_1 , which has been turbo encoded and decoded, brings additional priori information in the decoding process and helps improve the reliabilities of class A_2 as well.

In AWGN, the $PPHTC^{(2)}$ iterative convergence is resumed to almost two iterations for both evaluation platforms, LTE and random. Using LTE elements, class A_1 gains almost 0.5 dB, while class A_2 approximately 0.6 dB between the first and last iterations, and at 10^{-2} . On the random platform, the A_1 gain is of 0.4 dB, while A_2 reaches almost 0.7 dB, at the same BER of 10^{-2} .

In HT200, the two convergence iterations remain visible, yet the gain is not remarkable on neither one of

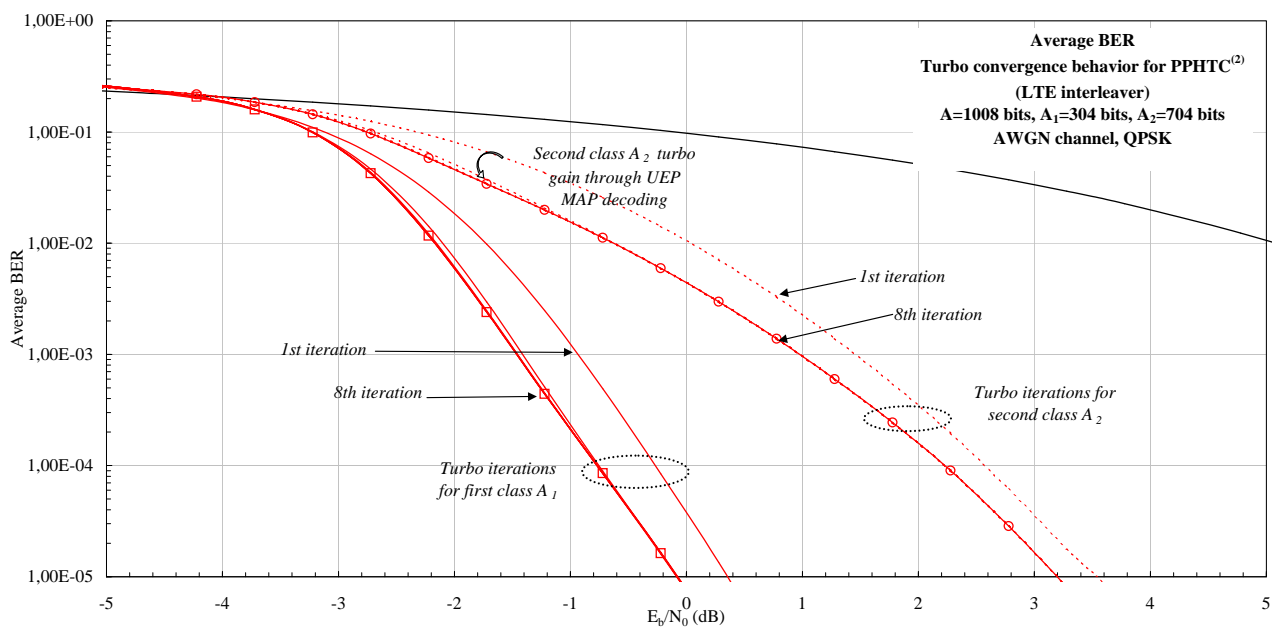


Figure 3.17. AWGN $PPHTC^{(2)}$ turbo iterative behavior, LTE platform.

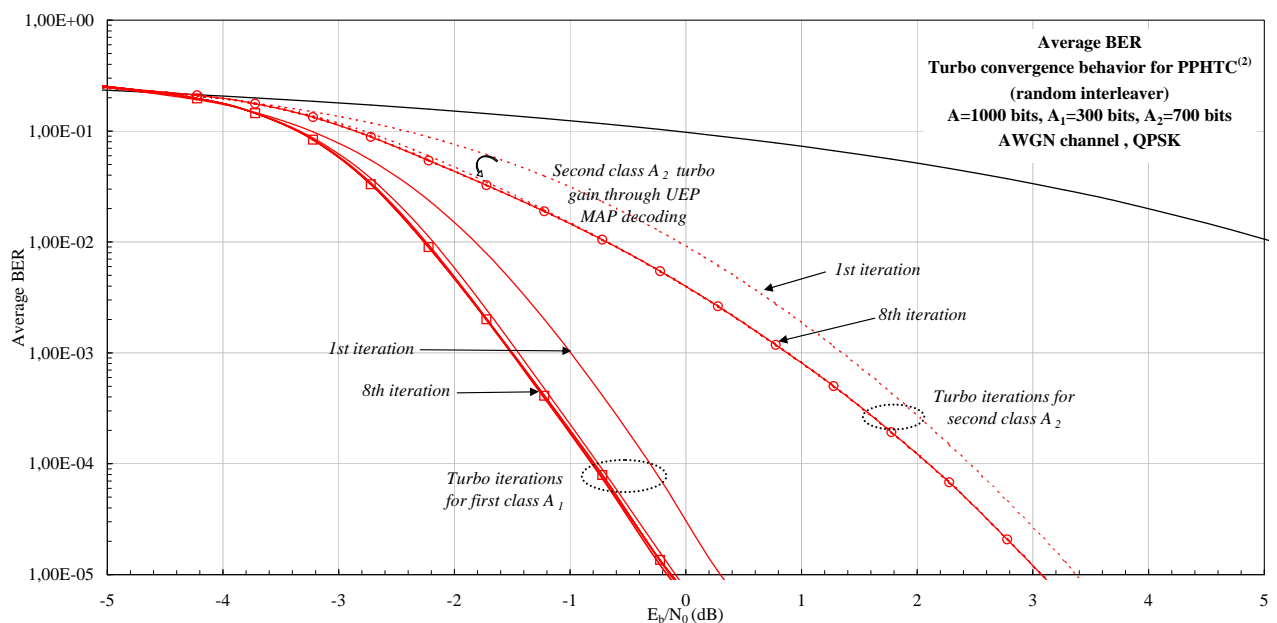


Figure 3.18. AWGN $PPHTC^{(2)}$ turbo iterative behavior, random platform.

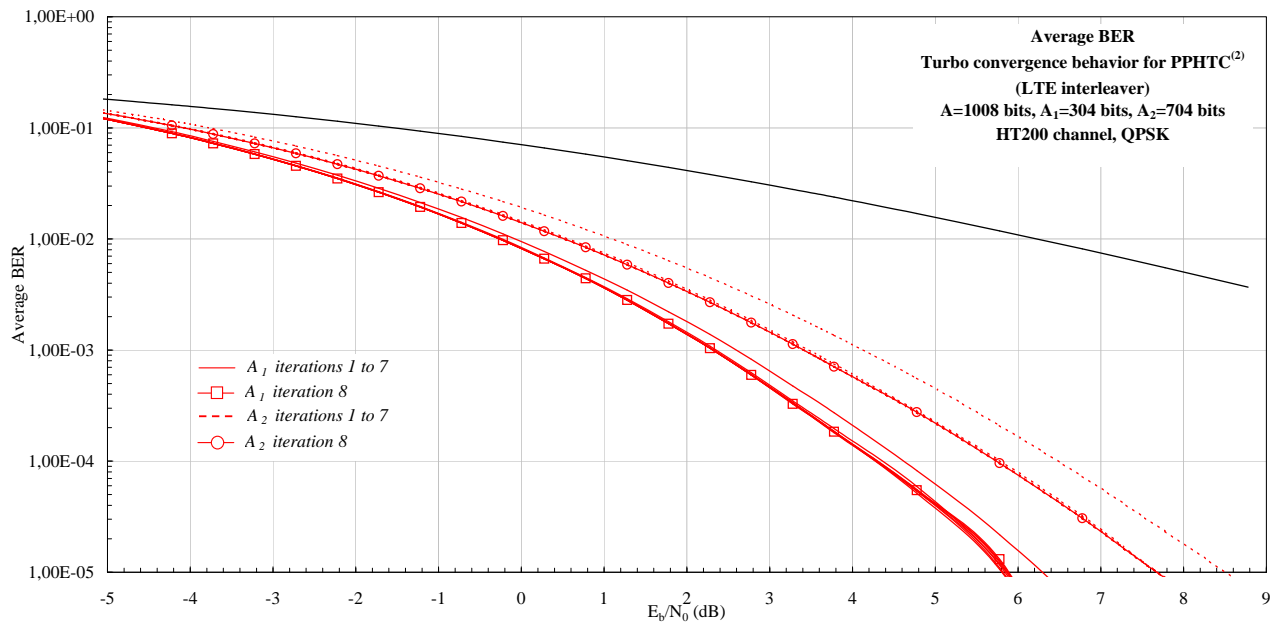


Figure 3.19. HT200 $PPHTC^{(2)}$ turbo iterative behavior, LTE platform.

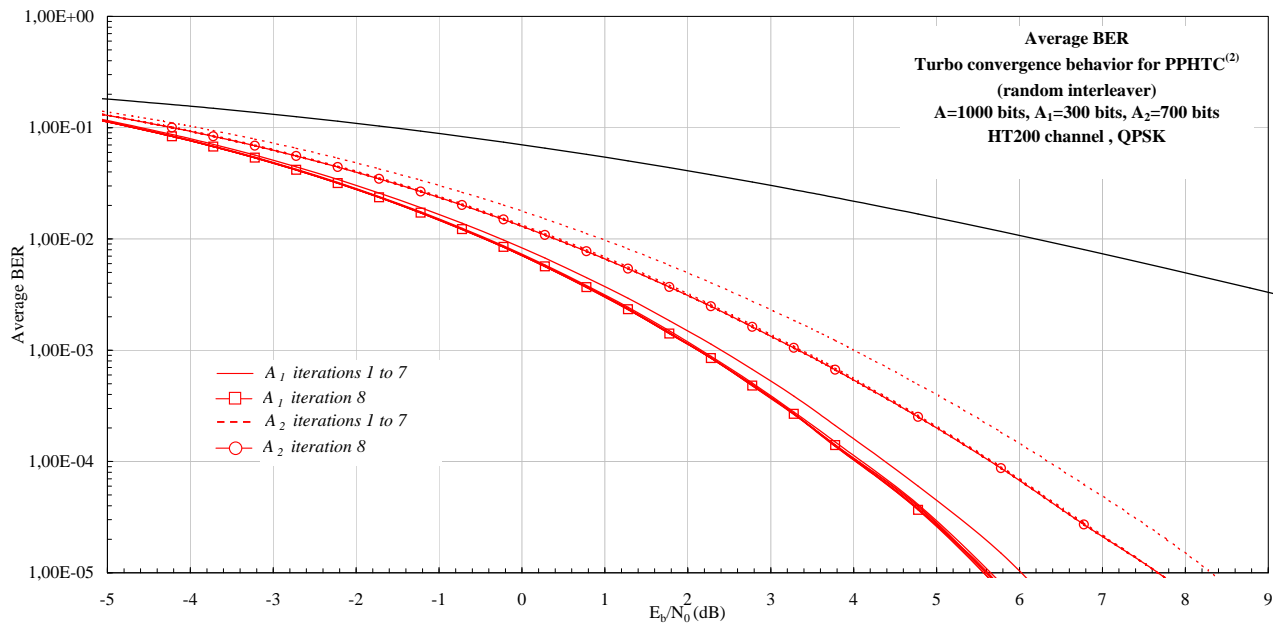


Figure 3.20. HT200 $PPHTC^{(2)}$ turbo iterative behavior, random platform.

the platforms. For a BER of 10^{-2} , class A_1 gains merely 0.2 dB, while class A_2 counts for almost 0.5 dB.

SPHTC

The iterative behavior for the first serial scenario, or $SPHTC^{(1)}$, is presented in Fig. 3.21 and Fig. 3.22, considering LTE and random elements respectively and AWGN channel. The HT200 performances are given in Fig. 3.23 and Fig. 3.24. For the opposite serial scenario, S_2 , the $SPHTC^{(2)}$ turbo LTE and random convergence is given in Fig. 3.25 and Fig. 3.26 respectively for AWGN, and in Fig. 3.27 and Fig. 3.28 for HT200.

The performances given by the $SPHTC^{(1)}$ decoding resemble those of the $PPHTC^{(1)}$, but considering the fact that the transmission rate for class A_1 is not 1/3, but 1/4. Our purpose was to evaluate the default structures' behavior and not use puncturing mechanisms that might alter them. Thus, the $SPHTC^{(1)}(A_1)$ is transmitted at a code rate of 1/4, while $SPHTC^{(1)}(A_2)$ is of rate 1/2. But class A_2 is spread between the bits of a code block of $2 \times N_1$, which corresponds to the encoded A_1 by the outer RSC, therefore a larger A_1 weight.

This explains the larger turbo gain visible on the SPHTC figures between the first and eighth iterations for class A_2 . As expected, with more priori values of class A_1 , the improvement of A_2 during iterations is considerable.

In AWGN, the class A_1 waterfall is particularly steep. It is nonetheless the decoding of a serial structure, for which it is widely accepted that the error floor is much lower than for parallel structures. The LTE and random platforms give similar results, even though we may observe that the random elements platform performs almost better than the LTE one. Of course, these elements are not optimized for optimum performances and are used for an evaluation of the code general behavior. Thus, class A_1 gains 1 dB between its first and last iterations over both platforms, but the random gains are shifted lower with 0.2 dB than the LTE ones. As for class A_2 , the iterative gain goes up to 3 dBs over LTE and almost 3.2 dB over the random platform. From the encoder perspective, these results highlight the importance of the input block code weight, as the same class $A_2 = 300$ bits is encoded by the same RSC in both $SPHTC^{(1)}$ and $PPHTC^{(1)}$ cases, but the serial structure proposes a higher weight through the encoded class A_1 . From the decoder perspective, class A_1 brings more priori

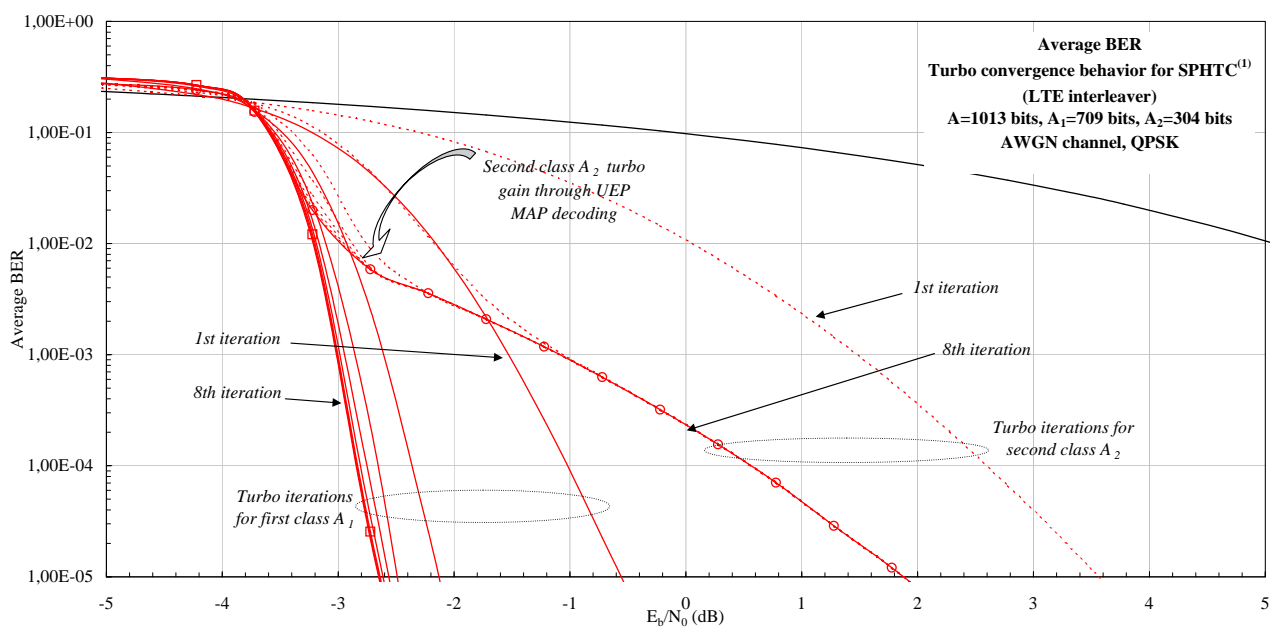


Figure 3.21. AWGN $SPHTC^{(1)}$ turbo iterative behavior, LTE platform.

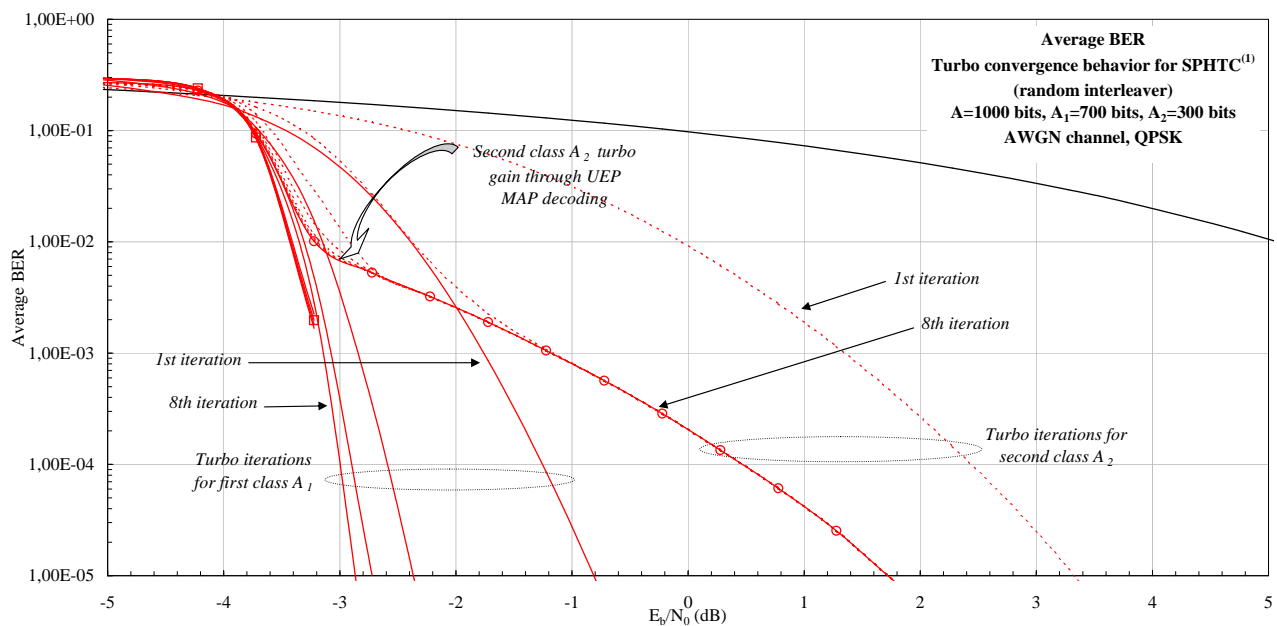


Figure 3.22. AWGN $SPHTC^{(1)}$ turbo iterative behavior, random platform.

probabilities and thus the UEP-MAP can better exploit the hidden redundancy of A_1 for improving A_2 .

The HT200 figures show very interesting gains for class A_2 , while the class A_1 turbo gain remains modest. Visible gains are registered at low BER values, of 10^{-5} , where A_1 gains 0.8 dB approximatively on both platforms, and A_2 benefits of 3.2 dB of improment between its first and last iterations.

The $SPHTC^{(2)}$ performs as expected. However, we can observe in AWGN that the last iteration of class A_1 begins to reach its error floor, while the gain for class A_2 is larger than the same scenario for $PPHTC^{(2)}$. In this serial case, class A_2 is spread over a larger encoded A_1 , i.e. 2×300 bits, compared to only 300 bits in the parallel structure. The maximum achievable weight is therefore larger.

This gain difference is also visible on HT200 performances. Evaluating the code on both platforms, LTE and random, gives a good overview of the code behavior. Using a particular interleaver instead of another does not bring consequent gains for the structure, even though this can affect the error floor at low E_b/N_0 .

We note that, in all figures shown here, for both **PPHTC** and **SPHTC**, the first iteration of class A_2 is

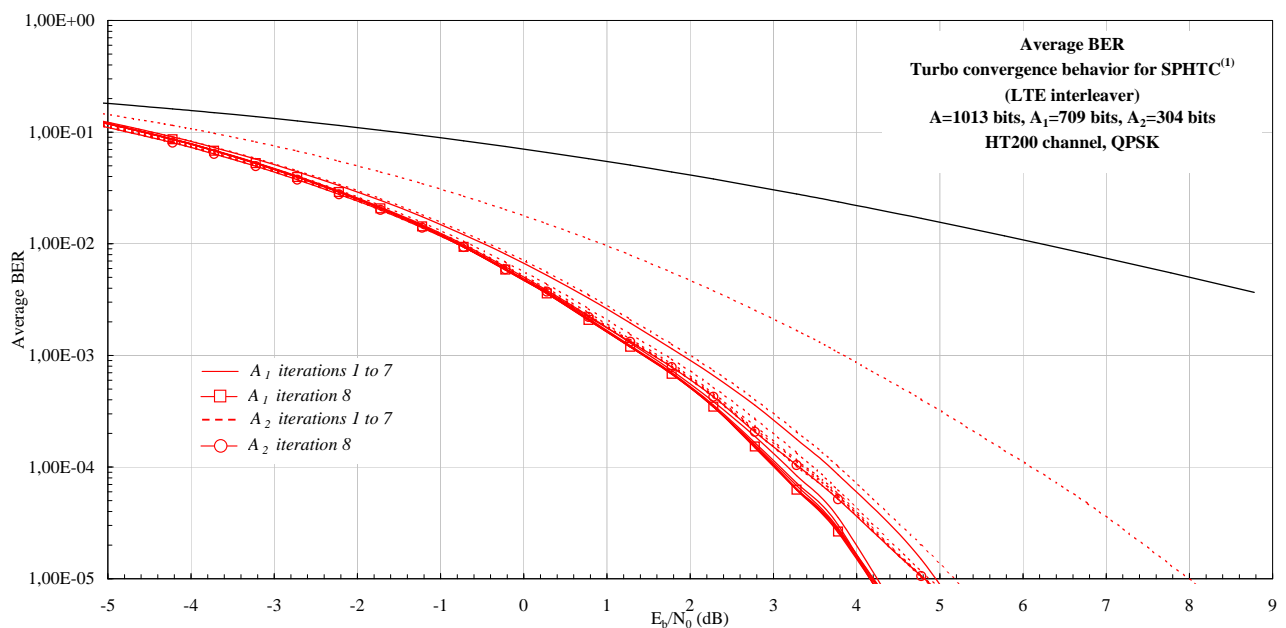


Figure 3.23. HT200 $SPHTC^{(1)}$ turbo iterative behavior, LTE platform.

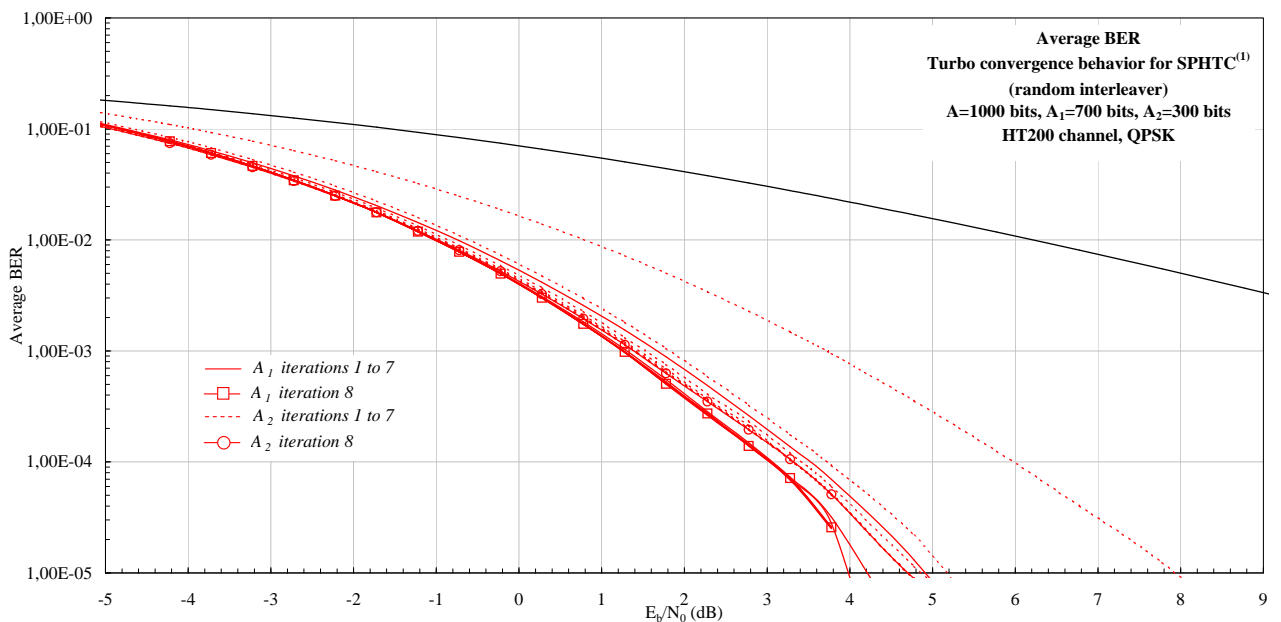


Figure 3.24. HT200 $SPHTC^{(1)}$ turbo iterative behavior, random platform.

highly similar to the convolutional decoding, while its last iteration presents a more or less strong convergence behavior. This proves the theoretical analysis, which shows that the decoding performances approach those of an ML algorithm when the size of A_2 becomes more important than the size of A_1 . Also, the last convergence is the result of the influence of A_1 over A_2 . This influence is shown by both mathematical expressions of the UEP-MAP decoder and the weight coefficients. Thus, the supplementary weight w_1 added by the presence of A_1 in the RSC encoding of A_2 , is fully exploited by the UEP-MAP decoder through the A_1 priori probabilities. A_1 behaves as a hidden redundancy, whose weight improves the decoding of the convolutionally encoded A_2 .

On the contrary, the turbo decoding waterfall of A_1 is more or less steep. This is obviously due to the presence of A_2 . In the UEP-MAP equations, this is translated by the absence of A_2 priori probabilities. And in the weight equations for class A_1 , we have noted the addition of weight w_2 corresponding to A_2 in the turbo structure. Thus, depending on the weight of A_2 and the importance that the convolutional encoding/decoding takes, the turbo waterfall of A_1 is modified.

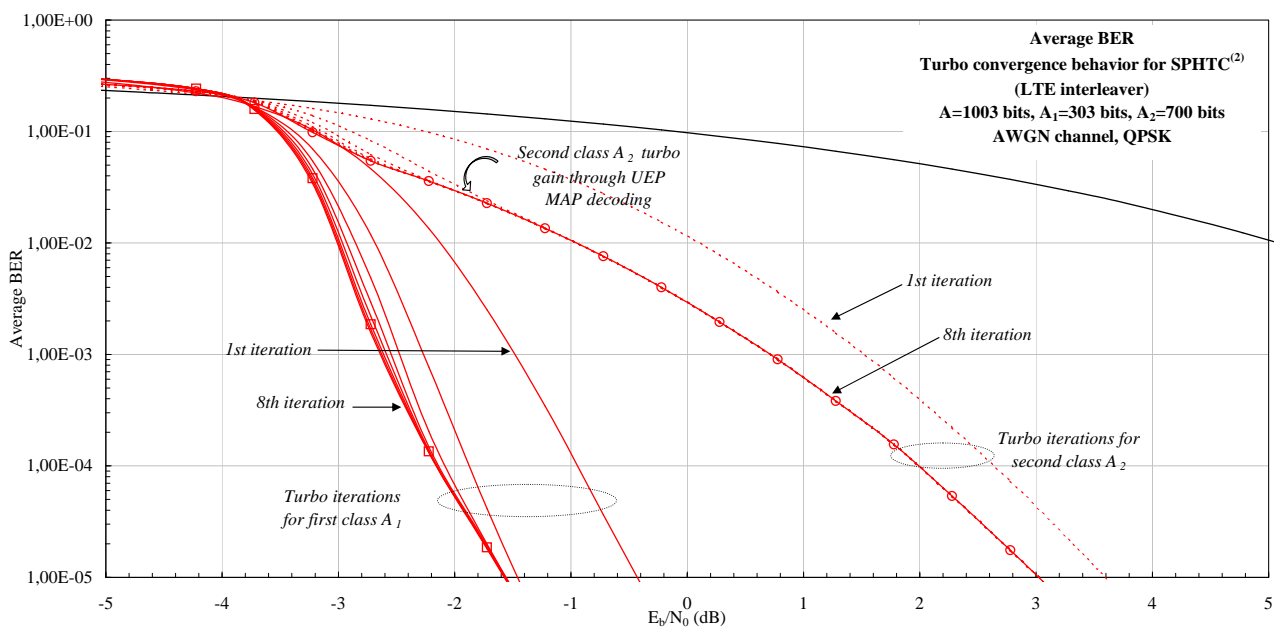


Figure 3.25. AWGN $SPHTC^{(2)}$ turbo iterative behavior, LTE platform.

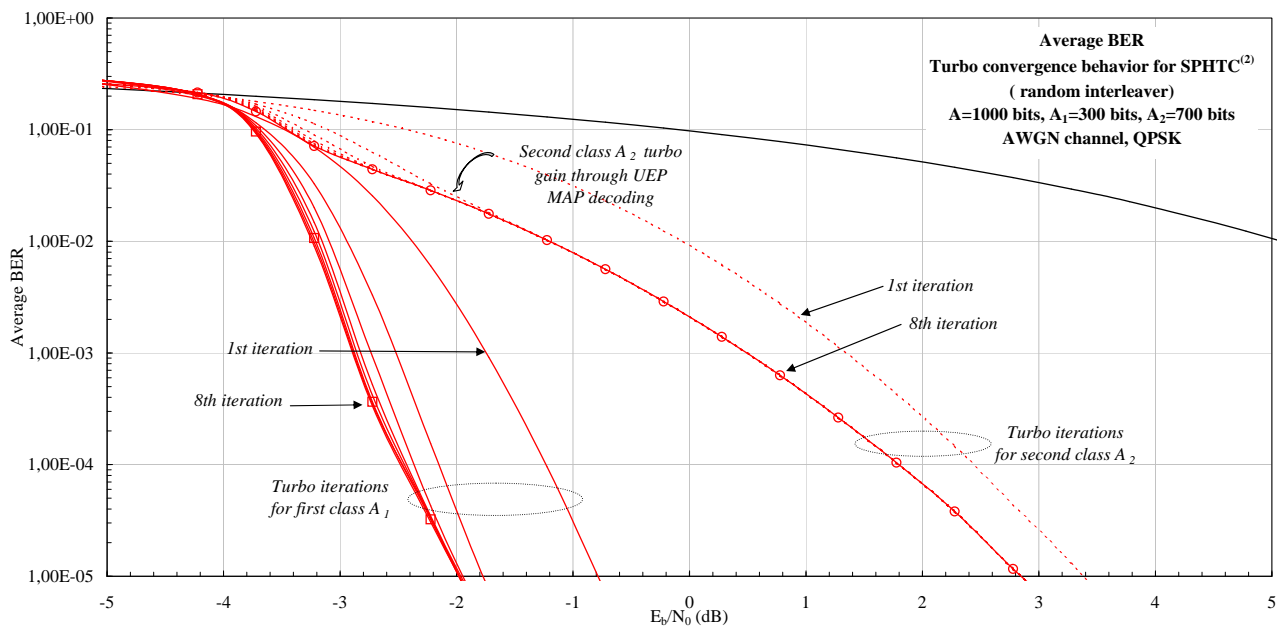
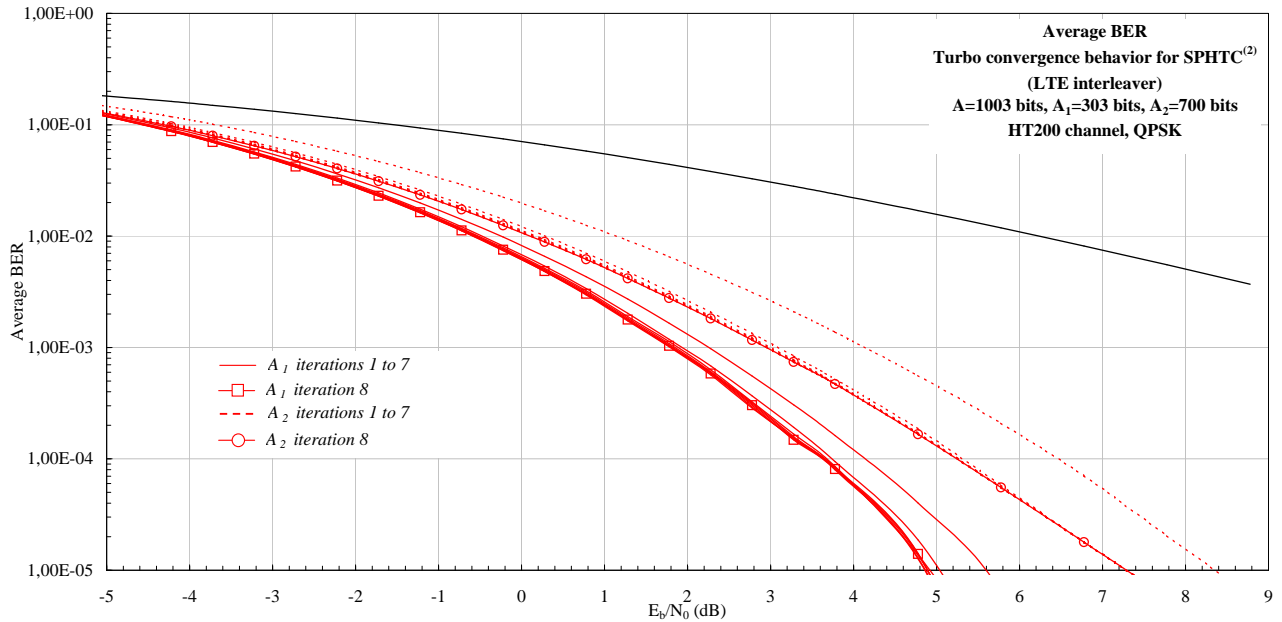
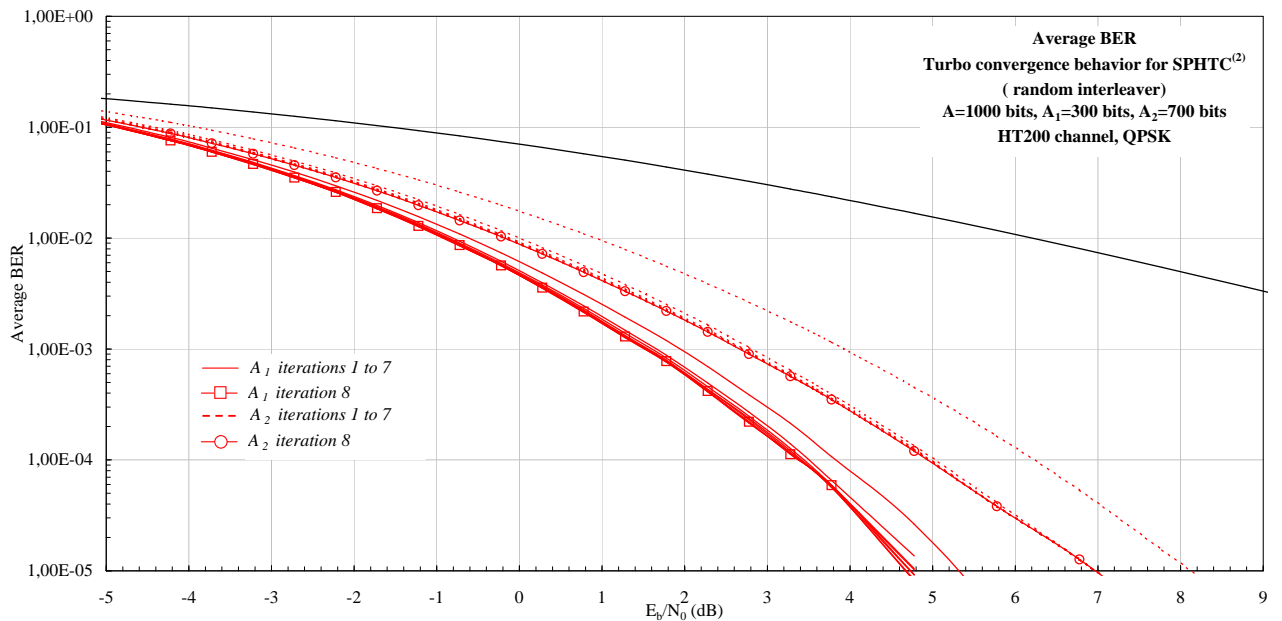


Figure 3.26. AWGN $SPHTC^{(2)}$ turbo iterative behavior, random platform.

Figure 3.27. HT200 $SPHTC^{(2)}$ turbo iterative behavior, LTE platform.Figure 3.28. HT200 $SPHTC^{(2)}$ turbo iterative behavior, random platform.

3.4.3.2 Pilot insertion codes

This paragraph highlights the PPHTC and SPHTC characteristics regarding pilot insertion codes. For both parallel and serial versions, and on both evaluation platforms, we quantify the expected performance gains for the 2-D case. Here, only the AWGN results are given, while their corresponding HT200 behavior is illustrated in the Appendix D, in subsection D.1.3.

The two classes' iterative convergence is presented for the two opposite scenarios, for the PPHTC and SPHTC respectively. In each scenario, alternatively, each class is supposed perfectly known by the transmitter and receiver, and its pilot effect on the remaining class is estimated. For identification, in the pilot insertion case, we denote the turbo convergence of each of the classes by *asymptotic*. In the following figures, the turbo UEP convergences is represented in red, while the pilot insertion code iterations are presented in blue.

In Fig. 3.29 and 3.30, the $PPHTC^{(1)}$ performances are given on the LTE and random platforms. The oppo-

site parallel scenario, $PPHTC^{(2)}$, is highlighted in Fig. 3.31 and 3.32. In Fig. 3.33 and 3.34, the $SPHTC^{(1)}$ performances are given on the LTE and random platforms. The opposite parallel scenario, $SPHTC^{(2)}$, is highlighted in Fig. 3.35 and 3.36.

Considering class A_1 as pilot, we compare the asymptotic results of class A_2 (in blue) with its UEP turbo convergence (in red). The pilot decoder converges after one iteration only on the random platform, and A_2 decoding with pilot insertion is asymptotically equivalent with A_2 UEP decoding. On the LTE platform, we note the slight difference between the first and eighth iterations. This is due to the structure of the rate matcher, where the streams are fed even though puncturing is not used. Thus, several dummy bits are introduced before channel transmission. These rate matching bits introduce some unexpected errors which need at least one iteration for correction. As expected, the iterative result of A_2 converges towards its asymptotic performance on both platforms, for both PPHTC and SPHTC, and for their two opposite scenarios respectively. We note that, for this class A_2 , the last UEP-MAP red iteration is perfectly superposed to the blue pilot code last iteration. Class A_2

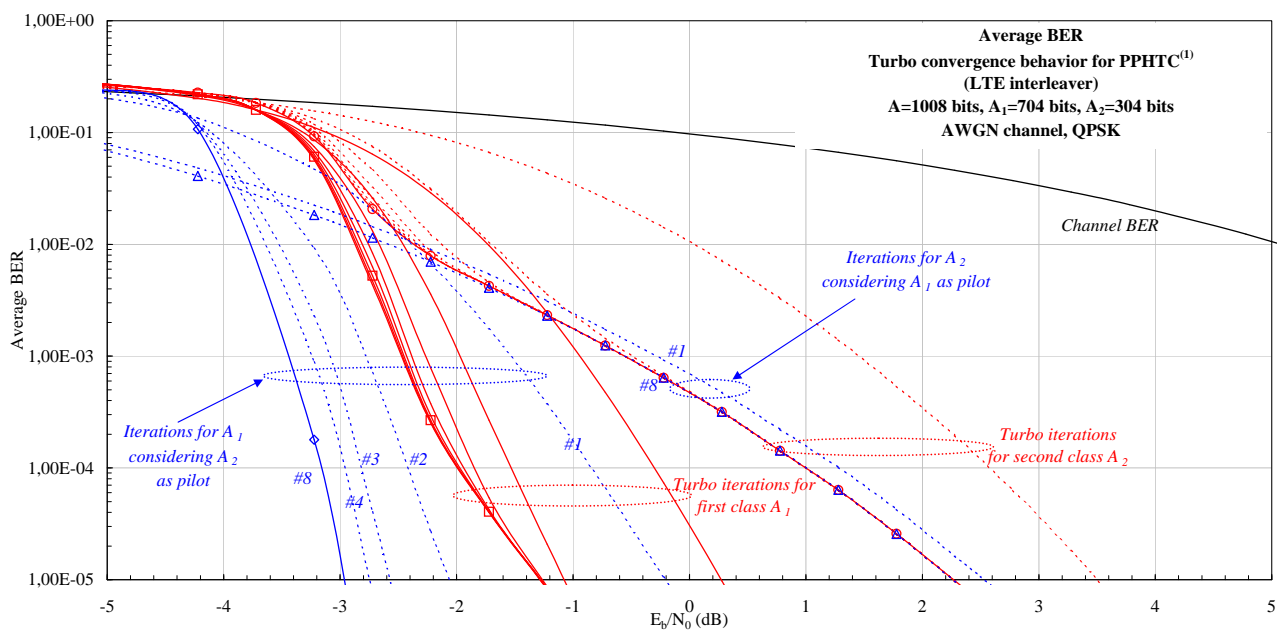


Figure 3.29. AWGN $PPHTC^{(1)}$ pilot insertion behavior, LTE platform.

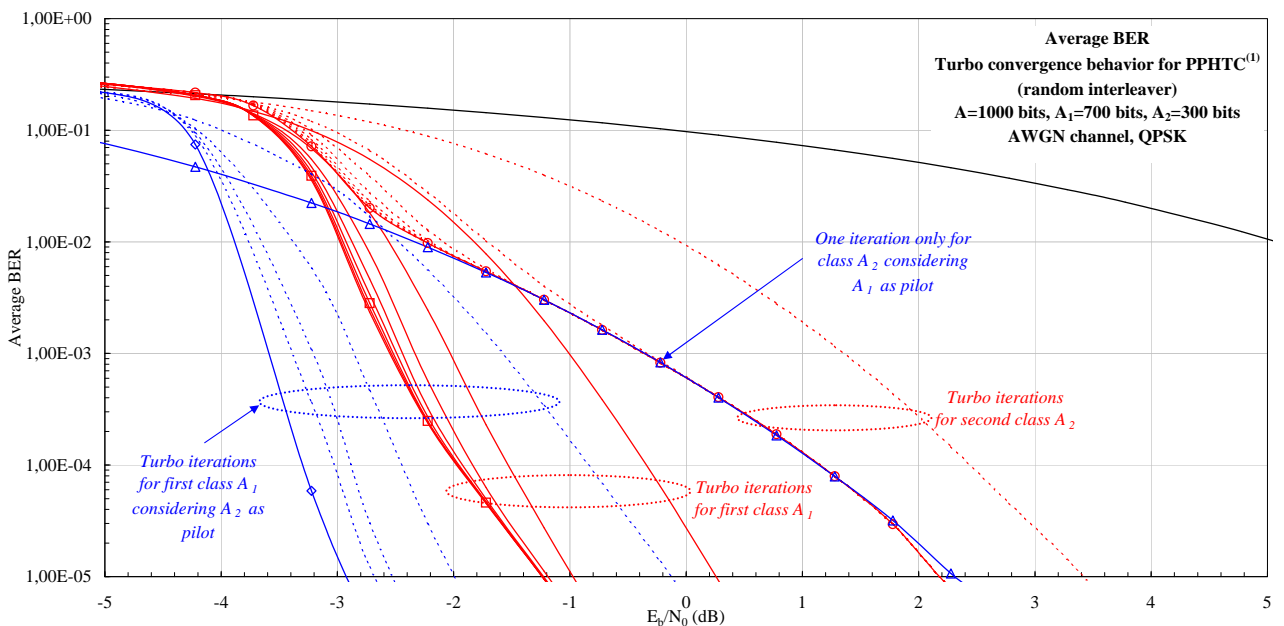


Figure 3.30. AWGN $PPHTC^{(1)}$ pilot insertion behavior, random platform.

decoding is performed by the UEP-MAP decoder with a perfect knowledge of the weights of A_1 code words. The blue behavior of class A_2 is in fact predicted by the weight coefficients, which show a convolutional encoder whose input weights have been modified.

In fact, in the PPHTC and SPHTC structures, the turbo decoded class A_1 acts as *pilot* for class A_2 decoding in the first place (the red performances). Or, we might rephrase this by saying that, from the point of view of class A_2 , the PPHTC and SPHTC structures are equivalent with *insertion convolutional encoders*. Thus, A_1 is interleaved with sequence A_2 before convolutional encoding. Obviously, in the UEP-MAP decoder, the estimation of A_2 is performed considering higher reliability bits, i.e. A_1 . Therefore, the estimation of class A_2 is improved with every turbo iteration until the maximum reliability status has been reached for class A_1 , and this hidden redundancy can not be exploited any longer. Therefore, in the UEP-MAP decoding of A_2 , the turbo decoded A_1 behaves exactly like a pilot. This is why the last red A_2 iteration can not go beyond the blue pilot estimation.

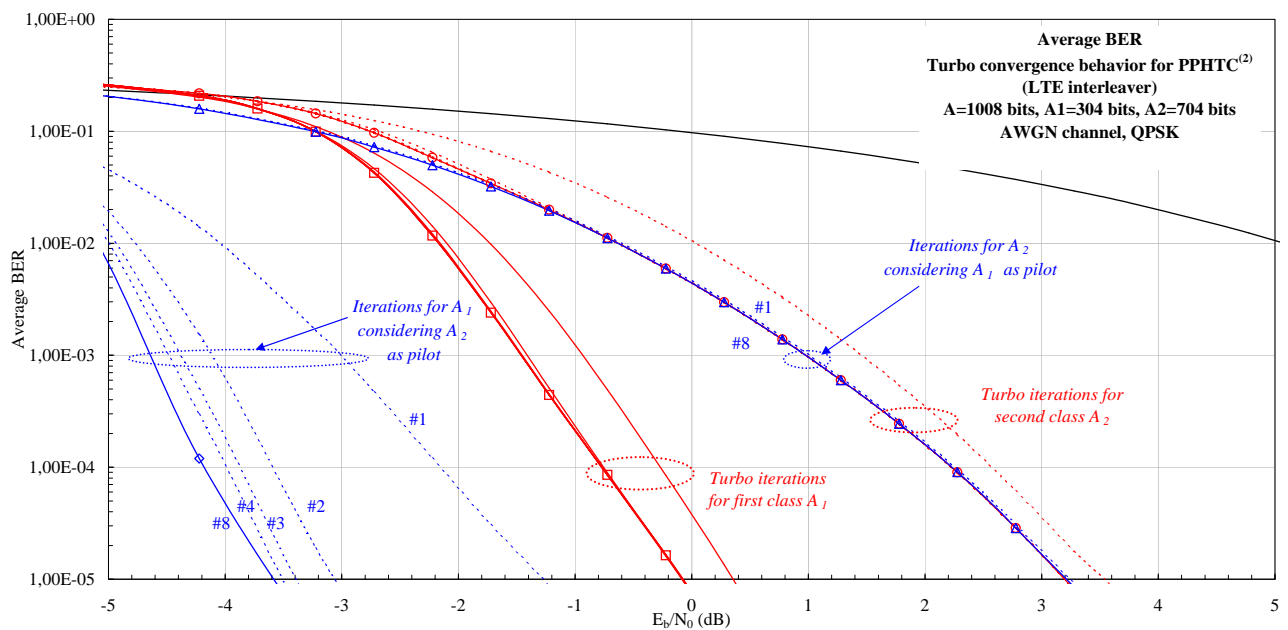


Figure 3.31. AWGN PPHTC⁽²⁾ pilot insertion behavior, LTE platform.

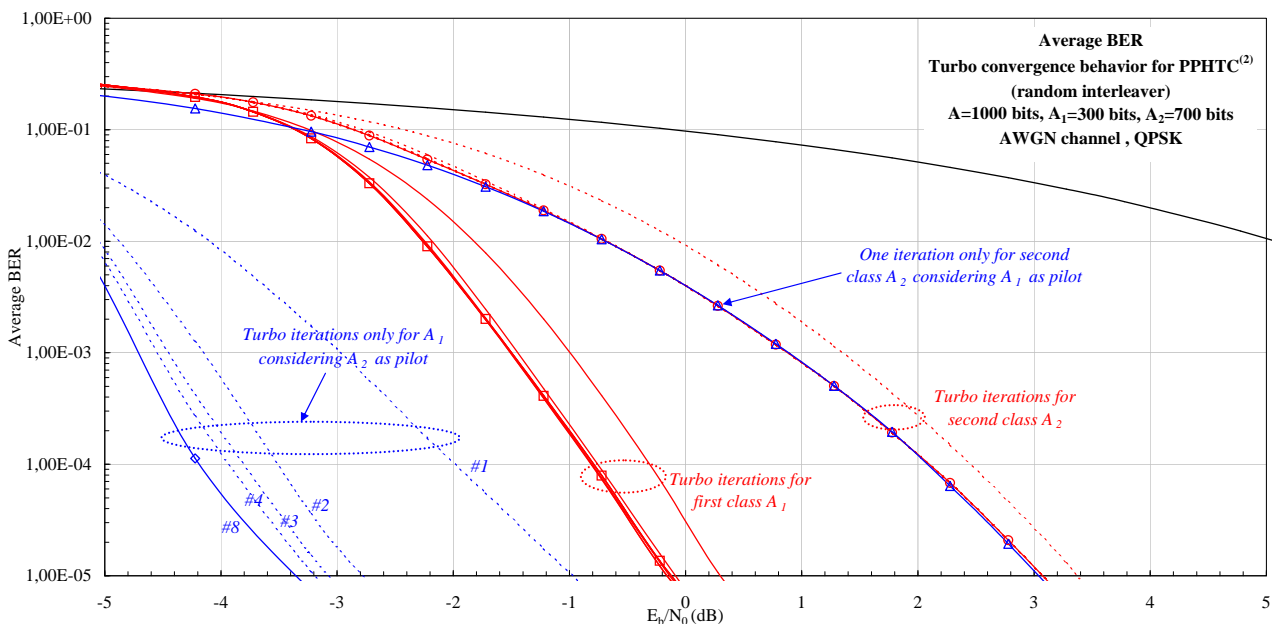


Figure 3.32. AWGN PPHTC⁽²⁾ pilot insertion behavior, random platform.

In the opposite case, i.e. supposing A_2 as **pilot**, we estimate class A_1 . Here, the pilot insertion code behavior is perfectly verified. The turbo decoder performances are improved as the turbo waterfall becomes steeper with the increasing pilot length. This is not only an insertion convolutional encoder, but a *pilot insertion turbo code*. However, we must observe that the pilot is only partly inserted, since it is not inserted before encoding, but during the encoding process, for both PPHTC and SPHTC. But this is sufficient for improving the turbo convergence. This improvement is also predicted by the weight coefficients of class A_1 . Thus, inserting perfectly known code word weights in the encoding process helps improving the decoder's estimations. We note that in both parallel and serial cases, the LTE turbo convergence is faster and steeper than over the random platform. The LTE interleaver type proves its effectiveness through these improved performances.

Also, we note that, in the serial structures case, the weight of the outer encoded A_1 is much larger and therefore, the A_2 performances benefit of a larger weight input for the inner RSC. The improvement of A_1 decoding performances when A_2 is considered as pilot is less impressive than in the parallel case. This is also

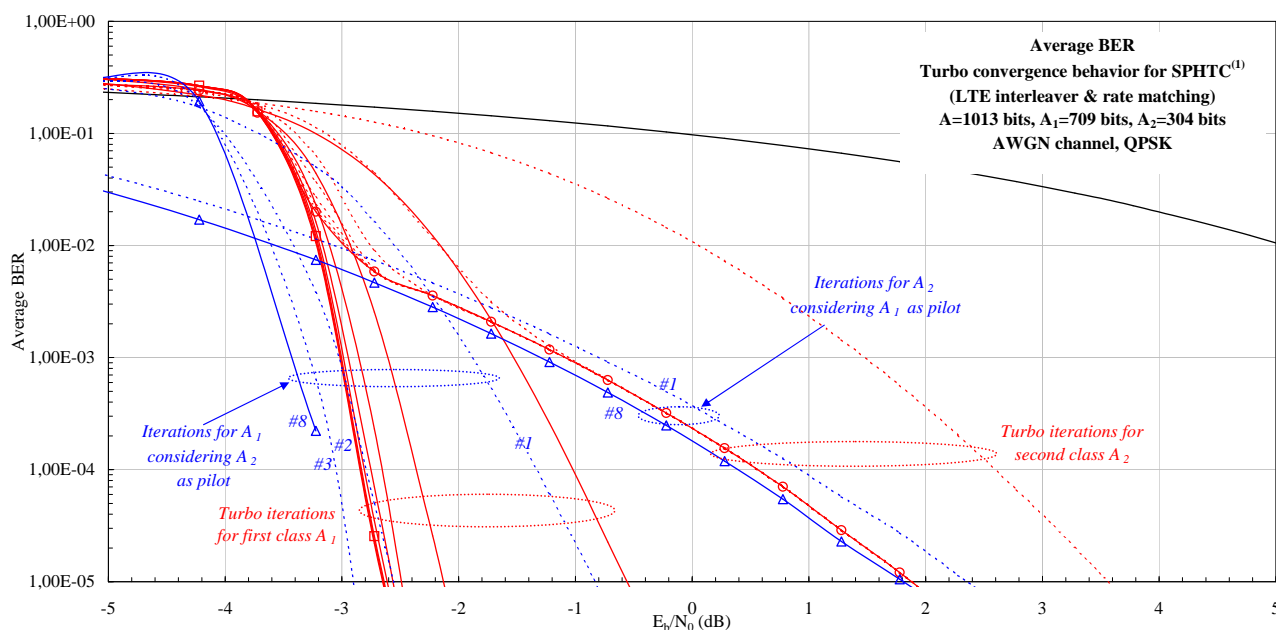


Figure 3.33. AWGN $SPHTC^{(1)}$ pilot insertion behavior, LTE platform.

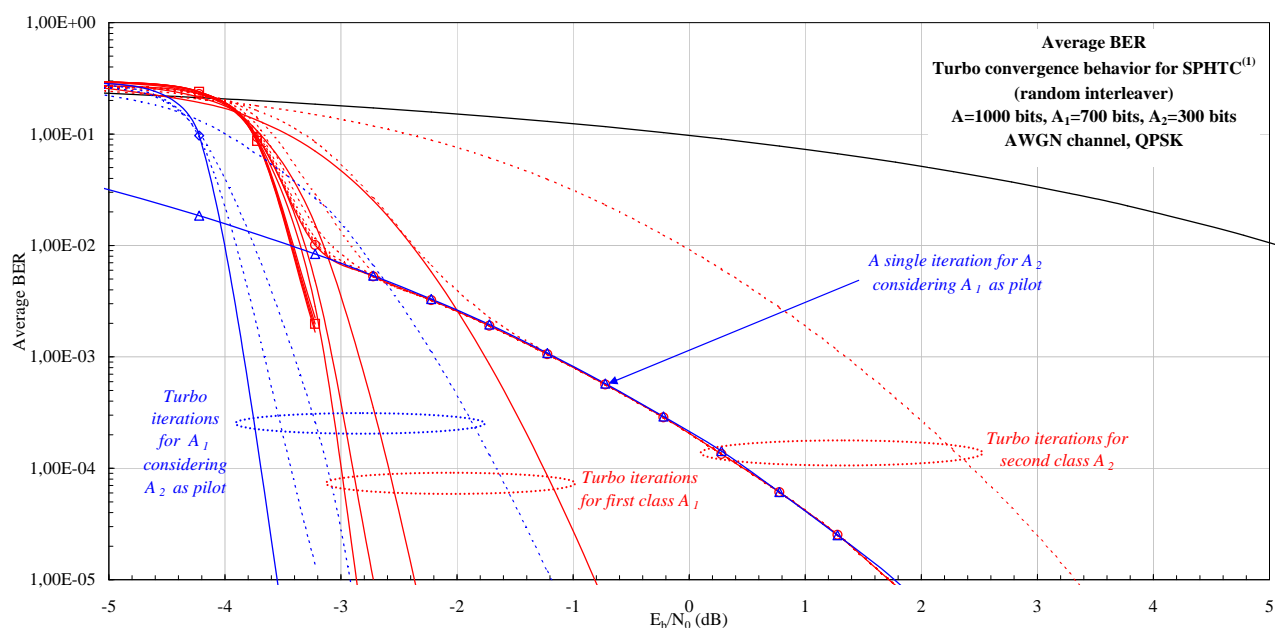


Figure 3.34. AWGN $SPHTC^{(1)}$ pilot insertion behavior, random platform.

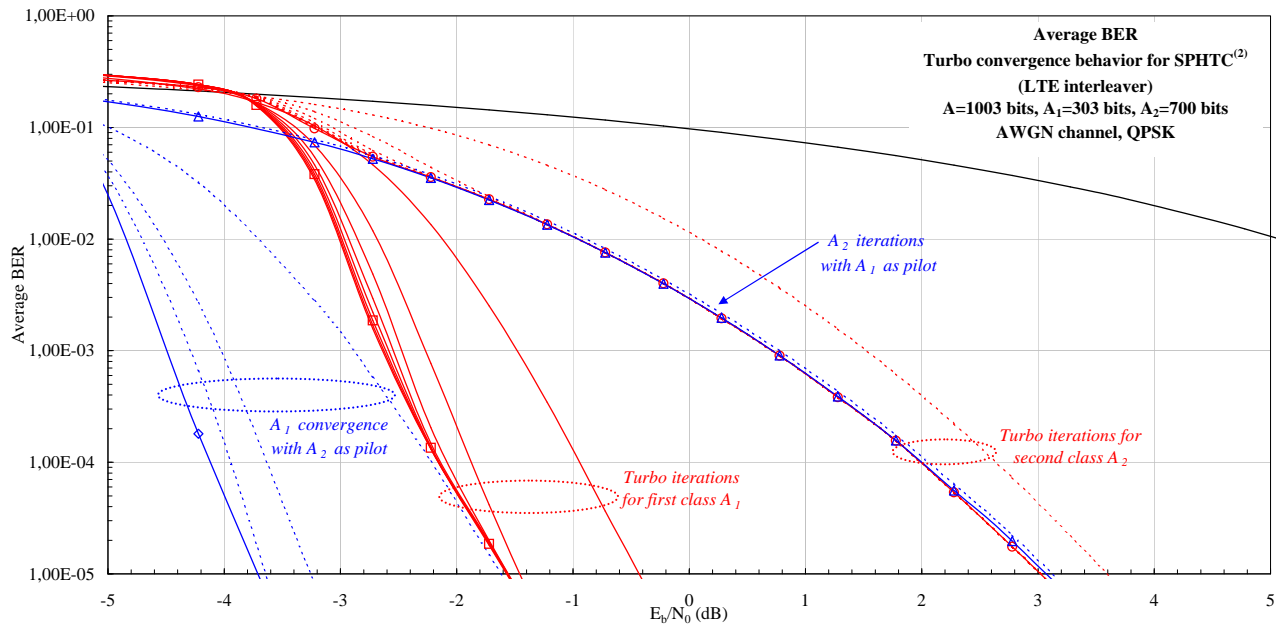


Figure 3.35. AWGN SPHTC⁽²⁾ pilot insertion behavior, LTE platform.

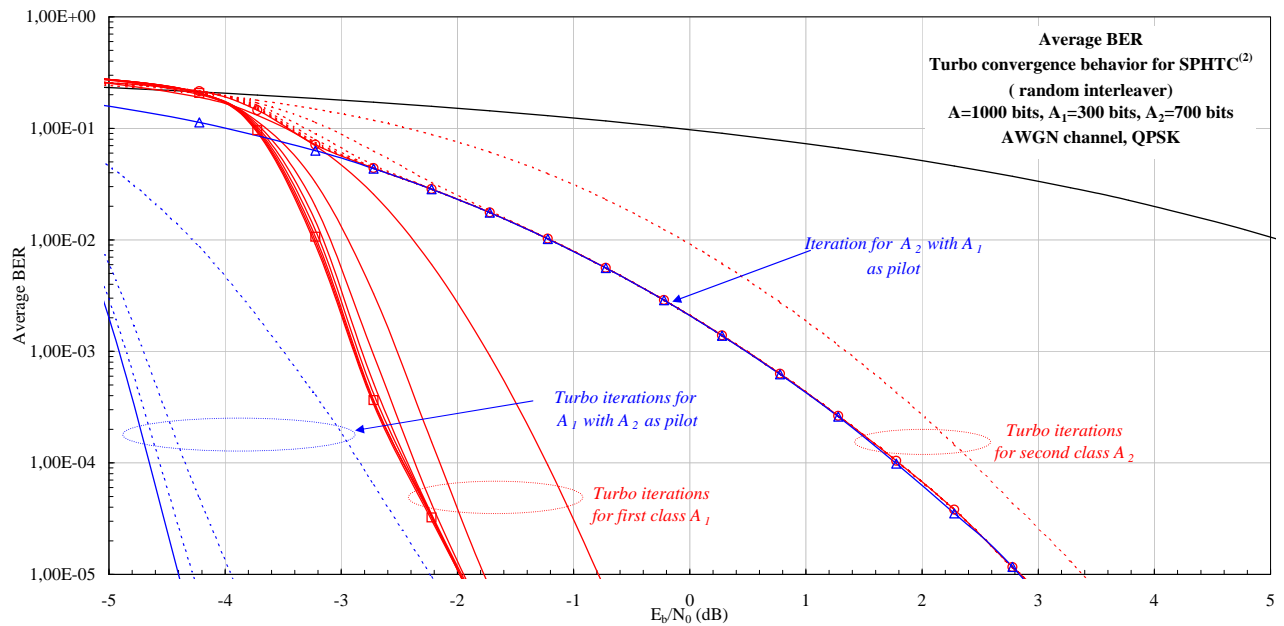


Figure 3.36. AWGN SPHTC⁽²⁾ pilot insertion behavior, random platform.

due to the serial RSC concatenation, and the fact that the serial decoding is performed on both systematic and parity bits of its respective input. The weight of A_2 becomes less important for the MAP decoding of A_1 .

3.4.3.3 AWGN Channel Performance Comparison

The AWGN code performances have been evaluated on both LTE and random platforms, also considering the benchmarks' performances, as indicated in Table 3.1. These results are given here for the average bit error rates (BER) as a function of the bit energy to noise ratio (E_b/N_0), while their corresponding performances in frame error rates (FER) are given in Appendix D, subsection D.1.4. The UEP decoded classes A_1 and A_2 are compared with turbo and convolutional benchmarks, supposing equivalent input-equivalent output. The comparison must be considered by pairs of classes, or the overall frame, as to objectively analyse the trade-off between performances and complexity.

PPHTC

The $PPHTC^{(1)}$ AWGN results are given in Fig. 3.37 and 3.38, evaluated over the LTE and random platforms respectively.

From a turbo UEP perspective, both classes are turbo encoded/decoded either together, either separately. The $PPHTC^{(1)}(A_1)$ and $PPHTC^{(1)}(A_2)$ performances can be evaluated compared with the $PCCC1/3(A_1)$ and $PCCC1/2(A_2)$ respectively. From a complexity point of view, we have showed in Table 3.1 that the PPHTC complexity is smaller than the complexity of the two PCCCs together. Fig. 3.37, presenting the LTE platform, shows that $PPHTC^{(1)}(A_1)$ closely follows $PCCC1/3(A_1)$ as low as 10^{-3} , where the UEP estimation begins to follow its error floor. $PPHTC^{(1)}(A_2)$ remains better than the $PCCC1/2(A_2)$ until 3×10^{-4} , and shows a gain of almost 2 dB for a BER of 10^{-2} . Therefore, on this LTE platform and for BER of interest of 10^{-2} , the PPHTC performances are largely superior to its PCCC counterpart. For the random platform on the other hand, from Fig. 3.38, even though $PPHTC^{(1)}(A_2)$ are very good compared to the $PCCC1/2(A_2)$, the

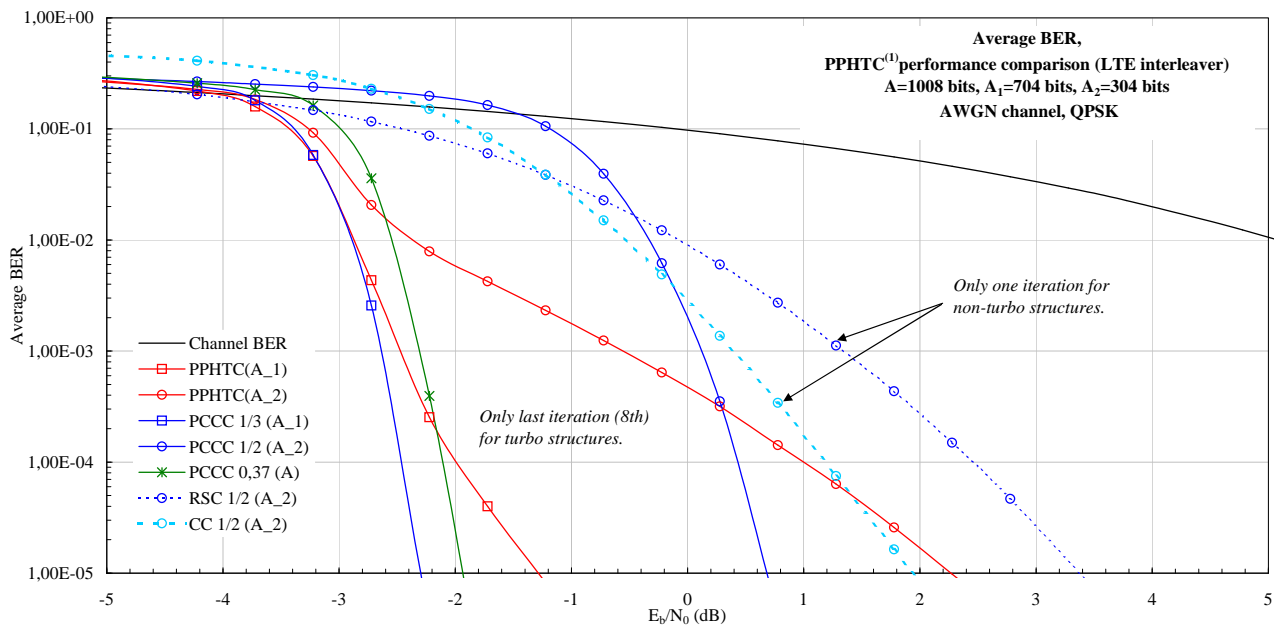


Figure 3.37. AWGN $PPHTC^{(1)}$ turbo performances comparison, LTE platform.

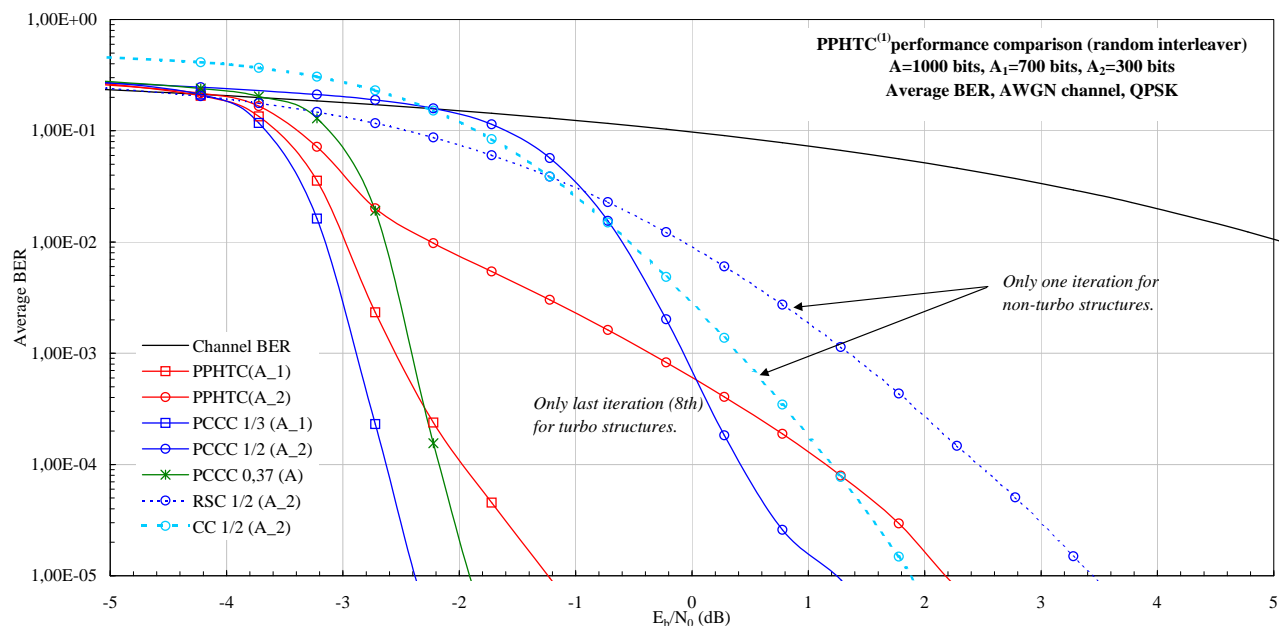


Figure 3.38. AWGN $PPHTC^{(1)}$ turbo performances comparison, random platform.

$PPHTC^{(1)}(A_1)$ estimations are 0.2 dB lower than over the LTE platform.

From a classical UEP scheme perspective, class A_1 is turbo encoded, while class A_2 is convolutionally encoded. Here, and for both platforms, we thus compare the results of $PPHTC^{(1)}(A_1)$ and $PPHTC^{(1)}(A_2)$ with $PCCC1/3(A_1)$ and $CC1/2(A_2)$, or $RSC1/2(A_2)$. The astonishing thing is that the computational complexity for such schemes are highly similar and of the same order of magnitude. While class A_1 presents better results when protected by a $PCCC1/3$, the performances of class A_2 are much improved in the PPHTC case compared to the convolutional benchmarks, even for the very powerful $CC1/2$.

A third perspective is the comparison of the embedded UEP with the EEP approach. This comes to evaluating the $PPHTC^{(1)}(A_1)$ and $PPHTC^{(1)}(A_2)$ results with the $PCCC0.37(A)$, i.e. the punctured PCCC to an equivalent transmission rate. Already the complexity of the $PCCC0.37(A)$ is superior to the $PPHTC^{(1)}(A)$. The punctured PCCC gives very good performances over both platforms, but the $PPHTC^{(1)}(A_1)$ remains nevertheless better up to a BER of 3×10^{-4} . Even though the class A_2 estimations are inferior in the UEP case,

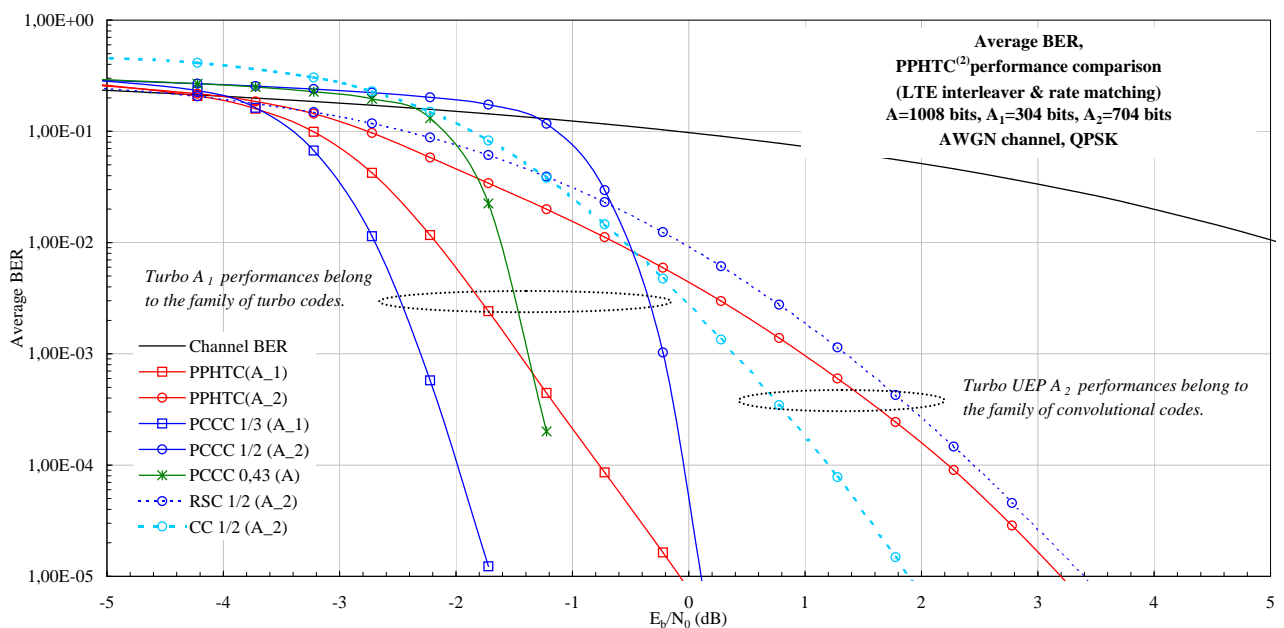


Figure 3.39. AWGN $PPHTC^{(2)}$ turbo performances comparison, LTE platform.

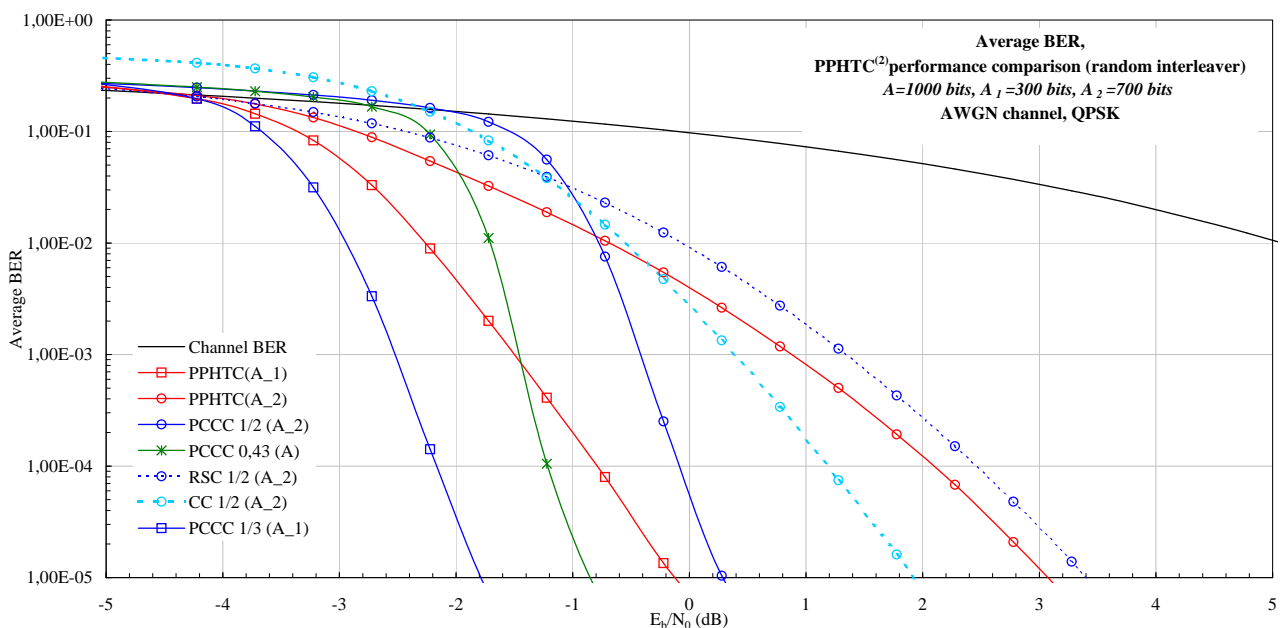


Figure 3.40. AWGN $PPHTC^{(2)}$ turbo performances comparison, random platform.

this is not cumbersome for some applications. For voice transmission for example, it is mainly the first class of bits that must have a good BER, while the second class bits influence is less visible in the final reconstructed signal. At a BER of 10^{-2} , $PPHTC^{(1)}(A_1)$ presents however a gain of approximately 0.4 dB compared to the EEP on both platforms.

The $PPHTC^{(2)}$ AWGN results are given in Fig. 3.39 and 3.40, evaluated over the LTE and random platforms respectively. Here, as the ratio between class sizes has changed, the performances are quite different.

From a turbo UEP perspective, the $PPHTC^{(2)}(A_1)$ remains inferior to $PCCC1/3(A_1)$. The $PPHTC^{(2)}(A_2)$ performances however are better than the $PCCC1/2(A_2)$ until 10^{-2} . On both platforms, it is not clear whether the PPHTC can be more efficient than the independent UEP offered by the PCCC. Depending on the applications, the PPHTC utility might be questioned. Nevertheless, from a complexity point of view, in Table 3.1, the numbers prove that the complexity of the PPHTC is almost half of the sum of the complexities for the $PCCC1/3(A_1)$ and $PCCC1/2(A_2)$.

From a classical UEP scheme perspective, the turbo encoded class A_1 is better with the $PCCC1/3(A_1)$ than the $PPHTC^{(2)}(A_1)$. But class A_2 presents better performances starting with 10^{-2} if protected by a $CC1/2(A_2)$ than if it were transmitted with the $PPHTC^{(2)}$, on both platforms. As for the $RSC1/2(A_2)$, since its behavior resembles the first iteration of the $PPHTC^{(2)}(A_2)$, it is obvious that it remains inferior to the $PPHTC^{(2)}(A_2)$. Here as well, the real value of the PPHTC remains to be seen in a real transmission scenario, where the final quality of the audio or video signal can be evaluated.

For the third perspective, the $PPHTC^{(2)}(A_1)$ and $PPHTC^{(2)}(A_2)$ results are better than the punctured EEP PCCC, i.e. $PCCC0.43(A)$. On both platforms, class A_1 PPHTC estimation intersects the PCCC evaluation at 10^{-3} . Undoubtedly, the embedded UEP approach remains better than the EEP punctured PCCC.

SPHTC

The $SPHTC^{(1)}$ AWGN results are given in Fig. 3.41 and 3.42, evaluated over the LTE and random platforms respectively.

These figures present very good results, and from all three evaluation perspectives.

From a turbo UEP perspective, both classes are turbo encoded/decoded either together, either separately by serial structures. The $SPHTC^{(1)}(A_1)$ and $SPHTC^{(1)}(A_2)$ performances are compared with the $SCCC1/4(A_1)$ and $SCCC1/2(A_2)$ respectively. Table 3.1 gives the complexity estimations, where the SPHTC complexity is smaller than the sum of complexities of the two SCCCs. In both Fig. 3.41 and 3.42, $SPHTC^{(1)}(A_1)$ and $SPHTC^{(1)}(A_2)$ results are better than their SCCC counterparts. Thus, $SPHTC^{(1)}(A_1)$ begins to visibly improve at 10^{-2} and 0.1 dB can be gained at 10^{-5} . As for the class A_2 , $SPHTC^{(1)}(A_2)$ performances are largely superior to those of $SCCC1/2(A_2)$. However, we must note that the puncturing used for the $SCCC1/2$ has not been optimized for use with serial structures and may degrade the SCCC performances. But the SPHTC global overview, and particularly regarding class A_1 compared to a non punctured SCCC, gives us reasons to believe that the SPHTC approach remains better than the independent UEP SCCC encoding of the two classes.

From a classical UEP scheme perspective, class A_1 is turbo SCCC encoded, while class A_2 is convolutionally encoded. Here, and for both platforms, the performances of both $SPHTC^{(1)}(A_1)$ and $SPHTC^{(1)}(A_2)$ remain superior to $SCCC1/4(A_1)$ and $CC1/2(A_2)$, or $RSC1/2(A_2)$, for complexities of the same order of magnitude.

As for the third perspective, the comparison of the embedded UEP with the EEP approach, $SPHTC^{(1)}(A_1)$ remains better than the $SCCC0.29(A)$ with up to 0.6 dB, and for both platforms approximately. The UEP A_2 estimations are inferior to the EEP case only lower than 10^{-2} . However, as class A_1 is undoubtedly much better than the punctured SCCC, the SPHTC scheme remains more interesting than the EEP one with a lower complexity as well.

The $SPHTC^{(2)}$ AWGN results are also very good, since the $SPHTC^{(2)}(A_1)$ performances remain above all benchmarks. These evaluations are given in Fig. 3.43 and 3.44, over the LTE and random platforms respectively.

Except the fact that class A_2 has lost in turbo convergence, the behavior of $SPHTC^{(2)}$ remains similar to $SPHTC^{(1)}$, when compared with equivalent benchmarks. The differences between the SPHTC and its

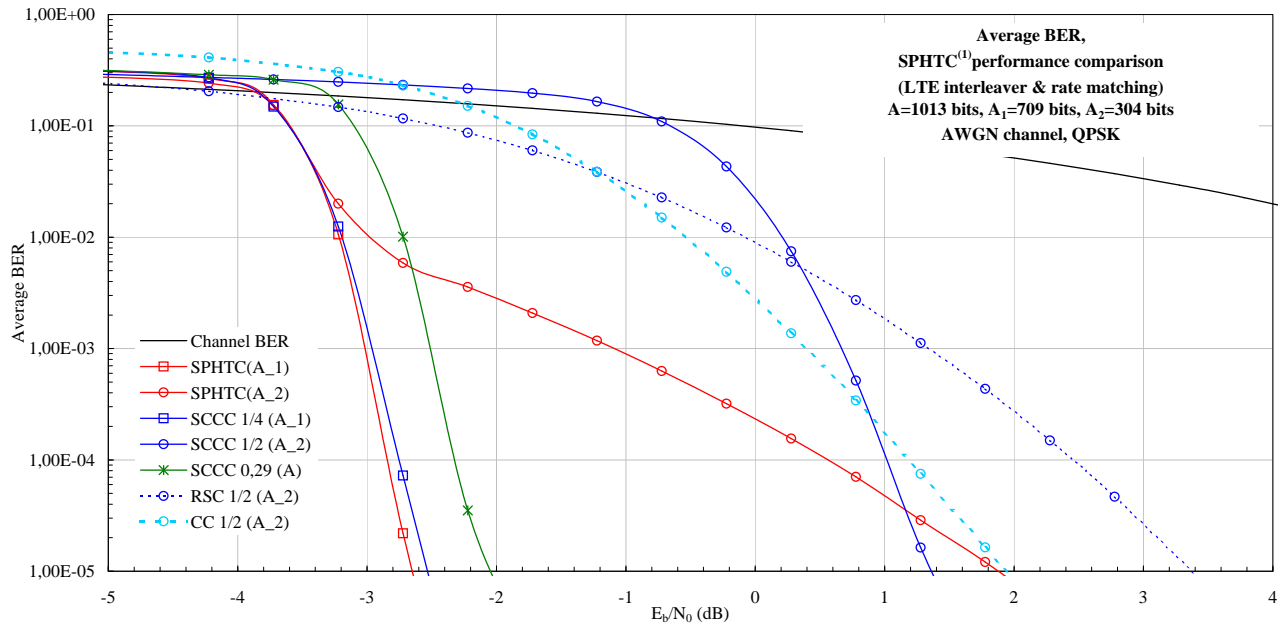


Figure 3.41. AWGN $SPHTC^{(1)}$ turbo performances comparison, LTE platform.

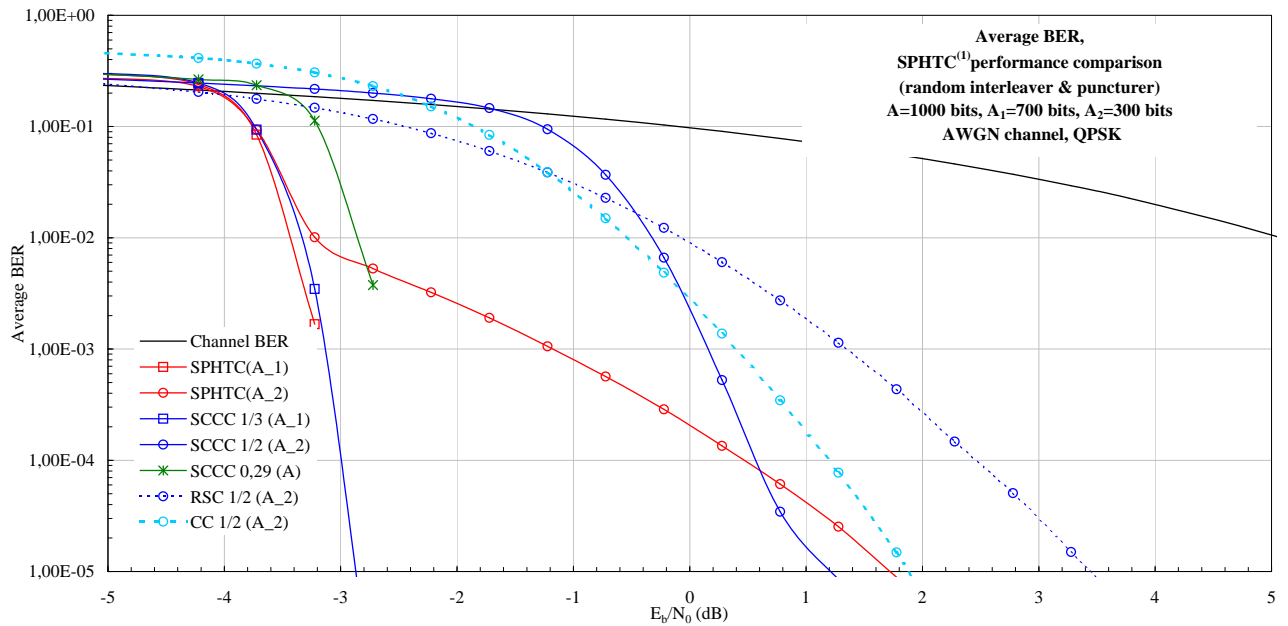


Figure 3.42. AWGN $SPHTC^{(1)}$ turbo performances comparison, random platform.

benchmarks for the three perspectives are even accentuated.

Thus, from a turbo UEP perspective, $SPHTC^{(2)}(A_1)$ and $SPHTC^{(2)}(A_2)$ remain better than the $SCCC1/4(A_1)$ and $SCCC1/2(A_2)$ respectively, for a target BER of 10^{-2} . As for the classical UEP and the EEP comparison perspectives, the SPHTC presents the best compromise between its performances and complexity compared to chosen benchmarks.

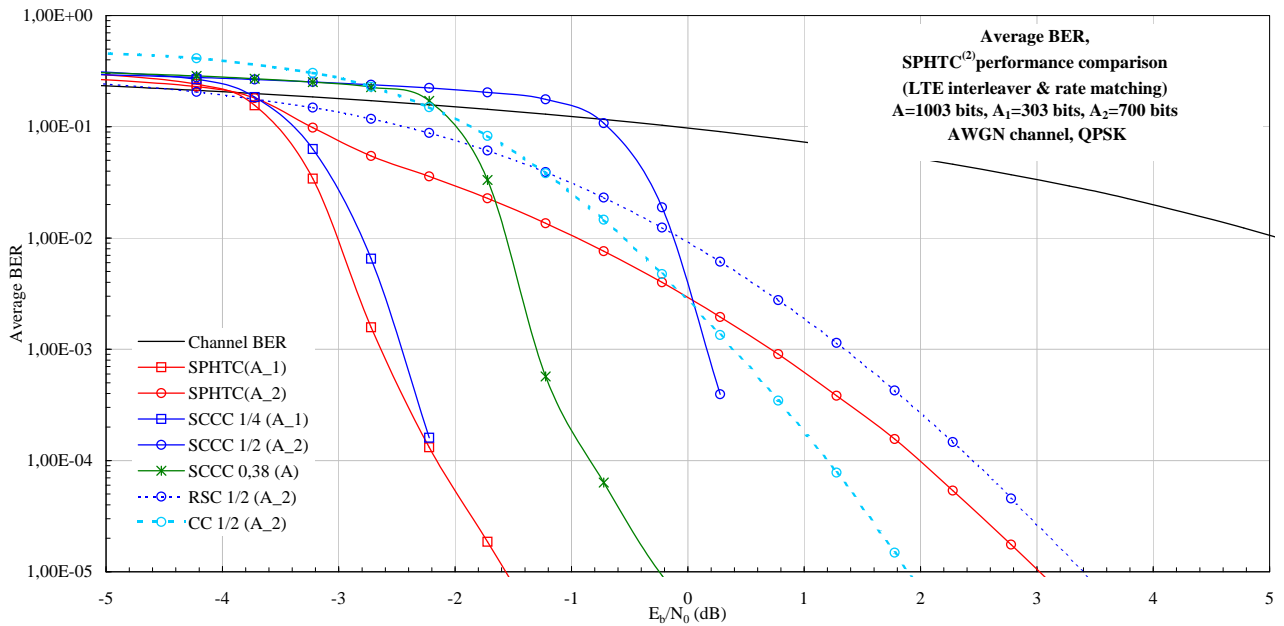


Figure 3.43. AWGN $SPHTC^{(2)}$ turbo performances comparison, LTE platform.

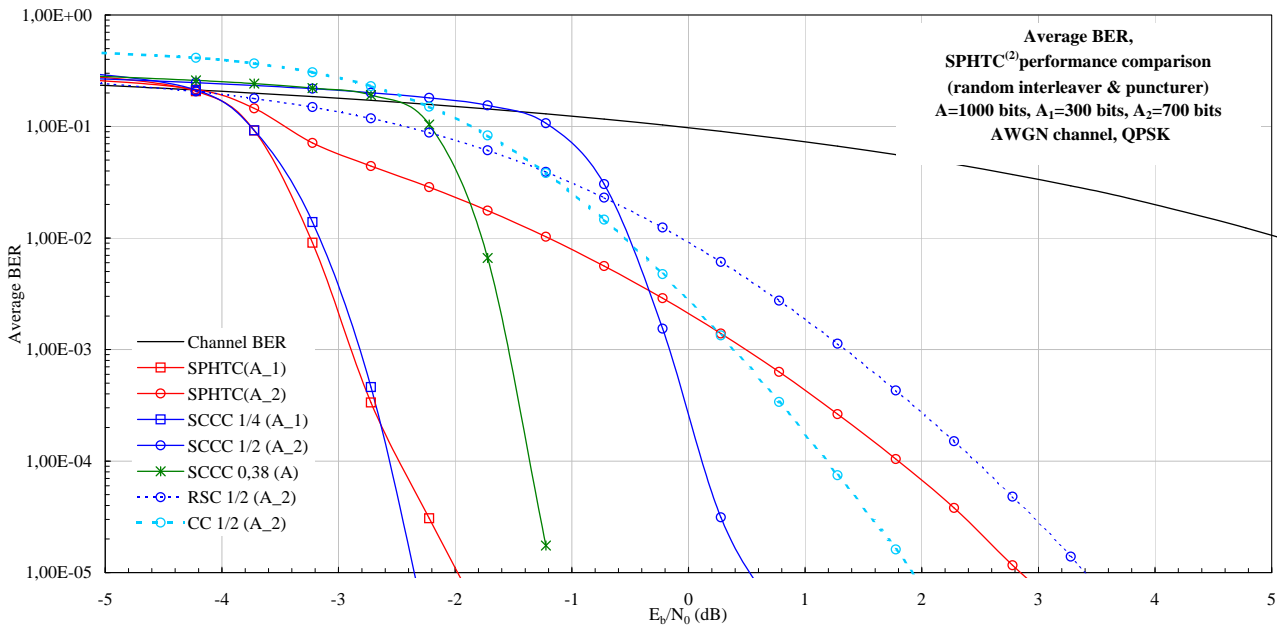


Figure 3.44. AWGN $SPHTC^{(2)}$ turbo performances comparison, random platform.

3.4.3.4 Rayleigh Channel Results

The Rayleigh channel results are given in this section considering only the average BER. The corresponding results given in average FER are presented in Appendix D, section D.1.5.

PPHTC

The $PPHTC^{(1)}$ HT200 results are given in Fig. 3.45 and 3.46, evaluated over the LTE and random platforms respectively. The performances are very flattened compared to the AWGN results, but remain however very interesting.

By looking at both platform evaluations, we notice that most of the class A_2 results are grouped together, with the exception of the $PPHTC^{(1)}(A_2)$ and the EEP $PCCC 0.37(A)$. Thus, from all three perspective

of evaluation, the $PPHTC^{(1)}$ estimations are undoubtedly better than benchmark schemes. Over both platforms, the $PPHTC^{(1)}(A_1)$ remains visibly the best, with 0.2 to 0.6 dB better than the $PCCC 1/3(A_1)$ or $PCCC 0.37(A)$, at a BER of 10^{-5} . $PPHTC^{(1)}(A_2)$ follows closely, and, in the case of LTE, remains even better of up to 0.1 dB than the $PCCC 0.37(A)$. Compared to the independent encoding provided by either $PCCC 1/2(A_2)$ or convolutional codes, there is a gain of up to 3 dB at a BER of 10^{-2} . The LTE platform gives better results than the random one, except only for the punctured PCCC, i.e. $PCCC 1/2(A_2)$, whose performances are visibly better on the random platform.

The $PPHTC^{(2)}$ HT results are given in Fig. 3.47 and 3.48, evaluated over the LTE and random platforms respectively. If the AWGN performances did not allow us to conclude on the utility of this UEP scheme, the HT200 results are most impressive. The $PPHTC^{(2)}$ is very good, and especially on the LTE platform.

Evaluating the performances from a turbo UEP perspective, it appears that the $PPHTC^{(2)}$ is preferable to the independent UEP encoding as $PCCC 1/3(A_1)$ and $PCCC 1/2(A_2)$. Even though the equivalent trans-

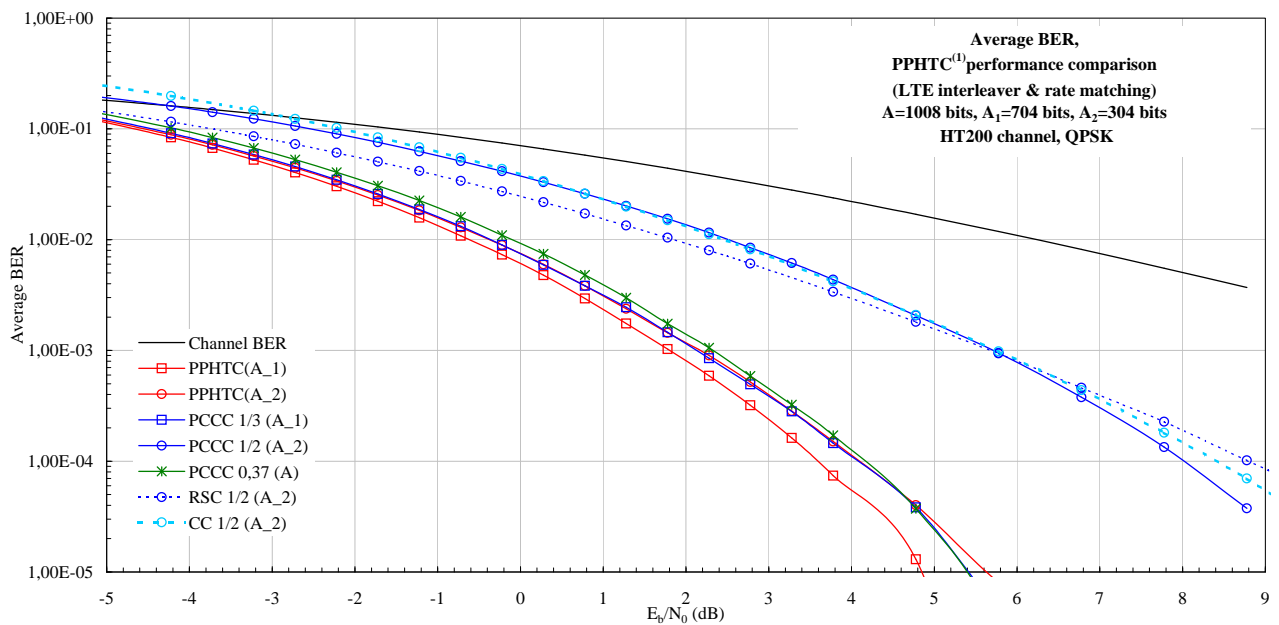


Figure 3.45. HT200 $PPHTC^{(1)}$ turbo performances comparison, LTE platform.

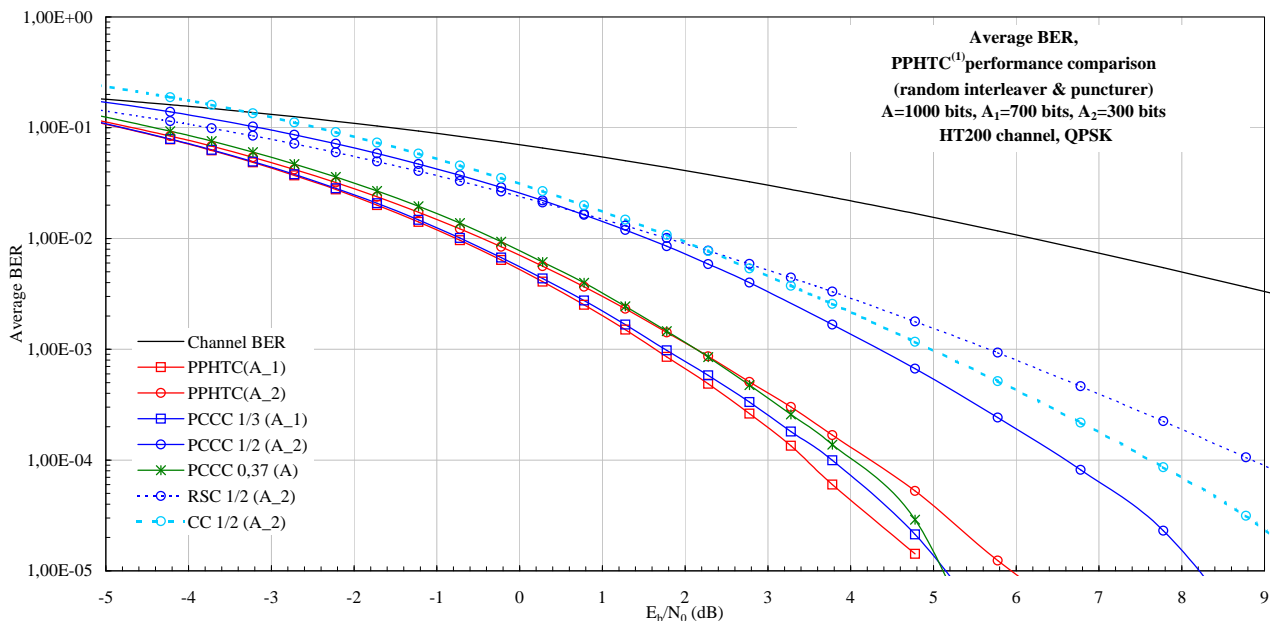


Figure 3.46. HT200 $PPHTC^{(1)}$ turbo performances comparison, random platform.

mission rate is the same for the two schemes, with the same input, the difference comes from the virtual rate of the PPHTC or simply the encoding of both classes together. In the HT200, it is obvious that any supplementary redundancy transmitted over the channel has a very high price. Thus, even if the mother code rate of $PPHTC^{(2)}(A_1)$ is $1/3$, its performances are improved considerably compared to the $PCCC 1/3(A_1)$. This is due to the extra redundancy introduced by A_2 in the PPHTC encoding process, i.e. $2 \times 700 = 1400$ extra bits, or what we have called the virtual code rate. Over the LTE platform, this translates in a gain of 0.5 dB for $PPHTC^{(2)}(A_1)$ compared to the $PCCC 1/3(A_1)$, gain expanding to 1 dB at 10^{-5} . In the random case, on the other hand, their respective results are quasi identical. The same phenomenon is registered for class A_2 as well. $PPHTC^{(2)}(A_2)$ remains greatly improved compared to the $PCCC 1/2(A_2)$. Over LTE platforms, a gain of 1.5 dB is observed at 10^{-2} , and 1.2 dB in the random case.

As for the classical UEP and EEP perspectives, the $PPHTC^{(2)}$ performances are undoubtedly best, and on both LTE and random platforms. For the classical UEP, $PPHTC^{(2)}(A_1)$ presents better or similar results

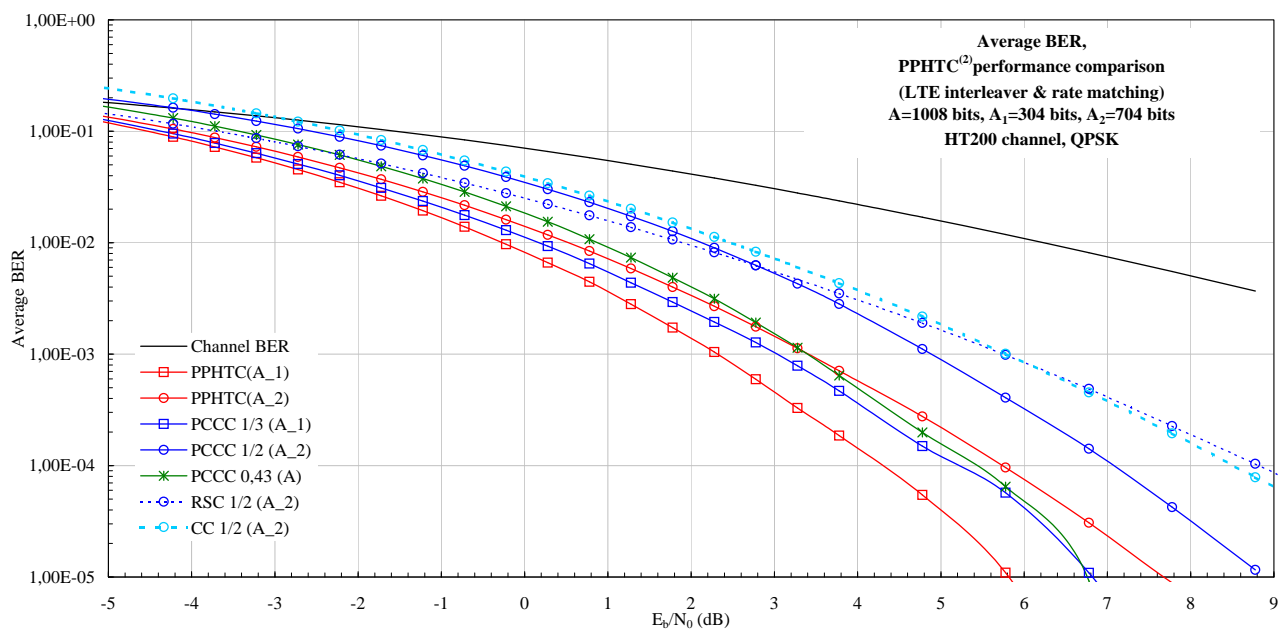


Figure 3.47. HT200 $PPHTC^{(2)}$ turbo performances comparison, LTE platform

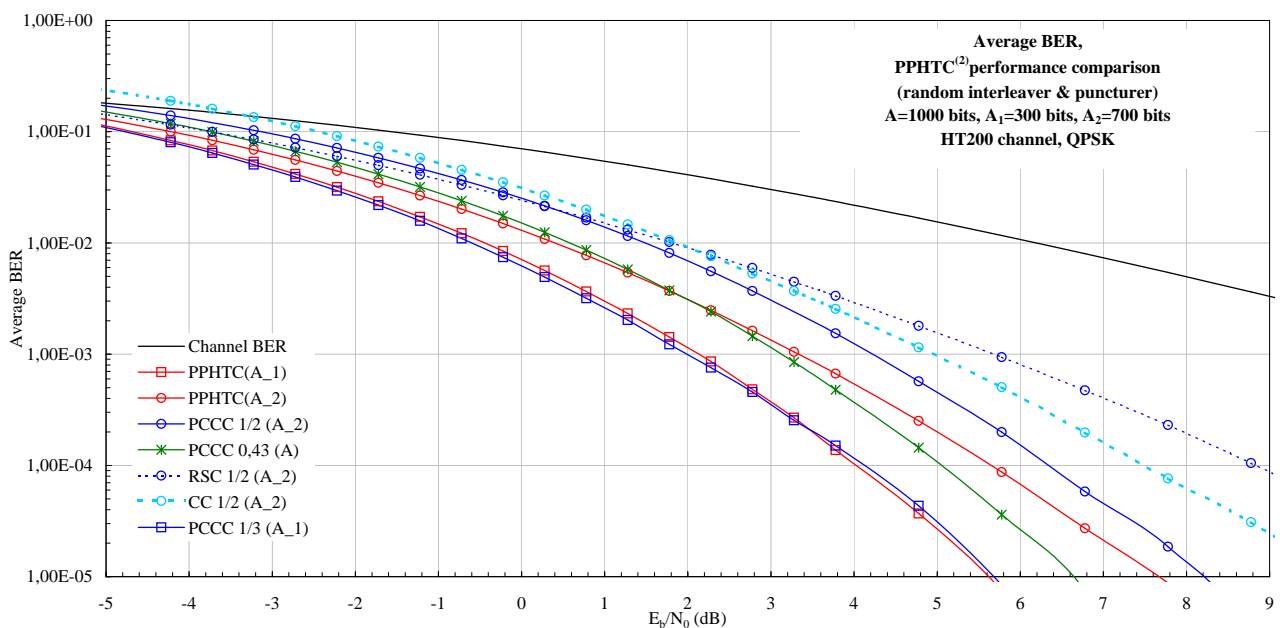


Figure 3.48. HT200 $PPHTC^{(2)}$ turbo performances comparison, random platform.

to the $PCCC\ 1/3(A_1)$, while $PPHTC^{(2)}(A_2)$ is largely superior to convolutional performances. As for the EEP, $PPHTC^{(2)}(A_1)$ shows a gain of almost 1 dB compared to the $PCCC\ 0.43(A)$, while $PPHTC^{(2)}(A_2)$ is hardly shadowed by this $PCCC\ 0.43(A)$.

SPHTC

The $SPHTC^{(1)}$ HT200 results are given in Fig. 3.49 and 3.50, evaluated over the LTE and random platforms respectively. As expected, both figures show very good evaluation performances for this $SPHTC^{(1)}$. For both evaluation platforms, the $SPHTC^{(1)}$ performances for classes A_1 and A_2 remain visibly best. Even the $SPHTC^{(1)}(A_2)$ surpasses the results of those of turbo codes applied to A_1 .

The $SPHTC^{(2)}$ HT200 results are given in Fig. 3.51 and 3.52, evaluated over the LTE and random platforms respectively. As in the case of its parallel counterpart, $PPHTC^{(2)}$, the performances for this serial UEP

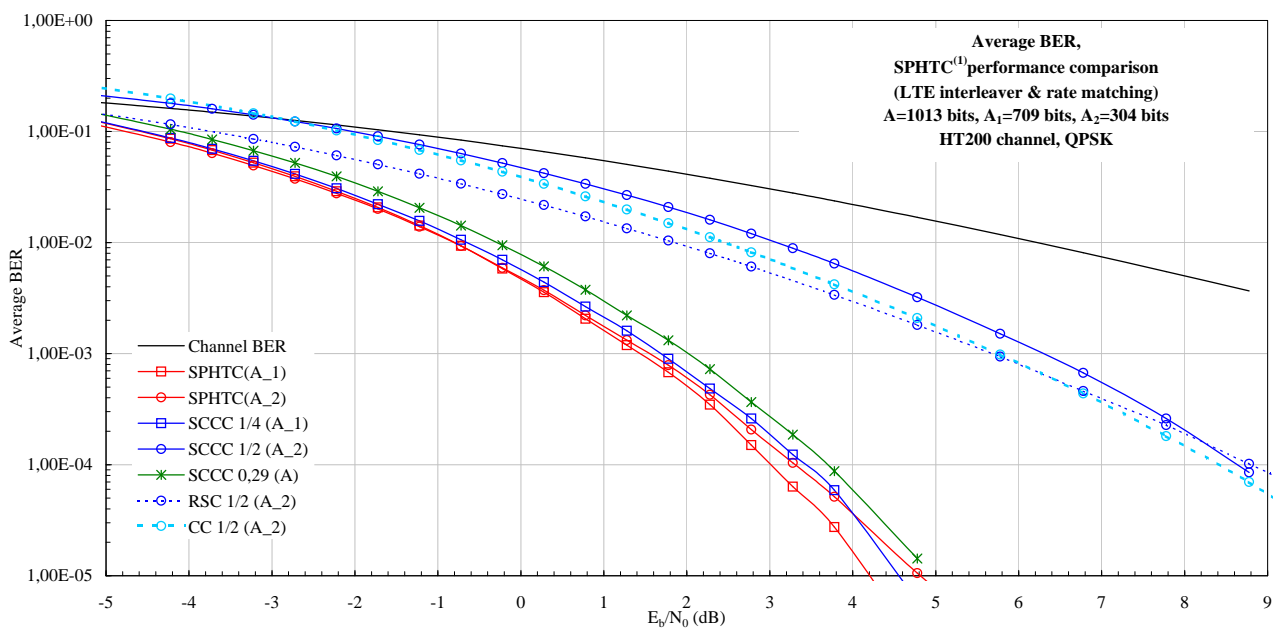


Figure 3.49. HT200 $SPHTC^{(1)}$ turbo performances comparison, LTE platform.

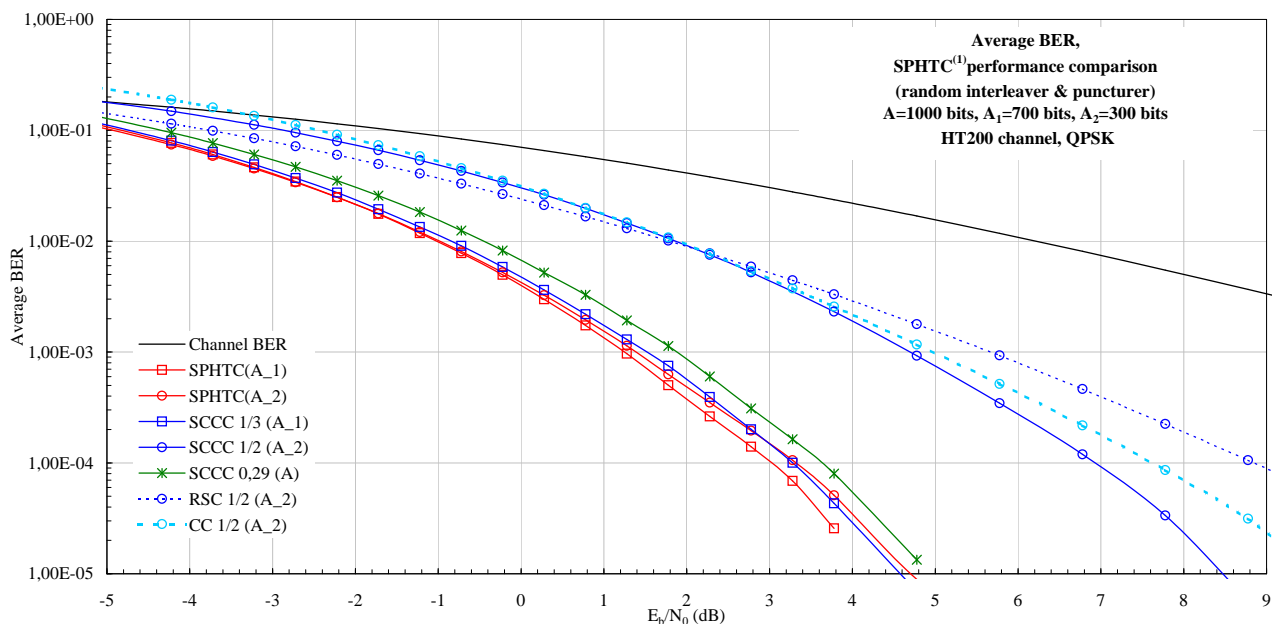


Figure 3.50. HT200 $SPHTC^{(1)}$ turbo performances comparison, random platform.

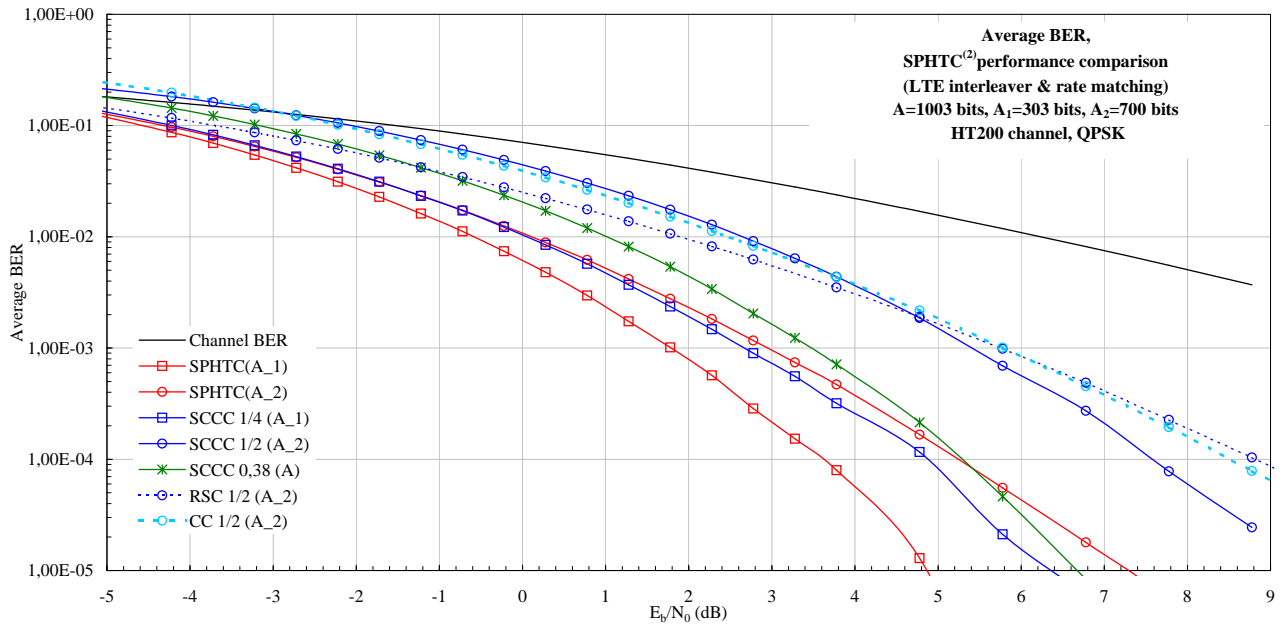


Figure 3.51. HT200 $SPHTC^{(2)}$ turbo performances comparison, LTE platform.

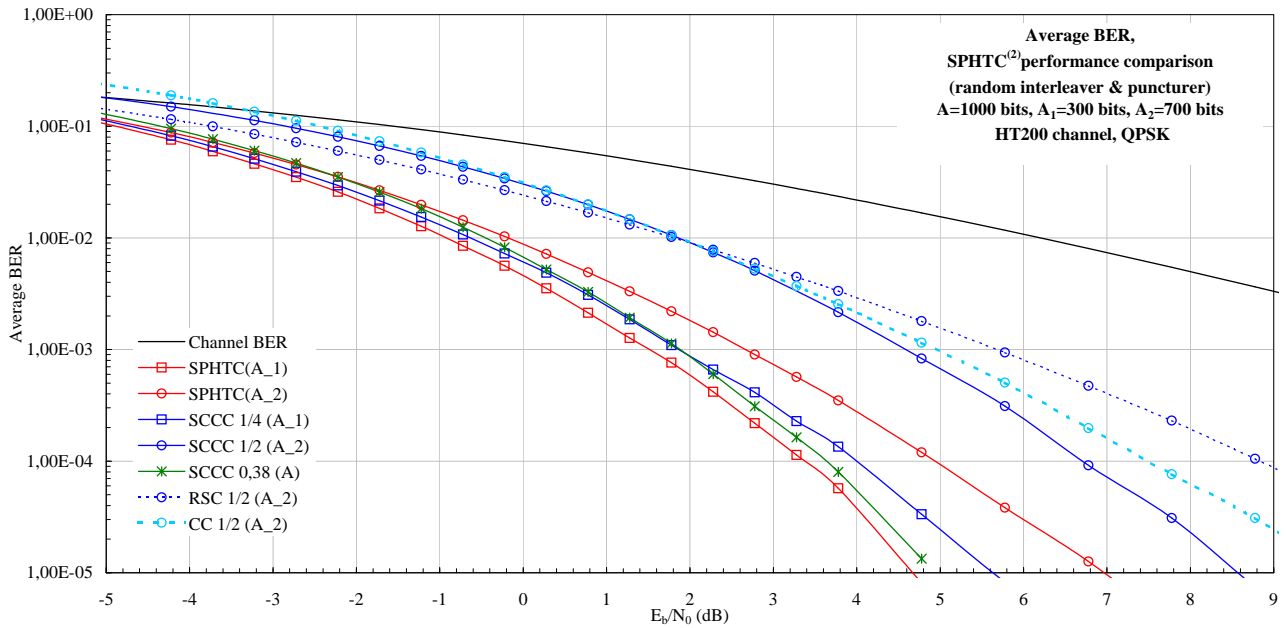


Figure 3.52. HT200 $SPHTC^{(2)}$ turbo performances comparison, random platform.

scenarios are surprisingly good.

The results of $SPHTC^{(2)}(A_1)$ are best for both evaluation platforms. With LTE elements, the gain is remarkable compared to the other benchmark codes. The extra channel redundancy, or the virtual code rate, provided by A_2 helps $SPHTC^{(2)}(A_1)$ gain 0.8 dB at 10^{-2} and up to 1.4 dB at 10^{-5} , compared to the $SCCC 1/4(A_1)$. The $SPHTC^{(2)}(A_2)$ performance is also impressive, gaining more than 2 dB compared to convolutional and $SCCC 1/2(A_1)$ benchmarks. Both $SPHTC^{(2)}(A_1)$ and $SPHTC^{(2)}(A_2)$ remain mostly best compared to the EEP $SCCC 0.38(A)$. As for the random platform, even though the $SPHTC^{(2)}(A_2)$ results are surpassed by the EEP $SCCC 0.38(A)$, the SPHTC results remain very good. From whatever perspective the comparison is made, either only UEP turbo encoding, or classical UEP with convolutional encoding, or EEP transmission, the global behavior of the $SPHTC^{(2)}$ remains highly competitive compared to the other codes.

3.5 Conclusion

In this chapter, we have proposed UEP turbo codes which modify the turbo encoder and decoder by embedding UEP principles in these high performance structures themselves. Progressively inserting new data at each encoding step is equivalent with virtually increasing the code rate for each class, together with enhancing the input output weights of respective block codes. The hierarchical encoding provides each class with the rate proportional to its defined level of protection, with a high flexibility regarding used codes and puncturing schemes.

The decoding is performed in a turbo performance perspective. Each class is progressively extracted from the decoding process. The n th class performances prove to be intermediate between the RSC decoding and the turbo decoding. This is explained by the duality between the ML and MAP decoding algorithms, since in the UEP-MAP this class does not possess any priori informations of itself.

The PPHTC and SPHTC prove to be very good codes whose results are surprisingly good in both AWGN and fading channels. Progressively introducing new information before interleaving and re-encoding proves to be quite efficient and perfectly applicable to any UEP scheme. While maintaining a turbo steep waterfall for the best protected data, the gains for the progressively introduced class of information are particularly visible in AWGN, showing turbo improvements of 0.5 up to 3 dBs between the first and eighth iterations. The comparison with benchmark codes confirms the good behavior, the UEP schemes remain better with up to 0.6 dBs than the EEP transmission. In the HT200 transmission channel, turbo iterative gains for the less protected class may go up to 3.2 dBs in most favorable configurations. And even though some weak gains of particular configurations in AWGN channel discourage the code usage for very low bit error rates, results in the fading environment prove the code efficiency even at these low error rates. The graphs show that, for one same code rate, embedded UEP results are improved for the classes of bits compared to benchmark codes. The UEP scheme can provide up to 1 dB of better gains than its EEP counterpart for these low rate configurations.

The UEP gains obtained for a same air throughput may translate in a better received signal quality or, for a constant quality, an increased number of subscribers. The embedded UEP code helps improving the system spectral efficiency. This gain is in part due to the virtual class rate, but also to the increased weights of the classes encoded together. The progressive turbo decoding exploits the correlation and dependence between frame bits. The scheme may prove to be very useful in real time UEP applications for which a high rate is required.

PPHTC and SPHTC structures with different constituent encoders and other types of interleavers are a very interesting topic for future research. Specific UEP interleavers that would exploit the existence of several UEP classes would also be very interesting for future investigations. These UEP interleavers could be configured for an optimal distribution of lower level classes bits in between the higher level classes bits. Thus, the iterative decoding would benefit of an optimal distribution of errors, which would enhance the decoder's performances. Further optimizations can be performed by analyzing the influence of the weights of encoded code words on the final performances. This would engender optimization rules as a function of the code words' length, i.e. the size of the different classes in the overall frame, but specific to the turbo constituent codes. The investigation can further be extended to the computation of optimization rules for the turbo constituent codes themselves. The progressive hierarchical turbo codes thus propose an evolution for the existent turbo codes and their UEP schemes, and open many interesting research perspectives.

Bibliography

- [1] D. Costello and G. Forney, "Channel coding: the road to channel capacity," in *Proceedings of the IEEE*, vol. 95, Jun. 2007, pp. 1150–1177.
- [2] F. Burkert, G. Caire, J. Hagenauer, T. Hindelang, and G. Lechner, "Turbo decoding with unequal error protection applied to GSM speech coding," in *IEEE Global Telecommunications Conference*, vol. 3, p. 2044.
- [3] A. Hottinen and K. Pehkonen, "A flexible multirate CDMA concept with multiuser detection," in *IEEE 4th International Symposium on Spread Spectrum Techniques and Applications*, vol. 2, p. 556.
- [4] B. Masnick and J. Wolf, "On linear unequal error protection codes," *IEEE Transactions on Informations Theory*, vol. IT-3, pp. 600–607, Oct. 1967.
- [5] S. Borade, B. Nakiboglu, and L. Zheng, "Unequal error protection: an information theoretic perspective," *IEEE Transactions on Informations Theory*, vol. 55, pp. 5511–5539, Dec. 2009.
- [6] C. Berrou, A. Glavieux, and P. Thitimajshima, "Near Shannon limit error-correcting coding and decoding: Turbo-codes," in *IEEE International Conference on Communications*, vol. 2, May 1993, pp. 1064–1070.
- [7] S. Benedetto, D. Divsalar, G. Montorsi, and F. Pollara, "Serial concatenation of interleaved codes: performance analysis, design and iterative decoding," *IEEE Transactions on Informations Theory*, vol. 44, pp. 909–926, May 1998.
- [8] E. Boutillon, C. Douillard, and G. Montorsi, "Iterative decoding of concatenated convolutional codes: implementation issues," in *IEEE International Conference on Communications*, vol. 95, Jun. 2007, pp. 1201–1227.
- [9] H. Jin and R. McEliece, "Coding theorems for turbo code ensembles," *IEEE Transactions on Informations Theory*, vol. 48, pp. 1451–1461, Jun. 2002.
- [10] P. Regalia and J. M. Walsh, "Optimality and duality of the turbo decoder," in *Proceedings of the IEEE*, vol. 95, Jun. 2007, pp. 1362–1377.
- [11] S. Benedetto and G. Montorsi, "Unveiling turbo codes: Some results on parallel concatenated coding schemes," *IEEE Transactions on Informations Theory*, vol. 42, pp. 409–428, Mar. 1996.
- [12] S. Benedetto, G. Montorsi, D. Divsalar, and F. Pollara, "Iterative decoding of serially concatenated codes with interleavers and comparison with turbo codes," in *IEEE Global Telecommunications Conference*, vol. 2, Nov. 1997, pp. 654–658.
- [13] A. Ambroze, G. Wade, and M. Tomlinson, "Iterative MAP decoding for serial concatenated convolutional codes," in *IEEE Proceedings - Communications*, vol. 145, Apr. 1998, pp. 53–59.
- [14] A. Mohammadi and A. Khandani, "Unequal error protection on turbo encoder output bits," *IEEE Electronic Letters*, vol. 33, pp. 730–734, Feb. 1997.
- [15] G. Caire and E. Biglieri, "Parallel concatenated codes with unequal error protection," *IEEE Transactions on Communications*, vol. 46, pp. 565–567, May 1998.
- [16] G. Caire and G. Lechner, "Turbo codes with unequal error protection," *IEEE Electronic Letters*, vol. 32, pp. 629–631, Mar. 1996.
- [17] M. M. Salah, R. A. Raines, M. A. Temple, and T. G. Bailey, "A general interleaver for equal and unequal error protections of turbo codes with short frames," in *International Conference on Information Technology: Coding and Computing*, 2000, pp. 412–415.

- [18] M. Aydinlik and M. Salehi, "Turbo codes with unequal error protection," *IEEE Transactions on Communications*, vol. 57, pp. 1215–1220, May 2009.
- [19] F. Babich, G. Montorsi, and F. Vatta, "Design of rate-compatible punctured serial concatenated convolutional codes," in *IEEE International Conference on Communications*, vol. 1, Jun. 2004, pp. 552–556.
- [20] —, "Partially systematic rate-compatible punctured SCCC," *IEEE Transactions on Communications*, vol. 8, pp. 241–243, Mar. 2004.
- [21] A. G. i Amat, G. Montorsi, and F. Vatta, "Design and performance analysis of a new class of rate compatible serially concatenated convolutional codes," *IEEE Transactions on Communications*, vol. 57, pp. 2280–2289, Aug. 2009.
- [22] A. G. i Amat, F. Brannstrom, and L. K. Rasmussen, "On the design of rate-compatible serially concatenated convolutional codes," *European Transactions on Communications*, vol. 18, pp. 519–527, Aug. 2007.
- [23] R. Morelos-Zaragoza and H. Imai, "Binary multilevel convolutional codes with unequal error protection capabilities," *IEEE Transactions on Communications*, vol. 46, pp. 850–853, Jul. 2009.
- [24] B. Frey and D. MacKay, "Irregular turbocodes," in *IEEE International Symposium on Information Theory*, 2000.
- [25] A. Huebner, J. Freudenberger, R. Jordan, and M. Bossert, "Irregular turbo codes and unequal error protection," in *IEEE International Symposium on Information Theory*, 2001.
- [26] D. Divsalar and F. Pollara, "Multiple turbo codes," in *IEEE Military Communications Conference*, vol. 1, p. 279.
- [27] C. Ravazzi and F. Fagnani, "Minimum distance properties of multiple-serially concatenated codes," in *6th International Symposium on Turbo Codes and Iterative Information Processing*, Sep. 2010, pp. 78–82.
- [28] J. Han and O. Takeshita, "On the decoding structure for multiple turbo codes," in *IEEE International Symposium on Information Theory*, 2001.
- [29] V. Z. S. Host, R. Johannesson, "Woven convolutional codes I: Encoder properties," *IEEE Transactions on Information Theory*, vol. 48, pp. 149–161, Jan. 2002.
- [30] R. Jordan, S. Host, M. Bossert, R. Johannesson, , and V. Zyablov, "Woven convolutional codes II: Decoding aspects," *IEEE Transactions on Information Theory*, vol. 50, pp. 2522–2529, Oct. 2004.
- [31] R. Jordan, S. Host, M. Bossert, and V. Zyablov, "Woven convolutional codes and unequal error protection," in *IEEE International Symposium on Information Theory*, 2001.
- [32] V. Pavlushkov, R. Johannesson, and V. Zyablov, "Unequal error protection for convolutional codes," *IEEE Transactions on Information Theory*, vol. 52, pp. 700–708, Feb. 2006.
- [33] V. Pavlushkov, R. Jordan, and V. Zyablov, "Some simulation results for woven convolutional codes with outer warp and two-levels unequal error protection," in *4th International ITG Conference Source and Channel Coding*, 2002.
- [34] C. Tanriover, B. Honary, J. Xu, and S. Lin, "Improving turbo code error performance by multifold coding," *IEEE Communications Letters*, vol. 6, pp. 193–195, May 2002.
- [35] C. Tanriover and B. Honary, "Image transmission using unequal error protection combined with two-fold turbo coding," in *Joint First Workshop on Mobile Future and Symposium on Trends in Communications, SympoTIC '03*, Oct. 2003.
- [36] C. Berrou, A. G. i Amat, Y. Ould-Cheikh-Mouhamedou, and Y. Saouter, "Improving the distance properties of turbo codes using a third component code: 3D turbo codes," *IEEE Transactions on Communications*, vol. 57, pp. 2505–2509, Sep. 2009.

- [37] C. Schlegel and L. Perez, "On error bounds and turbo codes," *IEEE Communications Letters*, vol. 3, pp. 205–207, Jul. 1999.
- [38] S. Benedetto and E. Biglieri, *Principles of Digital Transmission with Wireless Applications*. Kluwer Academic, Plenum Publishers, 1999.
- [39] A. Neubauer, J. Freudenberger, and V. Kuhn, *Coding Theory - Algorithms, Architectures and Applications*. John Wiley & Sons, 2007.
- [40] F. Daneshgaran, M. Mondin, and P. Mulassano, "Linear subcodes of turbo codes with improved distance spectra," *IEEE Transactions on Information Theory*, vol. 50, pp. 3291 – 3294, Dec. 2004.
- [41] A. Kadhim and A. Hamad, "Turbo codes with internal pilot insertion," in *IEEE NGMAST*, Sep. 2008.
- [42] T. Breddermann and P. Vary, "EXIT functions for parallel concatenated insertion convolutional codes," in *IEEE Global Telecommunications Conference*, Dec. 2011, pp. 1–5.
- [43] J. Cheng, A. Nimbalkar, Y. Blankenship, B. Classon, and T. K. Blankenship, "Analysis of circular buffer rate matching for LTE turbo code," in *IEEE Vehicular Technology Conference*, Sep. 2008, pp. 1–5.
- [44] C. Komninakis, "A fast and accurate Rayleigh fading simulator," in *IEEE Global Telecommunications Conference*, vol. 6, Dec. 2003, pp. 3306–3310.

Chapter 4

PMR Evolution: Design of Radio Efficient Voice over LTE

Abstract — This chapter proposes a design enhancement for voice transmission over packet bearer in next generation radio technologies. Broadband evolution is regarded as the first step for the convergence of all services over mobile radio, including voice and high rate video. One problem of these emerging technologies is their unique packet perspective which still has unsolved issues, especially regarding voice communications. We propose the evaluation of an optimally designed channel code for the improvement of packet bearer transmission of multimedia services over highly dispersive radio channels. This new perspective uses embedded unequal error protection (UEP) mechanisms for the progressive encoding of multimedia bits, according to their sensitivities to channel distortions. The code performances are highlighted for voice communications using a Long Term Evolution (LTE) transmission platform in a public safety context. The average error rates are correlated with the perceptual evaluation of speech quality (PESQ) for an objective evaluation of radio distortions, as well as both radio and audio decoding distortions. Results show the effectiveness of UEP concepts at the physical layer and the necessity of correlating PESQ results with channel error rates for an optimal system design.

4.1 Introduction

For public safety users, voice communications are essential in mobile networks. Therefore, effective mechanisms for voice transmission are an absolute necessity for future broadband Private/Professional Mobile Radio (PMR). However, Long Term Evolution (LTE) voice transmission remains a key issue, where many open questions remain. One issue regarding the network architecture and transmission protocols has been addressed by the Third Generation Partnership Project (3GPP). Two possibilities have been thus recommended: the voice over circuit switched technology in the first deployment stages, followed by full voice over internet protocol (IP) in later stages. But except the IP transmission, which has been receiving considerable attention over the years, voice over radio has also other interesting characteristics that may be exploited for a more efficient system.

Not strictly restricted to voice, but for all multimedia applications in a general manner, the most important element in evaluating a transmission system is the user perceived quality. The final reception quality represents the ultimate measure of the effectiveness of any network. This quality is usually obtained through a well calculated compromise between the radio efficiency (spectrum use) and the level of protection against channel errors (channel coding and modulation techniques). Naturally, the higher the perceived signal quality, the higher the used channel protection, and the more use of spectral resources. But all multimedia frames have an interesting characteristic: when used in the reconstruction of the signal, every bit has a different influence on the level of perceived user quality. A trivial example may be given for voice frames. Voice coders transmit parameters like pitch amplitude, the position of formants and a codebook index [1]. Channel errors on the bits describing the pitch would be intolerable, but errors on the last formant would not even be noticed by the listener. It is natural to observe that the same level of channel protection for the bits describing the pitch and those corresponding to the last formant is by no means necessary. On the contrary, it would only mean a useless loss of spectral

resources. Therefore, even from the beginning of voice over radio - the Global System for Mobile Communications (GSM), the unequal error protection (UEP) transmission techniques have been proposed. These concepts have also been adapted to PMR networks, as shown in chapter 2. Their purpose is to enhance the system spectral efficiency by providing only the necessary level of protection for every bit of multimedia applications.

In this chapter, our purpose is twofold. Firstly, we give an overview of the voice transmission mechanisms over LTE as to highlight the interconnections between higher network layers and lower radio layers. The comprehension of these mechanisms is essential in proving the necessity of cross-layer optimizations. Secondly, we will be evaluating the performances of the newly proposed UEP channel code, the parallel progressive hierarchical turbo code (PPHTC), for voice transmission over LTE. The voice codec employed is of typical PMR use and the radio performances are given for PMR European allocated bandwidths in hilly terrain (HT), as well as for an additive white Gaussian noise (AWGN) channel. The physical layer average error rates will be correlated to the perceptual evaluation of speech quality (PESQ) for an objective evaluation of radio distortions, as well as both radio and audio decoding distortions.

The chapter is structured as follows. Section 4.2 gives an overview of the existent voice over packet switched network architecture, and further describes the proposed UEP evolution, integrating the PPHTC concept. Also, we highlight here the issue of turbo encoding of short frames, which is of real interest as voice frames are short frames that must be effectively transmitted using turbo codes in next generation radio networks. The LTE evaluation platform together with the benchmark channel codes are detailed in section 4.3. The results and comments are presented in section 4.4. And finally, the conclusion is given in section 4.5.

4.2 Voice Services over Packet Switched Network

In this section, the bearer establishment mechanisms are presented in subsection 4.2.1. In subsection 4.2.2, we focus the analysis on the physical layer techniques, and more particularly on the UEP channel encoding. Turbo codes have long been a subject of study for both data and voice communications, as to standardize and simplify the radio technologies. We further describe the proposed UEP enhancements, integrating the optimal channel code designed for voice over packet bearer transmission: the PPHTC.

4.2.1 Packet Bearer Architecture

As we have already discussed, LTE represents the evolution of the radio network architecture, part of the evolved packet system (EPS), which also includes the evolved packet core (EPC) or the core network. The EPS is based on a flat architecture, which means an end-to-end IP communication, therefore a packet transmission over both core and radio systems.

Transmitting voice information is a very sensitive matter for packet networks, since voice communications are performed in real time. Thus, their architecture must be designed to comply with speech transmission specific requirements or the defined quality of service (QoS), related to system delay, packet loss, jitter, guaranteed bit rate (GBR), allocation retention priority (ARP). In LTE, these parameters are referenced using the QoS class identifiers (QCI), which are assigned to EPS bearers. The bearer may be seen as a logical "circuit" or "tunnel" which maps the data flows coming from higher transport layers (i.e. IP) to lower layers and radio transport channels, between the different network elements. It is a simple way of saying that for the specific service flow, all transmission "tunnels" have been assigned the corresponding parameters, from higher layers to lower layers. The service class indicators are thus translated for all network layers and elements. The radio bearer for example will be used by the radio layer to establish radio scheduling elements like: buffer delay and radio allocation priority, modulation and coding schemes (MCS).

In [2], the elements that contribute significantly to good reception of speech are highlighted for public networks: the packet loss of less than 0.25 %, the maximum tolerated jitter of 5 ms, and the packet delay of at most 150 ms. The authors recommend the acceptable service flows or bearers for voice over packet transmission. The GBR QCI 1 and 3 seem to be their choice for voice services over LTE, with the latter being more robust when paired with other network domains. Table 4.1 resumes these QCIs applicable to voice communications. As for the core network transmission, they suggest the use of differentiated service (DiffServ) or integrated

services (IntServ) for the mapping of QoS information with transport protocols, i.e. IP. The DiffServ Expedited Forwarding (EF) is particularly recommended for delay sensitive applications, e.g. voice. The network architecture together with the control mechanisms behind the bearer establishment are presented in [3]. Different services having the same level of QoS may be aggregated to only one bearer, i.e. many-to-one mapping. But there is a one-to-one mapping between the higher layer transport bearers (IP bearers) and the lower layer EPS bearers.

Table 4.1
QCI values for voice transmission.

QCI	packet type	priority	packet delay	FER
1	GBR	2	100ms	10^{-2}
2	GBR	4	150ms	10^{-3}
3	GBR	5	50ms	10^{-3}

The mapping of QoS defined parameters between higher layers (above IP) and lower layers (below IP) is a delicate problem for voice services over packet networks that will influence the final reception perceived quality. The 3GPP have thus defined the following mechanisms, which are resumed in Fig. 4.1:

- the IP-CAN session, identified by one IP address prefix (@IP), the UE identity (UE-ID) and the packet data network identification (PDN-ID), i.e. end-to-end control session,
- the IP-CAN bearer, explained as an IP transmission path of defined capacity, delay and bit-rate, these parameters being equivalent to the CQI in the EPS,
- the service data flows (SDF), associated with one and only QCI, and having a one-to-one mapping with user IP address and EPS bearers.

The mapping between the SDF and the IP-CAN bearer meant to transport it is performed through the binding procedure. One IP-CAN session can incorporate one or more IP-CAN bearers. And, for the same IP-CAN session, the SDFs may be aggregated if they share the same EPS QCI. To resume, this means that for every user, several IP addresses may be defined, one IP address per delivered service. To each IP service, one IP-CAN bearer is associated with its corresponding level of QCI. And all IP-CAN bearers are controlled during the IP-CAN session. We note that the radio layer interprets the IP indicated level of QoS into the radio parameters regrouped under a class indicator - QCI, which are materialized by the radio transmission using the proper modulation and coding - MCS¹. LTE does provide different levels of QCIs and MCSs, but with a one-to-one mapping, which is translated in the EPS and IP external networks by a one-to-one bearer mapping configuration as well. No QCIs have been envisaged that would refer to several MCSs at a time for a single service. This is, undoubtedly, the legacy of 3GPP packet systems, where the UEP concepts have not been properly optimized, but rather emulated.

Emulated UEP has thus been proposed for voice packet transmission, ever since first packet networks were proposed, i.e. enhanced data rates for GSM evolution (EDGE) radio access network (GERAN). In [4], authors evaluate the voice quality when using UEP concepts for radio transmission. They use voice over IP packet transmission over general packet radio service (GPRS)/ enhanced GPRS (EGPRS) and compare the performances for equal error protection (EEP) MCS with the UEP approach. They note that the performance can be easily improved using UEP, but designing an optimal channel code adapted to voice transmission over packet bearer would require consistent standard modifications. Therefore, they propose the use of emulated UEP for efficient voice transmission over packet bearer. The UEP is simulated by using two different MCSs for the two classes of bits, and a cyclic redundancy check (CRC) code is used for further error detection for the

¹Obviously, the mechanisms for MCS choice are more complex and depend on the radio channel as well. The channel quality indicators (CQI) are also considered in LTE for optimal transmission of the packets, but they represent a separate problem and will not be discussed here.

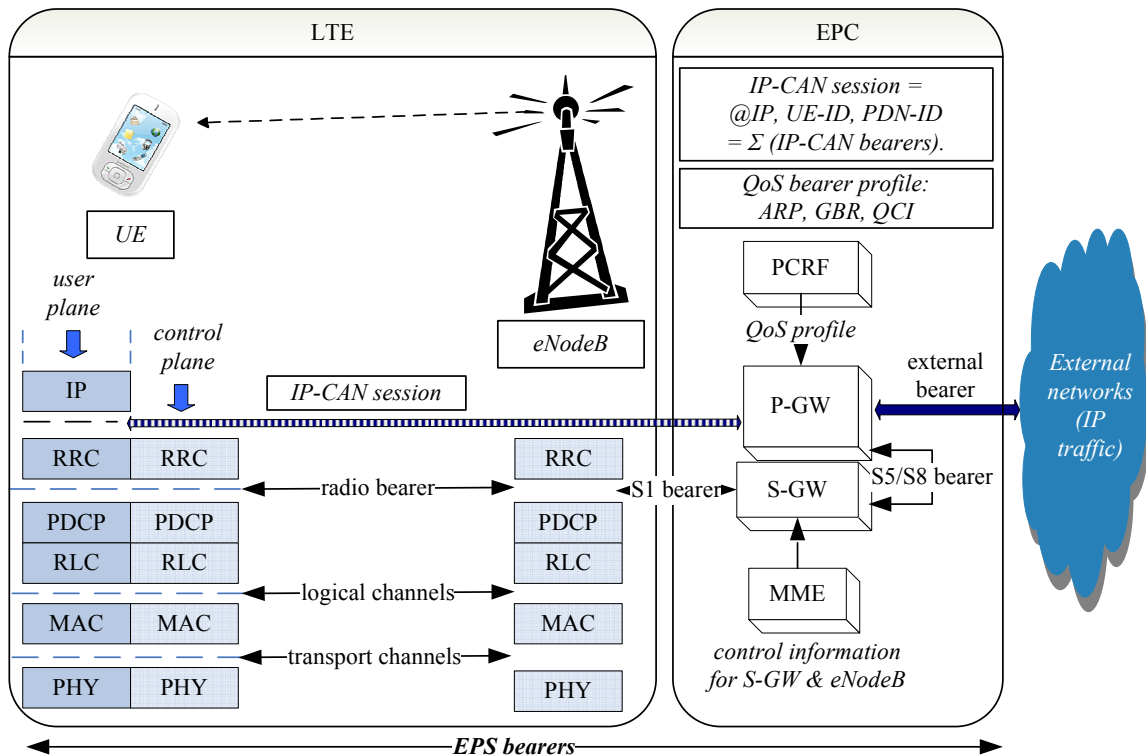


Figure 4.1. EPC bearer architecture.

first class bits. In later evolutions, as in universal mobile telecommunications system (UMTS), this emulated UEP was indicated by the higher layer bearer (core network) that was split in several logical channels, each one associated to one sub-bearer. The sub-bearer mechanisms had specific pre-defined parameters, including sizes for each of the UEP necessary data frames. Each sub-bearer was redirected to a different transport channel, and therefore was given a different MCS. But it seems these mechanisms have been lost in LTE, where a unique identification exists between the data radio bearer and the EPS bearer, and the notion of sub-bearer has disappeared. This would translate into the fact that, for any different required MCS, the specific service would have to be delivered on a different IP stream.

Contrary to video transmission, where each different scalable layer can indeed be transmitted using a separated IP stream, it is unimaginable to split voice packets in different IP streams as to create radio UEP. This is especially not recommended since the IP overhead is quite large compared to the short voice frame size. Voice communications over LTE can be optimized by using UEP MCS transmission. One solution with minimum standard modification would consist in designing a channel code adaptable to voice over packet transmission and based on the standard used turbo code. In this case, additional QCI parameters would be necessary for referencing the modified UEP code rates, but no considerable EPS or IP bearer modification would be necessary. Only a higher layer QoS enlarged palette of references would have to be envisaged.

4.2.2 Design of Embedded UEP MCS

In order to modify as little as possible the protocols associated to user elements (UE) and avoid significant backwards incompatibility, it is important to design system evolutions based on existent standard mechanisms. We thus propose an effective evolution of the 3GPP MCSs towards an embedded UEP perspective, by using an embedded UEP channel code. This new UEP channel code approach, the PPHTC, has been widely discussed in chapter 3. Our purpose is to optimize voice transmission over LTE by proposing an evolution of the existent turbo code towards an UEP embedded version of these parallel concatenated convolutional codes (PCCC).

Radio speech transmission using the UEP concepts has been proposed ever since the beginnings of GSM. UEP was seen as a necessary step due to the increased radio spectral congestion, as pointed out in [5]. The

authors highlighted the waste of resources if the bit stream were to be EEP encoded respecting the sensitivity of the more significant bits. And if the protection corresponded to the less significant bits, then the first class bits would be largely affected by errors. This is due to the fact that speech coders are designed to compress the audio information and exploit it at best for the human perception. The article reveals the mechanisms for measuring the bit error sensitivity of speech codecs and measures the performances of a punctured convolutional code for UEP radio transmission.

Later on, together with the development of packet data transmission, turbo codes were privileged for their low error rates. As a consequence, turbo encoding for voice communications started being addressed as a natural step towards the convergence of transmission techniques for all kinds of data.

In [6], the authors investigate the use of the PCCC for the transmission of speech frame in the GSM system. The speech frame measures 260 bits, separated in bits of class 1 (182 bits) and bits of class 2 (78 bits). Only the first class bits are PCCC encoded, while the last class bits are transmitted at a rate 1, without any channel protection. As the interesting bit error probabilities (BER) for voice are in the range 10^{-2} - 10^{-4} , it is noted that all interleavers yield the same performances for BER lower than 10^{-3} and the interleaver design becomes an issue below 10^{-5} . The UEP scheme using punctured turbo codes for the first class and no protection for the second class bits is compared to the GSM convolutional encoding in [7]. Significant gains are obtained for both classes of bits, but the authors conclude that with a more careful investigation of the bit's sensitivities and a more sophisticated design for the puncturing scheme, larger gains might be expected. In [8], turbo codes are also evaluated for voice over packet code division multiple access (CDMA) transmission. Using short frames of 192 bits for speech transmission, three turbo codes are evaluated for EEP encoding. The utility of the turbo encoding/decoding schemes is clearly demonstrated over the conventional non systematic convolutional code used in CDMA. The Advanced Multi-Rate (AMR) voice coder UEP transmission is proposed and analyzed in [9]. The serially concatenated turbo codes followed by carefully designed puncturing patterns are used for the efficient UEP channel coding scheme. Along with the perceptually most important bits, the header information is considered as crucial for the accurate detection of speech frames. Here as well, the UEP system outperforms the EEP benchmark.

Contrary to classical UEP schemes where puncturing techniques have been privileged, the PPHTC proposes a new encoding perspective, embedding the UEP concepts in the encoding structure of the turbo code itself. The UEP necessary rates are obtained by adjusting the input streams at the different encoding levels, and not by using puncturing. This common technique for modifying the transmission rates basically deletes bits at the channel code's output in order to modify the protection for certain bits. But this technique becomes quickly cumbersome when several levels of protection must be obtained for the same code. For example, if UEP was obtained for two classes using puncturing, the user should have perfect knowledge of the turbo code's internal interleaver, and of the constituent code's memory size as to identify the parity bits directly linked to the class two bits. Thus, only the second class bits would be punctured and their own protection only would be decreased. Another problem with puncturing techniques is that they become increasingly dangerous with short frames if not properly optimized. This complex problem is for example addressed in [10] for the AMR speech codec. Providing several levels of possible bit rates, AMR should benefit of the optimized UEP puncturing techniques for each one of these possibilities. Even though the proposed progressive symbol puncturing schemes seem promising, the corresponding puncturing table should be updated for every operating mode.

As discussed, the PPHTC encoding principles are very simple, yet very effective: the progressive encoding of the different classes of bits, by hierarchically introducing them in the encoding process. Thus, the level of protection of each class will be proportional to its own level of importance for the reconstructed signal. The progressive iterative decoding provides very good results, and exploits the hidden redundancy of the better protected classes in improving the decoding of the less protected classes.

Integrating the concepts of the PPHTC within LTE, we propose a new embedded UEP MCS, which can be translated to higher layers as an UEP embedded radio bearer. The radio packet bearer must be associated to the others EPS bearers with the appropriate UEP QCI. The UEP information needs to be forwarded between the user speech codec and the EPS network elements. The necessary correspondence between the IP DiffServ indicated QoS and the EPS UEP QCI must be correctly envisaged. These parameters will be mapped to the corresponding QCI and indicated to the radio bearer, along with the class sizes. The new proposed UEP embedded MCS design does not necessarily need the frame error rates (FER) for the lower level classes, since they

are naturally embedded in the code's structure and can be easily derived. The performances for the lower level classes are highly correlated to the first class and may be predicted. Puncturing may also be applied level by level for modifying the mother code rate. But UEP puncturing is no longer necessary since the UEP is already embedded in the code structure. A simple uniform puncturing at each level is enough for modifying the channel protection for each one of the classes. Fig. 4.2 presents this proposed UEP design for voice over packet bearer transmission.

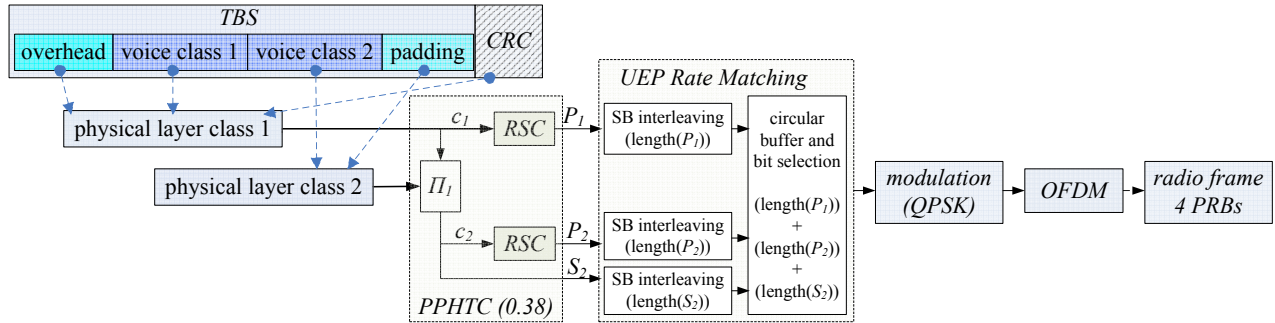


Figure 4.2. UEP embedded MCS.

The higher layer transmission regarding transport protocols and bearer establishment is LTE compliant. But at the layer one, we define a new embedded UEP MCS, where the channel code can provide n different levels of protection, and the modulation scheme is unique for the overall encoded frame. In this chapter, we suppose the existence of two levels of importance for the speech bits. The channel code thus provides two different innate code rates for the two classes, yet these classes are encoded together. This becomes a considerable advantage in the decoding process which better exploits the channel diversity. The PPHTC constituent elements are obviously those of the LTE turbo code, i.e. the constituent recursive systematic convolutional codes (RSC), the contention free internal interleaver based on quadratic permutation polynomial (QPP), and the rate matching (RM) schemes [11]. With the new encoding design, the RM subblock interleaving is slightly modified, as highlighted in Fig. 4.2. Due to the UEP code structure, the parity one (P_1) stream is shorter than the parity and systematic bits two (P_2 and S_2). Thus, each sub-block interleaver is initialized with the parity/systematic bits provided length, but the interleaving is still performed based on the 3GPP algorithm, using the 32 columns and the mapping patterns. The three interleaved streams are fed to the RM circular buffer, whose size is computed as the sum of the subblock output length streams. The bit selection formula is standard compliant. The resulting bit stream is afterwards mapped to quadrature phase shift keying (QPSK) modulation, and orthogonally frequency division duplex mapped (OFDM) before radio frame mapping and channel transmission.

4.3 LTE Evaluation Platform

We present the evaluation of this newly designed UEP embedded MCS over the LTE Release 9 simulation platform. Although in a simplified form, the platform gives an accurate estimation of the expected physical layer performances. Fig. 4.3 presents the emulated UEP architecture and Fig. 4.4 presents the design for the LTE EEP MCS.

The higher layers including the voice codec and transport protocols transmits a voice frame every T milliseconds. We have employed the advanced multi-band excitation (AMBE)² voice codec, the very low rate source codec used in chapter 2 as well for the LTE preliminary studies. Its UEP characteristics have been well defined by the constructors. Four classes of bits have thus been defined, u_0 , u_1 , u_2 and u_3 . The bit vector u_0 is defined as highly sensitive to bit errors and must be well protected, and a method of error detection of the uncorrectable bits should also be employed. u_1 must also be well protected. And while u_2 is considered moderately sensitive to errors, u_3 seems not very sensitive to errors.

²Registered Trademark from Digital Voice Systems Inc - DVSI.

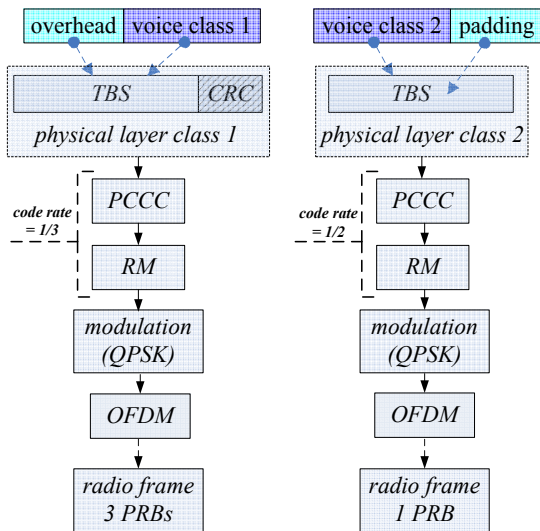


Figure 4.3. Emulated UEP simulated MCS.

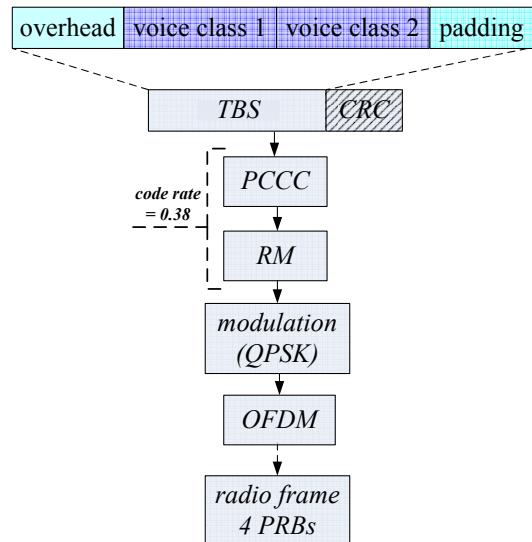


Figure 4.4. EEP simulated MCS.

Considering these constructor remarks, we have regrouped u_0 and u_1 in the so called *voice class 1* packet of bits, while u_2 and u_3 are regrouped in the *voice class 2* packet of bits, which will benefit of considerably less protection than class 1.

The higher layer constructed voice frame can contain a number of G aggregated voice packets. Thus, the classes of bits of the aggregated voice packets will be grouped together before transport protocol’s encapsulation. The transport protocol headers are added and the robust header compression is performed by the packet data convergence protocol (PDCP). The medium access layer (MAC) packet data unit (PDU) thus obtained is afterwards mapped on the transport channels and a transport block size (TBS) is chosen for physical layer processing. The realistic compressed overhead numbers as well as the TBS detailed computation “*Algorithm for Voice*” have been used as explained in chapter 2.

For the UEP transmission scenarios, the TBS will be split into different sensitivity classes of bits. The different strategies used for channel encoding will define the different types of MCS used for radio transmission. Thus, we evaluate the performances of the embedded UEP MCS in comparison with the emulated UEP MCS and the EEP MCS. The EEP benchmark represents the current 3GPP transmission mechanisms for any kind of packet data over the radio layer. The emulated UEP MCS is a straightforward adaptation of the UMTS mechanisms to today’s LTE, and what might be the most immediate adaptation to the UEP concepts. The chosen benchmarks naturally use those same elements of the 3GPP standard of the traditional parallel turbo code. The codes are configured as to obtain the same overall coding rate for every simulated MCS. Thus, for the same input TBS, after modulation and other physical layer mapping techniques, the LTE radio frame will be occupied at an equivalent level of P physical resource blocks (PRBs) for all three MCSs. Our purpose is to evaluate all MCSs and their physical layer performances at equivalent input (in number of bits - TBS) and equivalent output (number of channel bits - occupied PRBs).

These radio layer performances will be further translated for higher layer interpretation, i.e. voice quality analysis. The received frames are decoded using the iterative turbo decoding at the layer one, and the frame reliability is measured by a virtual CRC. This virtual CRC is simulated using the measurement of FER, i.e. if the FER of the *physical layer class 1* is non zero, than the entire received frame will be rejected. For replacing the rejected erroneous frame, the voice decoder AMBE will use the concealment mechanisms. This means that, for every rejected frame, the decoder will replace that frame with either the copy of the previous frame (for a fixed number of repetitions, R_{copy}^{max}), or with a muted frame if the number of maximum repetitions has been reached. These mechanisms are employed for a more comfortable audio signal reconstruction. The reconstructed audio signal quality is measured with a PESQ analyzer, a tool used for estimating the user perceived voice quality, i.e. the PESQ.

The PESQ notation system is an international telecommunication union (ITU) proposed method for evaluating the speech quality. The obtained mean opinion score (MOS) represents an objective metric for measuring the reliability of a network based on a large number of reference speech sequences. These speech sequences are based on a large number of speakers, as well as a large number of phonemes, i.e. different words and phrases in different languages.

4.4 Results and Comments

The results are given here for an objective evaluation of the proposed embedded UEP MCS. We present the average error rates that are useful for the reconstruction of the voice signal, as well as PESQ associated results. LTE performances are evaluated for both AWGN and HT (with a user mobility of 200 kmph - HT200) channel environments for downlink (DL). One antenna is supposed for the DL receiver in AWGN and two antennas are supposed for the DL receiver in HT200 for enhanced channel diversity.

The LTE physical layer configuration is performed in a simplified manner. The OFDM symbols are mapped on the radio frame, which remains nevertheless LTE representative. The radio frame is thus 10 ms long spanning 1.4 MHz of bandwidth, which in LTE terms is equivalent to 6 physical resource blocks (PRBs)³. The time transmission interval (TTI) corresponds to one sub-frame and is equal to 1 ms. For each TTI, we suppose that the first 4 OFDM symbols are allocated to the physical downlink control channel (PDCCH). The next available 8 OFDM symbols per TTI are entirely allocated to the user in blocks of PRBs. The channel estimation is supposed ideal, therefore the pilots are non necessary. The LTE radio structure has been detailed in chapter 2.

Table 4.2 presents the voice and MCS related parameters that have been used for computer simulations.

The average error rate performances are presented for the AWGN channel in Fig. 4.5 and Fig. 4.6, while the corresponding PESQ measurements are given in Fig. 4.9. The equivalent performances in HT200 transmission environment are presented in Fig. 4.7 and Fig. 4.8, and the dynamic channel estimated PESQ in Fig. 4.10.

The average speech quality is evaluated for 60 voice files, transmitted using a time division multiple access (TDMA) of 60, i.e. this represents a simulation of 60 independent voice communications over LTE. For each TTI, one voice file is transmitted, and its following packet will be emitted 60 ms later. For an objective interpretation of PESQ results, the transmitted files consist of female and male voices, with different spoken words and phrases in four different languages: English, French, German and Spanish. The simulation have been performed over a total of 600000 sub-frames, i.e. 10000 ms of radio transmission for each voice file. Therefore, the PESQ is averaged over 600 seconds of audio signal communication.

The audio signal reconstruction is made using the concealment mechanisms based on the FER. The computed FER over the *physical layer class 1* bits is a direct measurement of the number of correct detected frames. This FER represents a virtual CRC over these class 1 bits only. Once the frame has been detected as correct regarding its most sensitive bits, the voice bits are fed to the AMBE decoder. Here, the residual bit error rate (RBER) measures the number of erroneous bits of *class 2* that are globally fed to the voice decoder⁴. This latter error rate will mainly quantize the importance of the erroneous class 2 bits in the voice decoding algorithm.

In all figures, the embedded UEP MCS results are presented in red, the EEP MCS is given in green, and the emulated UEP MCS is shown in blue. For every MCS, two curves are shown each time, representing the two different physical layer classes - *PLC1* and *PLC2*. The PESQ figures present two flows of curves: the upper ones (triangle) give the PESQ for the *radio* measured distortions only, i.e. the received voice files are compared with the already AMBE encoded files. The lower flows (star) estimate the PESQ for the received voice files compared to the real original files, i.e. before AMBE encoding. This latter evaluation actually quantifies the impact of both radio and AMBE source codec distortions on the final *user* perceived audio signal. The symbol energy to noise (E_s/N_0) ratio represents the values of the channel used signal to noise ratio.

Concerning PLC1 performances in AWGN, Fig. 4.5 shows that the emulated UEP performances are the best since, here, the PLC1 bits are encoded alone using a PCCC 1/3. The embedded UEP PLC1 is slightly

³One PRB is defined as 12 OFDM symbols in the time domain spanning 12 frequency sub-carriers, spaced by 15 kHz. For simplicity, a measure of one PRB in the frequency domain refers to a pair of PRBs spanning an entire sub-frame of 1 ms.

⁴The RBER is measured at the physical layer over the entire *physical layer class 2* bits, including the TBS padding bits, but we consider these bits as negligible.

Table 4.2
LTE simulation platform parameters.

Network common parameters	Voice coder and bit rate	AMBE 2.45 kbps (49 bits for $T=20$ ms)
	UEP bit vectors	$u_0 = 12$ bits, $u_1 = 12$ bits, $u_2 = 11$ bits and $u_3 = 14$ bits
	Concealment mechanisms and aggregation	$R_{copy}^{max} = 3$ and $G = 3$
	Voice class 1 length	$3 \times 24 = 72$ bits
	Voice class 2 length	$3 \times 25 = 75$ bits
	Transport protocol overhead	6 bytes
	CRC	24 bits
	Modulation	QPSK
Embedded UEP MCS	TBS	208 bits
	Physical layer class 1 (PLC1)	144 bits (overhead + voice class 1 + CRC included)
	Physical layer class 2 (PLC2)	88 bits (voice class 2 + padding)
	LTE code block input to channel code	232 bits input to PPHTC rate 0.38
	Radio frame occupied PRBs	$P = 4$
EEP MCS	TBS	208 bits
	Physical layer class 1 (PLC1)	144 bits (overhead + voice class 1 + CRC included)
	Physical layer class 2 (PLC2)	88 bits (voice class 2 + padding)
	LTE code block input to channel code	232 bits input to punctured PCCC rate 0.38
	Radio frame occupied PRBs	$P = 4$
Emulated UEP MCS	TBS for physical layer class 1 (PLC1)	144 bits
	TBS for physical layer class 2 (PLC2)	88 bits
	Physical layer class 1 (PLC1)	144 bits
	Physical layer class 2 (PLC2)	88 bits (voice class 2 + padding)
	LTE code block PLC1 input channel code	168 bits input to PCCC rate 0.33
	LTE code block PLC2 input to channel code	88 bits punctured PCCC rate 0.52
	Radio frame occupied PRBs for PLC1	$P = 1$
Radio frame occupied PRBs for PLC2	$P = 3$	

underneath the latter, and remains better than the EEP MCS down to 1%. As for PLC2 results, we clearly see in Fig. 4.5 that the best class 2 results are those of the green EEP MCS, followed by the red embedded UEP, and the worst FER is registered for the emulated UEP as down as 1%. But the real class 2 influence over the PESQ may be estimated by looking at results given in Fig. 4.6. Considering that the green curve of the EEP MCS is the lowest, followed by the red of the PPHTC and, finally, the blue of the PCCC 1/2, we might conclude that, undoubtedly, the PESQ results will be best for the green EEP MCS. However, as shown in Fig. 4.9, the green EEP becomes better than the other two MCSs at only $E_s/N_0 = 2$ dB, when the channel has considerably improved. And up to $E_s/N_0 = 1.8$ dB, the newly proposed embedded UEP MCS gives the best results. The behavior is verified for both PESQ estimations, i.e. compared to the AMBE encoded (*radio* distortions only) and the original files (*user* perceived).

The performances are considerably different for the HT200 transmission channel. Since we are testing the LTE performances in a PMR use case, the carrier frequency F_c is equal to 450 MHz. Due to this VHF/UHF⁵ carrier and also the very low size input frame, the turbo code can not exploit very well the channel diversity. Therefore, the curves presented in Fig. 4.7 are particularly parallel to each other and the turbo code convergence waterfall is not visible, even though 2 antennas are used for reception with a maximum ratio combining (MRC) gain. A visual analysis proves that this dynamic channel behavior is the "transposition" of the very low E_s/N_0 area or the upper part of the curves from the AWGN channel from Fig. 4.5. Thus, in HT200, the proposed

⁵Very high frequency/ultra high frequency depending on the used frequency interval.

embedded UEP MCS performances are found in between the emulated UEP and the EEP for the class 1 bits. And its class 2 bits are second better after the EEP MCS. This "parallel" behavior is visible for the RBER as well in Fig. 4.8, where class 2 bits performances from the FER case are well proved here. The embedded UEP is second best after the EEP and better than the emulated UEP. These FER and RBER performances translate into a very interesting PESQ estimation. Fig. 4.10 shows that the proposed embedded UEP MCS performs better than any other MCS, with a gain of $E_s/N_0 = 0.4$ dB for the *radio* distortions for a PESQ of 4. The emulated UEP, which has been known as performing better than the EEP, is verified up to $E_s/N_0 = 4.5$ dB, where the speech can be already qualified as perfect for the human ear. The curves follow the same pattern when considering the *user* perceived quality, even though the distance between the MCSs is compressed due to the AMBE voice decoding. However, the proposed MCS remains better in the area of audio interest, i.e. above a score of 2.

What is most interesting from these curves is to detect the point of quality inflexion, i.e. the point where the

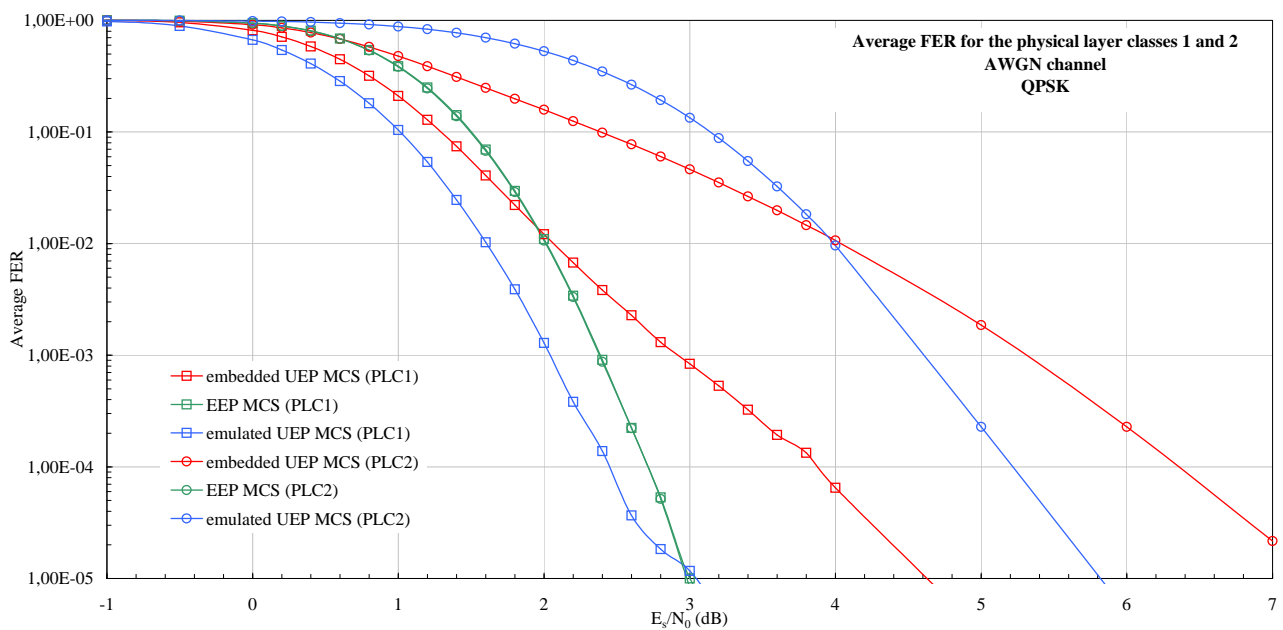


Figure 4.5. Average frame error rate (FER) for the AWGN transmission (for both physical layer classes - PLC).

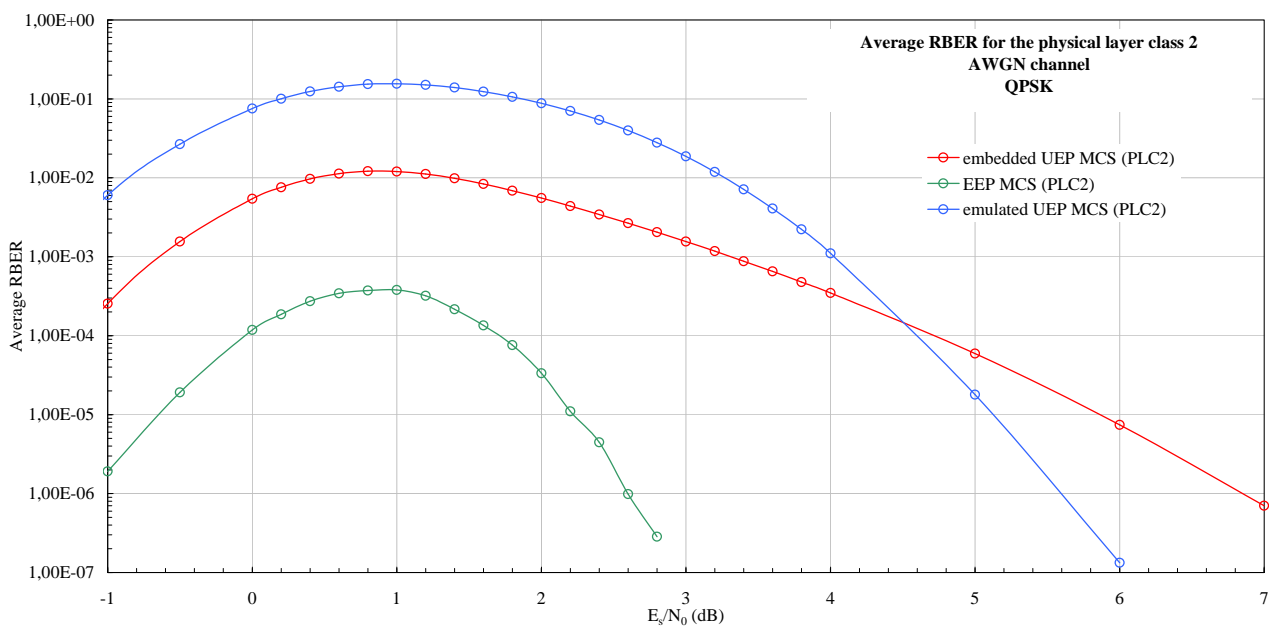


Figure 4.6. Average residual bit error rate (RBER) for the AWGN channel transmission (for the physical layer class 2 only - PLC2).

class 1 bits have fully contributed to the speech quality and where the bits of class 2 start making a difference. This will give us the necessary numbers for the expected FER for class 1 bits and the corresponding RBER for class 2 bits for an optimal audio quality. The presented figures show an interesting point in AWGN at $E_s/N_0 = 2$ dB, where the FER is equal to 1%. Here, we have an equivalent FER rate for class 1 bits for both EEP (green) and the embedded UEP (red). By looking at the RBER, it is clear that the green EEP is much better than the red embedded UEP. Therefore, by evaluating the PESQ at this particular point, we conclude that starting with this point, only class 2 bits will help with the audio quality. This point is visible in both AWGN and HT200 PESQ figures for $E_s/N_0 = 2$ dB. And we can see that the main importance in the reconstruction of the speech signal has been played by class 1 bits, and the influence of class 2 bits remains considerably smaller.

The proposed embedded UEP MCS imposes itself as a very interesting approach, since it performs a natural compromise between the protection needed for the two classes of bits. Both AWGN and HT200 performances show a noticeable gain in the area of interest for a good speech quality (scores between 2 and 4, knowing that,

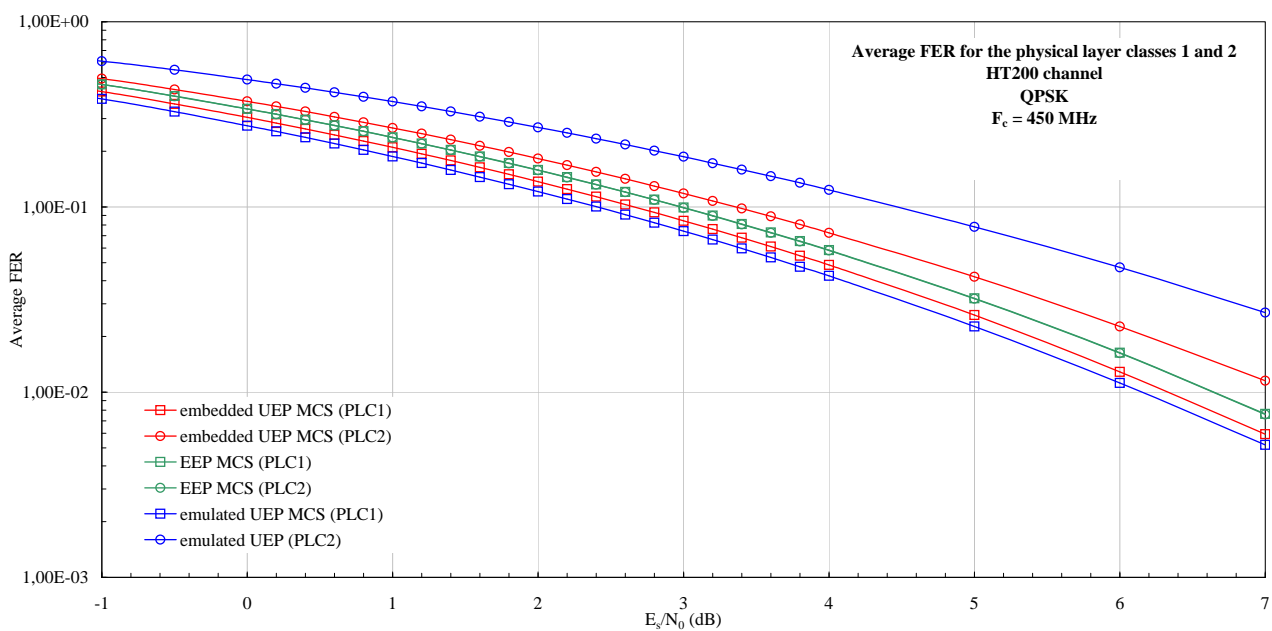


Figure 4.7. Average frame error rate (FER) for the HT200 transmission (for both physical layer classes - PLC).

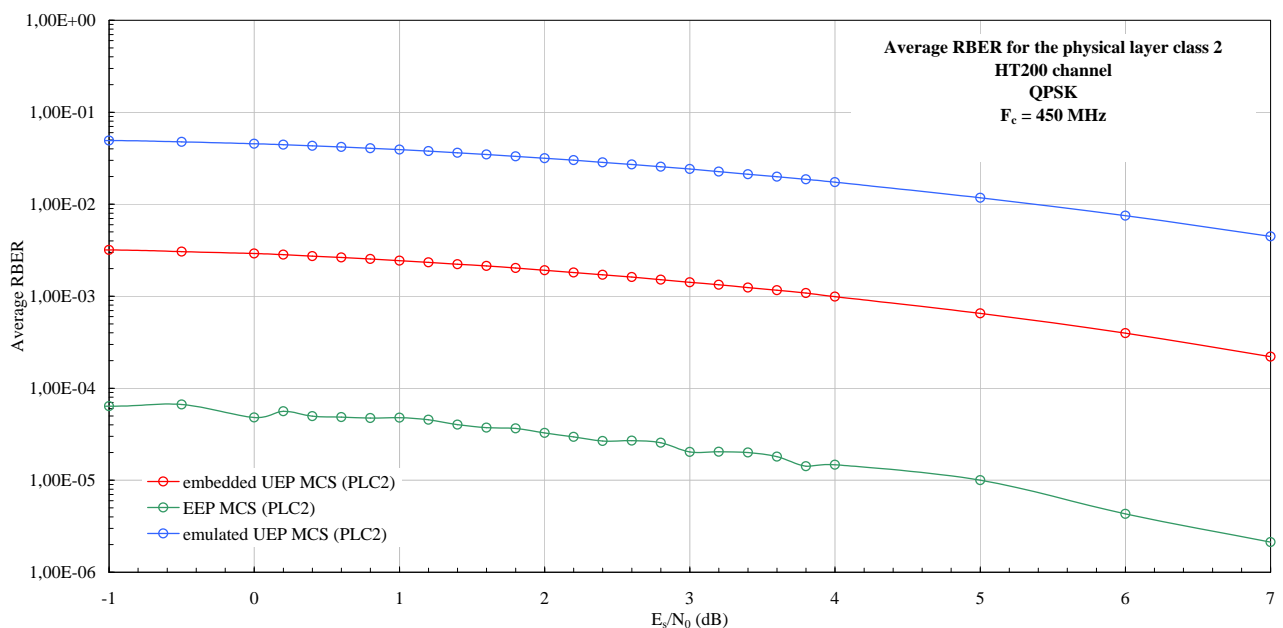


Figure 4.8. Average residual bit error rate (RBER) for the HT200 channel transmission (for the physical layer class 2 only - PLC2).

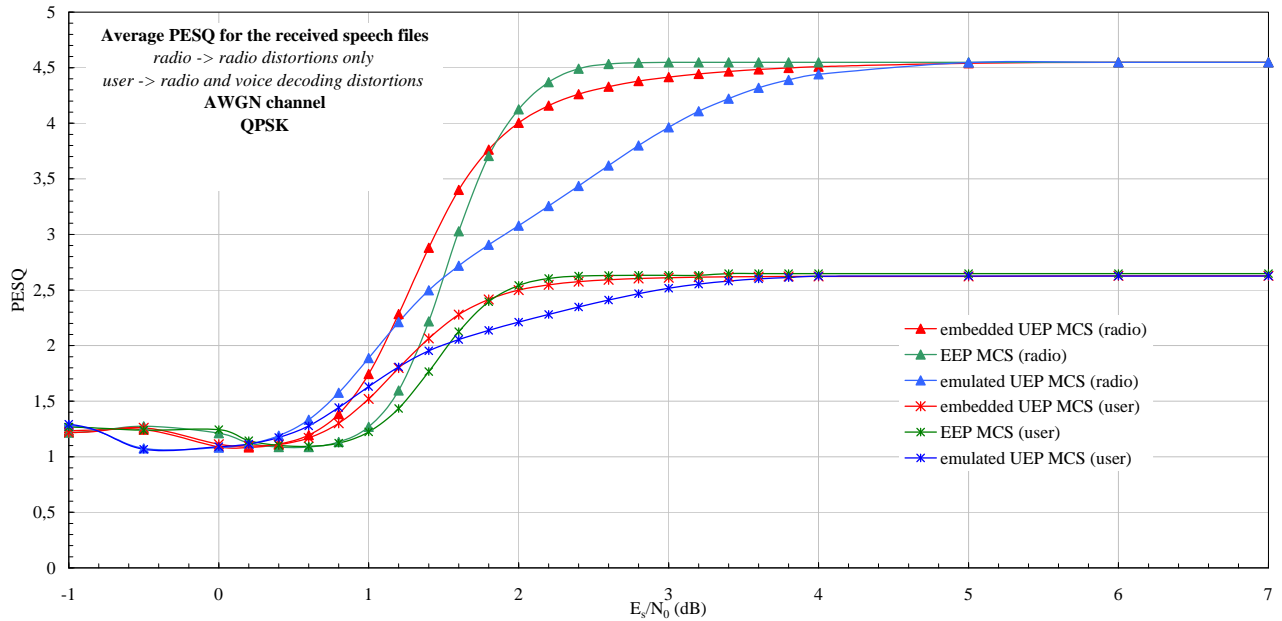


Figure 4.9. Average PESQ for the AWGN transmission, estimated considering radio distortions only, and both radio and speech reconstruction distortions.

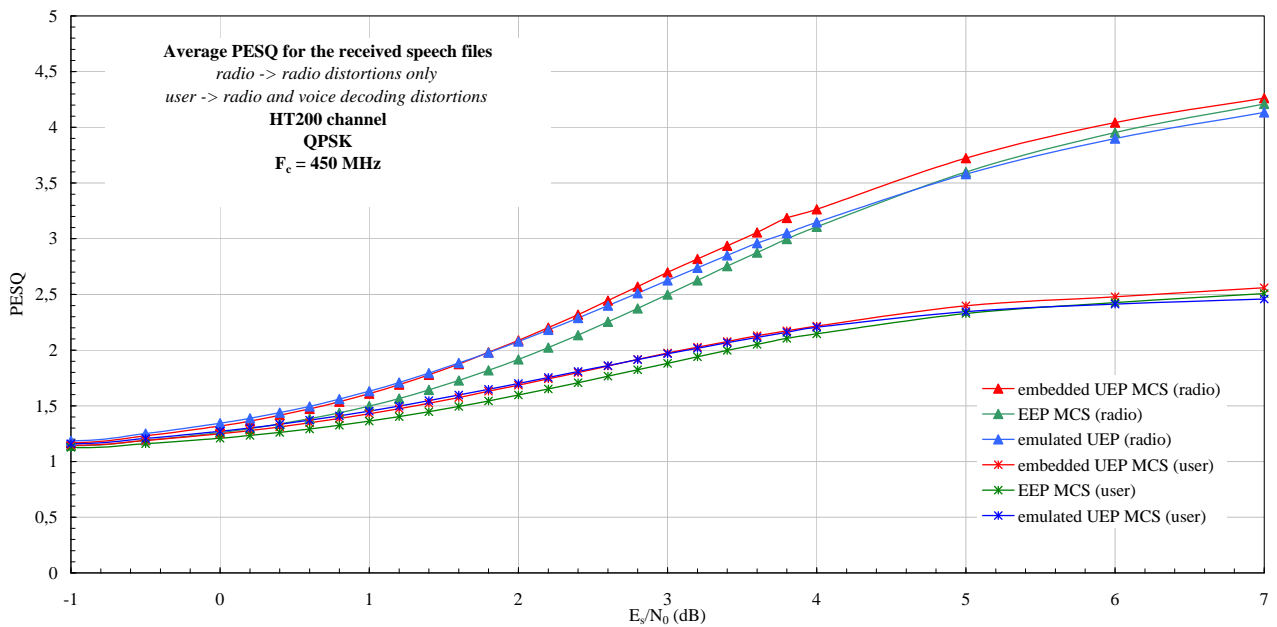


Figure 4.10. Average PESQ for the HT200 transmission, estimated considering radio distortions only, and both radio and speech reconstruction distortions.

beyond, audio gains are hardly hearable). The proposed embedded UEP MCS, integrating the PPHTC concept, remains the best approach in dynamic environment. However, the turbo code can not exploit the reduced channel diversity and the obtained gained is at most of 0.4 dB. This is also due to the small length encoded code words, for which it is well known that the turbo code's performances are limited. Contrary to results presented in chapter 3, we have chosen here a 232 bits input frame. Nevertheless, the PPHTC's behavior for small frames is better than that of the classical turbo code, due to its hybrid structure which encodes part of the frame only convolutionally. Also, an important factor that influences the PPHTC's performances is the ratio of the two classes of encoded data, which are not configured for optimum performances, and the size of the first class bits on which the frame rejection decision is taken. The FER ratio is computed considering all class 1 bits, i.e. 144 bits. In real systems, only a fraction of the class 1 bits are used for frame rejection. Therefore, we can expect the PPHTC FER to improve compared to the EEP FER. This hypothesis is proved by results given in chapter

3. Results from chapter 3 show that we can expect up to 1 dB of gain for the PPHTC 0.43, compared to its EEP counterpart, in fading environment. Expressed in bit error rates (BER), the latter prove the absolute gain of the PPHTC configuration compared to the other benchmarks. We can thus expect 1 dB gain for the 30%-70% configuration for a large enough input frame. If 3 AMBE users were multiplexed before channel encoding⁶, and the encoded classes ratios were set to 30%-70%, such gains could be expected for voice transmission in PMR networks as well. The input frame size would be extended, as to increase the turbo code's memory, and the ratios of the classes would allow a very favorable UEP scheme compared to the EEP case. Furthermore, this configuration would better exploit the LTE resources and would allow a total of 180 simultaneous calls (Erlangs) in a 1.4 MHz bandwidth, which would prove particularly interesting.

Nonetheless, for the LTE system using AMBE 2.45 evaluated here, even though not fully optimized, we can quantify the advantage of the embedded UEP MCS compared with the EEP MCS. The gain of 0.4 dB can be reported on the carrier to interference ratio (C/I), necessary for the computation of the reuse factor, i.e. cluster size. For a given PESQ of 4 measuring the voice quality, we note in Fig. 4.10 that an $E_s/N_0 = 6.2$ dB is obtained for the EEP MCS, and an $E_s/N_0 = 5.8$ dB is measured for the embedded UEP MCS⁷. These values can be roughly estimated as equivalent to the value of C/I in fading environment. We have shown in chapter 2 that the reuse factor can be computed including both fading and shadowing degradations. Referring to equations (2.5), (2.6) and (2.8), we can estimate the LTE maximum calls' capacity, reuse factor and corresponding spectral efficiency. Thus, for both MCS schemes, the maximum LTE call capacity is of 60 Erlangs in the deployed bandwidth of 1.4 MHz. The EEP MCS estimated reuse factor is of 5.26, which results in a spectral efficiency equal to 8.15 Erlangs/MHz/cell. The embedded UEP MCS, with a reuse factor of 4.99, engenders an LTE spectral efficiency of 8.6 Erlangs/MHz/cell. The newly proposed transmission scheme is 5% better than the existent EEP scheme for the LTE system using the AMBE vocoder. However, for 1 dB of channel coding gain only, we can expect up to 12% better results with the newly proposed embedded UEP MCS configuration compared to the EEP MCS.

4.5 Conclusion

We have proposed in this chapter a new approach for transmitting voice over packet bearer networks. This new perspective introduces an embedded UEP MCS, and integrates the recently proposed PPHTC in the LTE physical layer. For a maximum backwards compatibility, the PPHTC is introduced for UEP speech packets transmission as an evolution of the LTE standard turbo code. Through the embedded UEP structure of the code, the UEP encoding of voice packets is optimized for a more efficient radio transmission. Thus, the code protection is distributed between the different classes of bits, as a function of their sensitivity to channel errors. The proposed embedded UEP MCS is designed considering layer one characteristics and implies minor higher layer modifications. For such a transmission scheme, no significant IP and radio bearers evolution would be necessary, except a larger choice in QoS values mapping. The given results highlight the necessity of the use of UEP for an enhanced optimization of the radio layer. The estimated PESQ clearly underlines the importance of improving the protection of very sensitive bits for a better user perceived quality. The proposed UEP method shows very good performances, remaining the best choice for voice over packet bearer transmission especially in dynamic environment. However, to obtain higher gains and better exploit the new scheme's potential, new optimizations and LTE modifications will have to be envisaged. One such perspective would be multiplexing several users before channel encoding without protocol overhead. But such a configuration would engender consistent LTE evolutions, where the protocol stack would be altered. Also, for future PMR use, further optimizations and investigations regarding system parameters related to the vocoder's characteristics are needed, e.g. UEP classes' configurations, frame detection and rejection criteria. Even though many LTE aspects remain to be analyzed for its full evolution towards the PMR, the embedded UEP transmission scheme presented here provides interesting new perspectives for increased gains and public safety requirements.

⁶No protocol overhead assumed, and 3 voice frames aggregated per user, with u_0 bits in first class, and u_1, u_2, u_3 in class 2.

⁷Here, we do not suppose a SISO antenna configuration, but a SIMO antenna configuration, therefore the final results benefit from the MRC gain.

Bibliography

- [1] E. Shearer, "TETRA - a platform for multimedia," in *IEEE Colloquium on Mobile Computing and its Applications*, Nov. 1995.
- [2] N. Nageshar and R. Olst, "Regulation of bearer/service flow selection between network domains for voice over packet switched wireless networks," in *Proceedings of ITU Kaleidoscope 2011: The Fully Networked Human? - Innovations for Future Networks and Services (K-2011)*, Dec. 2011, pp. 1–6.
- [3] J. Shin, K. Jung, and A. Park, "Design of session and bearer control signaling in 3GPP LTE system," in *IEEE Vehicular Technology Conference*, Sep. 2008, pp. 1–5.
- [4] N. Paul, J. Brouet, C. Thirouard, J. Antoine, A. Wautier, and L. Husson, "Efficient evaluation of voice quality in GERAN (GSM EDGE radio access network)," in *IEEE Vehicular Technology Conference*, vol. 3, Sep. 2001, pp. 1402–1406.
- [5] R. Cox, J. Hagenauer, N. Seshadri, and C. Sundberg, "Subband speech coding and matched convolutional channel coding for mobile radio channels," *IEEE Transactions on Signal Processing*, vol. 39, pp. 1717–1731, Aug. 1991.
- [6] S. Benedetto, R. Garello, and G. Montorsi, "Parallel concatenated coding schemes for wireless applications," in *IEEE International Conference on Universal Personal Communications*, vol. 2, Oct. 1998, pp. 807–811.
- [7] F. Burkert, G. Caire, J. Hagenauer, T. Hindelang, and G. Lechner, "Turbo decoding with unequal error protection applied to GSM speech coding," in *IEEE Global Telecommunications Conference*, vol. 3, Nov. 1996, pp. 2044–2048.
- [8] P. Jung and M. Nasshan, "Results on turbo-codes for speech transmission in a joint detection CDMA mobile radio system with coherent receiver antenna diversity," *IEEE Transactions on Vehicular Technology*, vol. 46, pp. 862–870, Nov. 1997.
- [9] J. Wang, N. Othman, J. Kliewer, L. Yang, and L. Hanzo, "Turbo-detected unequal error protection irregular convolutional codes designed for the wideband advanced multirate speech codec," in *IEEE Vehicular Technology Conference*, vol. 2, 2005, pp. 927–931.
- [10] A. Bernard, X. Liu, R. Wesel, and A. Alwan, "Speech transmission using rate-compatible trellis codes and embedded source coding," *IEEE Transactions on Communications*, vol. 50, pp. 309–320, Feb. 2002.
- [11] J.-F. Cheng, A. Nimbalkar, Y. Blankenship, B. Classon, and T. Blankenship, "Analysis of circular buffer rate matching for LTE turbo code," in *IEEE Vehicular Technology Conference*, Sep. 2008, pp. 1–5.

Chapter 5

Conclusions and Perspectives

In this dissertation, we have discussed on the possibility of LTE becoming the next professional mobile radio technology. Being at crossroads in their evolution, the world of PMR has envisaged the migration to broadband opportunities. But considering the key requirements of mission critical communications, LTE has to most likely follow an evolutionary path before being adopted as the next step PMR. This broadband candidate has been conceived for high throughputs, with low latencies over an all IP architecture.

The technological gaps between current PMR systems and LTE are considerable and the design philosophies are completely different. Our first approach was to analyse their respective architectures and identify the elements that might help minimizing the gap between these two perspectives. Therefore, we have evaluated the behavior of LTE considering PMR specific applications, i.e. low rate voice and video transmissions. The results were surprising, highlighting LTE lacks, starting with higher layer transport protocols, and down to lower layer proposals for channel protections and radio allocations. Higher layer transport protocols, e.g. IP, are not dimensioned for the radio transmission of low rate data. Our study has proved the inefficiency of such an approach if it were to be used as such for PMR networks. Further, the LTE physical layer is not conceived for such low rates. Even though the proposed transmission rates and radio allocations are considerable, the options are very limited for efficient low rate communications. New features must be considered for enhancing the LTE spectral efficiency for these low throughput communications if the standard is to be envisaged for PMR evolution.

Among the abundance of possible LTE enhancements for PMR, we have focused our attention on unequal error protection channel coding techniques. The concept has been long used and with good results for all networks dealing with voice communications. Therefore, if a possible upgrade of LTE were possible, which would help improving the transmission of voice packets over the radio link, this would mean a victory in itself. Voice communications are considered to be very representative for both low rate communications and delay stringent applications. And the unequal error protection channel coding techniques can be used with any type of sensitive data, including video.

Considering LTE legacy in terms of channel coding, we have therefore searched to integrate unequal error protection concepts into the existing turbo codes. This search resulted in patented technological innovations, the parallel progressive hierarchical turbo codes and the serial progressive hierarchical turbo codes. The idea behind these concepts is very simple and is based on the fact that the input data can be hierarchised considering its levels of sensitivity to channel errors. Every one of the hierarchised packets thus obtained is progressively inserted in the encoding process at its corresponding step. This new approach provides to the transmitted frame an embedded unequal error protection, proportionally to each of its sensitivity levels. The decoding process performs surprisingly good, showing a good compromise between the performances of sensitivity packets. We have therefore performed both a theoretical and computer simulation detailed analysis for a better understanding of these technological innovations. Good results were obtained, which encourage the use of these new channel codes in radio systems.

The next step in our study was to obviously test the behavior of the parallel progressive hierarchical turbo codes over LTE for voice communications. The patented code performances were compared to LTE specific transmission techniques, considering realistic parameters. The physical layer error rates results were correlated with higher layer measured voice quality. Thus, the estimation of the user perceived signal quality provides an objective evaluation of the expected gains. Undoubtedly, the proposed code proves to be a very interesting

approach to voice transmission over LTE.

Nevertheless, even though we have tried an exhaustive analysis of these technological innovations, they represent a new approach to unequal error protection turbo codes and open new research perspectives.

The codes themselves can be further optimized, by trying any of the existent techniques, i.e. different interleavers, different types of constituent codes and even puncturing techniques. One can even envisage their optimization for certain applications through the number of concatenated codes. Hybrid structures are also possible, by combining together different parallel and serial elements.

Source related optimizations would also be very interesting. Source reliability informations can be introduced at the decoder level for improving the decoding process, for either voice or video transmissions. The video unequal error protection can be envisaged in different forms. For example, the highest level of protection can be given to base images, while the lower levels of redundancy can protect supplementary video images. This might prove to be a very interesting approach for future cloud streaming, where resources will have to be used wisely and distributed to a large number of users.

At the physical layer, due to their hierarchical and progressive structure, the codes can be paired with different mechanisms for enhanced performances. The embedded unequal error protection of data can be correlated to different levels of modulation, and thus provide an unequal error protection channel modulation. Also, the code reliabilities on different packets can be exchanged with the channel turbo equalizer, and improve the channel estimation. HARQ mechanisms can also fully benefit of the code provided branches. In a general perspective, different versions of HARQ packets can be obtained. One can imagine the progressive hierarchical encoding of one HARQ version, with the highest level of redundancy for the first half of the packet, and the lower protection for the second half of the packet. For the second version of the packet, the level of redundancy is switched between the two packets. The receiver will most likely have a double pilot behavior, because each turbo decoded half-packet will have the effect of a pilot when considered on the remaining branch for the other half's progressive decoding. The HARQ perspective can offer considerable gains.

As we have shown here and in each previous chapter, the research perspectives are abundant for both the proposed technological innovations, and LTE. The task of providing a broadband technology evolution for PMR networks seems rather complex given recent market evolutions. The LTE candidate to PMR development will either be modified to integrate specific mission critical requirements, or, the PMR world will modify its perception of these requirements. Radio systems are meant to evolve to new technologies and acquire new spectrum, and the current stream of ideas is orientated only towards high throughputs. However, the era of low rate communications is not over, since machine to machine communications for future smart grid networks are envisaged to use broadband technologies. Therefore, at one point, as the consumer exchange over smart grids will grow, the broadband optimization for low rate data transmission will be envisioned by large operators and industry actors themselves.

Appendix A

List of Publications

During this doctorate, the following conference papers were published:

- 1 A. A. Florea, L. Martinod, P. Mege and H. Nguyen, **Multi-layer Realistic Voice Capacity Evaluation in LTE Rel. 9 and Performance Comparison with PMR and GSM**, in *World Telecommunications Congress*, Miyazaki, Japan, March 2012.
- 2 A. A. Florea, H. Nguyen, L. Martinod and C. Molko, **Serial Progressive Hierarchical Turbo Codes**, in *IEEE Global Communications Conference*, Houston, USA, Dec. 2011.
- 3 A. A. Florea, H. Nguyen, L. Martinod and C. Molko, **Parallel Progressive Hierarchical Turbo Codes**, in *IEEE International Conference on Wireless and Mobile Computing*, Shanghai, China, Oct. 2011.

During this doctorate, the following patents were published:

- 1 A. A. Florea, H. Nguyen, L. Martinod and C. Molko, **Procédé de codage correcteur d'erreur, procédé de décodage et dispositifs associés/Error Correction Encoding Method, Decoding Method and Associated Devices**, *FR2972876/WO2012123516*, Sep. 21st, 2012.
- 2 A. A. Florea, H. Nguyen, L. Martinod and C. Molko, **Procédé de codage correcteur d'erreur, procédé de décodage et dispositifs associés/Error Correction Encoding Method, Decoding Method and Associated Devices**, *FR2972877/WO2012123511*, Sep. 21st, 2012.
- 3 P. Mege, H. Nguyen, A. A. Florea and L. Martinod, **Procédé de codage correcteur d'erreur, procédé de décodage et dispositifs associés/Error Correction Encoding Method, Decoding Method and Associated Devices**, *FR2972878/WO2012123517*, Sep. 21st, 2012.

Appendix B

Puncturing Adaptation

B.1 Puncturing Mechanisms

Existent puncturing mechanisms may be used to modify class rates. The puncturing may modify the transmission rates per class individually. To modify the rate for a certain class, A_k , the only constraint is that the puncturing pattern must be applied only at the specific level of encoding, k . The amount of punctured bits is determined as a function of the remaining levels of encoding, $k + 1$ to n .

From a general perspective, we can compute the needed punctured size per class of bits in order to respect some higher layer defined transmission code rate, as explained hereafter. If the system level defined code rates, r_s , defined as $r_s = (r_{A_1}, r_{A_2}, \dots, r_{A_n})$ for the n classes of bits are different from the default code rates (or mother code rate), r_d , known as $r_d = (r_1^{(d)}, r_2^{(d)}, \dots, r_n^{(d)})$, then we can compute the necessary quantity of bits to be deleted (punctured) as

$$\Delta_k = (r_k^{(d)} - r_{A_k}) C_k, \quad (\text{B.1})$$

with $k = 1 \dots n$. Therefore the new level k constituent code punctured rate will be

$$r_k = \left(\frac{1}{\frac{1}{r_{A_k}} - \frac{1}{r_{A_{k+1}}}} \right)_{1 \leq k < n}, \quad \text{for PPHTC}, \quad (\text{B.2})$$
$$r_k = \left(\frac{r_{A_{k+1}}}{r_{A_k}} \right)_{1 \leq k < n}, \quad \text{for SPHTC},$$

with the last encoding level code rate equal with the last class code rate $r_{A_n} = r_n$. The puncturing is highly flexible, as any kind of uniform or non uniform puncturing may be applied differently per class and per level of encoding.

B.2 Illustrative Results

We provide here some representative results of the PPHTC behavior using LTE style puncturing, i.e. rate matching. We suppose the transmission of code block $A = 1008$ bits, with constituent classes $A_1 = 504$ bits and $A_2 = 504$ bits. These performances are given for the AWGN channel transmission, and for three transmission rates. The two "punctured" performances are derived from the same mother rate code. Fig. B.1 gives the turbo iterative behavior for the PPHTC, using the RSC default rates, or mother rates. Therefore, the default code rates are $R_{A_1} = 1/3$ and $R_{A_2} = 1/2$. The first puncturing scheme, given in Fig. B.2, uses rate matching and the rates become $R_{A_1} = 1/2$ and $R_{A_2} = 1$. Finally, Fig. B.3 presents the performances for extreme rates $R_{A_1} = 2/3$ and $R_{A_2} = 1$.

These figures show an interesting property of the PPHTC. The second class of bits, A_2 , presents an important gain compared to the channel bits given its punctured transmission rate of 1. Basically, class A_2 does not have any redundancy of its own and still its performances are improved through the iterative decoding. The

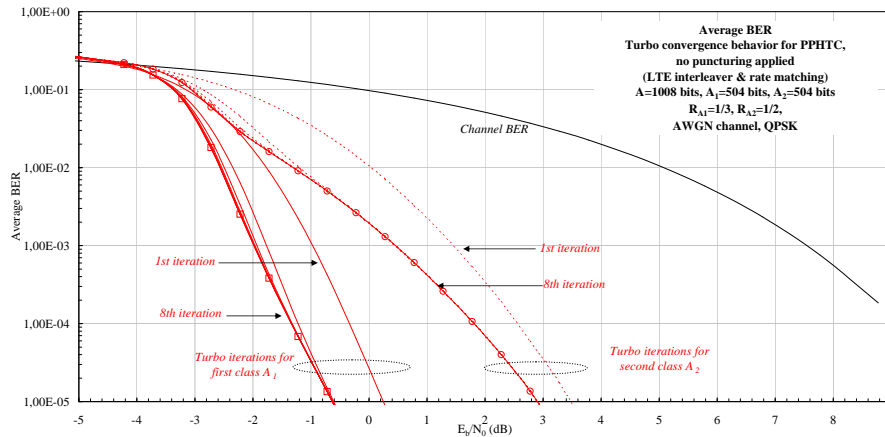


Figure B.1. *PPHTC* turbo iterative behavior without puncturing, $r_{A_1} = 1/3$ and $r_{A_2} = 1/2$ - average BER, LTE platform

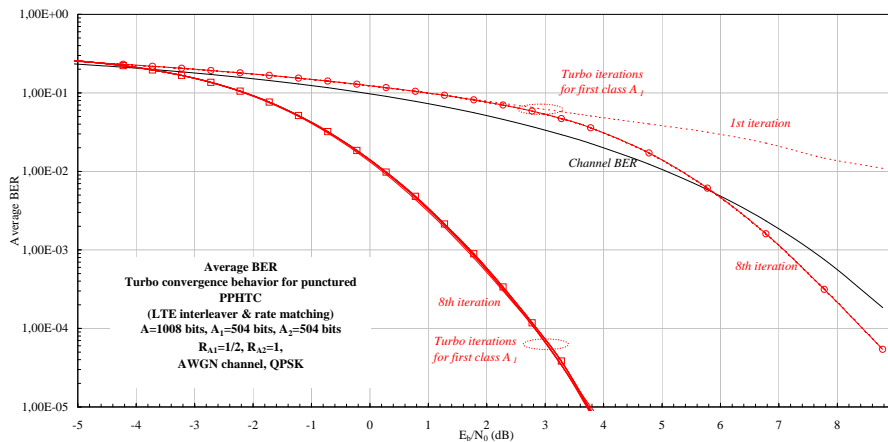


Figure B.2. Punctured *PPHTC* turbo iterative behavior, $r_{A_1} = 1/2$ and $r_{A_2} = 1$ - average BER, LTE platform

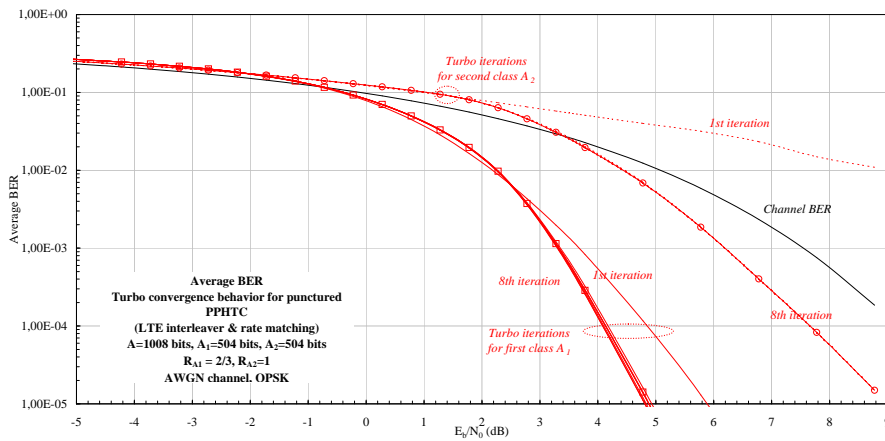


Figure B.3. *PPHTC* turbo iterative behavior, $r_{A_1} = 2/3$ and $r_{A_2} = 1$ - average BER, LTE platform

advantage of such a structure becomes obvious compared to current systems. In PMR networks, the last class of bits may be sent over the channel non protected, at a rate of 1. The PPHTC proves its efficiency even in this extreme case, where class A_2 must have the rate of 1.

Appendix C

The Tangential Sphere Bound

In today's literature, a certain number of theoretical bounds exist, that predict the maximum likelihood (ML) theoretical decoding error probability in AWGN channels. Within these bounds, the most widely used are the union bound and the tangential sphere bound (TSB). The tangential sphere bound is believed to be tighter than the union bound, especially for low and moderate values of E_b/N_0 .

The theoretical bounds are very useful in estimating the turbo codes error floors, and of course help in lowering them. The bit or block error probability for the ML theoretical decoding is upper-bounded by these bounds. The union bound, for example, sums the contributions of all error paths of the encoded weights. All possible combinations of input and output weights for error events are considered at the enumerator term. In [1], the authors note that the bound may diverge beyond the value equal to 1. The transition occurs very abruptly for large block lengths and for values of E_b/N_0 below the threshold determined by the cutoff rate of the code.

The computational cutoff rate is defined as the maximum achievable rate for a given code having a specific metric. For an AWGN channel with bipolar inputs (BPSK), the cutoff rate for a code with rate R is:

$$E_b/N_0 = -\frac{\ln(2^{(1-R)})}{R} \quad (\text{C.1})$$

The standard union bound gives a good estimation of the performance of turbo codes only in the region below the cutoff rate. This means that, in general, this bound is useful for low levels of noise, for codes with moderate lengths and where levels of 10^{-3} to 10^{-4} for error rates are necessary. Often, the minimum distance of the code is mainly useful for computing this bound. This term corresponds to the first term only of the distance spectrum of the code. At high levels of noise, the union bound becomes a very poor estimate of the error probabilities, i.e. 0.01 to 0.1.

Turbo codes yield performances between the cutoff rate and the Shannon capacity of the channel. Therefore, a tighter upper bound, like the TSB, has been recently privileged for the computation of turbo codes theoretical performances. This bound is called tight because it predicts the behavior for SNRs very close to Shannon limits, where the channel is largely affected by noise. The TSB has been firstly proposed by Poltyrev in [2]. The TSB in itself is obtained through the combinations of two other existing bounds: the sphere bound of Hughes [3], and the tangential bound of Berlekamp [4].

In [5], authors have improved the tangential sphere bound for theoretical ML decoding and demonstrated that this bound is a good approximation for the performances of iteratively decoded turbo codes (using Log-MAP). The TSB has been adapted and computed for unequal error protecting (UEP) turbo codes in [6], where the UEP is obtained through puncturing.

The TSB is calculated using the distance spectrum of the codes or the weight enumerating functions (WEF). More exactly, it is the error coefficient, $\varphi_{h(i)}$, determining the contribution of the codeword with weight h_i to the bit error probability, that is used for the TSB estimation.

We recall that the PPHTC error coefficient, $\varphi_{h(i)}^{(C_p)}$, is computed as

$$\varphi_{h_i}^{(C_p)} = \sum_{w_i=1}^{N_i} \frac{w_i}{N_i} A_{w_i, h}^{(A_i)}. \quad (\text{C.2})$$

And the SPHTC error coefficient is computed as

$$\varphi_{h(i)}^{(C_s)} = \sum_{w_i=1}^{N_i} \frac{w_i}{N_i} A_{\omega_i, h}^{(i)}. \quad (C.3)$$

The TSB parameters must be computed as shown in [6] and [5]. This upper bound for each class i uses the following parameters:

$$\begin{aligned} r_{z_1} &= \left(1 - \frac{z_1}{\sqrt{NE_s}}\right) r, \\ \beta_k(z_1) &= \frac{r_{z_1}}{\sqrt{1 - \frac{\delta_k^2}{4NE_s}}} \frac{\delta_k}{2r}, \\ \alpha_k &= r \sqrt{1 - \frac{\delta_k^2}{4NE_s}}, \end{aligned} \quad (C.4)$$

where N represents the output length, δ_k refers to the Euclidian distance between two antipodal symbols as $\delta_k = \sqrt{kE_s}$, and E_s represents the symbol energy.

The TSB upper bound for each class i for the PPHTC (C_p) or the SPHTC (C_s) is written as

$$\begin{aligned} P_{b,i} \leq & \int_{-\infty}^{+\infty} \left\{ \sum_{k: \frac{\delta_k}{2} < \alpha_k} \left\{ \varphi_{h_i}^{(C_{p/s})} \int_{\beta_k(z_1)}^{r_{z_1}} \frac{1}{\sqrt{2\pi\sigma}} \bar{\gamma} \left(\frac{N-2}{2}, \frac{r_{z_1}^2 - z_2^2}{2\sigma^2} \right) \exp \frac{-z_2^2}{2\sigma^2} dz_2 \right\} + \right. \\ & \left. + 1 - \bar{\gamma} \left(\frac{N-1}{2}, \frac{r_{z_1}^2}{2\sigma^2} \right) \right\} \frac{\exp \frac{-z_1^2}{2\sigma^2}}{\sqrt{2\pi\sigma}}, \end{aligned} \quad (C.5)$$

where σ^2 denotes the AWGN noise variance, and $\bar{\gamma}$ the normalized incomplete γ function. The remaining parameters are explained hereafter.

The TSB computes the theoretical limits based on the theoretical expression

$$Prob(A) \leq Prob(z \in B, A) + Prob(z \notin B). \quad (C.6)$$

A represents a decoding error, that might or might not be a part of the decoding dimensions of the received message. B refers to the decoding message space, conceived as an n -dimensional cone with a half angle θ and radius $r = \sqrt{nE_s} \tan \theta$. z_1 represents the noise vector added to the received message, and this vector can be decomposed between the tangential and the radial components. But here, only the radial component, $z_1^{(r)}$, modifies the code word weight. The code word supposed to be placed at distance r of the center of the sphere represents the correct code word. When the vector $z_1^{(r)}$ is added (oriented towards the center of the sphere), the code word weight decreases and its position is altered. Its new position belongs to a new sphere of square radius r_{z_1} , this latter sphere being obtained through errors.

The TSB performs an integration on all values of the radial component of the noise vector, z_1 , on the n dimensional sphere, and performs an estimation of the probability of error as the maximum or lowest achievable values. But the tightest upper bound is performed with an optimal radius r , determined from the equation

$$\sum_{k: \frac{\delta_k}{2} < \alpha_k} \varphi_{h_i}^{(C_{p/s})} \int_0^{\theta_k} \sin^{N-3} \phi d\phi = \frac{\sqrt{\pi} \Gamma \left(\frac{N-2}{2} \right)}{\Gamma \left(\frac{N-1}{2} \right)}, \quad (C.7)$$

where

$$\theta_k = \cos^{-1} \left(\frac{\delta_k}{2r} \frac{1}{\sqrt{1 - \frac{\delta_k^2}{4NE_s}}} \right) = \cos^{-1} \frac{\delta_k}{2\alpha_k}. \quad (C.8)$$

In other words, the optimum radius is obtained for valid angle values such as $\frac{\delta_k}{2\alpha_k} < 1$.

The mathematical functions are defined as:

$$\Gamma(x) = \int_0^{\infty} t^{x-1} \exp -tdt, \quad (\text{C.9})$$

and

$$\bar{\gamma}(a, x) = \frac{1}{\Gamma(a)} \int_0^x t^{a-1} \exp -tdt. \quad (\text{C.10})$$

for positive values of a and x .

Considering the computer computation and simulation of all these equations and their respective parameters, we have made some approximations of the PPHTC and SPHTC theoretical ML bounds. However, due to the required computation complexity, we present here only our first results obtained on very small length code words.

Fig. C.1 presents the theoretical TSB computed for the PPHTC, with input $A = 56$ bits, from which class $A_1 = 28$ bits and class $A_2 = 28$ bits. The TSB results are compared with average BER performances for the PPHTC considering an AWGN channel and BPSK modulation (random interleaver).

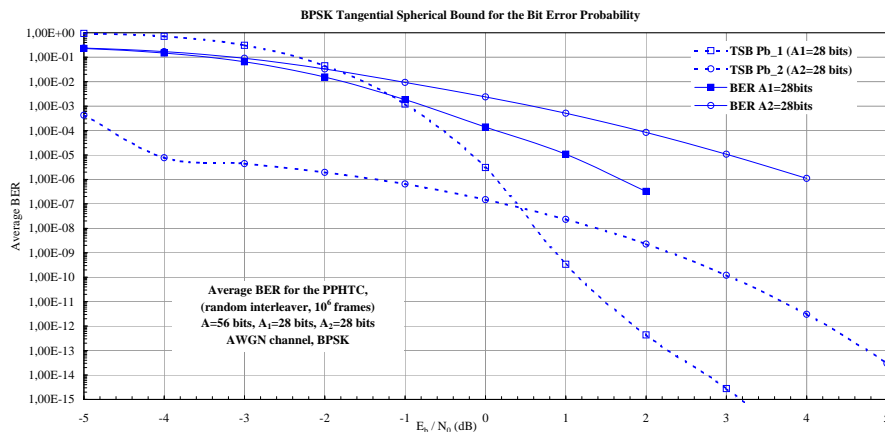


Figure C.1. Comparison of the bit error probability theoretical upper bound for theoretical ML decoding with PPHTC simulations results for iterative decoding, random platform.

Fig. C.2 presents the theoretical TSB computed for the SPHTC, with input $A = 60$ bits, from which class $A_1 = 30$ bits and class $A_2 = 30$ bits. The TSB results are compared with average BER performances for the SPHTC considering an AWGN channel and BPSK modulation (random interleaver).

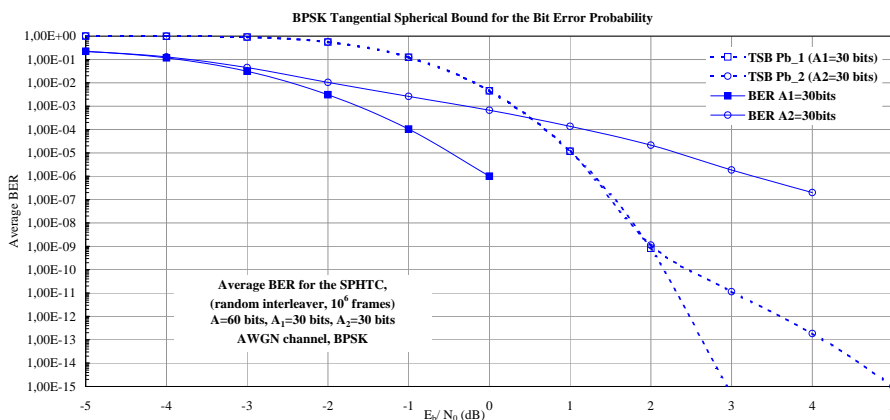


Figure C.2. Comparison of the bit error probability theoretical upper bound for ML decoding with SPHTC simulations results for iterative decoding, random platform.

We particularly note the difference between the bounds computed for the second class A_2 . This shift of the TSB from the parallel case to the serial case might be caused by the minimum distance difference. In the

PPHTC case, the convolutional encoding of A_2 is performed on $N_1 + N_2$ bits, i.e. 56 bits. This means that the maximum possible input weight is 56, compared to the all zero codeword. But in the SPHTC case, the convolutional encoding of A_2 is performed on $2N_1 + N_2$ bits, i.e. 90 bits. Therefore, its maximum achievable input weight is equal to 90 compared to the all zero codeword. The error floor is reached faster by the PPHTC than by the SPHTC, and for both classes.

These performances are especially visible at a larger scale, e.g. on the average BER figures for input $A = 1000$ bits. The performances of the SPHTC decoded A_2 are always improved compared to the PPHTC case. And also, the PPHTC average BER tends to reach the error floor faster than the SPHTC, which is visible particularly on the performances of class A_1 .

The TSB gives an immediate overview of the error floor. The moment when the error floor is reached, the TSB curve shifts and the waterfall becomes less steeper, and more horizontal. In the turbo structure case, we note this behavior especially in Fig. C.1, where the class A_1 upper bound starts shifting. This horizontal shift provides an insight to the maximum achievable ML theoretical decoding for class A_1 . Even though we have performed simulations on 10^6 frames, obtaining these theoretical limits through computer simulations would need much higher order simulations. For the turbo behavior of class A_2 on the other hand, the TSB shift is well visible on both Fig. C.1 and C.2. The descent towards lower probability of errors is smoother and resembles a convolutional code. We might as well say that it is the behavior of a convolutional code, but with an enhanced input weight, which virtually modifies its minimum distance properties.

Bibliography

- [1] D. Divsalar, S. Dolinar, F. Pollara, and R. McEliece, "Transfer function bounds on the performance of turbo codes," in *TDA Progress Report*, Aug. 1995, pp. 42–122.
- [2] G. Poltyrev, "Bounds on the decoding error probability of binary linear codes via their spectra," *IEEE Transactions on Information Theory*, vol. 40, pp. 1284–1292, Jul. 1994.
- [3] B. Hughes, "On the error probability of signals in additive white Gaussian noise," *IEEE Transactions on Information Theory*, vol. 37, pp. 151–155, Jan. 1991.
- [4] E. Berlekamp, "The technology of error-correcting codes," in *Proceedings of the IEEE*, vol. 68, May 1998, pp. 564–593.
- [5] I. Sason and S. Shamai, "Improved upper bounds on the ML decoding error probability of parallel and serial concatenated turbo codes via their ensemble distance spectrum," *IEEE Transactions on Information Theory*, vol. 46, pp. 24–47, Jan. 2000.
- [6] M. Aydilink and M. Salehi, "Performance bounds for unequal error protecting turbo codes," *IEEE Transactions on Communications*, vol. 57, pp. 1215–1220, May 2009.

Appendix D

Complementary Results

D.1 2-D Results

D.1.1 UEP Turbo behavior: AWGN FER Performances

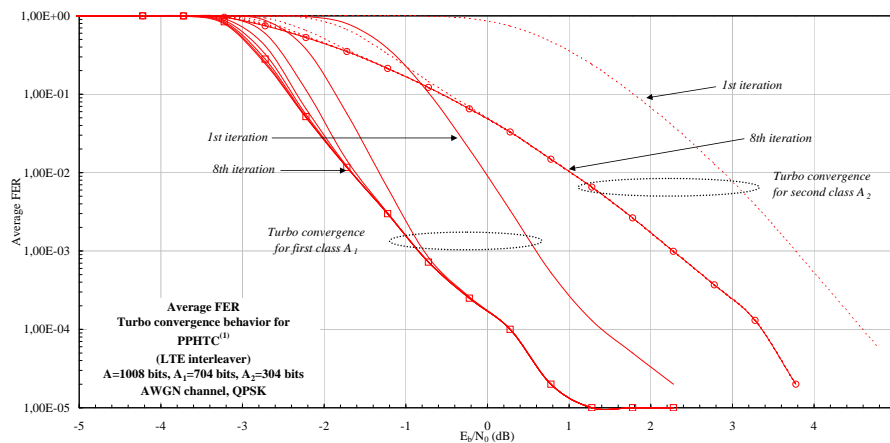


Figure D.1. AWGN $PPHTC^{(1)}$ turbo iterative behavior - average FER, LTE platform

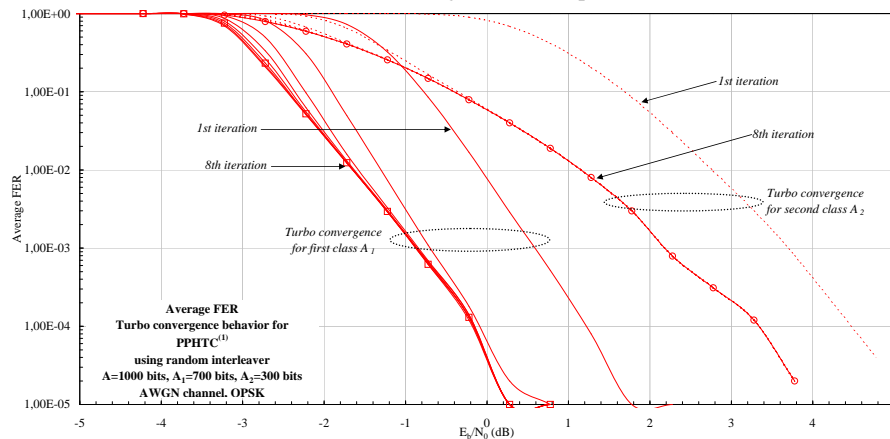


Figure D.2. AWGN $PPHTC^{(1)}$ turbo iterative behavior - average FER, random platform

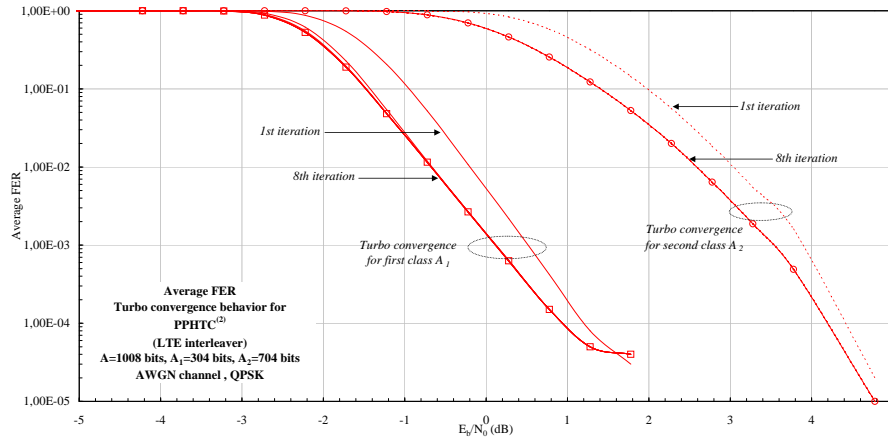


Figure D.3. AWGN PPHTC⁽²⁾ turbo iterative behavior - average FER, LTE platform

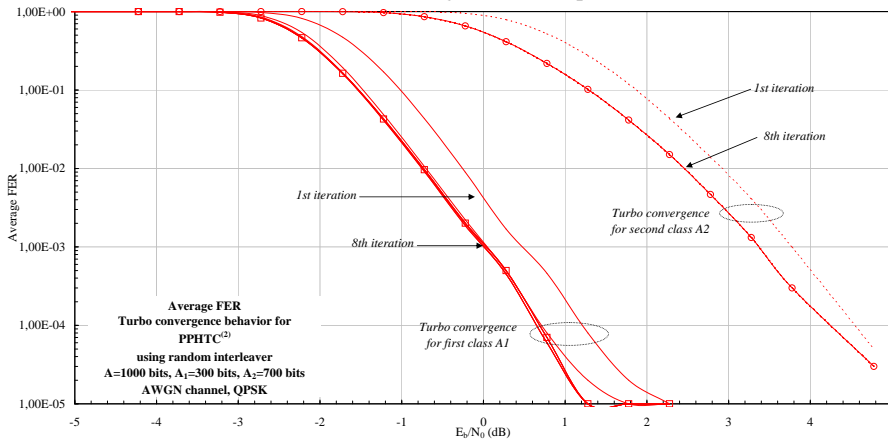


Figure D.4. AWGN PPHTC⁽²⁾ turbo iterative behavior - average FER, random platform

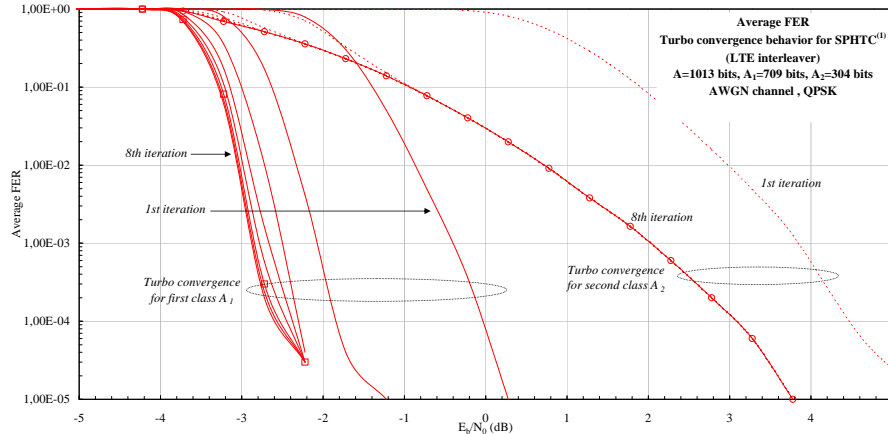


Figure D.5. AWGN SPHTC⁽¹⁾ turbo iterative behavior - average FER, LTE platform

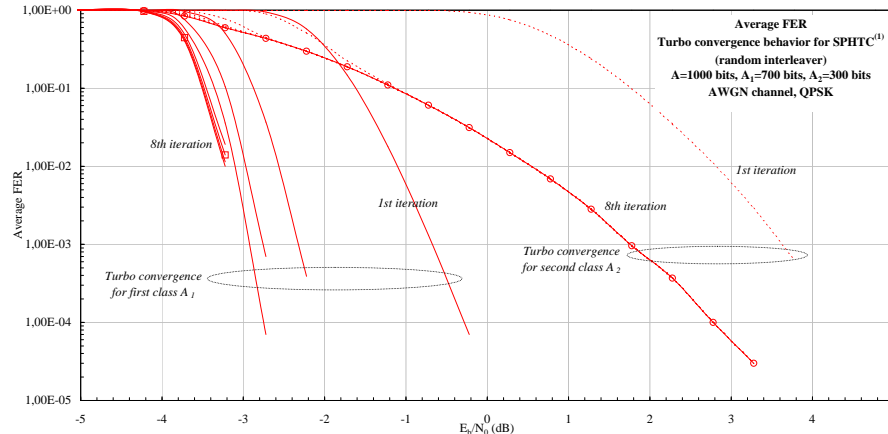


Figure D.6. AWGN SPHTC⁽¹⁾ turbo iterative behavior - average FER, random platform

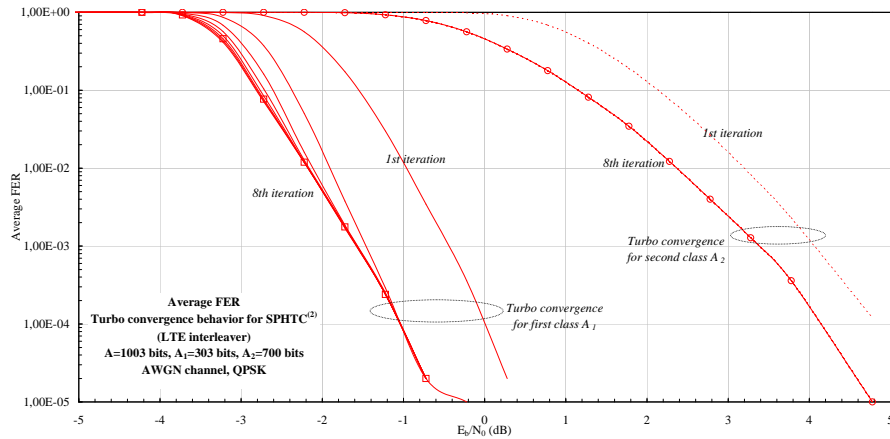


Figure D.7. AWGN SPHTC⁽²⁾ turbo iterative behavior - average FER, LTE platform

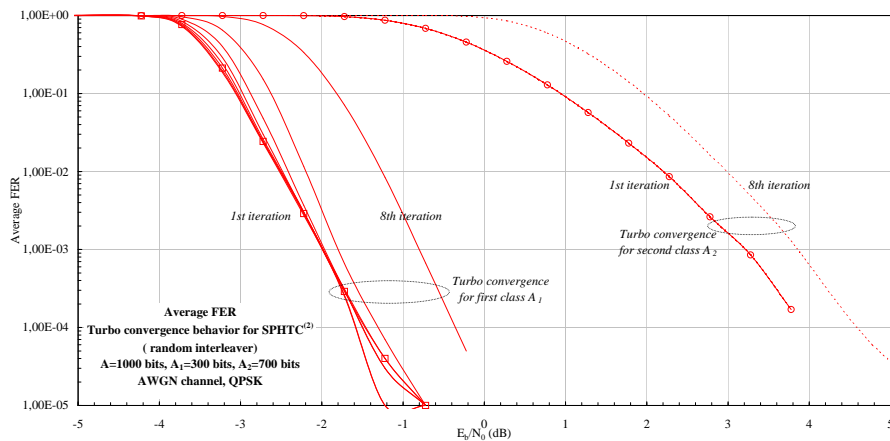


Figure D.8. AWGN SPHTC⁽²⁾ turbo iterative behavior - average FER, LTE platform

D.1.2 UEP Turbo behavior: HT200 FER Performances

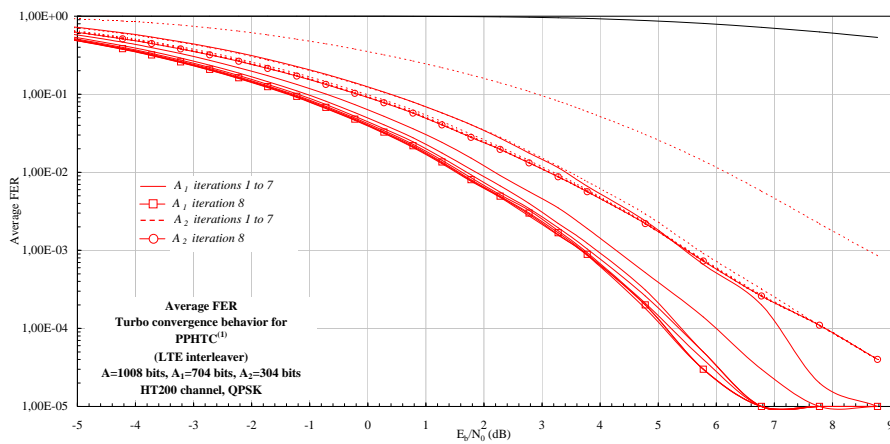


Figure D.9. HT200 PPHTC⁽¹⁾ turbo iterative behavior - average FER, LTE platform.

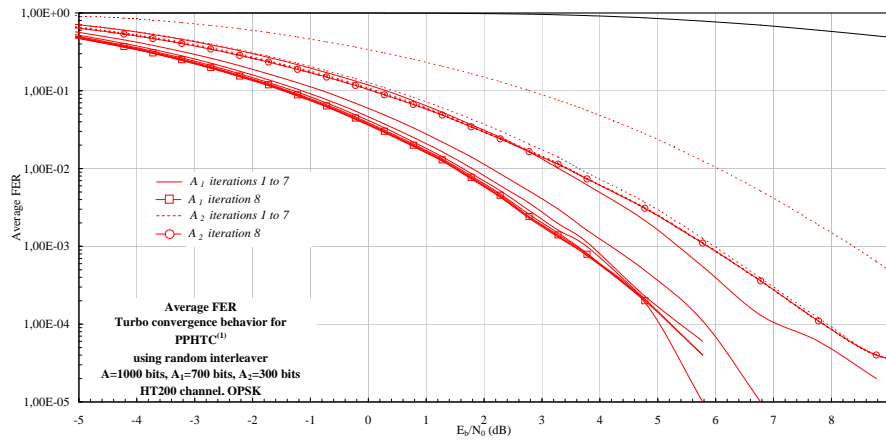


Figure D.10. HT200 $PPHTC^{(1)}$ turbo iterative behavior - average FER, random platform.

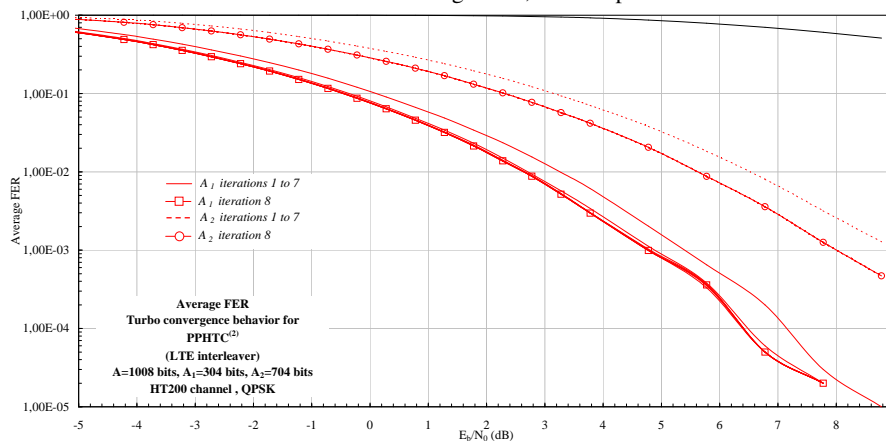


Figure D.11. HT200 $PPHTC^{(2)}$ turbo iterative behavior - average FER, LTE platform.

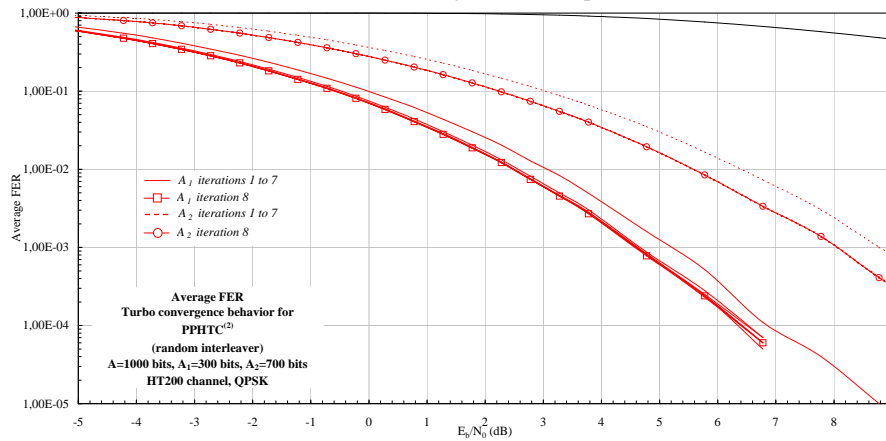


Figure D.12. HT200 $PPHTC^{(2)}$ turbo iterative behavior - average FER, random platform.

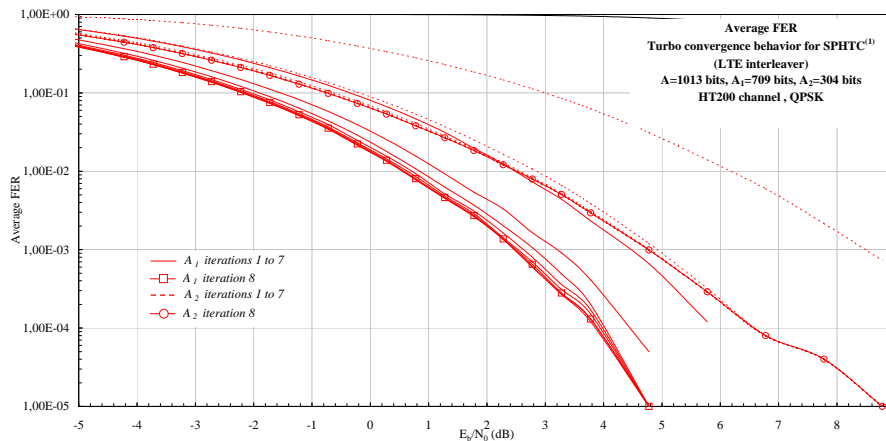


Figure D.13. HT200 $SPHTC^{(1)}$ turbo iterative behavior - average FER, LTE platform.

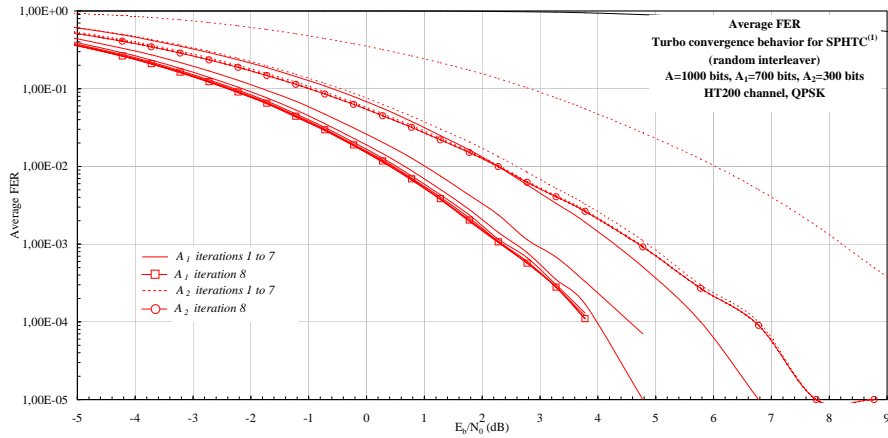


Figure D.14. HT200 SPHTC⁽¹⁾ turbo iterative behavior - average FER, random platform.

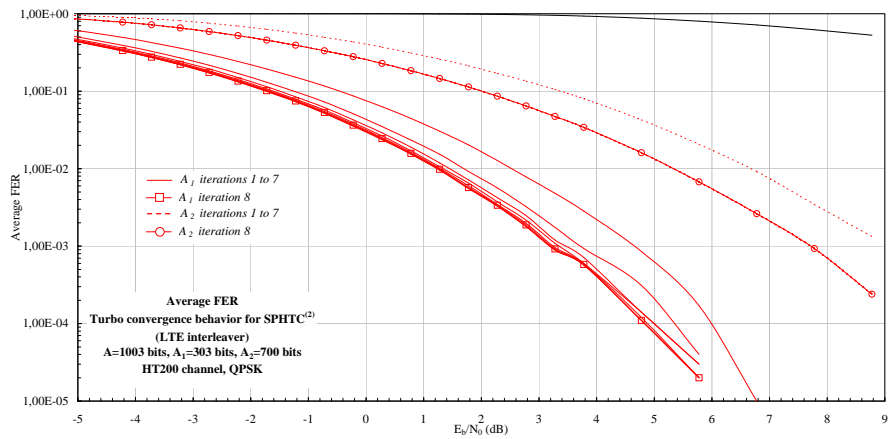


Figure D.15. HT200 SPHTC⁽²⁾ turbo iterative behavior - average FER, LTE platform.

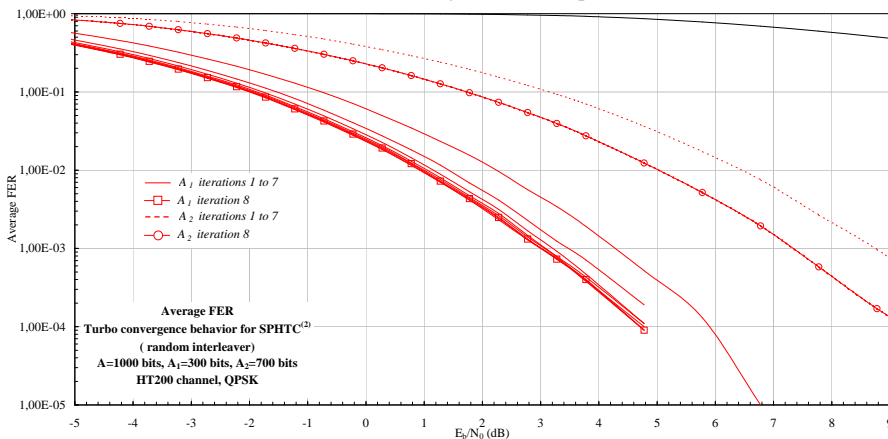


Figure D.16. HT200 SPHTC⁽²⁾ turbo iterative behavior - average FER, random platform.

D.1.3 HT200 Pilot Code Performances

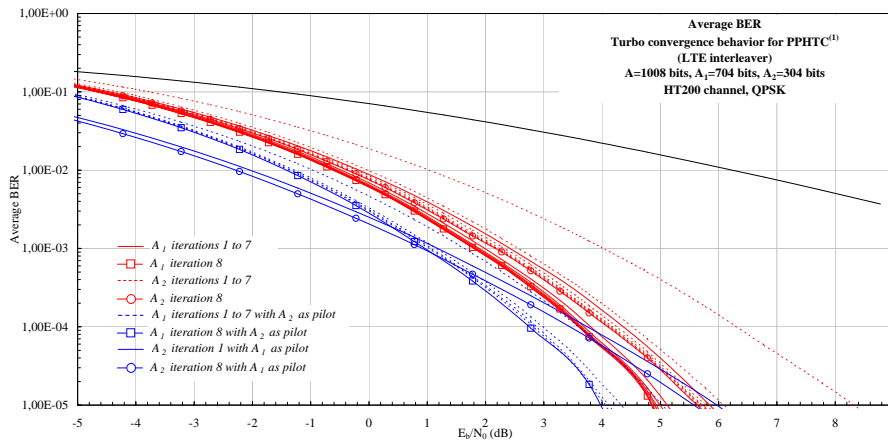


Figure D.17. HT200 *PPHTC*⁽¹⁾ pilot insertion behavior, LTE platform.

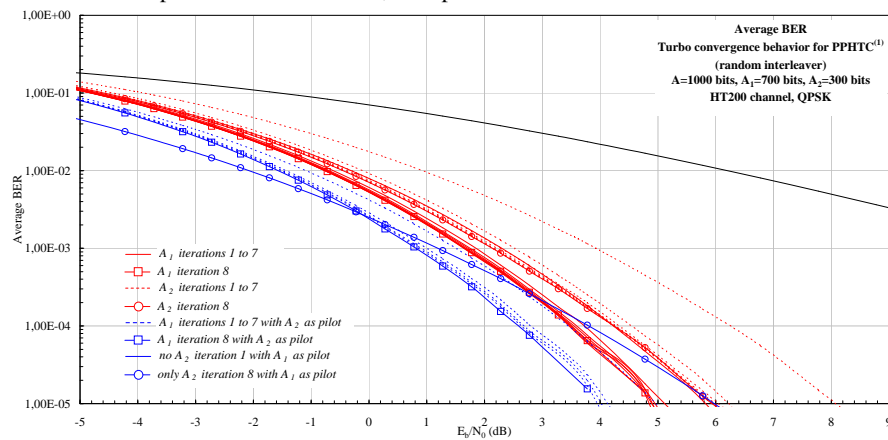


Figure D.18. HT200 *PPHTC*⁽¹⁾ pilot insertion behavior, random platform.

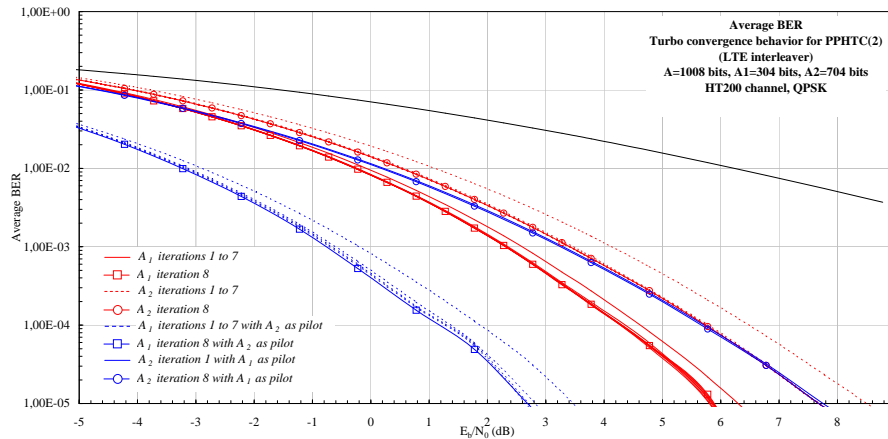


Figure D.19. HT200 *PPHTC*⁽²⁾ pilot insertion behavior, LTE platform.

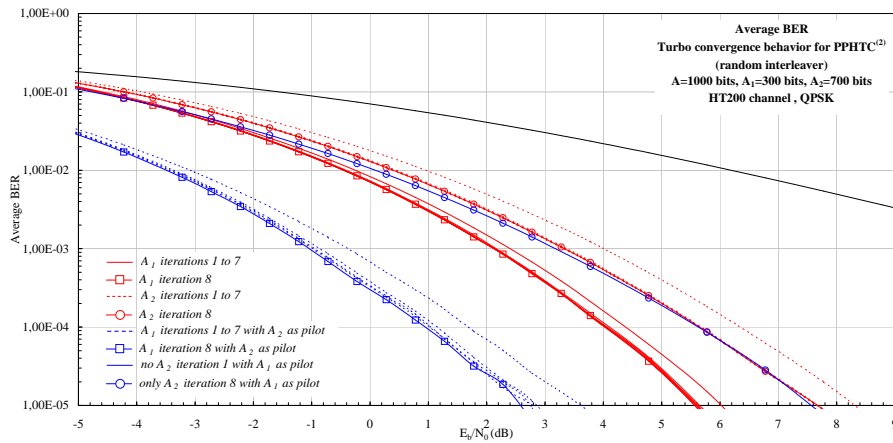


Figure D.20. HT200 $PPHTC^{(2)}$ pilot insertion behavior, random platform.

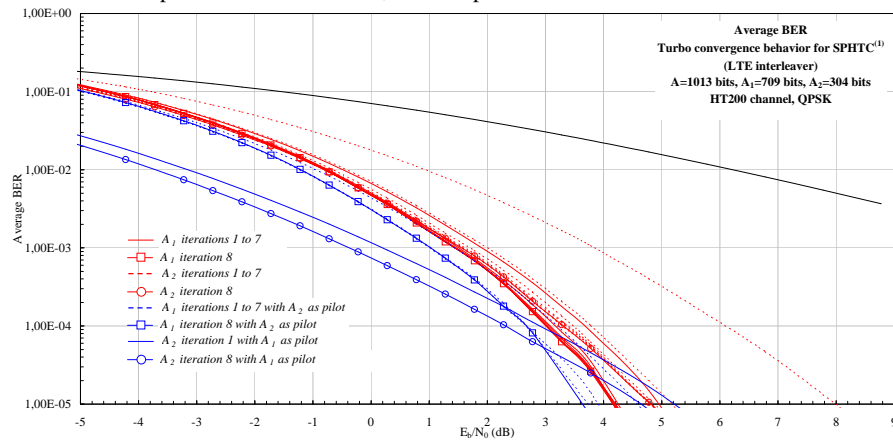


Figure D.21. HT200 $SPHTC^{(1)}$ pilot insertion behavior, LTE platform.

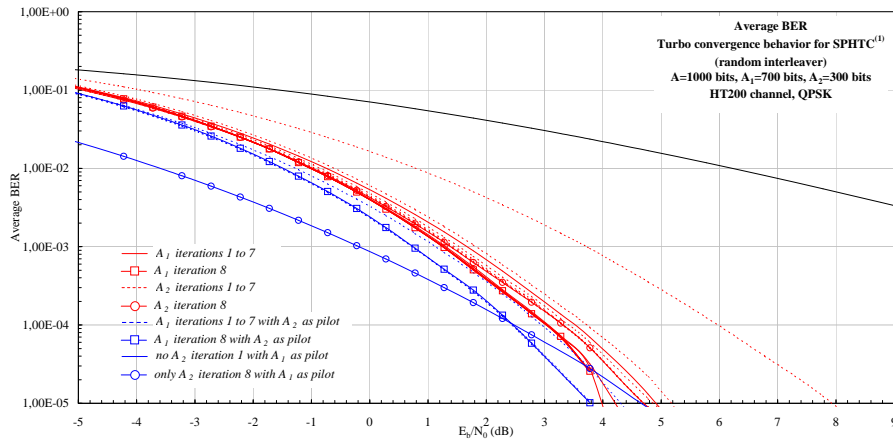


Figure D.22. HT200 $SPHTC^{(1)}$ pilot insertion behavior, random platform.

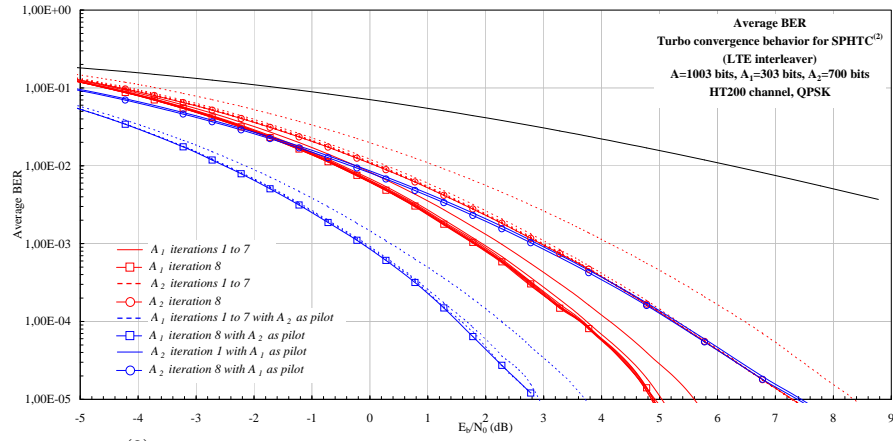


Figure D.23. HT200 $SPHTC^{(2)}$ pilot insertion behavior, LTE platform.

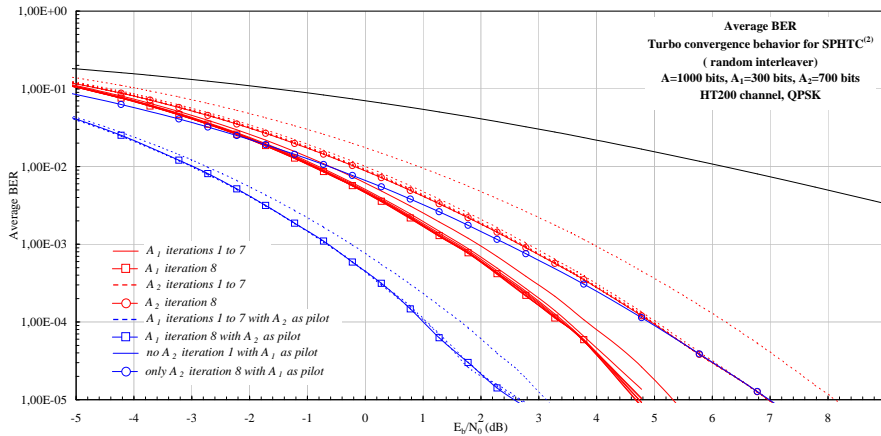


Figure D.24. HT200 SPHTC⁽²⁾ pilot insertion behavior, random platform.

D.1.4 AWGN FER Performance Comparison

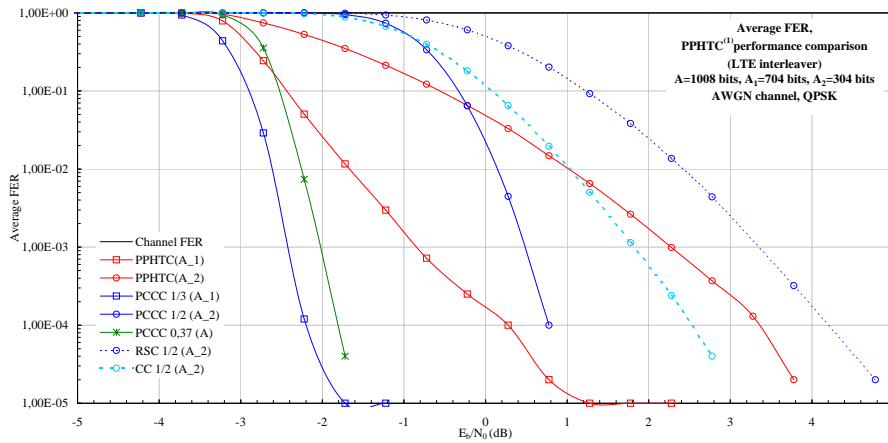


Figure D.25. AWGN PPHTC⁽¹⁾ turbo performances comparison - average FER, LTE platform.

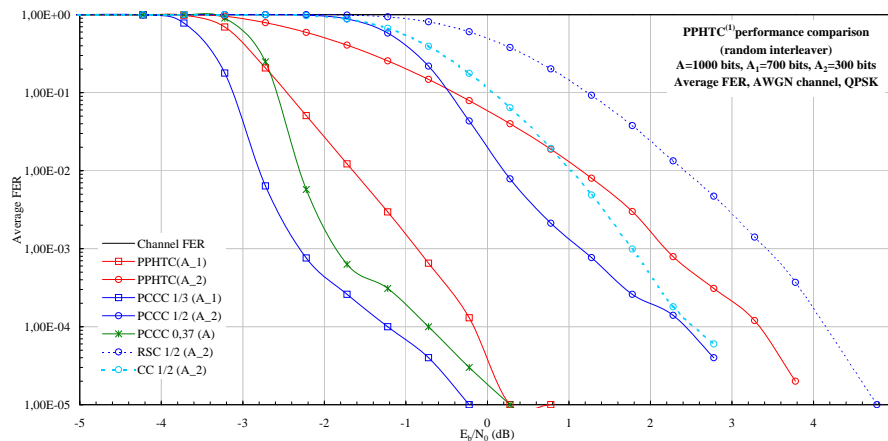


Figure D.26. AWGN PPHTC⁽¹⁾ turbo performances comparison - average FER, random platform.

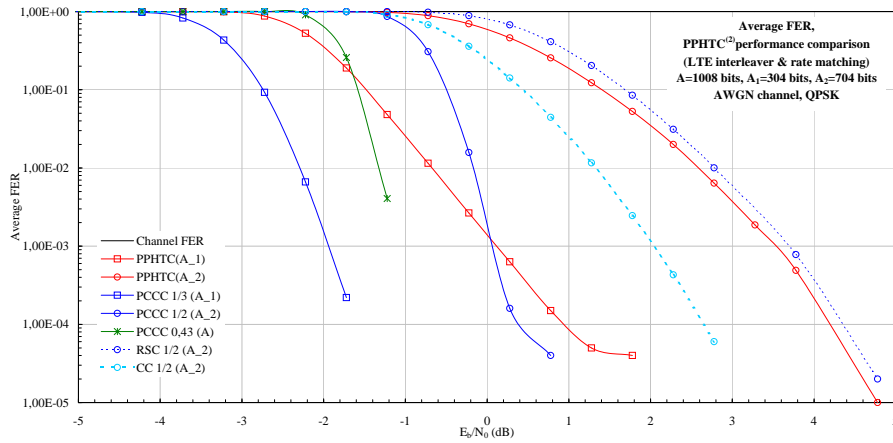


Figure D.27. AWGN PPHTC⁽²⁾ turbo performances comparison - average FER, LTE platform.

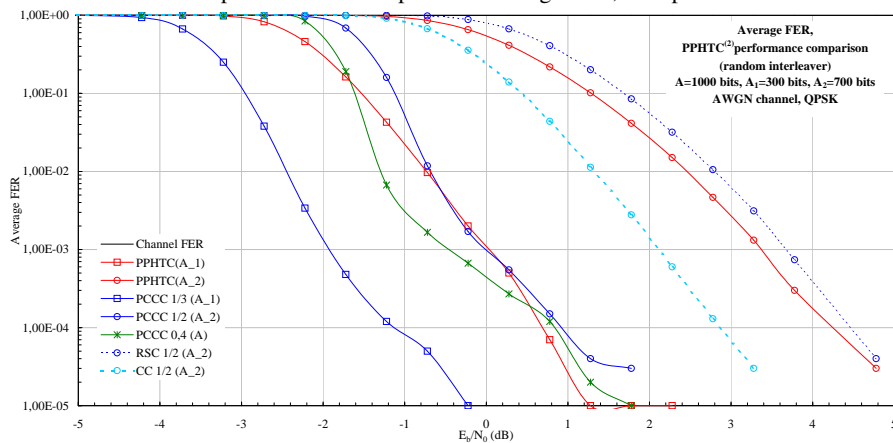


Figure D.28. AWGN PPHTC⁽²⁾ turbo performances comparison - average FER, random platform.

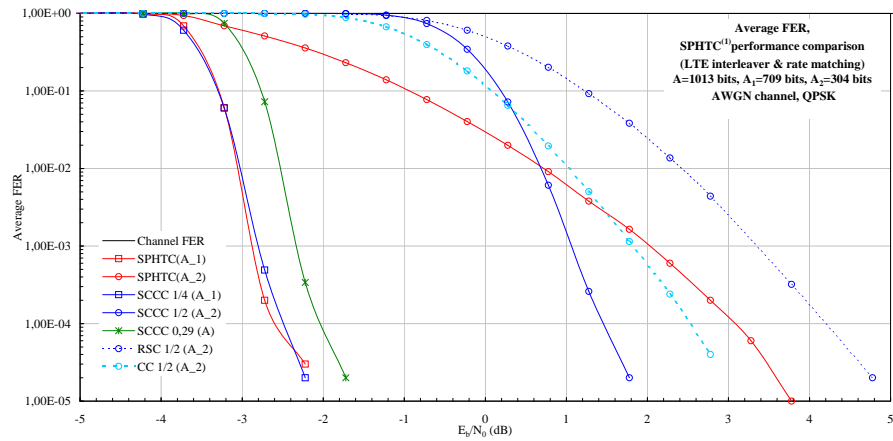


Figure D.29. AWGN SPHTC⁽¹⁾ turbo performances comparison - average FER, LTE platform.

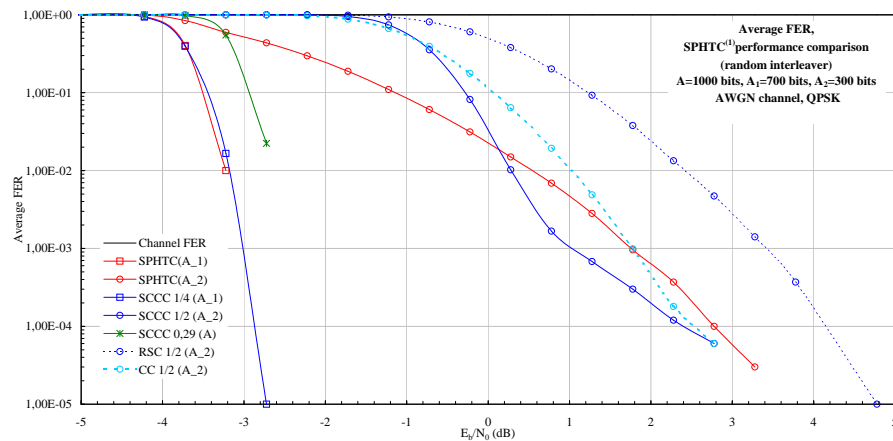


Figure D.30. AWGN SPHTC⁽¹⁾ turbo performances comparison - average FER, random platform.

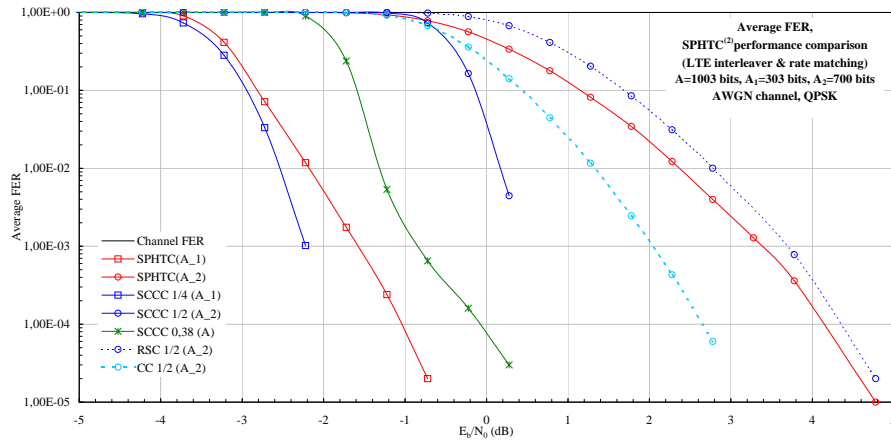


Figure D.31. AWGN *SPHTC*⁽²⁾ turbo performances comparison - average FER, LTE platform.

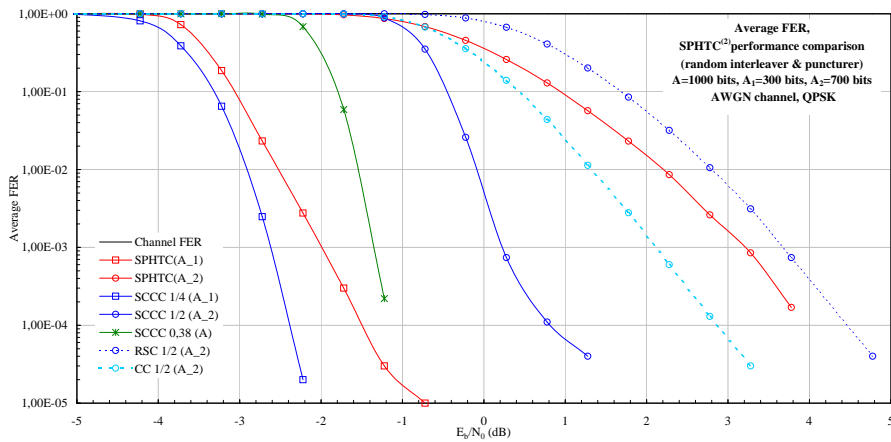


Figure D.32. AWGN *SPHTC*⁽²⁾ turbo performances comparison - average FER, random platform.

D.1.5 HT200 FER Performance Comparison

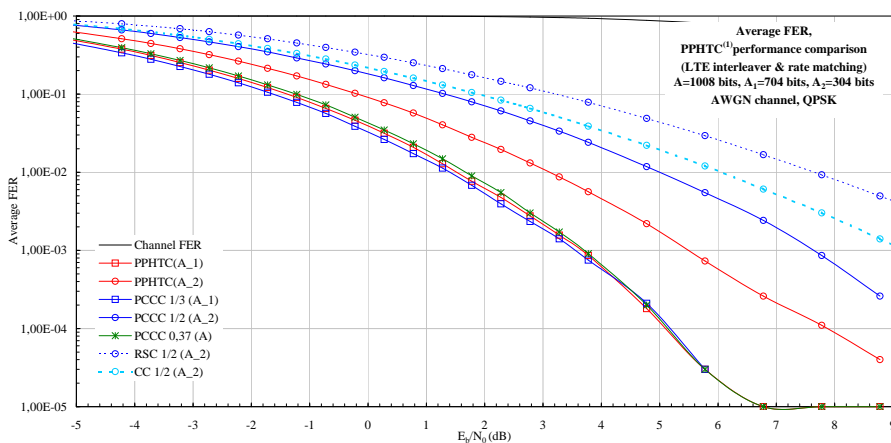


Figure D.33. *PPHTC*⁽¹⁾ turbo performances comparison - average FER, LTE platform, HT200.

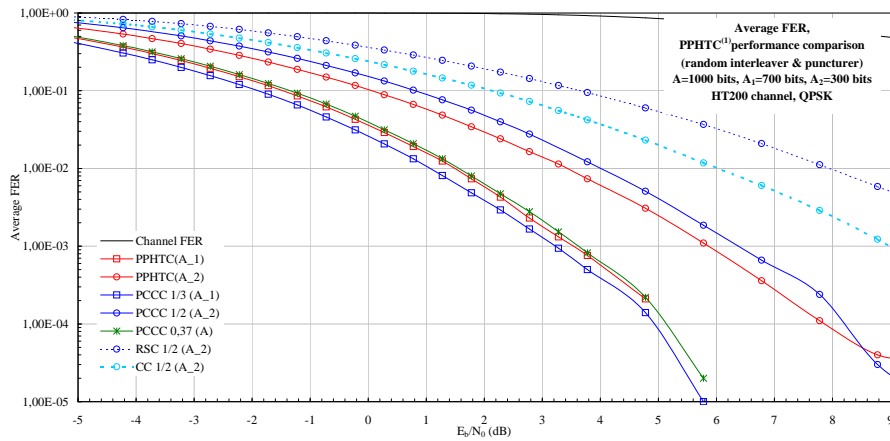


Figure D.34. $PPHTC^{(1)}$ turbo performances comparison - average FER, random platform, HT200.

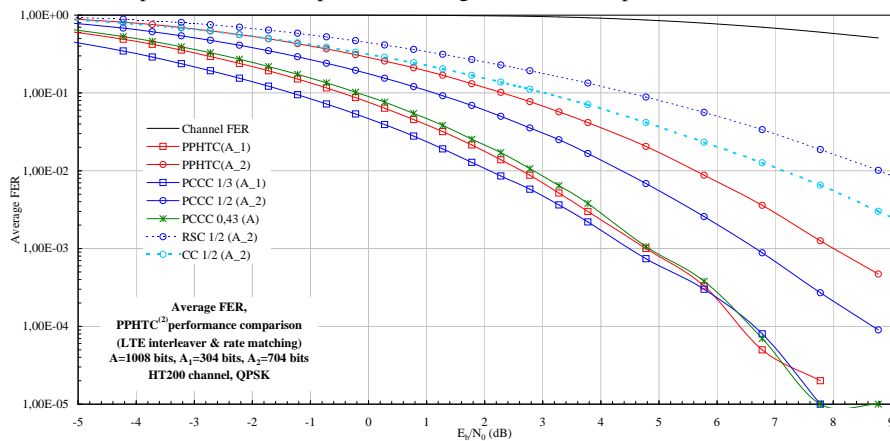


Figure D.35. $PPHTC^{(2)}$ turbo performances comparison - average FER, LTE platform, HT200.

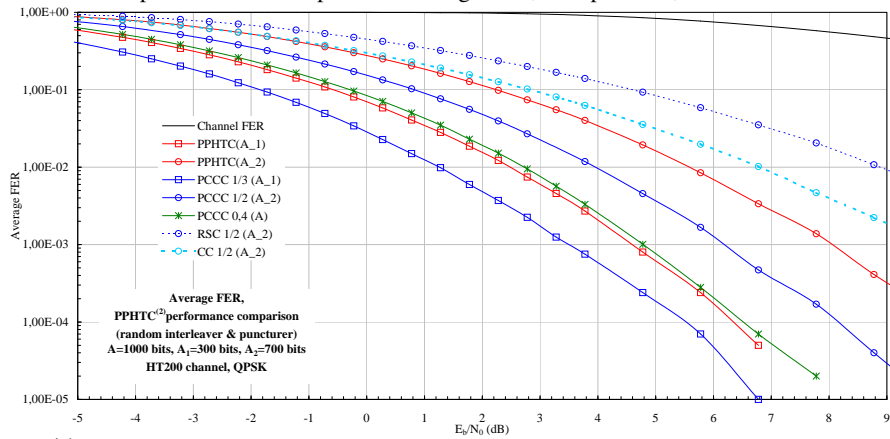


Figure D.36. $PPHTC^{(2)}$ turbo performances comparison - average FER, random platform, HT200.

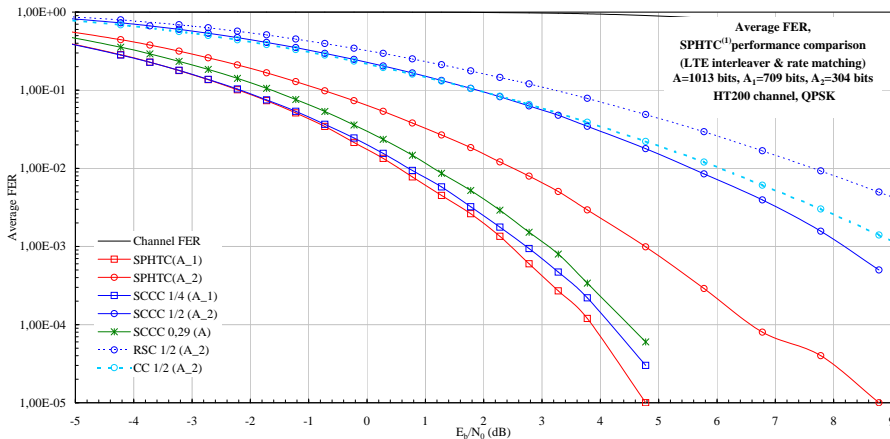


Figure D.37. $SPHTC^{(1)}$ turbo performances comparison - average FER, LTE platform, HT200.

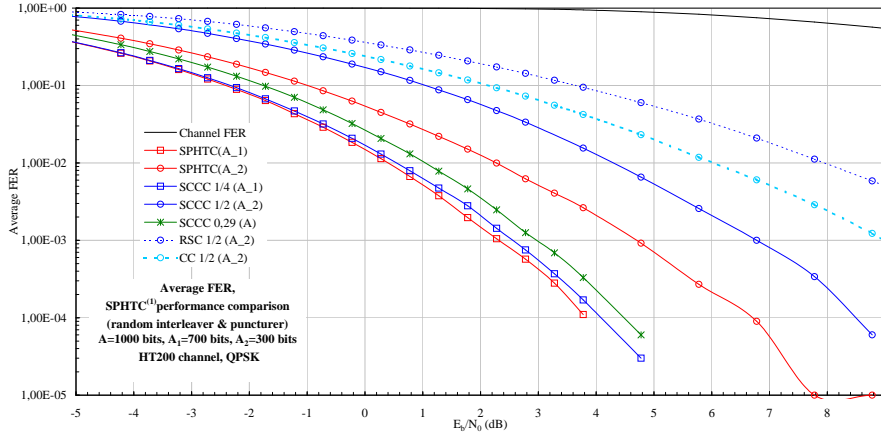


Figure D.38. *SPHTC*⁽¹⁾ turbo performances comparison - average FER, random platform, HT200.

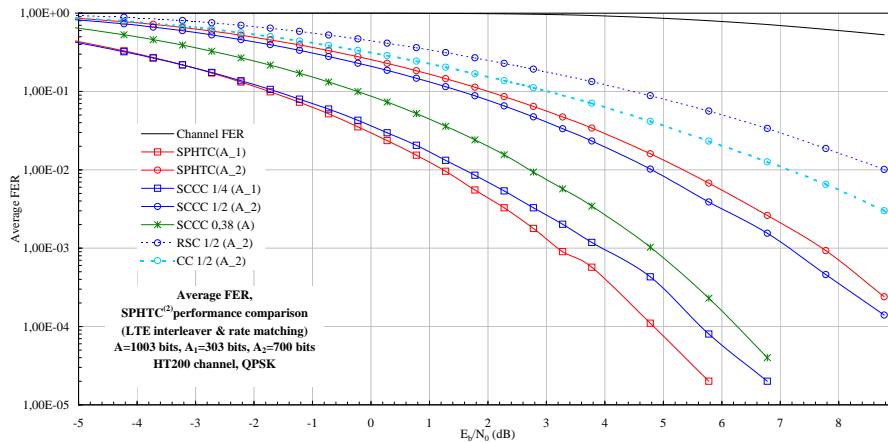


Figure D.39. *SPHTC*⁽²⁾ turbo performances comparison - average FER, LTE platform, HT200.

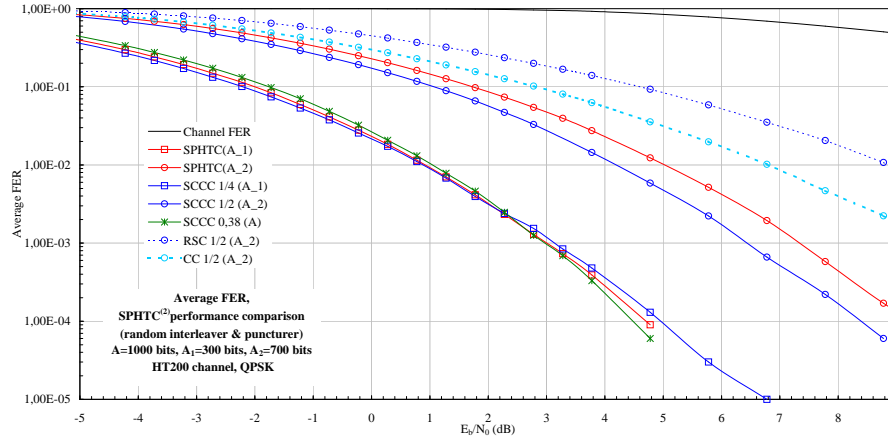


Figure D.40. *SPHTC*⁽²⁾ turbo performances comparison - average FER, random platform, HT200.

D.2 3-D Performances

For an illustration of higher level performances, we present here some performances for the $n = 3$ case, i.e. three constituent codes for the PPHTC and SPHTC respectively, and three transmitted UEP classes. As expected, the results show a full turbo behavior for higher level classes, A_1 and A_2 . These classes benefit of three and two concatenated RSCs each respectively. Not surprisingly, the third class A_3 also presents an iterative behavior. Through the eight iterations, A_3 gains are considerable between its first and eighth iteration.

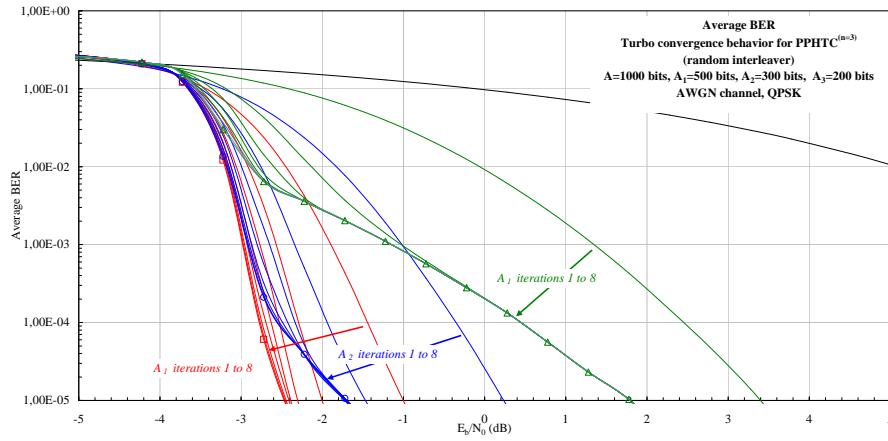


Figure D.41. AWGN PPHTC⁽ⁿ⁼³⁾ convergence behavior $A_1 > A_2 > A_3$ - average BER, random platform.

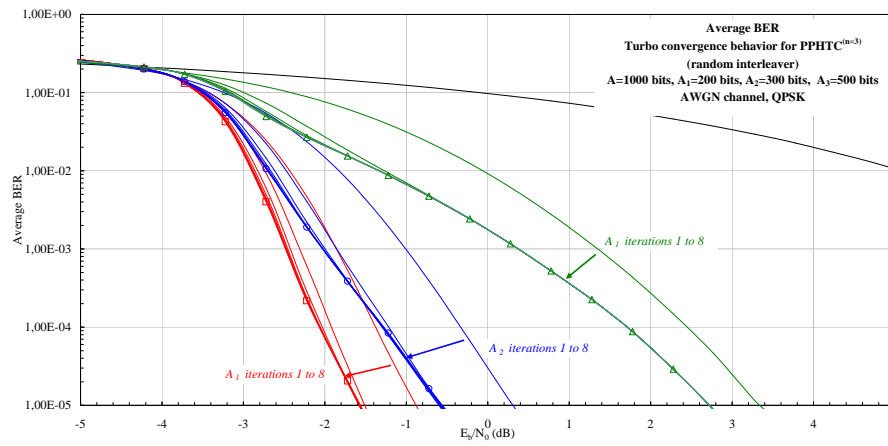


Figure D.42. AWGN PPHTC⁽ⁿ⁼³⁾ convergence behavior $A_1 < A_2 < A_3$ - average BER, random platform.

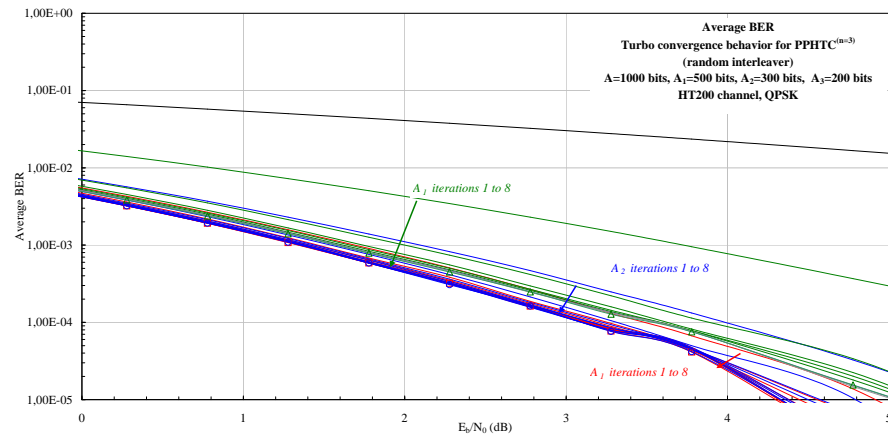


Figure D.43. HT200 PPHTC⁽ⁿ⁼³⁾ convergence behavior $A_1 > A_2 > A_3$ - average BER, random platform.

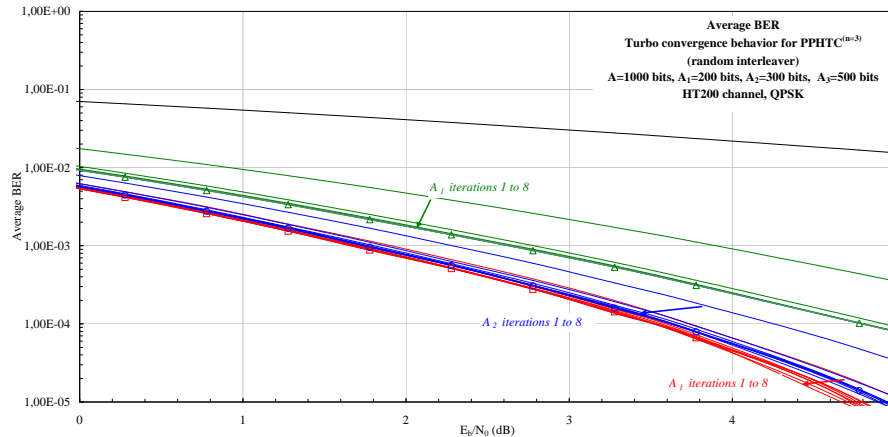


Figure D.44. HT200 PPHTC⁽ⁿ⁼³⁾ convergence behavior $A_1 < A_2 < A_3$ - average BER, random platform.

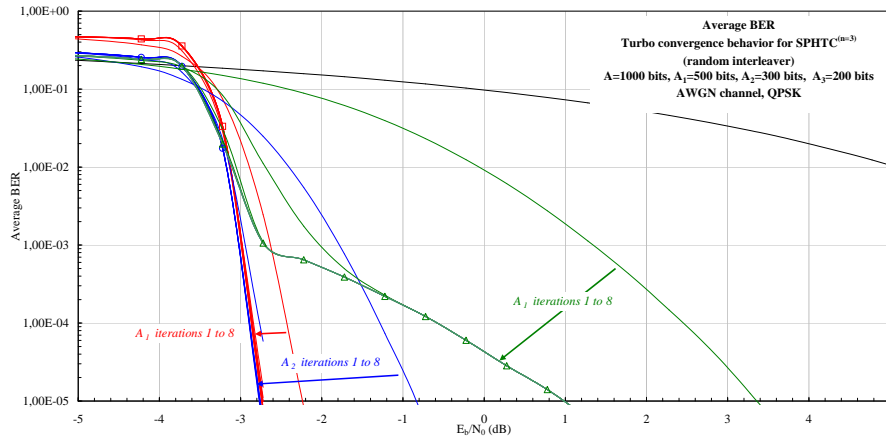


Figure D.45. AWGN $SPHTC^{(n=3)}$ convergence behavior $A_1 > A_2 > A_3$ - average BER, random platform.

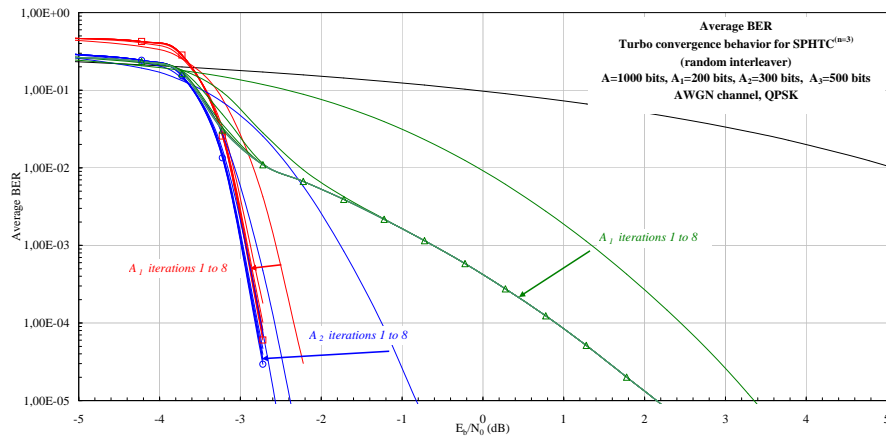


Figure D.46. AWGN $SPHTC^{(n=3)}$ convergence behavior $A_1 < A_2 < A_3$ - average BER, random platform.

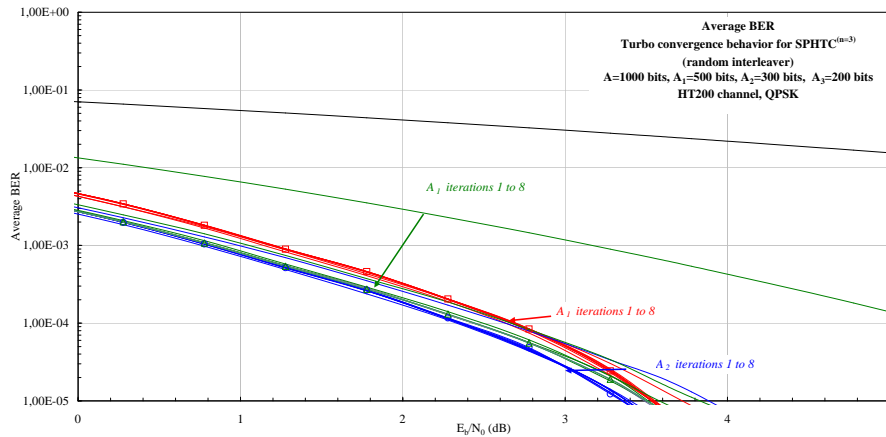


Figure D.47. HT200 $SPHTC^{(n=3)}$ convergence behavior $A_1 > A_2 > A_3$ - average BER, random platform.

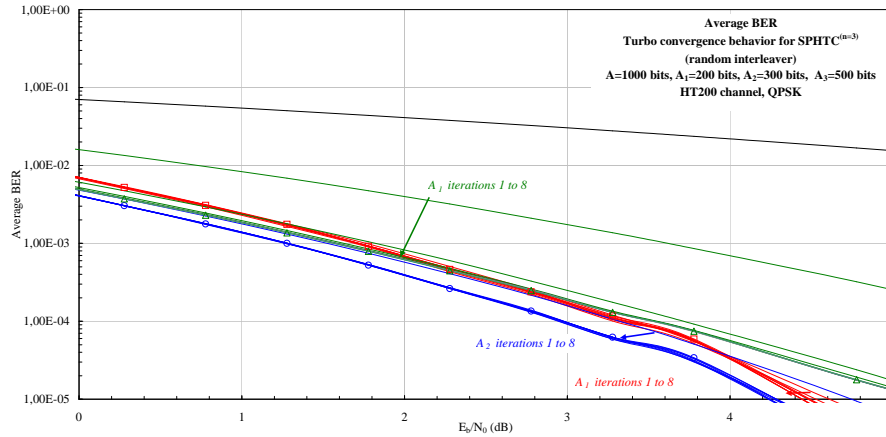


Figure D.48. HT200 $SPHTC^{(n=3)}$ convergence behavior $A_1 < A_2 < A_3$ - average BER, random platform.